Universidade Vigo

Escola Internacional de Doutoramento

Iago Algarra Cajide

TESE DE DOUTORAMENTO

Moisture transport associated with Atmospheric Rivers and Low Level Jets at global scale

Dirixida por:

Dr. Luis Gimeno Presa

Dra. Raquel Olalla Nieto Muñiz

2020

"Mención internacional"

Universidade Vigo

Escola Internacional de Doutoramento

Dr. Luis Gimeno Presa, catedrático do Departamento de Física Aplicada da Universidade de Vigo e Dra. Raquel Olalla Nieto Muñiz, profesora titular do Departamento de Física Aplicada da Universidade de Vigo:

FAN CONSTAR que o presente traballo, titulado ***"Moisture transport associated with Atmospheric Rivers and Low Level Jets at global scale"*** que presenta Iago Algarra Cajide para a obtención do título de Doutor pola Universidade de Vigo con Mención Internacional, foi elaborado baixo a súa dirección no programa de doutoramento *"Auga, sustentabilidade e desenvolvemento"* baixo a modalidade de compendio de publicacións.

Ourense, 31 de xaneiro de 2020

Os directores da tese de doutoramento

Dr. Luis Gimeno Presa

Dra. Raquel Olalla Nieto Muñiz

Campus Universitario de Ourense, Universidade de Vigo

Departamento de Física Aplicada | Environmental Physics Laboratory (EPhysLab)

Iago Algarra Cajide (ialgarra@uvigo.gal)

AGRADECEMENTOS

En primeiro lugar, o meu agradecemento vai para aos meus directores, Luis e Raquel, por terme dando a oportunidade de poder levar a cabo o doutoramento. O meu recoñecemento a súa entrega, paciencia e confianza dende o principio ate o final.

Agradecemento especial a Jorge pola súa dedicación e traballo en diferentes partes do mundo, a súa axuda foi moito máis alá da académica.

As miñas gracias tamén para Marta, Rogert e Milica, os cales foron imprescindibles no desenvolvemento desta tese co seu apoio continuo, e para os compañeiros de laboratorio cos que partillei o día a día, a Danica, Lucía, Orlando, Anita, Santiago e Coral. A tódalas persoas que pasaron ou forman parte do grupo EPhysLab.

Agradecer a contribución de tódolos coautores das publicacións que conforman o corpo deste traballo, a súa dedicación fixo posible a realización deste documento.

Dar as grazas ao Dr. Gonzalo Miguez-Macho (Santiago de Compostela, USC), a Dra. Francina Domínguez (Urbana-Champaign – Illinois, UIUC, USA) e o Dr. Alexandre M. Ramos (Lisboa, ULisboa) a oportunidade de poderes facer respectivas estadías nos seus grupos de investigación durante o transcurso desta etapa de doutoramento.

Na parte máis persoal, agradecer de xeito especial os meus pais e a miña irmá, polo seu apoio ó longo de todo este tempo. Tamén as miñas avoas, unha é a culpable de todo isto. E a Bea polo seu apoio constante, paciencia e compresión.

En Allariz, un 26 de xaneiro do 2020

Este traballo foi posible a través do proxecto EVOCAR (CGL2015-65141-R) cofinanciado polo Ministerio de Economía, Industria e Competitividade e polo Fondo Social Europeo (Convocatoria de contratos predoutorais para a formación de doutores 2016, BES-2016-078240).

CONTENTS

RESUMO

A continua sucesión de etapas a través da cal a auga pasa da atmosfera á terra, denantes de retornar de novo á atmosfera, coñécese como o ciclo hidrolóxico. Trátase dun ciclo pechado, no cal a taxa de evaporación das rexións oceánicas, xeralmente, excede á taxa de precipitación, e así pois os océanos son considerados coma as grandes fontes de humidade globais; acontecendo o contrario nas rexións continentais, onde xeralmente, a taxa de precipitación é maior ca taxa de evaporación, o que fai que as rexións continentais sexan consideradas coma sumidoiros de humidade. Aínda que os océanos conteñen aproximadamente o 97% das reservas mundiais de auga, e son a principal fonte de humidade para a precipitación continental, algúns estudos sinalan a forte importancia da evaporación sobre terra para a precipitación continental a través de procesos de reciclaxe da humidade. Unha vez que a auga é evaporada, reside na atmosfera un tempo medio de entre 8 a 10 días na atmosfera, e nese tempo é transportada e redistribuída fundamentalmente pola acción do campo de ventos. O transporte de humidade na atmosfera constitúe a rama atmosférica do ciclo hidrolóxico e é considerado o nexo de unión entre a evaporación oceánica e a precipitación continental. O transporte de humidade e a súa redistribución na atmosfera fai que as rexións fonte de humidade difiran das rexións sumidoiro, condicionando en grande medida a dispoñibilidade dos recursos hídricos a través dos patróns de precipitación. De modo que, a unha escala rexional, un transporte anómalo de humidade pode conducir a eventos de inundacións ou secas, comprometendo as reservas e recursos hídricos.

A alta sensibilidade do contido de vapor de auga na atmosfera coa temperatura suxire unha atmosfera máis húmida baixo futuros escenarios de quecemento global. Espéranse maiores relacións de evaporación e precipitación e polo tanto unha intensificación do ciclo hidrolóxico actual. Un maior contido de vapor de auga proxectará un maior transporte global de humidade.

Esta tese de doutoramento céntrase no estudo das dúas principais estruturas meteorolóxicas responsables da maior parte do transporte de humidade a escala global: unha é particularmente importante en rexións tropicais e subtropicais – os Chorros de Baixo Nivel (ou *Low-Level Jets, LLJ,* na súa nomenclatura en inglés) – mentres que a outra é fundamental en rexións extratropicais – os chamados Ríos Atmosféricos (*Atmospheric Rivers, AR).*

Os LLJs poden ser definidos como corredores de vento no que o seu máximo de velocidade ocorre dentro do primeiro quilómetro da troposfera. Trátanse de fenómenos moi localizados tanto no espazo coma no tempo, o que dificulta substancialmente o estudo destas estruturas meteorolóxicas. Amosan frecuentemente un marcado ciclo diario, cun máximo de intensidade á noite, e veñen sendo chamados LLJs nocturnos, ou en inglés *Nocturnal Low-Level Jets* (NLLJ) formados principalmente polo desacoplamento da capa limite planetaria (en inglés, *Planetary Boundary Layer, PBL).* Aínda cos LLJ poden estar presentes durante todo o ano, adoitan ser máis activos na estación cálida. Nos últimos anos, o interese polos LLJs está a aumentar debido ao feito de que estas estruturas, como xa se comentou, son o principal mecanismo de transporte de humidade nas rexións tropicais e subtropicais, e é precisamente nestas áreas onde se concentra a maior cantidade do vapor de auga na troposfera inferior. O estreito vínculo entre os LLJs e transporte de humidade, fai que estean asociados inequivocamente cos patróns de precipitacións rexionais, polo que calquera modificación baixo os diferentes escenarios de quecemento global agardados para o futuro poden modificar substancialmente o ciclo hidrolóxico rexional, pero tamén a nivel planetario.

O outro mecanismo de transporte de humidade no cal que se centra esta tese de doutoramento son os Ríos Atmosféricos. Estas estruturas son responsables do transporte de grandes cantidades de auga ao longo de correntes relativamente estreitas dende os trópicos ata latitudes medias. O concepto de Río Atmosférico foi amplamente empregado debido a natureza intuitiva do termo, xa que reflicte que a cantidade de humidade transportada por estas estruturas é comparable ao caudal dos grandes ríos continentais do mundo, comparable á descarga coma o Amazonas. Porén, non foi ata fai relativamente pouco tempo que a súa definición formal foi incorporada ao *Glosario de Meteoroloxía* da *Sociedade Meteorolóxica Americana (Glossary of Meteorology, GoM – American Meteorological Society, AMS).* Xeralmente, acéptase que os ARs proporcionan a maior parte do transporte de humidade a longa distancia, o cal representa cerca do 90% do fluxo de vapor de auga meridional. Polo tanto, cando un AR alcanza terra frecuentemente está asociado a eventos de precipitación extrema e a posibles inundacións posteriores. Por exemplo, os ARs intensos son identificados coma a principal causa de danos económicos na costa oeste de América do Norte. Así e todo, os ARs débiles son beneficiosos para un aumento das reservas hídricas. Polo tanto, cambios na intensidade (en termos de

humidade transportada) ou mesmo modificacións na súa frecuencia en escenarios futuros de quecemento global, poden comprometer a dispoñibilidade de recursos hídricos.

O principal obxectivo desta tese de doutoramento é investigar o vínculo entre os principais mecanismos de transporte de humidade, os citados LLJs e ARs, e o transporte global de humidade, co suposto xeral da forte advección de vapor de auga por parte de ámbalas dúas estruturas meteorolóxicas. A localización e caracterización das principais rexións onde estes sistemas toman a súa humidade para ser despois transportada é o punto central deste traballo. A análise da variabilidade destas fontes de humidade é particularmente relevante debido ao feito de que un aumento (ou unha diminución) na dispoñibilidade de vapor de auga afecta dunha forma directa a un maior (ou menor) transporte desta polos ARs e LLJs. Esta humidade transportada é a responsable da precipitación corrente abaixo destas estruturas, sobre as rexións coñecidas como sumidoiros. Son particularmente vulnerables aos cambios aquelas rexións continentais onde a entrada de humidade, e polo tanto o patrón de chuvias, depende só destas estruturas, xa que calquera modificación nestes sistemas meteorolóxicos (frecuencia, posición, intensidade) poden pois comprometer a cantidade de precipitación.

Para a análise do comportamento de humidade empregáronse as saídas globais do modelo de transporte de Lagranxiano FLEXPART (*FLEXible PARTicle dispersion model*) na súa versión 9.0 (Stohl et al., 2015). O uso deste modelo permite rastrexar, ben cara adiante ou ben cara atrás no tempo, as parcelas de aire coa finalidade de localizar aquelas rexións onde estas gañan humidade (fontes de humidade) ou onde a perden (sumidoiros de humidade). Nos últimos anos, o modelo FLEXPART está sendo amplamente empregado no estudo da rama atmosférica do ciclo hidrolóxico, converténdose nunha robusta ferramenta de análise de transporte de humidade. Así pois, este modelo e a metodoloxía asociada ao seu uso, é a escollida na maioría dos estudos que conforman esta de tese de doutoramento para estimar os cambios de humidade ao longo de traxectorias e así identificar as principais fontes e sumidoiros de humidade asociados aos LLJs e ARs. Nas simulacións realizadas, FLEXPART é alimentado con datos da reanálise ERA-Interim do Centro Europeo de Previsións Meteorolóxicas a Medio Prazo (*European Centre for Medium-Range Weather Forecasts, ECMWF)* cunha resolución horizontal de 1º en latitude e lonxitude nos 61 niveis da vertical, dende 0.1 ata 1000 hPa. A densidade de niveis verticais é maior en superficie que en niveis altos, acorde co maior contido de vapor de auga na baixa troposfera. O modelo divide

homoxeneamente a atmosfera en aproximadamente dous millóns de parcelas de aire (ou partículas), as cales son advectadas acorde ao campo tridimensional de ventos. As variacións de humidade poden ser expresadas a través da taxa de cambio neto do contido de vapor de auga de cada unha delas mediante a seguinte ecuación: $e\text{-}p=m(dt/dq)$, onde m, é a masa das parcelas de aire, a cal é constante ao longo da simulación, e onde e e p representan o aumento ou a diminución de humidade, ou o que ven sendo a evaporación e precipitación, respectivamente. Unha das principais vantaxes do emprego do modelo FLEXPART é que este permite o seguimento individual das parcelas de aire cara atrás ou cara adiante no tempo, de maneira que é capaz de reconstruír dun xeito preciso as súas traxectorias. Para obter un balance total de humidade é preciso integrar na vertical os cambios de e-p de tódalas parcelas de aire que residen na columna atmosférica que se quere estudar. Desta forma, obtemos o balance de $(E - P)$, onde E é a evaporación e P a precipitación por unidade de área. Así, a análise cara atrás no tempo permite a identificación de rexións onde a ganancia de humidade dunha masa de aire é superior á perdida $((E – P) > 0)$. Estas rexións son consideradas como fontes de humidade, que no caso deste tese serán as fontes de humidade asociadas aos principais mecanismos de transporte de humidade, ARs e LLJs. Por outra banda, na análise das traxectorias cara adiante no tempo, as rexións onde prevalece a precipitación fronte á evaporación $((E – P) < 0)$ son consideradas como sumidoiros de humidade, é dicir, onde a humidade contribúe á precipitación.

O tempo de integración das parcelas de aire limitouse a 10 días, considerado o tempo de residencia medio do vapor de auga na atmosfera, e no cal as traxectorias poden ser consideradas relativamente precisas. Os resultados derivados de enfoques lagranxianos son realmente sensibles ao tempo de integración empregado nas análises, de xeito que o emprego dun tempo de integración baixo limita a identificación de fontes de humidade mais remotas. No transcurso desta tese de doutoramento foi publicado un estudo no que se establecen os tempos de integración óptimos para estudos lagranxianos de fontes de humidade, polo que un dos traballos, que é posterior a esta publicación, emprega estes novos tempos óptimos de integración.

Coa finalidade de investigar aquelas rexións que proporcionan vapor de auga aos LLJs e ARs, é necesario identificar previamente que áreas están baixo a influenza de ámbolos dous mecanismos de transporte de humidade. Así pois, para a identificación de eventos de LLJ empregouse o índice de actividade nocturna de LLJ proposto por Rife et

al. (2010). Este índice é aplicado a escala global, baseándose na variación vertical da estrutura temporal do vento e no feito de que os LLJ son mais intensos durante a medianoite en hora local. O índice de actividade nocturna de LLJ incorpora dúas condicións que deben ser cumpridas simultaneamente para definir un evento coma LLJ: (i) a velocidade do vento debe ser maior na medianoite que ao mediodía local; (ii) a velocidade do vento en superficie a medianoite local debe maior que en altura. Para identificar os LLJs empregáronse datos da reanálise ERA-Interim (ECMWF) en dous niveis sigma na vertical (para garantir a altura da medida con respecto á elevación do terreo): o nivel 53 para os datos en superficie (que aproximadamente acércanse a 500 m sobre o nivel do mar) e o nivel 42 para os de altura (aproximadamente situado a uns 4000 m).

Na identificación dos ARs empregouse como partida a base de datos desenrolada por Guan e Waliser (2015) que se basea nun limiar de intensidade do fluxo vertical integrado de vapor de auga (en inglés, *integrated water vapour*, *IVT*) ao que se lle engaden limitacións xeométricas acorde á coherencia das estruturas dos ARs. A resolución orixinal dos datos é de 1.5º en latitude e lonxitude sobre o que se realizou un acumulado espacial a 12º (baixando a resolución) para identificar ao longo de todas as costas continentais aquelas rexións que posúen unha frecuencia maior ao 10% dos días totais de ARs a nivel global. Todas aquelas rexións que superan este limiar son identificadas nun primeiro momento como rexións de alta actividade de ARs. De seguido, analízase cada rexión en termos de anomalías de presión media do nivel do mar *(Mean Sea Level Pressure, MSLP)*, coa finalidade de que estas rexións previamente identificadas estean todas asociadas á presenza de sistemas baroclinos.

O corpus desta tese de doutoramento consiste nun total de cinco artigos publicados en revistas especializadas incluídas na listaxe do *Journal Citation Reports (JCR)* e outro enviado a publicar. O conxunto de datos utilizados nos cálculos nas diferentes investigacións vai sendo actualizado progresivamente, polo que o período de análise de cada artigo publicado varía segundo o comezo de cada estudo e a dispoñibilidade do conxunto de datos. Cabe sinalar tamén, que a orde dos artigos presentados na tese de doutoramento non se corresponde coa orde de publicación dos mesmos, polo que poden aparecer algunhas inconsistencias nos períodos analizados durante a lectura deste manuscrito.

O primeiro dos seis artigos que conforman o corpus da tese de doutoramento é un artigo de revisión no que se realiza unha exhaustiva actualización sobre o coñecemento actual da relación fontes-sumidoiros de humidade. Neste artigo, destácase o papel dos principais mecanismos de transporte de humidade, LLJs e ARs, revisándose os adiantos recentes do papel dos mesmos a escala global e preséntanse algúns dos desafíos fundamentais para futuras investigacións.

De seguido a este artigo de revisión, a estrutura da tese divídense entre o estudo de LLJs e ARs. Nun primeiro lugar, ámbalas dúas estruturas son abordadas (de xeito individual en artigos separados) dende un enfoque global, para despois presentar estudos particulares ou nalgunha rexión específica.

Comézase pola análise dos LLJs realizando unha identificación global de eventos de LLJs e estudando o transporte de humidade asociado a estas estruturas en termos de días de LLJ e días de non LLJ. Primeiramente, identifícanse globalmente as principais rexións de ocorrencia de LLJ mediante o índice de actividade nocturna, o cal foi aplicado os meses de xaneiro (verán austral) e xullo (verán boreal) acorde ao comportamento estacional destes sistemas meteorolóxicos. Identificáronse un total de 33 rexións de alta actividade de LLJ, 20 rexións no hemisferio norte e 13 no hemisferio sur. A distribución xeográfica das áreas de máxima ocorrencia de LLJs ocorre maioritariamente en rexións tropicais, confirmando polo tanto que o transporte de humidade debido a estes sistema é de grande importancia no ciclo hidrolóxico. A análise da relación fonte-sumidoiro de humidade, amosa unha importante modulación do transporte de humidade por parte dos LLJs. A influencia de eventos de LLJs amosa un sumidoiro de humidade mais remoto cando sucede un día de LLJ, acorde coa gran advección de vapor de auga vinculado a estas estruturas.

Para o caso de estudo, o foco é posto no *Great Plains low-level jet (GPLLJ),* un LLJ que modula a entrada de humidade, e polo tanto, do patrón de precipitacións no súeste dos Estados Unidos. Se ben, o GPLLJ é excepcionalmente un LLJ ben documentado, neste traballo cuantifícase o seu transporte de humidade a través dunha novidosa técnica euleriana de etiquetado de humidade baseada na replicación das ecuacións de prognóstico relativas a humidade total. Para isto, é necesario definir previamente a fonte de humidade, a cal é identificada mediante un enfoque lagranxiano empregando o modelo FLEXPART, metodoloxía apropiada anteriormente descrita. Os resultados amosan que o GPLLJ é responsábel de máis do 80% de humidade do transporte de humidade no sur dos Estados

Unidos. E que a medida que aumenta a latitude (é dicir, cara máis ao norte), a proporción de humidade transportada polo GPLLJ vai diminuíndo, pero aínda así esta estrutura é capaz de explicar case a metade da humidade que se atopa ao sur dos Grandes Lagos en América do Norte.

A segunda rama desta tese de doutoramento céntrase no estudo do transporte de humidade dos ARs, recordemos nesta altura que son principais mecanismos de transporte de humidade en rexións extratropicais. Realízase unha identificación global das principais rexións de alta actividade de ARs para despois pasar a analizar as areas que proporcionan humidade a estes sistemas para ser transportada cara os continentes. Como xa se comentou previamente mediante o emprego da base de datos de ARs desenvolvida por Guan e Waliser (2015), identifícanse un total de 20 rexións de alta actividade de ARs. As cales correspóndense fundamentalmente con rexións localizadas na costa occidental en latitudes medias. O estudo de análise de humidade anómala amosa que a principal rexión na que os ARs toman humidade é a rexión da piscina cálida do hemisferio occidental (*Western Hemisphere Warm Pool*, *WHWP*). Desta fonte toman anomalamente humidade practicamente tódolos ARs que ocorren no Atlántico Norte, rexión cunha alta densidade de rexións de ocorrencia de ARs, ao norte e en ámbalas caras da conca oceánica. O estudo da variabilidade interannual revela un aumento significativo nas rexións de absorción anómala de humidade dos AR cun escalado próximo a Clausius-Clapeyron (CC).

Para o estudo particular dos ARs centrámonos no Ártico, rexión especialmente vulnerable ao quecemento global. Emprégase de novo a base de datos de ARs desenrolada por Guan e Waliser (2015) para identificar estacionalmente as rexións de máxima pegada polos ARs que alcanzan a latitude de 60ºN (límite ao sur para a definición da rexión ártica). Deste xeito o traballo conclúe que son os sectores do Atlántico Norte e Pacífico Norte os que constitúen fundamentalmente as portas de entrada para os ARs que alcanzan o dominio Ártico. De seguido, e facendo uso do modelo lagranxiano FLEXPART analízase a contribución anómala de humidade dos ARs que foron previamente identificados. Nesta análise evidénciase que as principais fontes anómalas de humidade para estes eventos de ARs esténdense maiormente sobre estas mesmas rexións oceánicas, máis en particular sobre a súa parte occidental na banda latitudinal entre 30º e 40ºN. Asociadas á estación cálida aparecen tamén importantes fontes de humidade anómala en rexión continentais en América do Norte e sobre Eurasia. Tampouco é depreciable a contribución de humidade local sobre a rexión de máxima actividade dos ARs. Ademais,

os resultados confirman unha importante intensificación na absorción de humidade sobre as fontes climatolóxicas..

Como xa se explicou, os LLJs e ARs gobernan o transporte de humidade a diferentes latitudes. Os LLJs principalmente en latitudes tropicais, mentres que os ARs en latitudes medias e altas. Así e todo, un pódese preguntar se ámbalas dúas estruturas poderían estar conectadas en termos de transporte de humidade. Para iso, no derradeiro artigo científico que forma parte desta tese de doutoramento, examínase o vínculo entre a dinámica atmosférica en América do Sur e as precipitacións invernais en Sudáfrica. Atopouse que unha particular fase do *South American Low-Level Jet (SALLJ)* coñecida como *No Chaco Jet Event (NCJE)* transporta humidade dende a rexión continental de América do Sur (particularmente, dende unha rexión que inclúe a conca do río Paraná e a conca sur do río Amazonas) cara a conca oceánica do Atlántico Sur occidental e central. Esta humidade é posteriormente recollida e transportada polos ARs que alcanzan a costa oeste de Sudáfrica. O traballo confirma o sumidoiro anómalo de humidade sobre o Atlántico Sur occidental para os días de NCJE e así poder xustificar as anomalías de IVT para os días de ARs que chegan a Sudáfrica durante o inverno. Polo tanto, as dúas marxes do Atlántico Sur amosan estar conectadas pola combinación de dúas das estruturas máis importantes de transporte de humidade.

A estrutura desta tese de doutoramento presentada na modalidade de compendio de artigos de investigación, componse de cinco capítulos principais, dispostos na orde que a continuación se describe. No capítulo primeiro preséntase unha breve introdución ao ciclo hidrolóxico e aos principais mecanismos de transporte de humidade global, LLJs e ARs. No capítulo segundo amósanse os seus principais obxectivos. No capítulo terceiro descríbense os métodos e as técnicas empregadas. O cuarto capítulo inclúe un compendio dos cinco artigos publicados en revistas científicas ao longo do transcurso do presente traballo de doutoramento, e mais un sexto artigo enviado a publicar no momento de redacción final deste manuscrito. Finalmente, no capítulo quinto expóñense as principais conclusións obtidas. Pecha esta tese de doutoramento o material suplementario e a listaxe de referencias empregadas na redacción do presente documento.

ABSTRACT

The research presented in this dissertation investigates the role of the two meteorological structures responsible for most moisture transport on a global scale. One is particularly important in tropical and subtropical regions, i.e., Low-Level Jets (LLJs), whereas the other is important in extratropical regions, i.e., Atmospheric Rivers (ARs). Both structures shape the atmospheric branch of the hydrological cycle, transporting most of the available moisture in the atmosphere to latitudes further than its origin, and they describe the link between evaporation from the ocean/continent and precipitation over the continents.

This thesis is structured into five chapters: Chapter 1 presents a brief introduction to the hydrological cycle and describes the main mechanisms of moisture transport on a global scale, whereas Chapter 2 lists the main objectives of the thesis. Chapter 3 describes the methods and datasets used. Chapter 4 includes a compendium of five manuscripts published in scientific journals. Finally, the main conclusions and possible avenues of future research are presented in Chapter 5.

The corpus of this thesis is the five research articles published in scientific journals included in the *Science Citation Index* (SCI), included in *Chapter fourth: Set of Publications*.

The first article is a review article, which provides an update on recent advances in the source-sink moisture relationship in the distribution of rainfall. The role of the main moisture transport mechanisms, AR and LLJ, as triggers of hydrological extremes such as droughts and floods are highlighted. Finally, some of the fundamental challenges for future research are presented.

The next four articles correspond to two studies examining LLJs and two more for ARs, with the same structure. The first article in each case focused on the global scale, and the second examined a particular structure or a specific region.

In the global analysis of LLJs, 33 regions of occurrence were identified, with 20 and 13 regions in the northern and southern hemispheres, respectively. The global distribution of the high activity regions of LLJs is consistent with the potential moisture transport of these systems in tropical and subtropical regions. The analysis of the moisture source-sink relationship shows an essential modulation of the moisture transport of LLJs.

The amount of moisture transported is highly asymmetric, with structures such as the Great Plains low-level jet (GPLLJ) or the South American low-level jet (SALLJ) or LLJs linked to monsoon regimens, transport a large amount of moisture. Nevertheless, LLJs that develop over Africa are more linked to the transport of dust. The comparison of jet and non-jet days showed significant differences in the sink of moisture, being more remote when an LLJ event occurs according to the intense moisture advection. For the particular case of LLJ, the focus was on the GPLLJ, which modulates the entry of moisture, and hence, the precipitation pattern in the south-eastern centre of the United States. Although it is one of the most studied LLJs, in this research was quantified the moisture transport. To address this question, a combination of Lagrangian and Eulerian techniques was used to identify and quantify the moisture transport associated with the GPLLJ objectively. The results show that the GPLLJ is responsible for more than 80% of the moisture transported to the southern United States. As the latitude increases, the proportion of moisture transported at the GPLLJ pole decreases, but the GPLLJ can explain more than half of the moisture that reaches the south of the Great Lakes.

In the global analysis of ARs, 20 regions of high AR activity were identified, which corresponds to regions mainly located on the western coast of mid-latitudes. The anomalous moisture analysis shows that the primary region through which the ARs uptake moisture is the Western Hemisphere Warm Pool (WHWP). The study of global variability shows a significant increase, with an escalation close to Clausius-Clapeyron (CC), suggesting higher moisture transport by ARs under future global warming scenarios. For this particular study, the focus was on the ARs that reach the Arctic system, a region especially vulnerable to global warming. An increase in moisture transport to this region is associated with a decrease in the extent of sea ice. The ARs represents one of the main mechanisms involved in the transport of moisture; hence, latent heat from the tropics to higher latitudes. All ARs that exceed 60 ºN were seasonally identified to analyse their exceptional contribution of moisture. The North Atlantic and North Pacific sectors constitute the main entryways for the ARs that reach the Arctic; they are also the primary sources of moisture for ARs events. Intensification in the uptake of moisture is observed on the sources of moisture climatology during AR events.

The sixth article focuses on examining the links between ARs and LLJs in terms of moisture transport from South America, which results in winter rainfall over South Africa. The results show that the particular phase of the SALLJ known as the No Chaco

Jet Event (NCJE) transports moisture from the continental region of South America (particularly, from a region that includes the Paraná river basin and the southern basin of the Amazon River) towards the western and central South Atlantic Ocean basin. This moisture is then transported by ARs to the west coast of South Africa. Anomalous moisture sink for the NCJE days and IVT anomalies for ARs days have been detected, confirming the existence of this link. Thus, the two margins of the South Atlantic Ocean appear connected by a combination of two of the essential meteorological structures for the moisture transport, i.e., the LLJ and the ARs.

This thesis has substantial scientific and socio-economic implications. LLJs and ARs can modulate extreme precipitation events, i.e., an intensification (or reduction) of moisture transport modifies precipitation anomalies, hence inducing flooding (or drought). The possible changes in the position and frequency of LLJs and ARs with their climatological behaviour can alter the rainfall patterns substantially. In the context of a changing climate, the high sensitivity of water vapour content to temperature leads to higher evaporation and precipitation rates in a warmer scenario, and hence, an intensification of the hydrological cycle, with implications in the large moisture transport via ARs and LLJs. Therefore, this analysis of the main moisture transport mechanisms helps to understand future changes in precipitation patterns.

LIST OF FIGURES

LIST OF TABLES

LIST OF ACRONYMS

The following abbreviations are used in this manuscript:

ANYAS	Annals of the New York Academy of Sciences
AMS	American Meteorological Society
AMU	Anomalous Moisture Uptake
AR	Atmospheric River
CC	Clausius-Clapeyron relationship
COSMO	Consortium for Small-scale Modeling
ECMWF	European Centre for Medium-Range Weather Forecast
EPhysLab	Environmental Physics Laboratory
ESD	Earth System Dynamics
ESR	Earth-Science Reviews
FLEXPART	FLEXible PARTicle dispersion model
FLEXTRA	FLEXible TRAjectory
GFS	Global Forecast System
GoM	Glossary of Meteorology
GPCP	Global Precipitation Climatology Project
GPLLJ	Great Plains low-level jet
GPWv4	Gridded Population of the World Version 4.0
ISSN	International Standard Serial Number
ITCZ	Intertropical Convergence Zone
IVT	Integrated Water Vapour Transport
IWV	Integrated Water Vapour
JCR	Journal Citation Reports
LLJ	Low-level jet
LPDM	Lagrangian Particle Dispersion Model
MM5	Fifth-Generation Penn State/NCAR Mesoscale Model
MSLP	Mean Sea Level Pressure
MSWEP	Monthly Multi-Source Weighted-Ensemble Precipitation
NAO	North Atlantic Oscillation
NCEP	National Centre for Environmental Prediction

NCJE	No Chaco Jet Event
NLLJ	Nocturnal Low-Level Jet
PBL	Planetary Boundary Layer
SALLJ	South American low-level jet
SCI	Science Citation Index
SEDAC	Socioeconomic Data and Applications Center
SST	Sea Surface Level
UTC	Universal Time Coordinated
WHWP	Warm Hemisphere Western Pool
WRF	Weather Research and Forecasting
WRF-TT	WRF-Tracers Tool
WVT	Numerical Water Vapour Tracers

1
Introduction

1.1 The importance of the hydrological cycle

Water is a fundamental component of the climate system and is an essential resource for life. Although the water vapour represents only 0.25% of the total mass in the atmosphere (Seidel, 2002), it is crucial in the regulation of global climate and weather patterns (Held and Soden, 2000). Furthermore, the relative large heat capacity of the water is related to the storage of large amounts of energy. The continuous succession of stages through which water passes from the atmosphere to the Earth before returning to the atmosphere is known as the hydrological cycle (Fig. 1) (Peixoto and Oort, 1992; OMM, 2012). In oceanic regions, evaporation exceeds precipitation and therefore the oceans are considered as a net source of moisture allowing moisture to be transported by atmospheric winds to the continents. Over landmasses, the pattern is reversed. Precipitation exceeds evapotranspiration; hence, the continental regions act as sinks of moisture favouring the runoff that flows to the rivers and eventually to the ocean, thus completing the hydrological cycle (Trenberth et al., 2011). Only 1 out of 10 litres of water vapour that evaporates from the oceans is transported to continents where it precipitates; the rest precipitates again over the oceans (Oki et al., 2005). Although this amount of water vapour may seem relatively small, it is essential and constitutes the atmospheric branch of the hydrological cycle, which encompasses all the processes that go from oceanic evaporation to continental precipitation.

In essence, the hydrological cycle can be summarized as evaporation in one place and precipitation in another one, which is balanced by the atmospheric, oceanic, and

hydrological transport of water. Understanding the processes that govern the evaporation of water from the oceans and the atmospheric transport of moisture is one of the main challenges facing atmospheric sciences (Gimeno, 2013). It is essential to understand the hydrological cycle's intensity and evolution over time from the perspective of global warming and variability. Researchers usually attempt to investigate the atmospheric branch of the hydrological cycle to establish the source-sink relationship of atmospheric moisture, and the diagnosis of their sources and their transport could provide a better understanding of the impact of global warming on the hydrological cycle (Gimeno et al., 2012).

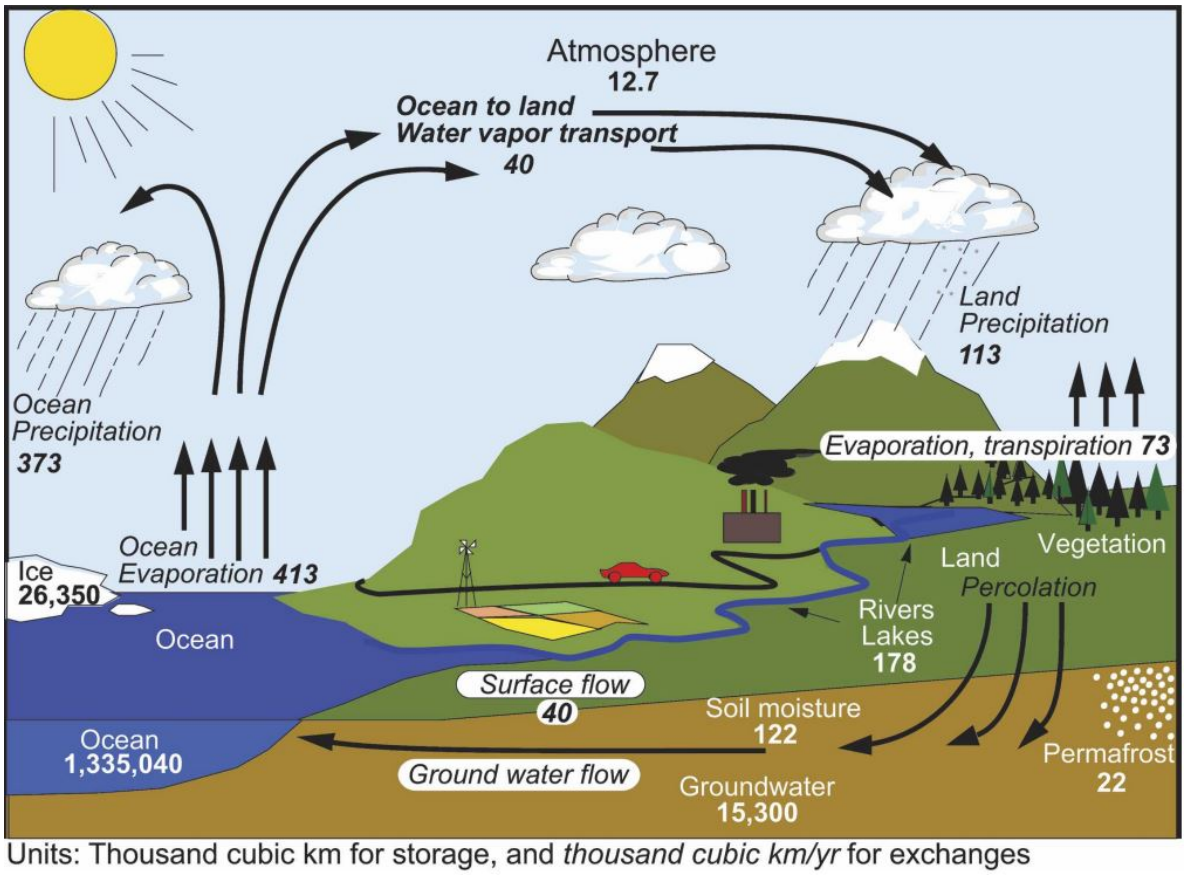

Figure 1. **The hydrological cycle**. Estimates of the main water reservoirs observed and flow of moisture (1000 km^3 for storage and 1000 km^3 yr^{-1} for exchanges) adjusted from Trenberth et al. (2007).

1.2 From evaporation to precipitation: the transport of moisture

The oceans contain approximately 97% of the world's water reserves (Baumgartner and Reichel, 1975), and it can be considered as the primary source of moisture for continental precipitation (Gimeno et al., 2010). Evaporation can be defined as the conversion of water into steam. In global terms, 86% of the moisture that evaporates annually comes from the oceans, while the rest has its origin in the continents (Trenberth, 2007). Nevertheless, some authors (e.g., van der Ent and Savenije, 2011; van der Ent et al., 2010) show the importance of recycling, in which approximately 40% of the precipitation on land comes from continental evaporation instead of oceanic evaporation.

The air-water interface over oceanic areas can be estimated through Fairral parameterisation (*1*):

$$E = c_e U dq = c_e U\big(q_s(SST) - q_a(T_{air}, RH)\big) \qquad (1)$$

where c_e is a turbulent exchange coefficient; U is the wind speed closer to oceanic surface; q_s is the saturation specific humidity at the sea surface; q_a is the near-surface atmospheric specific humidity (i.e., a function of air temperature T_{air} and relative humidity RH); and $d_q = q_s - q_a$ as described by Fairall et al. (2003). Therefore, evaporation is a function of the radiative energy balance and presents a pattern similar to that of shortwave solar radiation and the distribution of sea surface temperature (SST). Generally, evaporation is higher when there is high wind speed over the ocean surface (U), low moisture in the air (RH), and when the sea surface temperature (SST) is high (Gimeno et al., 2012).

Following the evaporation patterns, the maximum evaporative regions, which are also the high moisture source areas, are located in the subtropical zones and the western border current zones (mainly the Gulf current and the Kuroshio current) (Gimeno et al., 2012; Castillo et al., 2014). In these regions, evaporation is supported by relatively dry intense winds that are transported on a warm ocean surface. It is generally accepted that water vapour has an average residence time in the atmosphere of nearly ten days (Numaguti, 1999; van der Ent et al., 2017) and is mainly transported by the wind field from oceanic areas to landmass regions. Thus, water vapour is redistributed by the atmospheric moisture transport processes, where instability mechanisms that favour the condensation and precipitation of the atmospheric water vapour may arise. Globally, moisture source regions exhibit asymmetrical and specific roles to the precipitation over land (Gimeno et al., 2012; Castillo et al., 2014). Thus, precipitation regions, which can

be considered as large sinks of moisture, are located on the intertropical convergence zones (ITCZ) and secondary highs at medium latitudes mainly in the winters associated with the storm-track (Gimeno et al., 2012; Nieto et al., 2019).

Within the water cycle, evaporation and recycling provide the moisture that precipitates over the globe and is redistributed by transport processes. Because the wind field advects moisture, the circulation of winds is strongly related to the seasonality of rainfall. Nevertheless, special attention must be paid to the transport of large-scale moisture, such as the transport of moisture between the tropics and the extratropics.

1.3 The intensification of the hydrological cycle: the influence of global warming

The availability of water vapour in the atmosphere is part of the closed cycle in which the distribution of moisture in the atmosphere depends on temperature, evaporation, and precipitation. The saturation vapour pressure in the atmosphere can be approximated as an exponential function of the temperature (Clausius-Clapeyron relationship, *CC*). Thus, the distribution of water vapour in the atmosphere generally decreases with the height (approximately half of water vapour is below 1500 metres) and with latitude (there is an excess of steam of water in the tropics compared to higher latitudes) (Held and Soden, 2006; Pierrehumbert et al., 2008). According to Trenberth et al. (2011), general patterns and temporal variations of water vapour over the oceans are related to sea surface temperature (SST), since, according to the Clausius-Clapeyron equation, the saturation water vapour pressure is a nonlinear function of temperature. Thus, a change in the Clausius-Clapeyron equation of only 1 °C causes a change of approximately 7% in the water vapour content (Held and Soden, 2006; Wentz et al., 2007; O'Gorman and Muller, 2010).

Given the strong dependence of saturated vapour pressure on temperature, a global warming scenario as expected (IPCC, 2014) suggests an increase in water vapour content in current source-receptor atmospheric moisture ratios could be altered. According to the Clausius-Clapeyron relationship, the ability of the atmosphere to retain water increases with the increasing temperature in the atmosphere (Held and Soden, 2006). Consequently, a wetter atmosphere will lead to an increase in evaporation, and therefore, precipitation, which will lead to an intensification of the water cycle (Fig. 2) (Gimeno et al., 2012). Large moisture source regions are expected to increase their capacity to send water vapour

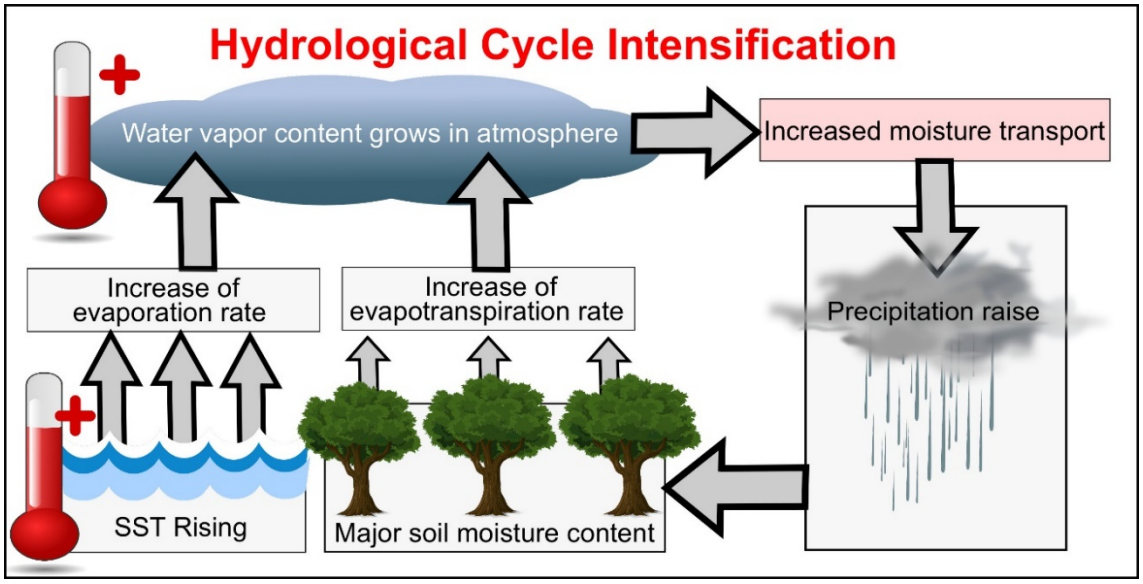

Figure 2. Summary scheme of the intensification of the hydrological cycle. The larger capacity of water vapour retention in the atmosphere associated with a global warming scenario suggests a huge water vapour content in the atmosphere, and hence, an intensification of moisture transport.

to other regions according to the relentless upward trend in temperature observed in recent decades. Consequently, a warmer scenario can result in a generalised mechanism of "*the dry becomes drier and the damp gets wet*" as the response of thermodynamic pattern in which the rainfall increases as the gross stratification of moisture increases (Held and Soden, 2006; Chen et al., 2019).

1.4 Major mechanisms of transport of moisture at global scale: Atmospheric Rivers and Low-Level Jets

The transport of moisture, i.e., from the oceans to the continents, is the main component of the atmospheric branch of the water cycle, which forms a bridge between the evaporation in the ocean and the precipitation over the continents (Peixoto and Oor, 1992). On a global scale, the main mechanisms of atmospheric moisture transport are the Low-Level Jets (LLJs) and Atmospheric Rivers (ARs) (Gimeno et al., 2016). Both structures transport the significant part of the available moisture in the atmosphere to latitudes further than its origin, modulating the global and regional precipitation pattern over the continents, thus playing an essential role in the availability of water resources (Dettinger et al., 2011; Gimeno et al., 2012). Globally, robust thermodynamic changes have been found to be related to a warming climate in precipitation extremes but more uncertain dynamic changes at regional scales (O'Gorman and Schneider, 2009).

On the one hand, the thermodynamic response leads to an intensification of the transport of moisture as a consequence of larger water vapour holding capacity in a global warming scenario (Held and Soden, 2006). Besides, changes in atmospheric circulation patterns can alter the variation in the occurrence and frequency regions of ARs and LLJs, affecting the moisture flux and the hydrological balance, hence compromising the availability of the water resources. Nevertheless, there is still a high degree of uncertainty associated with these changes under a warmer future world.

1.4.1 Atmospheric Rivers (ARs)

Although the term of Atmospheric River (AR) appeared for the first time in the modern scientific literature in the early 1990s, it was used during the 20 years due to the intuitive nature of the term. It was not until recently when a formal definition of the Glossary of Meteorology of the American Meteorological Society (2019), was finally admitted. The definition states that an AR is: *"a long, narrow, and transient corridor of strong horizontal water vapour transport that is typically associated with a low-level jet stream ahead of the cold front of an extratropical cyclone. The water vapour in ARs is supplied by tropical and/or extratropical moisture sources. ARs frequently lead to heavy precipitation where they are forced upward - for example, by mountains or by ascent in the warm conveyor belt. Horizontal water vapour transport in the mid-latitudes occurs primarily in ARs and is focused in the lower troposphere. ARs are the largest "rivers" of fresh water on Earth, transporting on average more than double the flow of the Amazon River"* (http://glossary.ametsoc.org/wiki/Atmospheric_river last view 31 January 2020). The horizontal and vertical characteristics of ARs are schematically represented in Fig. 3.

It is generally accepted that ARs transport more than 90% of the total midlatitudes vertically integrated water vapour (IWV) flux. If we take a screenshot of the IWV, at all times, i.e., 3 to 5 temporally ephemeral filamentary features are present in each hemisphere providing transport of large quantities of water vapour in midlatitudes (Newell et al., 1992; Zhu and Newell, 1998). Therefore, AR landfalling is closely linked with extreme precipitation events and flash floods, primarily due to orographic lift over mountainous topography (e.g., Ralph et al., 2006; Dettinger, 2011; Dominguez et al.,

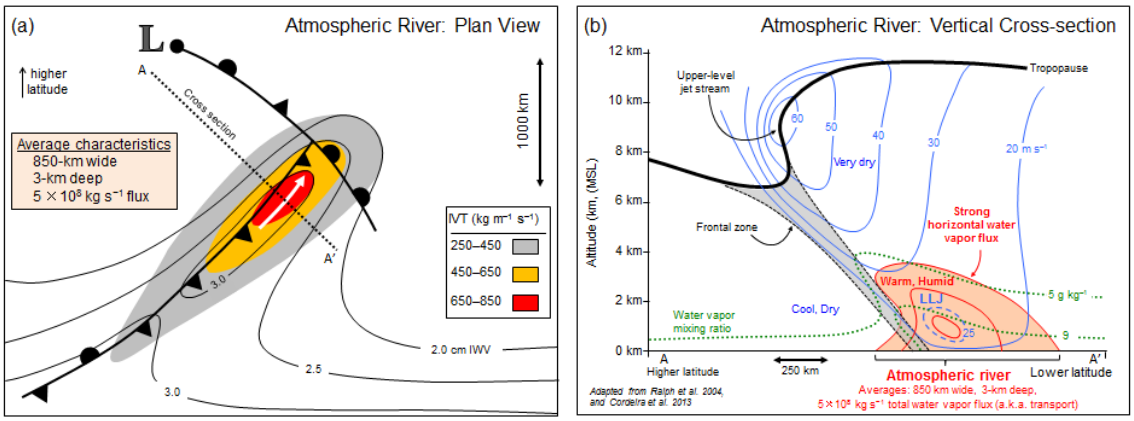

Figure 3. Schematic summary of the structure and the strength of an average midlatitude ARs from AMS Glossary (2019). Both figures are based on dropsonde measurements and reanalyses. Complete information in http://glossary.ametsoc.org/wiki/Atmospheric_river.

2018). A summary of the geographical position of the ARs is displayed in Fig. 4 (Gimeno et al., 2016). To better understand the relationship between AR and flood damage, Ralph et al. (2019) recently developed an intensity scale that describes the strength of the ARs. Two parameters dominate the hydrologic outcomes and impacts of ARs, i.e., the vertically integrated water vapour transport, and the AR duration. The strength and hence, the riskiness of AR damage is increased as the amount of transported water vapour increases and will last for the duration of the event. The scale recognises that weak ARs are often most beneficial because they can enhance water supply and snowpack. Nevertheless, stronger AR causes billions of dollars in flood damage (Corringham et al., 2019).

In a warmer climate, ARs will become more intense (Espinoza et al., 2018) as well as the amount of water vapour transported from remote locations (Nusbaumer and Noone, 2018). As the ARs increase in intensity, the delivered precipitation that landfall will be reinforced, which will result in more frequent and stronger extreme precipitation events even as the overall frequency of precipitation decreases at an increase in future precipitation volatility (Gershunov et al., 2019). This will lead to a significant increase in the damages caused by these systems (Cordeira et al., 2019; Corringham et al. 2019). As an example, in the west coast of the United States, where the extreme precipitation events are almost entirely linked to ARs, future projections show a global increase in the frequency and strength of ARs (Espinoza et al., 2018; Massoud et al., 2019), modulating the future availability of freshwater; and there is evidence that the warming observed in the Pacific Ocean is related to an increase in the intensity of these systems (Gershunov et

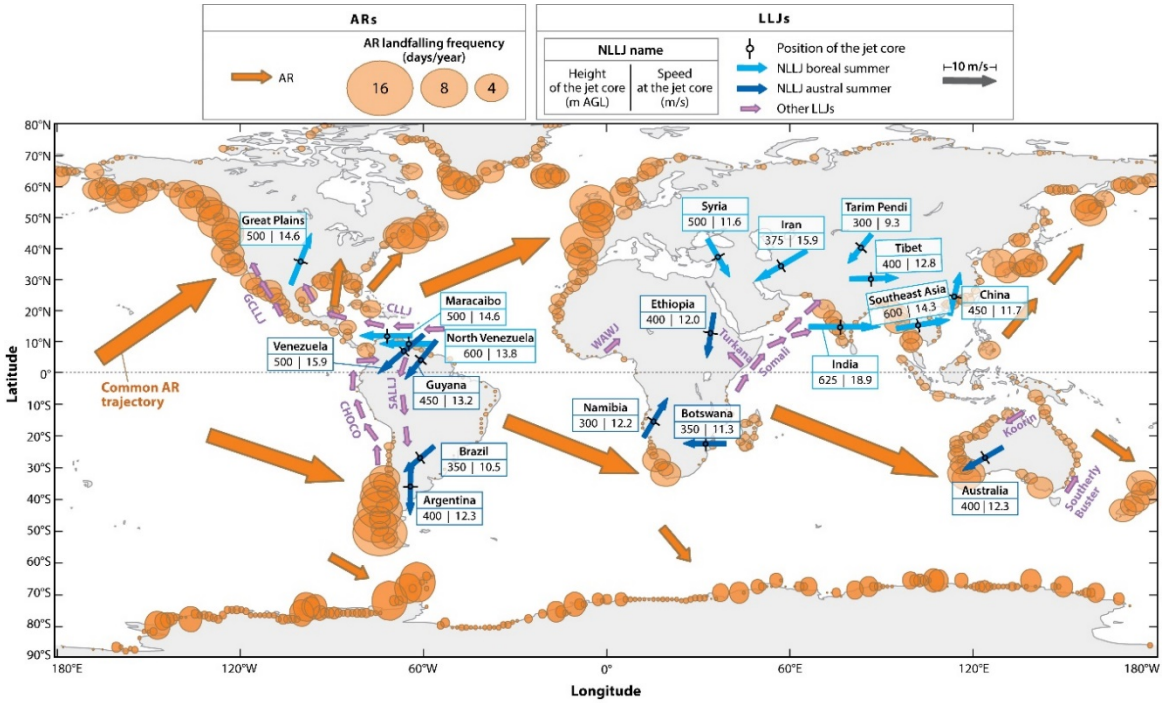

Figure 4. Global distribution of ARs and LLJs. LLJs are mainly confined in tropical latitudes (blue and purple arrows) while regions of high AR activity are located in extratropical latitudes (orange arrows and large orange circles). Figure from Gimeno et al. (2016).

al., 2019). In Europe, Sousa et al. (2019) indicate migration of the ARs to higher latitudes in the northern Atlantic region, which will lead to a significant decrease in rainfall over the Iberian Peninsula due to the combined effect of subtropical expansion and the higher water retention capacity in a warmer atmosphere.

1.4.2 Low-Level Jets (LLJs)

A Low-Level Jet (LLJ) can be simply defined as filamentous regions or corridors of anomalously high wind speeds that are located within the first kilometre of the troposphere (Nicholson, 2016). Some authors establish wind intensity fixed thresholds when defining and categorising an LLJ event; however, this may add some subjectivity in their definition (Blackadar, 1957; Bonner, 1968; Whiteman et al., 1997). They are primarily a warm-season phenomenon; coastal LLJs are generally in geostrophic equilibrium, and they are associated with topography and daily land-sea contrast cycles, while topographic, inertial effects, or both, induce inland LLJ. Often, LLJs exhibit a daily cycle with maximum intensity at night and labelled as nocturnal low-level jets (NLLJs), triggered mainly by the decoupling of the Planetary Boundary Layer (PBL).

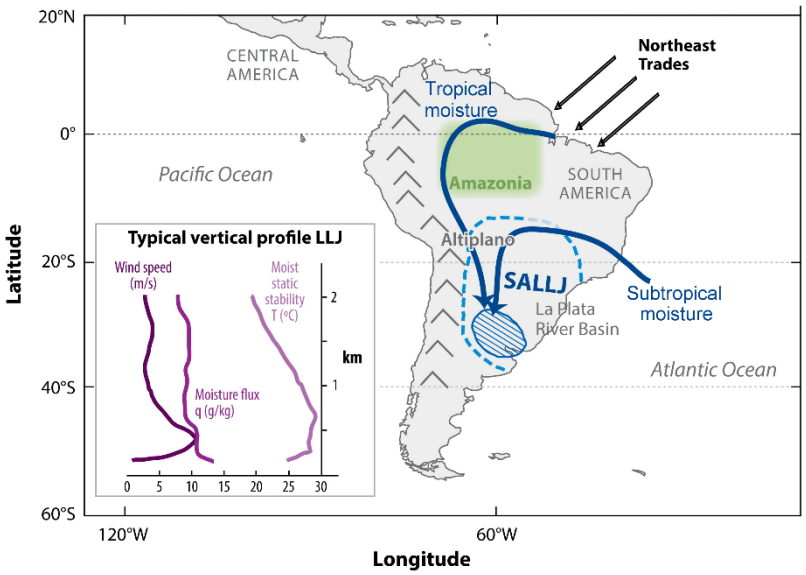

Figure 5. Schematic plan view and vertical profile of the South American low-level jet (SALLJ). The trade winds (black arrows) penetrate the north of South America, forming an LLJ-shaped structure. The SALLJ transports moisture into South America from the tropical and subtropical South Atlantic Ocean basin reaching La Plata basin (dashed blue lines - diagonal stripes indicate intense precipitation). A typical vertical profile of LLJ is shown in the box inside. Figure from Gimeno et al. (2016), adjusted from Vera et al. (2006) and Martins et al. (2013).

The greatest challenge in studying LLJs is the lack of data at high temporal and spatial resolutions and the fact that LLJs are very localised phenomena (in space and time). The LLJs have been described in several regions around the world (Stensrud, 1996; Rife et al., 2010), and they are particularly important in tropical and subtropical regions (see Fig. 4). Only a few LLJ studies have approached the topic from a global perspective. For example, Rife et al. (2010) used a reanalysis hourly dataset and a novel algorithm based on the vertical variation of the wind's temporary structure to identify 21 regions of LLJ occurrence worldwide. In a companion paper, Monaghan et al. (2010) investigated the linkages between nocturnal precipitation extremes and NLLJs detected previously through a statistical approach. They reported a strong relationship between the occurrence of NLLJs and nocturnal rainfall extremes in at least ten regions around the world, thus playing an essential role in the contribution to extreme rainfall in the oceans and coastal regions near the NLLJs.

The climatological interest in LLJs is increasing because they are understood as the main meteorological structure of moisture transport in tropical and subtropical regions. However, there are currently no studies that explicitly link the moisture transport at lower latitudes by the LLJs (i.e., related to the precipitation variability), with their

changes in position and intensity. The bulk of the moisture contained in the atmosphere is concentrated in the lower troposphere where the maximum wind intensity associated LLJ is also located. Therefore, this renders LLJs as high potential moisture transport structures. The close link between LLJ and the transport of moisture suggests that these systems are strongly associated with precipitation patterns. Therefore, changes under different scenarios of global warming may substantially modify the global and regional hydrological cycle.

The LLJs modulate the annual cycle of moisture transport and precipitation and provide a link to the tropic-extratropical interactions, i.e., for instance, the case of the Great Plains low-level jet (GPLLJ) and the South American low-level jet (SALLJ). The former is one of the most studied LLJs, which modulates the entry of moisture in the eastern centre of the United States mainly during the warm season (Bonner, 1968). The GPLLJ is considered as the northern branch of the Caribbean low-level jet, which develops over the Caribbean Sea due to the influence of trade winds. Given the amount of moisture that is transported from the Gulf of Mexico and the Caribbean Sea, the GPLLJ has been identified as responsible for extreme precipitation events often triggering massive flooding over the southeastern United States (e.g., Moore et al., 2012). Contrarily, the latter is present throughout the year and blows parallel to the Andes mountain range, transporting moisture from the Amazon basin to the Rio de la Plata basin (Fig. 5). Changes in land use in the Amazon (mainly forest to grazing lands) caused a change in the moisture ratio transported by the SALLJ which transports a lower amount of moisture to the Rio de la Plata basin, thus compromising the availability of water resources in this region (Marengo, 2005).

1.5 Scope of this thesis

Unequal distribution of freshwater along with the continuing demand of a growing population, accentuate the pressure of water resources already limited. Global warming will intensify the hydrological cycle, with higher evaporation and precipitation rates. Similarly, changes in atmospheric circulation patterns are expected, compromising the availability of water resources. Given the fragility of water resources, there is a growing need to understand the changes caused by global warming in order to ensure a sufficient supply of water resources. ARs and LLJs constitute the main moisture transport

mechanisms that redistribute almost all of the available moisture in the atmospheric branch of the hydrological cycle, hence regulate precipitation patterns. There is a need for a complete analysis of the anomalous moisture transported by these mechanisms of moisture transport at a global scale over its regions of high activity, as well as the global identification of the sources.

The identification and associated variability of sources of moisture have become a fundamental tool for understanding the atmospheric branch of the hydrological cycle at different time scales since it allows establishing a source-sink relationship through the transport of moisture. Changes in moisture transport affect the availability of water resources. Given that there will likely be a rise in extreme events, associated with a more abundant water availability and transport by LLJs and ARs under different global warming scenarios (e.g., Harding and Snyder 2014; Ramos et al., 2016; Gershunov et al., 2019), a precise identification of moisture source/sink regions will provide reliable insights for future works related to the projection of changes linked to the referred climate change scenarios.

Significant effort has been made to modulate the transport of moisture by LLJs and ARs within the hydrological cycle. Nevertheless, it is still challenging to reliably simulate the frequency, intensity, and spatial pattern of precipitation linked to these main structures of transport of moisture. The intensification (or reduction) of transport of moisture by ARs or LLJs modify precipitation anomalies and the subsequent flooding (or drought). The possible changes in the position and occurrence of LLJs and ARs with their climatological behaviour can alter precipitation patterns. Over the last decade, the analysis of these structures was studied in regional studies (e.g., Moore et al., 2012; Ramos et al., 2016) despite its undeniable influence on the global hydrological cycle. Moreover, no research has evaluated global sources and sinks from a Lagrangian perspective, i.e., which regions are uptaking moisture from which of the transports systems and whether there is variability in these evaporation sources. A detailed study of the transport of moisture could provide a better understanding of current and future changes in precipitation patterns (Gimeno et al., 2012; Gimeno, 2013).

2
Objectives

As it was previously commented, there are two meteorological structures responsible for most of the moisture transport on a global scale. One is particularly important in tropical and subtropical regions, i.e., the Low-Level Jets (LLJs), and the other is important in extratropical ones, i.e., the so-called Atmospheric Rivers (ARs). The review paper by Gimeno et al. (2016) indicates the need for additional analysis of the impacts of these structures to understand the extremes of precipitation in terms of atmospheric moisture transport and its evolution over time. The Lagrangian techniques have allowed the analysis of moisture sources and sinks for regions of interest, i.e., to analyse where the moisture in a given region comes from or which are the areas most influenced by it in terms of moisture contribution. The study of moisture sources is one of the main challenges of the atmospheric sciences and an initial step for a better understanding of the variability of precipitation (Gimeno, 2013).

This section sets out the objectives to be achieved in the development of this work.

The main objective of the current study is to **investigate the global transport of moisture associated with the Atmospheric Rivers (ARs) and Low-Level Jets (LLJs)**, with the overall assumption of the strong advection of water vapour by both meteorological structures. This thesis focused on the research of locating the primary regions where these systems obtain moisture. The variability of these moisture source regions is particularly relevant because an increase (or decrease) in the availability of moisture can leads to a higher (or lesser) transport of moisture by LLJs or ARs. Those regions that depend solely on these structures for moisture are particularly vulnerable. Therefore, modifications associated with these systems (i.e., frequency or amount of

moisture transported) can compromise the availability of water resources over large continental areas. To successfully achieve the main objective, a set of specific objectives are listed below:

1. **Update knowledge of the sources of moisture through a complete review of recent articles published in this field:**
   a) Report the main current advances in the methods used to establish the source-receptor relationship,
   b) Update knowledge about the latest regional studies of sources and moisture sinks,
   c) Assess the anomalous transport of moisture as a trigger for hydrometeorological extremes: droughts and floods,
   d) Review recent studies on the main mechanisms of transport of moisture, and
   e) Establish future challenges in the field of sources and transport of moisture.

This objective is addressed in the first article titled: ***Recent progress on the sources of continental precipitation as revealed by moisture transport analysis*** published in 2020 in the *Earth-Science Reviews* Journal.

2. **Analyse the transport of moisture by LLJs from a global approach:**
   a) Objective identification of those regions of maximum occurrence of LLJs on a global scale,
   b) Locate the significant sources and sinks of moisture associated with those regions of maximum activity of LLJs using the Lagrangian model, i.e., FLEXPART,
   c) Contrast differences in transport of moisture between days with LLJ or not, and
   d) Assess the role of the transport of moisture by LLJs from a socioeconomic perspective.

This objective is addressed in the second article titled: ***Global climatology of nocturnal low-level jets and associated moisture sources and sinks*** published in 2019 in the *Atmospheric Research* Journal.

3. **Analyse a particular LLJ: Quantify the transport of moisture by the Great Plains LLJ (GPLLJ):**
    a) Quantify the average moisture contribution from the oceanic source by GPLLJ through the Eulerian model, i.e., WRF Tracers Tool (WRF-TT).

This objective corresponds to the third paper presented in this manuscript with the title: ***On the assessment of the moisture transport by the Great Plains low-level jet*** published in 2019 in *Earth System Dynamics* Journal.

4. **Analyse the role of the transport of moisture by ARs from a global approach:**
    a) Objective identification of the regions of high activity of ARs on a global scale,
    b) Locate the regions that provide moisture to be transported by the identified meteorological structures using the Lagrangian model, i.e., FLEXPART, and
    c) Analyse the inter-annual variability in terms of anomalous moisture uptake of the regions that provide moisture to the ARs.

This objective is addressed in a submitted article titled: ***On the origin of the anomalous uptake of water vapor by landfalling Atmospheric Rivers***.

5. **Study a particular region of AR occurrence: Analysis of the moisture transport to the Arctic domain:**
    a) Identify the main longitudes for the entry of ARs to the Arctic system,
    b) Locate the regions that provide moisture to the meteorological structures, and
    c) Analyse the anomalous moisture uptake during ARs events.

This objective corresponds to the fifth paper titled: ***Atmospheric Rivers over the Arctic: Lagrangian Characterisation of Their Moisture Sources*** published in 2019 in *Water* Journal.

6. On the link between LLJs and ARs in terms of moisture transport:

LLJs and ARs mostly occur at different latitudes, at tropical zones and in the mid and higher latitudes, respectively, but they could be connected in terms of moisture transport. Finally, the last study focused on the South Atlantic Ocean Basin and its continental margins to analyse both meteorological structures.

a) Identification of the anomalous moisture sources for ARs that make landfall over the western coast of South Africa, and
b) Based on the sources of moisture identified, assess the role of the moisture transport by the South American LLJ to the South Atlantic Ocean.

This objective corresponds to the sixth paper titled: ***From Amazonia to southern Africa: atmospheric moisture transport through low-level jets and atmospheric rivers*** published in 2019 in *Annals of the New York Academy of Sciences (ANYAS)*.

3
Methodology

The atmospheric moisture transport analysis, along with the location of sources and moisture sinks, is based on the capabilities of a Lagrangian approach developed by Stohl and James (2005). The robustness and the reliability of FLEXPART (FLEXible PARTicle Dispersion Model), supported by an extensive list of peer-reviewed publications where the model is applied and validated, make FLEXPART attractive for this study. Thus, FLEXPART model is applied on a global scale to analyse the transport of moisture and to estimate sources and sinks of moisture associated with the main meteorological mechanisms of moisture transport in the atmosphere, i.e., **Atmospheric Rivers (ARs)** and **Low-Level Jets (LLJs)** (Gimeno et al., 2016). The methodology used for the global identification of the regions of occurrence of nocturnal low-level jets is detailed as well as the characteristics of the database used for detecting atmospheric rivers. Finally, additional datasets used for this study were included.

3.1 The FLEXPART model: A Lagrangian approach

The FLEXible PARTicle dispersion model (hereafter, FLEXPART) is an open-source Lagrangian particle dispersion model (LPDM) initially developed in the mid-1990s for studying long-range and mesoscale dispersion of air pollutants from point sources. LPDM is a three-dimensional model able to calculate the trajectories of a large number of particles. FLEXPART evolves from the FLEXible TRAjectory model (FLEXTRA) (Stohl et al., 1998; 2005). Over the past decades, successive versions of the model have been improved in different aspects, from several technical changes and bug fixes, as well as improved representation of physical processes forming FLEXPART, i.e.,

comprehensive and useful tool for multi-scale atmospheric transport analysis and modelling. Nevertheless, FLEXPART model has been used successfully in a wide variety of fields of application such as air pollution studies (Zhang et al., 2016; He et al., 2017), exchange between the stratosphere and troposphere (Langford et al., 2015; 2018) or in the global water cycle (Gimeno et al., 2010; 2012).

Since the launch of FLEXPART more than two decades ago (Stohl et al., 1998), the software has been available for free under the GNU General Public License (GPL) Version 3. Although in this study is used FLEXPART in version 9, recently, version 10.3 has been published (Pisso et al., 2019).

FLEXPART is an off-line model; in our study, it was fed with input data from the global ERA-Interim reanalysis dataset (Dee et al., 2011). Nevertheless, it can be also fed with other meteorological data from the Global Forecast System (GFS) or the National Centre for Environmental Prediction (NCEP). Moreover, it can be used with other outputs from mesoscale models such as the Weather Research and Forecasting (WRF), COSMO, or MM5, for instance, when they are defined by a hybrid coordinate system.

To execute FLEXPART, three-dimensional fields and two-dimensional fields are required as input data. On the one hand, three-dimensional fields include temperature data, horizontal and vertical winds components and specific humidity data. On the other hand, the two-dimensional fields include surface pressure, total cloud cover, 10 m horizontal wind components, 2 m temperature, dew point temperature, large-scale and convective precipitation, sensible heat flux, east/west and north/south surface stress, topography, land-sea-mask and the sub-grid standard deviation of topography (Stohl et al., 2005). Furthermore, FLEXPART has implemented a set of parameterisations, among which the parameterisation of turbulence and convection, are particularly relevant in the simulation of the effects of humidity.

One of the main advantages of the Lagrangian approach is it allows the understanding of the properties of each particle, along with its origin and destination. For every one of approximately two million particles, nine variables, listed in Table 1, are stored at every output time, i.e., at six hours (i.e., 00, 06, 12 and 18 UTC). FLEXPART can be executed in two different modes, i.e., forward and backward. In the forward mode, the particles are released from the target region and followed in time intending to analyse their destiny and the changes experienced along their trajectory. Contrarily, the particles

are followed back in time from a target region in the backward mode; therefore, it is useful for locating the sources of the particles.

Table 1. Output variables of FLEXPART model.

Parameter	Units
Latitude (Lat)	
Longitude (Lon)	
Height (H)	m
Topographic Height (TH)	m
Potential Vorticity (PV)	10^{-6} (m^2K/s kg)
Specific Humidity (q)	g/kg
Density of the air ()	Kg/m^3
Mixing height (hmixi)	m
Temperature (T)	K

In this study, some details of the FLEXPART model are highlighted. A complete description of improvements implemented in version 10.3, i.e., the latest version of FLEXPART, are available in Pisso et al. (2019). Furthermore, this work constitutes an update of the last published technical note equivalent to the FLEXPART version 6.2 by Stohl et al. (2005). More details can be found on https://www.flexpart.eu/.

3.2 FLEXPART as a tool for moisture transport

From a Lagrangian approach, a fluid can be represented by a discrete number of finite elements of a volume for which the position and the properties are known at every time step. Following this premise, the FLEXPART model divides the atmosphere homogeneously into several particles or air parcels (i.e., approximately 2.0 million in the simulation), which have a constant mass. Then, the particles (or the air parcels) are advected following a trajectory in equation (2):

$$\frac{dx}{dt} = v[x(t)] \quad (2)$$

where *dx* is the position of the parcel, and *v[x(t)]* is the spatial and temporally interpolated wind speed. From a Lagrangian point of view, it is assumed that the specific humidity changes along the trajectories are due to physical processes. Thus, the gain (i.e.,

evaporation from the environment, *e*) or loss (i.e., convection and precipitation, *p*) of the specific humidity (*q*) by each particle is calculated following equation (3):

$$e - p = m\frac{dq}{dt} \quad (3)$$

where (*e* - p) represents the difference between evaporation and precipitation, which is the freshwater flux of the particle, *m* represents the mass of each particle, *q* represents the specified humidity and t is the time. Regarding this last term in equation (3), fluctuations in the specify humidity were calculated at six hours intervals (i.e., 00, 06, 12 and 18 UTC). The diagnosis of the surface freshwater flux is calculated integrating (e - p) in the entire atmospheric vertical column for all the resident particles, equation (4):

$$(E - P) \approx \frac{\sum_{k=1}^{k}(e-p)}{A} \quad (4)$$

where *(E - P)* represent the surface freshwater flux, *K* is the number of particles in residence over a specific area, *A*.

3.2.1 Identification of moisture sources and sinks

Over the last decades, Lagrangian techniques for estimating sources and sinks of moisture have increased due to the reliability of the method. Notably, the FLEXPART particle dispersion Lagrangian model responds correctly from where the moisture that precipitates in a specific region originates. A global FLEXPART experiment was realised at the Environmental Physics Laboratory (EPhysLab) of the University of Vigo. To perform the experiments, the 6h ERA-Interim reanalysis data from the ECMWF was used (Dee et al., 2011) with a resolution of 1º in latitude and longitude, and with 60 vertical levels (Fig. 6).

The FLEXPART Lagrangian model is a useful tool to estimate the variation in specific humidity along the individual trajectory of each particle and identify those regions where the set of particles uptake or loss in moisture. From the global FLEXPART experiment, it is possible to compute (e - p) for each particle that resides in a region of interest, i.e., those particles that leave the region of interest (forward in time) or that reach this region (backwards in time). It is important to note that the number of particles considered will depend on the extension of the region of interest. Thus, along the individual trajectories, q fluctuations can occur for nonphysical reasons (e.g., because of

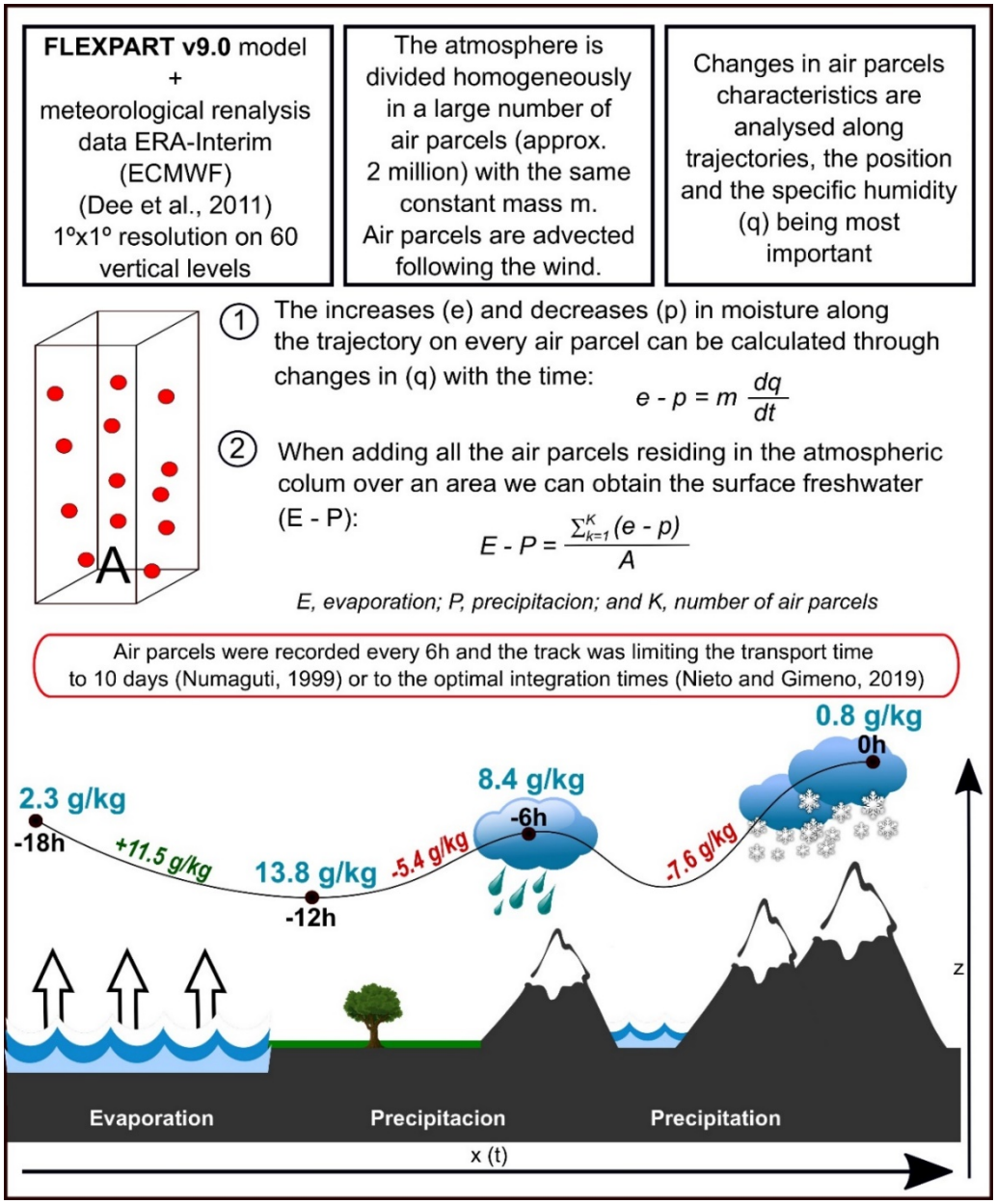

Figure 6. Lagrangian approach to identify sources and sinks of moisture. A scheme of the Lagrangian approach based on FLEXPART model used to estimate the moisture transport. Bottom figure: the black line represents the temporal trajectory of an air parcel during 18h, the black dots show the 6h-step. The specific humidity content (q, in g kg^{-1}) of the air parcel is given in blue for each time step - q increments (decreases) are shown in green (red) numbers. Figure adjusted from Gimeno-Sotelo et al. (2018) and Läderach and Sodemann (2016).

q interpolation or trajectory errors), this model limitation is partially compensated for by the presence of significant quantities of particles in the atmospheric column over the target area.

Once the associated study region is delimited, in this case, to moisture transport mechanisms, the particle trajectories are analysed for a specified period. This study

considered periods of 37 years and 38 years, i.e., 1980-2016 and 1980-2017, respectively, based on the availability of data. As noted previously, the FLEXPART model allows the tracking of particles along their trajectories backwards and forward in time. An analysis performed backwards in time distinguishes the origin of the atmospheric moisture in the air masses over the primary regions of moisture transport occurrence. Thus, in the backward experiment, a source of moisture is defined as that region in which the evaporation exceeds the precipitation, i.e., $(E - P) > 0$, and the net moisture budget of the tracked particles favours evaporation from the environment to the particles; thus, there is a positive contribution of moisture. On the other hand, a moisture sink is those regions where precipitation exceeds evaporation, i.e., $(E - P) < 0$, the moisture budget favours moisture loss from the tracked particles to the environment. In the forward experiment, the moisture loss computed in the air masses from a source over a target region is considered to contribute to the precipitation. Note that FLEXPART is not able to obtain a direct measurement of precipitation but of a difference the evaporation balance and precipitation (E - P), or an absolute value of the specific humidity.

3.2.2 The question of the residence time of water vapour: optimal integrations times for a Lagrangian Analysis

For the determining the sources and moisture sinks, the tracking of the particles was limited to ten days in the first part of this study, i.e., the most widely used integration time, derived from the average residence time of water vapour in the atmosphere (Numaguti, 1999; Trenberth, 1998). Nevertheless, the results are susceptible to the integration time of the trajectories used in the analysis. Longer integration times allows for identifying more remote sources and moisture sinks. Based on the offline tracking methods, Läderach and Sodemann (2016) estimate a shorter scale of 4-5 days for the global mean residence time. Nevertheless, van der Ent and Tuinenburg (2017) used reanalysis and modelling to derive the global average residence time of 8-10 days (i.e., close to the classical values of the residence time of water vapour in the atmosphere).

The residence time of water vapour in the atmosphere is a crucial variable to understand the hydrological cycle and is a topic of discussion in the current literature. Besides, it has a stationary cycle and not only does this time vary spatially, but it is highly dependent on processes such as advection, entrainment, phase changes, and diffusion. From a global point of view, the use of ten days is extensive in literature as a result of the global water balance.

The use of different periods to find sources and sinks of moisture could alter the initial results, the subsequent analyses, and the interpretations. It is, therefore, necessary to estimate the optimal integration time for these Lagrangian methods for estimating sources and sinks. In a recent study, Nieto and Gimeno (2019) proposed a new approach to address this scientific problem by estimating the optimal integration time for the identification of sources and sinks of moisture through Lagrangian methods. These new integration times are based on precipitation estimates from the Lagrangian approach using different times of integration with results obtained from ERA-Interim reanalysis and two precipitation dataset, i.e., the Multi-Source Weighted-Ensemble Precipitation (MSWEP) (Beck et al., 2017) and the Global Precipitation Climatology Project (GPCP) (Adler et al., 2003). Thus, in the second part of this study, the tracking of the particles is limited according to the relative new integration times proposed in Nieto and Gimeno (2019).

3.3 Advantages of a Lagrangian analysis and methods for diagnosing the atmospheric branch of the hydrological cycle

Moisture source study is analysed as a source-receiver relationship. Thus, over the last decades the Lagrangian approach applied for diagnosing the atmospheric moisture transport has increased in importance due to the reliability and robustness of the technique. Nevertheless, other methods used for the study of moisture transport and that establish a source-receiver relationship include analytical or box models, physical water vapour tracers (isotopes), and numerical water vapour tracers (i.e., Lagrangian and Eulerian approaches). A detailed inter-comparison of different methods is given in Gimeno et al. (2012), and the different studies concerning moisture budget analysis could be read in Gimeno et al. (2020).

On the one hand, **analytical or box models** in a target region are based on the vertically integrated balance of water vapour equation. This kind of model allows the identification of moisture inflow and outflow through the lateral boundary of the study region. Nevertheless, it is not able to provide information about the processes that occur inside the box. An analytical model has been extensively applied to compute the local recycling ratio. On the other hand, **physical water vapour tracers (isotopes),** are useful for validation since they use physical measurements but does not consider convection and rainwater precipitation. Finally, **numerical water vapour tracers (WVT)** are a useful

tool to determine the origin of atmospheric moisture. The results obtained depend on the capacity of the numerical model to simulate the processes included (such as wind advection, turbulence, and convection). Two approaches are distinguished: **Eulerian and Lagrangian models**. The main difference between the two approaches is the perspective of the atmospheric motion. In the Eulerian approach, the observer focuses on a specific location in the space through which the fluid flows as time passes. Nevertheless, in the Lagrangian approach, the observer follows a particle or air parcel of the individual fluid as it moves through space and time. The path along which the air parcel travels is called the trajectory. Thus, the Lagrangian formulation is formed by a finite number of fluid elements, for which the position and other properties are known at all times. Both methodologies have been widely used. Eulerian models provide detailed atmospheric processes, in which a realistic atmospheric circulation is represented. However, they do not include remote sources of moisture in a region. Therefore, Eulerian approaches are only able to estimate the ratio between the advected and the recycled moisture and to calculate moisture transport from pre-arranged sources or over the sink regions. They are unable to provide a direct identification of the moisture source regions, which has to be performed through very time-consuming computer-based Lagrangian techniques. Lagrangian approaches method allow the computation of air parcels or particles with a high spatial resolution in a global domain. The accuracy of the results obtained will depend on (i) the meteorological conditions, (ii) the correct use of parameterisations, (iii) the resolution of the dataset used, and (iv) the assimilation of the observations. However, one of the disadvantages is that evaporation and precipitation are not separable in some methods (e.g., FLEXPART model).

3.4 Nocturnal Low-Level Jet (NLLJ) detection: the NLLJ index

The global identification of the primary regions of occurrence of LLJs was obtained from the index of nocturnal activity proposed by Rife et al. (2010) for the period: 1980-2016. The identification of LLJ events was performed in the hemispheric summer (i.e., January and July) following the strong seasonal cycle of these structures. The nocturnal low-level jet (NLLJ) index is based on the vertical wind and the diurnal-nocturnal variation of the wind fields. The calculation of the NLLJ index was performed at each grid point on a global scale through equation (5) below:

$$NLLJ = \lambda\varphi\sqrt{[(u_{00}^{L1} - u_{00}^{L2}) - (u_{12}^{L1} - u_{12}^{L2})]^2 + [(v_{00}^{L1} - v_{00}^{L2}) - (v_{12}^{L1} - v_{12}^{L2})]^2} \quad (5)$$

where *u* and *v* represent the zonal and the meridional components of the wind fields, *00* and *12* are midnight and noon solar time, respectively, and *L1* and *L2* are the near-to-surface level and height level, respectively. According to the Rife criterion, to identify an LLJ event, it is necessary for the wind speed to be higher at midnight than at local noon and higher on the surface than at high levels:

$$\lambda = \begin{cases} 0, ws_{00}^{L1} \leq ws_{12}^{L1} \\ 1, ws_{00}^{L1} > ws_{12}^{L1} \end{cases} \quad (6)$$

$$\varphi = \begin{cases} 0, ws_{00}^{L1} \leq ws_{00}^{L2} \\ 1, ws_{00}^{L1} > ws_{00}^{L2} \end{cases} \quad (7)$$

Thus, λ (Eq. (6)) and φ (Eq. (7)) are two binary operators which assure that the LLJ event exists only if the wind module is higher at *L1* than at *L2*, and higher at *00* than at *12*. These operators are used to preserve the nocturnal and low-level restricted character of the detected systems. The 95th percentile of NLLJ index value was applied to determine a threshold that limits the spatial region occurrence of LLJ.

3.5 Atmospheric Rivers (ARs) detection

Based on the original resolution (i.e., 1.5º × 1.5º) of the AR database developed by Guan and Waliser (2015), a re-escalation was performed by multiplying the original resolution by eight to obtain a spatial resolution of 12º and to perform a higher accumulation of AR events over larger coastal areas. From this new coarser resolution, a threshold of 10% of the AR number of days (i.e., a period of 1388 days of ARs, from 1980-2017) was applied. Therefore, on a global scale, those regions with ARs frequency over this threshold are initially identified as regions of maximum occurrence of AR landfalling.

3.6 Weather Research and Forecast Tracers Tool (WRF-TT)

The innovative Eulerian 3D tracers tool coupled to the Weather Research and Forecast (WRF) mesoscale model (WRF-TT) (Eiras-Barca et al., 2017; Insua-Costa and Miguez-Macho, 2018) was used to quantify the moisture transport by the Great Plains

low-level jet (GPLLJ). It is a technique of tracing the moisture contained or crossing through in certain regions previously defined within the simulation domain with a defined 3D mask. This tool replicates all the equations concerning the advection, convection, turbulence, and phase change for the moisture contained in the initial mask solely. The labelled water vapour is followed in time and space during the simulation. Thus, after advancing several days in the simulation, it can be determined how much moisture present in any other region of the domain comes from the initially labelled region. This conclusion can be obtained for both specific humidity and precipitation. In the simulation, a resolution of 20 km and 38 vertical levels were used. The simulation period is 11 days, and it was started seven days before each GPLLJ event, which was sufficient time for the advection process through the Great Plains Low-Level Jet (GPLLJ). The initial and boundary conditions of the model have been provided by the ERA-Interim reanalysis model (ECMWF) (Dee et al., 2011). A complete description of the tool and its validation can be found in Insua-Costa and Miguez-Macho (2018).

3.7 Datasets

3.7.1 FLEXPART input

The FLEXPART model can be initialised with different datasets. In the present study, FLEXPART v9.0 model was fed with ERA-Interim reanalysis data (Dee et al., 2011) from the European Centre for Medium-Range Weather Forecast (ECMWF). We use a data collection for a period of 38 years, i.e., from 1980 to 2017. FLEXPART uses ERA-Interim global data at 6h intervals (i.e., 0000, 0600, 1200 and 1800 UTC) with a spatial resolution of 1º and 61 vertical levels from 0.1 to 1000 hPa (approximately 14 model levels below 1500 m and 23 below 5000 m). This concentration of surface levels is per water vapour transport, which mainly occurs in the lower troposphere, i.e., affected by the Earth's topography (Peixoto and Oort, 1992). To execute the FLEXPART model, three-dimensional and two-dimensional fields are required as input data. On the one hand, the three-dimensional fields include the horizontal and vertical wind components, temperature, and specific humidity. On the other hand, the two-dimensional fields include surface pressure, total cloud cover, 10 m horizontal wind components, 2 m temperature, dew point temperature, large-scale and convective precipitation, sensible heat flux,

east/west and north/south surface stress, topography, land-sea mask, and sub-grid standard topography deviation (Stohl et al., 2005).

3.7.2 NLLJ inputs

A 37-year output of 6h ERA-Interim reanalysis data (Dee et al., 2011) with longitude and latitude of 0.25º was obtained from the ECMWF. The NLLJ index is based on the vertical variation of the wind's temporary structure (Rife et al., 2010). Thus, regarding vertical levels, sigma levels have been used to consider the particularities of the global terrain. Particularly, for the calculation of the NLLJ index, the study used the zonal (u) and meridional (v) components of the wind at two height levels, i.e., a surface level (53 sigma level) and a height level (42 sigma level). The difference between both levels varies between 3000 m and 3800 m above sea level as a function of topography. Globally averaged, sigma level 53 had an average height of 550 m, whereas sigma level 42 had an average height of 4000 m.

3.7.3 ARs dataset

The global database developed by Guan and Waliser (2015) was used for detecting AR events. AR detection was based on a set of requirements on IVT intensity, direction, and geometry as described in detail by Guan and Waliser (2015). Although it is available for various datasets and different spatial and temporal resolutions, the study used the database based on data from the ERA-Interim reanalysis of the ECMWF model. This database is available at a spatial resolution of 1.5º and covers a period of 38 years, from 1980 to 2017.

3.8 Other datasets

Additional datasets were used to provide a proper interpretation of the results. A complementary set of data were used in the different articles that were part of this study, depending on the requirements of each specific objective:

3.8.1 Precipitation data from MSWEP

Monthly Multi-Source Weighted-Ensemble Precipitation (MSWEP) database (Beck et al., 2017) has a longitude and latitude resolution of 0.25º, accumulated over three-hour time periods. MSWEP was specially designed for hydrological modelling. The

new version, MSWEP v2, is available with a spatial resolution of 0.1º and covers the temporal coverage from 1979 to 2017 (Beck et al., 2019). MSWEP merge a wide range of precipitation information, with several characteristics: (i) it combines a wide range of precipitation data sources to provide reliable precipitation estimates around the world, including gauges, satellites, and atmospheric reanalysis models; (ii) it accounts for gauge under-catch and topographic effects using Q observations from 13762 stations worldwide; and (iii) it has a high temporal and spatial resolution. MSWEP was used to quantify the monthly precipitation over each sink NLLJ region. It is available upon request from http://www.gloh2o.org/.

3.8.2 Mean Sea Level Pressure (MSLP) from ERA-Interim

As ARs are linked to baroclinic systems, the regions of maximum occurrence of AR were evaluated during wintertime throughout anomalies of MSLP from ERA-Interim reanalysis (ECMWF; Dee et al., 2011).

3.8.3 Water Scarcity

An approach to the socioeconomic impact of LLJ was measured through data on water demand and affected population. Water demand data is calculated as the ratio of local bluewater footprint to the total bluewater availability. Blue water footprint is defined as the water sourced from the surface or groundwater resources. It is either evaporated, incorporated into a product or extracted from one water body and returned to another, or returned at a different time. The water scarcity dataset was obtained from waterfootprint.org at a longitude and latitude resolution of 0.5º and for a period of 10 years (from 1996 to 2005). More information on this dataset can be found in Mekonnen and Hoekstra (2016).

3.8.4 Population

Information on population was obtained from the Socioeconomic Data and Applications Center (SEDAC, http://sedac.ciesin.columbia.edu). In particular, the Gridded Population of the World (GPWv4) dataset, which provides an estimation of the human population using a combination of national censuses and population registers, was applied using the year 2015 as the representative year when the research was conducted.

4

Set of publications

The availability of water resources is governed by moisture transport. Over the years, the number of studies that focused on the analysis of the main moisture transport mechanisms has increased. Nevertheless, these studies focused mainly on specific regions, ignoring the global approach despite the importance of both meteorological systems, i.e., ARs and LLJs in the global regulation of the hydrological cycle. Therefore, there is a need to have an in-depth understanding of the processes that govern the global transport of moisture.

A total of five publications and one paper submitted have been used to construct this final document. Fig. 7 shows a scheme of the articles that make up the body of this study. It should be noted that the order of the articles does not necessarily correspond to the order of the date of publication. The analysis period varies as per the beginning of each study and the availability of data, which were progressively updated. Table 2 shows the title, the authors, the year of publication, and the journal where the articles have been published. In Table 3, a description of each journal and certain characteristics such as the quartile, the scientific impact factor, and the ISSN for the publications are listed. The supplementary material linked to each article is given in **Appendix A: Supplementary Material**.

The first article in this document is a review which updates the knowledge of the moisture source-sink relationship on rainfall distribution. Therefore, the recent advances of the significant mechanisms of moisture transport at a global scale are summarized, mainly ARs and LLJs, and a revisiting of their role as triggers of hydrological extreme due to its anomalous moisture transport was achieved in ***Recent progress on the sources***

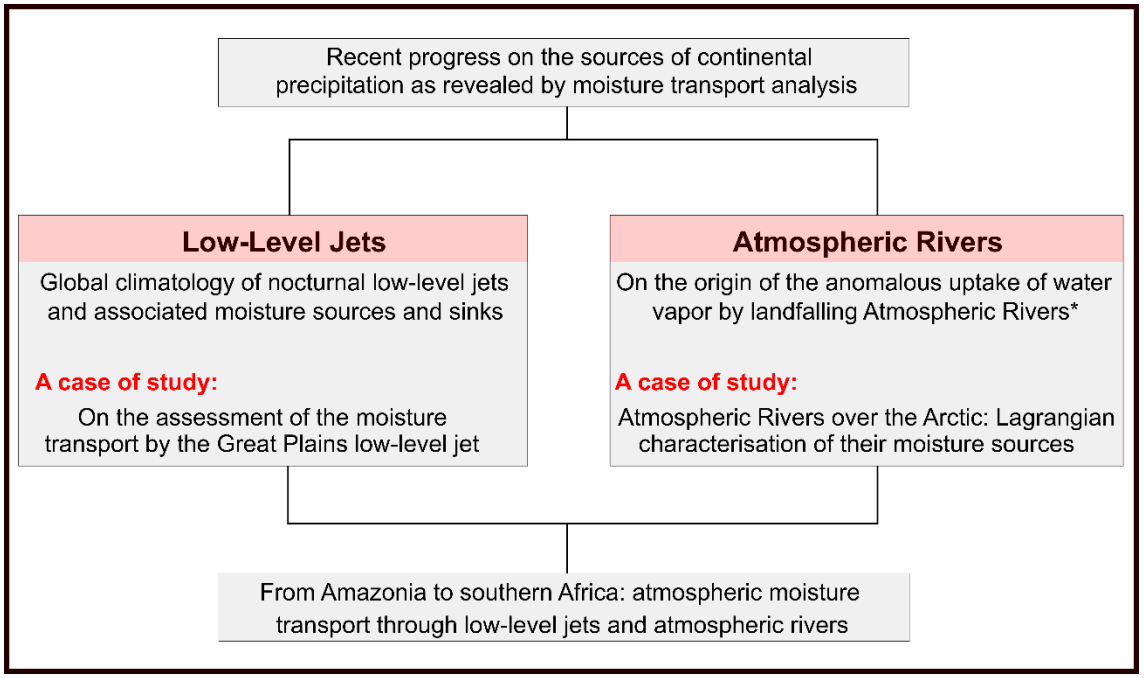

Figure 7. Scheme of the articles that make up the thesis. The thesis begins with a review that updates knowledge in recent years of moisture sources and their transport. Then, the document is divided into the study of LLJ and ARs. Both structures are studied primarily from a global approach to focus then on the study of a particular structure or region of occurrence. Finally, a link between AR and LLJ is reported by transporting moisture. (*) denotes submitted article.

of continental precipitation as revealed by moisture transport analysis by L. Gimeno, M. Vázquez, J. Eiras-Barca, R. Sorí, M. Stojanovic, **I. Algarra**, R. Nieto, A.M. Ramos, A.M. Durán-Quesada and F. Domínguez; published in 2020 in *Earth-Science Reviews*.

Subsequently, the thesis is divided into the study of LLJ and AR.

In the case of LLJs, global identification of LLJ is performed, and moisture transport is studied based on a jet and no-jet days. In a particular study of the LLJs, we focus on the Great Plains LLJ (GPLLJ), the LLJ that modulates the entry of moisture, hence, the precipitation pattern in the southeastern United States. While the GPLLJ is a well-documented LLJ, we focus on quantifying the transport of moisture of this structure through the WRF Tracers Tool.

The second article that forms part of this Thesis is titled ***Global climatology of nocturnal low-level jets and associated moisture sources and sinks*** by **I. Algarra**, J. Eiras-Barca, R. Nieto and L. Gimeno; published in 2019 in *Atmospheric Research*. This article makes a global identification of the primary regions of occurrence of NLLJ to provide the location of the primary sources and sinks of moisture associated with each

NLLJ. The role of moisture transport for jet days and no-jet days is evaluated. Finally, a contextualisation in terms of water demand and its link to the occurrence of NLLJ was presented.

The third article in this thesis: ***On the assessment of the moisture transport by the Great Plains low-level jet*** by **I. Algarra**, J. Eiras-Barca, G. Miguez-Macho, R. Nieto and L. Gimeno; published in the journal *Earth System Dynamics* in 2019, combines the Lagrangian and Eulerian approach, i.e. FLEXPART and WRF-TT, respectively; to address the general behaviour of the GPLLJ in terms of transport of moisture. Five representative simulations based on the intensity of the GPLLJ were performed to quantify the transport of moisture by this structure, which modulates much of the moisture input in the southeastern United States of America.

Regarding the study of ARs, a global identification of the primary regions with a high activity of ARs was done to analyse which areas provide anomalous moisture to these structures.

The fourth article submitted that forms the thesis, which is pending publication, is titled: ***On the origin of the anomalous uptake of water vapor by landfalling Atmospheric Rivers.*** In this article, the main landfalling regions around the globe of AR were identified to identify the anomalous moisture receiving areas over ARs periods. Then, a global inter-annual variability analysis was performed.

The fifth article is titled: ***Atmospheric Rivers over the Arctic: Lagrangian Characterisation of Their Moisture Sources*** by M. Vázquez, **I. Algarra**, J. Eiras-Barca, A.M. Ramos, R. Nieto, and L. Gimeno, was published in the journal *Water* in 2019. In this article, the primary regions of entry of ARs into the Arctic System were identified, and an anomalous moisture transport study of AR that reaches this region was performed.

Finally, the last article that makes up this thesis establishes a link between the two margins of the South Atlantic Ocean which appear connected by a combination of the two most critical meteorological structures for the moisture transport, i.e., the LLJ and the ARs. ***From Amazonia to southern Africa: atmospheric moisture transport through low-level jets and atmospheric rivers*** by A.M. Ramos, R.C. Blamey, **I. Algarra**, R. Nieto, L. Gimeno, R. Tomé, C. Reason and R. M. Trigo; published in the journal *Annals of the New York Academy of Sciences (ANYAS)* in 2019, links the South American atmospheric dynamics and the wintertime rainfall in South Africa for the first time. An interaction was

established between a phase of the SALLJ, known as No Chaco Jet Event (NCJE), and the ARs that make landfalling over the west coast of South Africa.

Table 2. List of publications.

Title	Authors	Year	Journal
Recent progress on the sources of continental precipitation as revealed by moisture transport analysis	L. Gimeno, M. Vázquez, J. Eiras-Barca, R. Sorí, M. Stojanovic, **I. Algarra**, R. Nieto, A. M. Ramos, A. M. Durán-Quesada and F. Domínguez	2020	Earth-Science Reviews (ESR)
Global climatology of nocturnal low-level jets and associated moisture sources and sinks	**I. Algarra**, J. Eiras-Barca, R. Nieto and L. Gimeno	2019	Atmospheric Research
On the assessment of the moisture transport by the Great Plains low-level jet	**I. Algarra**, J. Eiras-Barca, G. Míguez-Macho, R. Nieto and L. Gimeno	2019	Earth System Dynamics (ESD)
On the origin of the anomalous uptake of water vapor by landfalling Atmospheric Rivers	**I. Algarra**, R. Nieto and L. Gimeno	2020	Submitted to publication
Atmospheric Rivers over the Arctic: Lagrangian Characterisation of Their Moisture Sources	M. Vázquez, **I. Algarra**, J. Eiras-Barca, A. M. Ramos, R. Nieto and L. Gimeno	2019	Water
From Amazonia to southern Africa: atmospheric moisture transport through low-level jets and atmospheric rivers	A. M. Ramos, R.C. Blamey, **I. Algarra**, R. Nieto, L. Gimeno, R. Tomé, C. Reason and R. M. Trigo	2019	Annals of the New York Academy of Sciences (ANYAS)

Table 3. Summary of the impact and quality of the Journals in which the papers are published. The data correspond to the year 2018 (last year available at the date of preparation of this document).

Journal	Description	Journal characteristics
Earth-Science Reviews (ESR)	ESR is a monthly peer-reviewed scientific journal published by Elsevier. It covers all aspects of Earth sciences.	JCR Abbrev: *Earth-Sci. Rev.* JCR category rank: 3/196 Current Impact Factor: 9.530 5-year Impact Factor: 10.640 Quartile: Q1 in *Geosciences, Multidisciplinary* ISSN: 0012-8252
Atmospheric Research	Atmospheric Research is a peer-reviewed scientific journal that publishes scientific papers (research papers, review articles, letters and notes) dealing with the part of the atmosphere where meteorological events occur.	JCR Abbrev: *ATMOS RES* JCR category rank: 13/86 Current Impact Factor: 4.114 5-year Impact Factor: 4.024 Quartile: Q1 in *Meteorology & Atmospheric Sciences* ISSN: 0169-8095
Earth System Dynamics (ESD)	ESD is an international scientific journal dedicated to the publication and public discussion of studies that take an interdisciplinary perspective of the functioning of the whole Earth system and global change.	JCR Abbrev: *EARTH SYST DYNAM* JCR category rank: 16/196 Current Impact Factor: 4.351 5-year Impact Factor: 5.124 Quartile: Q1 in *Geosciences, Multidisciplinary* ISSN: 2190-4979
Water	Water is a peer-reviewed open access journal on water science and technology, including the ecology and management of water resources, and is published monthly online by MDPI.	JCR Abbrev: WATER-SUI JCR category rank: 29/91 Current Impact Factor: 2.524 5-year Impact Factor: 2.721 Quartile: Q2 in *Water Resources* ISSN: 2073-4441
Annals of the New York Academy of Sciences (ANYAS)	ANYAS is one of the oldest scientific journals in the United States. Edited in consultation with experts in their fields, Annals is rigorously peer reviewed and available in over 11,000 institutions worldwide.	JCR Abbrev: ANN NY ACAD SCI JCR category rank: 14/69 Current Impact Factor: 4.295 5-year Impact Factor: 4.788 Quartile: Q1 in *Multidisciplinary Sciences* ISSN: 0077-8923

Earth-Science Reviews 201 (2020) 103070

Contents lists available at ScienceDirect

Earth-Science Reviews

journal homepage: www.elsevier.com/locate/earscirev

Recent progress on the sources of continental precipitation as revealed by moisture transport analysis

Luis Gimeno[a,*], Marta Vázquez[a,b,c], Jorge Eiras-Barca[a,d], Rogert Sorí[a,b], Milica Stojanovic[b,c], Iago Algarra[a], Raquel Nieto[a], Alexandre M. Ramos[b], Ana María Durán-Quesada[e], Francina Dominguez[d]

[a] Environmental Physics Laboratory (EPhysLab), CIM-UVigo, Universidade de Vigo, Ourense, Spain
[b] Instituto Dom Luiz (IDL), Faculdade de Ciências, Universidade de Lisboa, 1749-016 Lisboa, Portugal
[c] Escola de Ciências e Tecnologia, Universidade de Trás-os-Montes e Alto Douro, Vila Real, Portugal
[d] Department of Atmospheric Sciences, University of Illinois at Urbana-Champaign, Urbana-Champaign, IL, USA
[e] Department of Atmospheric, Oceanic and Planetary Physics, University of Costa Rica, San José, Costa Rica

ARTICLE INFO

Keywords:
Moisture sources
Methods of linking moisture source-sink relationships
Precipitation extremes
Droughts and floods
Major mechanisms of atmospheric moisture transport
Atmospheric Rivers
Low-Level Jets

ABSTRACT

The assessment of sources of moisture is key to the understanding of the hydrological cycle at different time scales, because it enables the establishment of source-sink relationships and the identification of the main moisture transport conveyors and associated processes, the result of which is precipitation. Gimeno et al. (2012) provided a comprehensive review of the state-of-the-art in the assessment of moisture source-sinks and how different approaches can contribute to improving our knowledge of this component of the Earth's Climate System. Since then, a variety of studies have focused on more specific aspects of the moisture budget and the source-sink distribution across the globe by integrating observations, satellite-derived products, physical tracers and numerical modelling. Here, we summarise the main advances in the field related to the impact of the moisture source-sink relationship on rainfall distribution, and add to the scientific debate on the question of the residence time of water vapour. We also revisit some of the recent advances in the role of the major mechanisms of moisture transport at a global scale, mainly Atmospheric Rivers and Low-Level Jet systems (Gimeno et al., 2016), in terms of their effects on precipitation extremes. Finally, we set out some of the main challenges for future research.

1. Introduction

To explain the origin and variability of continental precipitation, there is a need to understand the rather complex internal processes of the hydrological cycle. The hydrological cycle consists of a continuous succession of stages through which water passes from the atmosphere to the Earth, before returning to the atmosphere (WMO, 2012). The atmospheric branch of this cycle plays a key role as a natural conveyor between water bodies (oceans, rivers, lakes), evaporation, and continental precipitation, but it also relates directly to the contribution of evaporation from land to local and remote precipitation (van der Ent et al., 2014; Gimeno et al., 2012). Oceans cover the greater proportion of the planet's surface (~71%) and contain 97% of the Earth's water. The water that evaporates from them becomes the principal source of moisture for continental precipitation (Gimeno et al., 2010; Gimeno et al., 2012; van der Ent and Savenije, 2013). However, some authors (e.g., Van der Ent and Savenije, 2011; van der Ent et al., 2010) have remarked that around 40% of the precipitation on land originates from continental rather than from oceanic evaporation, pointing to the importance of moisture recycling. Based on the understanding of source-sink relationships, Gimeno et al. (2012) performed a characterisation from several related studies to assess how continental regions are influenced by water from different moisture source regions. Numerous processes and factors are involved in driving the source-sink relationships; for example, changes in land cover affect vegetation-regulated moisture recycling, which is a critical source for adjacent sinks (Keys et al., 2016). Indeed, global changes in land cover averaged from 1850 to 2000 were shown to have increased discharge through reduced evapotranspiration (Bosmans et al., 2017). Human water use (irrigation, industrial use, etc.) also affects the natural patterns involved in runoff and groundwater reservoirs; it induces groundwater-to-atmosphere feedback, which potentially weakens continental sinks over arid

* Corresponding author at: Universidade de Vigo, Campus Da Auga, Rúa Canella da Costa da Vela, 12, 32004 Ourense, Spain.
E-mail address: l.gimeno@uvigo.es (L. Gimeno).

https://doi.org/10.1016/j.earscirev.2019.103070
Received 2 September 2019; Received in revised form 13 November 2019; Accepted 17 December 2019
Available online 19 December 2019
0012-8252/

watersheds (e.g., in southern Europe), possibly contributing to the drying of these areas (Keune et al., 2018). Furthermore, important modes of climate variability such as the El Niño-Southern Oscillation (ENSO), the Atlantic Multidecadal Oscillation (AMO), and the North Atlantic Oscillation (NAO) are associated with large-scale shifts in atmospheric circulation cells, and consequently have a strong effect on the modulation of global and regional precipitation (Stephens et al., 2018; Zhang et al., 2013).

As global warming continues over the short and long term (IPCC, 2014), the global climatological characteristics of the source-sink relationships of the atmospheric moisture as they are known today could be altered. Indeed, water vapour plays a key role in the warming of the atmosphere. Some studies have highlighted the crucial role of local and poleward moisture transport from lower latitudes to explain both Arctic warming and the decline in rainfall and sea ice extent in recent years in an area today considered a global 'hotspot' (Gimeno-Sotelo et al., 2019; Zhong et al., 2018). As the temperature of the atmosphere increases, so does its capacity to hold water according to the Clausius-Clapeyron relationship (Held and Soden, 2006). Accordingly, the thermodynamic response to idealised climate warming can be understood as a generalised mechanism of "dry gets drier and wet gets wetter", in which the greatest precipitation is enhanced the most from increased gross stratification of moisture (Chen et al., 2019). Observational and modelling studies suggest that the strong dependence of saturated vapour pressure on temperature will result in increased evaporation, and hence precipitation, leading to an intensification of the water cycle (Gimeno et al., 2015). From the connections already established, changes in certain hotspot moisture source regions (Nieto et al., 2014) will be directly related to projected increases in the intensity of extreme precipitation events, probably of unprecedented magnitude, throughout the 21st century (Giorgi et al., 2019). Marked differences between latitudes and continents are expected (Madakumbura et al., 2019), with a knock-on effect on the availability of freshwater resources (Cosgrove and Loucks, 2015), a topic of worldwide concern today and for the future. In a crowded world with populations still on the rise, and changing patters of consumption, humankind has not done enough to plan for and manage the future of water availability (FAO, 2011).

There has been a notable advance in the number of studies of the origins of precipitation, the identification of moisture sources, and the establishment of climatologies of moisture source-sink relationships following Gimeno et al. (2012). The results have provided new detailed insights regarding the role of synoptic-scale systems such as Low-Level Jets (e.g. Algarra et al., 2019; Zhang et al., 2019), Atmospheric Rivers (e.g. Dettinger et al., 2015; Ralph et al., 2017a; Eiras-Barca et al., 2017), and monsoons (e.g. Ordoñez et al., 2019; Sorí et al., 2018; Pathak et al., 2017; Hu and Dominguez, 2015) on precipitation over different continental areas. Additionally, a great number of studies have given further consideration to the role of moisture sources in the diagnosis of the occurrence of extreme hydroclimatic events (e.g., Drumond et al., 2019; Bohlinger and Sorteberg, 2018), even at multiple spatiotemporal scales (Herrera-Estrada et al., 2019). To this end, a number of authors have implemented classical Eulerian (Van der Ent and Savenije, 2011), Lagrangian (Stohl and James, 2004, 2005; Dominguez et al., 2006; Dirmeyer et al., 2014), and stable isotope approaches (Dansgaard, 1964), as well as new sophisticated and robust methods such as Eulerian mesoscale tracer tools (Insua-Costa and Miguez-Macho, 2018). The results of these studies have contributed to a deeper understanding of the functioning of the hydrological cycle on the planet and have provided support for socioeconomic planning. In the present review, we aim to provide an update of the most recent results (after Gimeno et al., 2012), and a broad characterisation of the genesis of continental precipitation and its associated mechanisms. The remainder of this article may be summarised as (1) methods and techniques for the identification of moisture sources, (2) the question of the residence time of water vapour, (3) the climatological position of the moisture sources for continental precipitation, (4) the role of meteorological structures at a planetary scale in terms of moisture transport (Low-Level Jets, Atmospheric Rivers, and monsoons), and (5) the role of oceanic and continental moisture sources in the development of extreme precipitation events.

2. Advances in methods used to establish source-receptor relationships

The novel methodologies applied in the establishment of source-receptor relationships related to moisture transport can be categorised using the classification contained in Gimeno et al. (2012). On the one side, analytical or box models provide simple paradigms to evaluate the vertically integrated balance of water vapour using a number of assumptions. These approximations (e.g., negligible changes in the storage of atmospheric water or a well-mixed atmosphere) make these models easy to implement and computationally cheap, but mean they lack any precise analysis of the physical phenomena involved in the moisture transport process.

On the other side, so-called numerical models (either Lagrangian or Eulerian) provide a more sophisticated analysis by considering a large number of physical processes by making use of moisture tracers throughout their residence time in the Troposphere.

A good comparison between the numerical approaches can be found in Winschall et al. (2014b). The authors support the convenience of relying on complementary results and interpretations provided by the two types of diagnostic tool. In fact, Lagrangian approaches are presented as more suitable for climatological analysis, while Eulerian formalism is more comprehensive for detailed case studies.

Finally, physical moisture tracers based on concentrations of Hydrogen and Oxygen isotopes contained in water vapour and precipitation provide the only appropriate means of validation of the methodologies mentioned above, together with additional valuable information where such data are available.

In this section, we describe the recent advances provided in the cited methodologies, together with some typical results derived from these.

2.1. Analytical models

The basis of the analytical or box model is the application of a simple Eulerian framework in the analysis of the vertically integrated balance of water vapour:

$$E - P = \frac{\partial W}{\partial t} + \nabla \cdot \overrightarrow{\Phi} \tag{1}$$

where the budget of evapotranspiration (E) minus precipitation (P) is evaluated through changes in the storage of water vapour in the integrated column (W) and the divergence of the integrated vapour transport ($\overrightarrow{\Phi}$ or IVT), i.e., advection of moisture into the box. Fields of IVT and W can be directly obtained by:

$$W = \frac{1}{g}\int_{ps}^{p} q\,dp \tag{2}$$

$$\overrightarrow{\Phi} = \frac{1}{g}\int_{ps}^{p} q\vec{U}\,dp \tag{3}$$

where both the specific humidity (q) and the horizontal wind field (U) are integrated over the vertical column from the surface pressure (ps) to the upper levels.

Starting from this basic idea behind all analytical models, substantial improvements, including the consideration of soil-atmosphere interaction, have been reported in the recent literature, for a range of different purposes.

Van der Ent and Savenije (2011) provide an analytical framework for calculating length and time scales of atmospheric moisture recycling without the restrictions associated with the dependence of scale or

shape on the region of analysis, as shown in previous studies. As well as providing average length scales for both precipitation and evaporation recycling, they also provide a global distribution of average depletion and replenishment times, as well as length scales for both evaporation and precipitation recycling.

Singh et al. (2016) provided the basis of a simple model in which the moisture flux divergence term in the atmospheric moisture budget (Eq. (1)) can be divided into the divergence of locally evaporated moisture and the convergence of remotely evaporated moisture for periods of more than a year when variations in the storage of water in the atmosphere are negligible. In these terms, the divergence term is written as:

$$-\nabla\cdot\overrightarrow{\Phi} = (FT - T)\overrightarrow{E} \tag{4}$$

where F is the Hollow convergence matrix whose non-diagonal elements are equal to the fraction of exported atmospheric water from the region j that precipitates in region i, T is the diagonal export matrix, whose elements are equal to the fraction of water vapour evaporated in each region i that diverges, and the vector of evaporation contains the evaporation for each region i.

2.2. Lagrangian models

The Lagrangian formalism applied to moisture transport relies on the analysis of both forward and backward trajectories of a certain number of particles dispersed in the atmosphere, and simulating the trajectories followed by the humid air parcels.

Stohl and James (2004, 2005) developed a methodology to account for the net loss and gain along trajectories using:

$$E - P = \frac{\sum (e - p)_k}{A} \tag{5}$$

for the dispersion of K particles over an area A, where for each particle:

$$(e - p)_k = m\frac{dq}{dt} \tag{6}$$

Numerous authors have been able to provide source-sink analyses for various regions (e.g., Gimeno et al., 2012). Within this simple framework, regions where $E-P > 0$ in backward analyses can be considered as sources, while regions where $E-P < 0$ in forward analyses can be considered as sinks.

In recent years, plenty of bibliographies have also provided improvements to and discussions on these Lagrangian methodologies.

Sun and Wang (2014) introduced what they termed the *areal source-receptor attribution method*. This extension to the traditional methods allows the determination of the contribution of different previously selected regions to the total release of moisture over the region of interest. They applied this characteristic to results obtained by FLEXPART model (Stohl and James, 2004, 2005) to analyse the moisture sources for a semiarid grassland in China. Under their scheme, the partial contribution to the release of moisture in the target region from each of the source regions can be determined. This approach typefies Eulerian mesoscale tracer tools (e.g., Eiras-Barca et al., 2017), which are computationally more expensive than their Lagrangian counterparts.

De Leeuw et al. (2017) introduced a technique that quantifies the amount of precipitation in terms of the variability of each of the physical processes involved, under the hypothesis that:

$$P \propto ST \times LOC \times AI \times AF \times NT \tag{7}$$

where ST is the surface temperature, LOC the location of origin, AI the ascent intensity, AF the ascent mass fraction, and NT the number of analyses over a given period of production of precipitation. They also applied this technique to the ROTRAJ model (Methven, 1997) in the analysis of summer precipitation over England and Wales.

Pérez-Muñuzuri et al. (2018) discussed the inconvenience of considering a constant mass of particles in Eq. (5). In particular, they achieved more realistic results in the analysis of Atmospheric River events over the Iberian Peninsula and the US West Coast when they considered accelerations due to external forces. Under this model, active tracers can be modelled by the momentum equation (e.g., Pérez-Munuzuri and Garaboa-Paz, 2016) rather than merely by following streamlines.

2.3. Eulerian regional models

Even though the analysis of moisture transport in the atmosphere has been classically addressed through the dispersion of particles within a Lagrangian framework, some of the more recently developed Eulerian water vapour tracers allow the exploration of source-receptor relationships, taking into account both grid-scale and parametrisation-solved interactions applied to global climate models or mesoscale models.

Where a tracer tool can be coupled to Eulerian global or regional models, changes in the source of moisture throughout the simulation are commonly analysed as:

$$\frac{\partial q_n}{\partial t} = -\vec{U}\cdot\nabla q_n + \nu_q\cdot\nabla^2 q_n$$

$$+\left(\frac{\partial q_n}{\partial t}\right)_{PBL} + \left(\frac{\partial q_n}{\partial t}\right)_{microph} + \left(\frac{\partial q_n}{\partial t}\right)_{cum}$$

where the first term represents advective processes, the second term accounts for molecular diffusion, and the remainder of the terms may take into account changes in moisture related to the planetary boundary layer, microphysics, and cumulus parametrisations, respectively. n represents the different species of moisture under consideration, including possibly vapour, cloud water, rainwater, snow, ice, and graupel.

One example of a recently developed tool that follows this formalism is the WRF Water Vapour Tracer (WRF-WVT), which provides a tracer capability to the well known Weather Research and Forecast (WRF) mesoscale model. The details of this tool can be found in Insua-Costa and Miguez-Macho (2018). This tool was previously applied to the analysis of the moisture recycling ratio in the Iberian Peninsula (Rios-Entenza et al., 2014), the analysis of moisture sources associated with the North America monsoon (Dominguez et al., 2016) and Atmospheric Rivers (Eiras-Barca et al., 2017), and more recently in the analysis of the fate of the moisture transported by the Great Plains Low-Level Jet (Algarra et al., 2019).

WRF-WVT is embedded within WRF and reproduces Eq. (4) for moisture contained within (3D feature) or previously evapotranspirated from (2D feature) a specific region labelled as a 'mask'. The fate of this tagged moisture of any species is followed throughout the domain of the simulation, and its changes of phase in the form of precipitation are analysed separately from the remainder of the total precipitation. The tool allows the identification of sinks of moisture from a forward perspective, together with the analysis of recycling ratios, among other applications.

At the same time, Knoche and Kunstmann (2013) implemented an analogous evaporation tagging (E-tagging) mechanism applied to the Eq. (4)-equivalent in the MM5 model, and they applied the tool in the analysis of recycling in West Africa. This formulation of MM5 was later extended and applied to the analysis of recycling in Southeast China by Wei et al. (2015).

A similar evaporation E-tagging tool to the WRF-WVT, and one which was also coupled to WRF, is presented in Arnault et al. (2016) where the authors also analysed precipitation recycling for West Africa.

Goessling and Reick (2013) showed that less expensive offline 2D WVT models achieve similar conclusions to 3D E-tagging tools only if the assumption of a 'well-mixed' vertical column is actually met. When it is not, errors occur due to rapid recycling, and advective processes tend to cause the results to diverge, which is a normal characteristic of

barotropic atmospheres.

2.4. Physical tracers

The use of stable water isotopes in climatology may be a useful means of providing a unique fingerprint of the origin of the water. Widely used in the interpretation of paleoclimatic proxy records, these physical tracers are commonly used in the interpretation of moisture sources. Although significant steps have been made in recent years regarding measurement techniques and the incorporation of isotopes in models, the fundamental theory of Craig (1961) and Dansgaard (1964) still applies.

The two stable isotopes of Hydrogen observable in nature, ^{1}H and ^{2}H (the latter usually being referred to as D for "deuterium") may combine with any of the three stable isotopes of Oxygen (^{16}O, ^{17}O, and ^{18}O) to create nine possible combinations of isotopologues, of which four are measured in nature with significant ratios in terms of their prevalence: $^{1}H_2{}^{16}O$ (~ 99.7%), $^{1}H_2{}^{18}O$ (~ 2‰), $^{1}H_2{}^{17}O$ (~ 0.5‰), $^{1}HD^{16}O$ (~ 0.3‰) (e.g., Jouzel et al., 2013).

The fraction of heavier isotopes over lighter ones is conventionally expressed using:

$$\delta = \left(\frac{R_{sample}}{R_{VSMOW}} - 1\right)\cdot 1000[‰]$$

where R_{sample} is the ratio of heavier isotopes over lighter ones for both hydrogen and oxygen and R_{VSMOW} is given by the Vienna Standard Mean Ocean Water (VSMOW) conventionalism:

$$R_{VSMOW,18O} = \left(\frac{^{18}O}{^{16}O}\right)_{average} = (2005.20 \pm 0.45)\cdot 10^{6}$$

$$R_{VSMOW,2H} = \left(\frac{^{2}H}{^{1}H}\right)_{average} = (155.95 \pm 0.08)\cdot 10^{6}$$

Heavier and lighter water both tend to show different behaviours at phase changes. Lighter water diffuses more rapidly and evaporates preferentially, while heavy molecules condense preferentially (Allen et al., 2017). This process, known as *equilibrium fractionation,* occurs at each phase change apart from sublimation and melting for compact ice, and is explained by the differences in latent heat for each change, due to differences in saturation vapour pressures and molecular diffusivity between the isotopologues. Is it noteworthy that no fractionation occurs in transpiration from plants. Thus, evaporated water is lighter than transpirated water.

The *meteoric water line* (MWL) relates $\delta^{18}O$ to δD via the well-known linear equation:

$$\delta D = 8\delta^{18}O + D - excess$$

Where D-excess provides some insight into the degree to which the precipitation has been affected by *kinetic fractionation* rather than *equilibrium fractionation* (Yoshimura, 2015).

Rayleigh distillation explains the linear relationship:

$$R = R_0 f^{\alpha-1}$$

where R_0 is the initial isotopic ratio, f is the fraction of the original moisture remaining after the phase change, and α is the fractionation factor that governs the phase change under equilibrium conditions, according to:

$$\alpha_{v,l}^{18O} = \frac{R_l^{18O}}{R_v^{18O}} = exp\left(\frac{1137}{T^2} - \frac{0.4156}{T} - 0.002067\right)$$

$$\alpha_{v,l}^{D} = \frac{R_l^{D}}{R_v^{D}} = \exp\left(\frac{24840}{T^2} - \frac{76.25}{T} + 0.0526\right)$$

where l and v respectively refer to the liquid and vapour state and T denotes the dependence of the fractionation process on temperature.

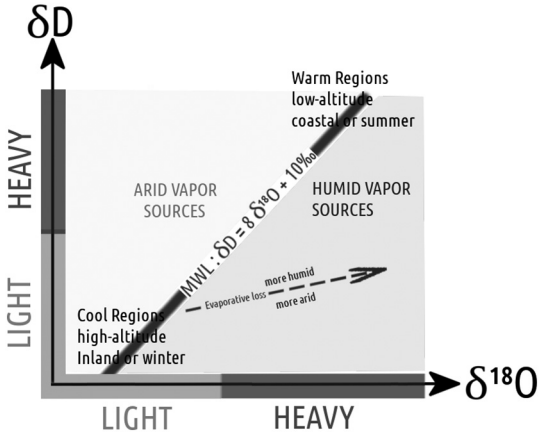

Fig. 1. Simple scheme summarising basic properties inferred from measurements regarding the meteoric water line and deviations from it, based on http://web.sahra.arizona.edu/programs/isotopes/oxygen.html.

Fig. 1 summarises the implications of this dependence through which the properties of the origin of water measured both in liquid or vapour states over the target area may be inferred.

Over the last decade, advances in the science of stable isotopes in both water vapour and precipitation have been continuously incorporated into all kinds of models. Eulerian general circulation models (GCMs, e.g., the SPEEDY-IER model, Dee et al., 2015), Eulerian regional circulation models (RCMs, e.g., the COSMO model, Pfahl et al., 2012), Lagrangian models along with Eulerian last-saturation tracers (e.g., Hurley et al., 2012), or even inverse modelling techniques of in-situ measurements (e.g., Galewsky and Rabanus, 2016) have been improved, developed and used widely both for model validations and analyses of moisture sources and paleoclimatic conditions. An in-depth review of the history and current advances in this area can be found in Yoshimura (2015) and Galewsky et al. (2016).

Regarding the techniques of measurement, ever since Dansgaard (1954) presented the first (both water vapour and precipitation) samples using freezing with dry ice and alcohol, numerous approaches have been developed and improved, some of them in more recent years.

Near-infrared laser absorption spectroscopy in-situ techniques have also been applied, together with the widely used Picarro cavity ring down spectroscopy (Crosson et al., 2002) and Los Gatos Research integrated cavity output spectroscopy (Baer et al., 2002), among others. A set of custom-made and commercial spectral analysers (such as the ISOWAT-II instrument, Dyroff et al., 2010) have been deployed in recent years on aircraft missions to measure isotope concentrations, both in the troposphere and the lower stratosphere (e.g., Landsberg et al., 2014). A detailed review of these methodologies together with some key results can be found in Galewsky et al. (2016).

With regard to remote sensing, some remarkable advances have been made possible using observations from space. For instance, the sunlight reflected in the shortwave infrared has been used by Frankenberg et al. (2013) and Boesch et al. (2013) to estimate concentrations of $^{1}H^{2}HO$ and $^{1}H_2O$. Especially notable are the δD dataset obtained from the MUSICA MetOP infrared atmospheric sounding interferometer, which was recently applied in the validation of moisture dispersion models (e.g., Schneider et al., 2017), and the TES high-resolution infrared-imaging Fourier transform spectrometer owned by NASA, with the largest available tropospheric water isotopologue dataset (e.g., Worden et al., 2012).

3. The question of residence time of water vapour

One of the key parameters of interest in the understanding of the global hydrological cycle is the residence time of water vapour in the

atmosphere. Classical studies based on the balance between the incoming or outgoing flux, the ratio between water in the local atmospheric column and evaporation/precipitation, or the use of age tracers in the global circulation model have all shown residence times of around 8–10 days (see van Der Ent and Tuinenburg (2017) for a review). This value is important not just from a theoretical point of view, but also because it has a clear influence on the estimation of other characteristics of the hydrological cycle, for instance in the determination of moisture sources and sinks.

Traditionally, in order to determine time scales for the assessment of moisture sources, the nearly 10-day threshold for residence of water vapour in the atmosphere is generally used. However, not only does this time vary spatially, but it is highly dependent on processes such as advection, entrainment, phase changes, and diffusion. Hence, using a fixed integration time may neglect both large- and eddy-scale processes affecting the concentration of water vapour, changing the saturated vapour pressure, modifying the transport or modulating rainout processes. From a global point of view, the use of a value of 10 days has been widely used as a result of the global water balance. This value was challenged by Läderach and Sodemann (2016), based on offline tracking methods; they proposed that a shorter scale of 4–5 days would be more appropriate. However, van Der Ent and Tuinenburg (2017) used reanalysis and modelling to derive residence time based on evaporation and precipitation, their results confirming the 8–10 day threshold as a global mean residence time for atmospheric moisture, and similar findings were also reported by Wang et al. (2018) over large continental areas. The authors highlighted a 2-day difference in residence time between ocean and land, the complexity of residence time of precipitation, and the presence of long-tailed PDFs with global medians of 5 days. Tuinenburg and van der Ent (2019) followed up on the problem of the detected variations in the daily cycle of atmospheric moisture residence time resulting from differences in the surface fluxes for various models. They concluded that there was a likelihood of a weaker daily cycle of residence time for ERA-I dataset to be an artefact of the surface flux forcing for the model, and attributed the differences in residence time between land and ocean to the effects of transpiration.

In a recent study, Nieto and Gimeno (2019) proposed a different focus for this scientific problem by identifying the optimal time of integration for Lagrangian studies, the most widely used parameter in the identification of moisture sources, rather than searching precisely for the residence time of water vapour. Fig. 2 shows the annual average of values of residence time for Läderach and Sodemann (2016), van Der Ent and Tuinenburg (2017), and integration times for Nieto and Gimeno (2019).

A simple comparisson suggests that the times found by Nieto and Gimeno (2019) over continents are more similar to van Der Ent and Tuinenburg (2017). For instance, over the Amazon basin 9–12 days were estimated in both studies, but the half by Läderach and Sodemann (2016). This fact also occur over Europe or Central Africa, showing that regionally the choice of a methodology could affect the results in the moisture quantification and it is critical for the identification of moisture sources and sinks.

4. Studies of source and sink regions

Following the moisture source-sink assessments made at the global scale (e.g., Rasmusson and Mo, 1996; Yanai and Tomita, 1998; Knippertz et al., 2013; Nieto et al., 2014), the scientific community has now turned to more specific local studies. In the last few decades a number of authors have investigated moisture transport at a regional scale. A summary of the main results obtained by continent is presented below, and a synthesis of the link between sinks and sources of moisture as found in the literature is presented in Fig. 3. Lines on the figure do not represent specific paths of moisture transport, rather they only relate to those areas that may affect regional precipitation.

4.1. Europe

Moisture transport towards Europe is strongly influenced by the North Atlantic contribution of cyclonic activity or Atmospheric Rivers (ARs) (e.g., Lavers and Villarini, 2013a, 2015). Lavers and Villarini (2015) showed that more than 30% of the mean monthly precipitation over Western Europe is linked with AR occurence; this percentage is even higher if only extreme precipitation is considered (Lavers and Villarini, 2013a). Many authors have identified the Atlantic Ocean as an important moisture source for Europe not only in autumn and winter, but also in summer months (e.g., Sodemann and Stohl, 2013; Gómez-Hernández et al., 2013). Over northern European regions such as Norway and Sweden, the Atlantic to the north of 50°N contributes significantly to precipitation events (Sodemann and Stohl, 2013; Gustafsson et al., 2010) – it was found that most of the moisture contribution over the Norwegian coast in December 2006 came from the North Atlantic between 50° and 70°N. Over this region, southern areas of the Atlantic Ocean increase their contribution associated with ARs (Sodemann and Stohl, 2013). The influence of the Atlantic Ocean over Eastern Europe was also identified, for example over France (Gómez-Hernández et al., 2013) and the Iberian Peninsula (Gimeno et al., 2010; Gómez-Hernández et al., 2013). In both cases the influence of this source is greater in winter. The Atlantic moisture contribution is not limited to the western sector; several studies have shown its effect over regions further east such as the Balkan Peninsula (Gómez-Hernández et al., 2013; Ciric et al., 2016), Italy (Gómez-Hernández et al., 2013) and Central Europe, where it is the major source of precipitation for the northern Alpine region, with a contribution of almost 40% of the annual moisture over this region (Sodemann and Zubler, 2009).

The influence of the Mediterranean and other enclosed Seas such as the Black and Caspian Seas on European precipitation was also demonstrated by several authors. For the Mediterranean, despite the contribution from this source being more intense over southern Europe, it actually affects most of the continent (Nieto et al., 2010). The Western Mediterranean modulates the seasonality of the Alpine precipitation, the maximum values from August to September being associated with an increase in moisture contribution from this area (Sodemann and Zubler, 2009). This region was also identified as an important moisture source for the Iberian Peninsula, Italy, France (Gómez-Hernández et al., 2013), and the Danube river basin (Ciric et al., 2016), and is the main winter moisture source over most of southern Europe (Gómez-Hernández et al., 2013; Ciric et al., 2016).

Finally, despite most of the moisture sources identified in the literature all having oceanic origins, some continental areas of Europe have been seen to be moisture sources in some cases, especially in dry months (spring and summer). Some authors have suggested the importance of recycling in precipitation over the Balkan Peninsula (Gómez-Hernández et al., 2013; Bisselink and Dolman, 2008; Ciric et al., 2016), especially for wet summers (Bisselink and Dolman, 2008); it was also identified as an important source of moisture over Central Europe (Sodemann and Zubler, 2009), Italy, France, and the Iberian Peninsula (Gómez-Hernández et al., 2013) during the dry season. Moisture sources with continental origins clearly gain in importance under dry conditions.

4.2. Asia and Oceania

The moisture sources for Asia show important regional differences. Over China three main contributors were detected by several authors, namely the Indian Ocean (mainly the Bay of Bengal), the western Pacific, and continental parts of Central-Eastern Asia (Sun and Wang, 2015; Wang and Chen, 2012; Wei et al., 2012; Drumond et al., 2011a; Hu et al., 2018; Ma et al., 2018). The oceanic moisture contribution in summer over this area, especially over Southern and Eastern China, was shown to be linked with the Indian and East Asian monsoon (Sun and Wang, 2015; Wang and Chen, 2012; Ding et al., 2009; Baker et al.,

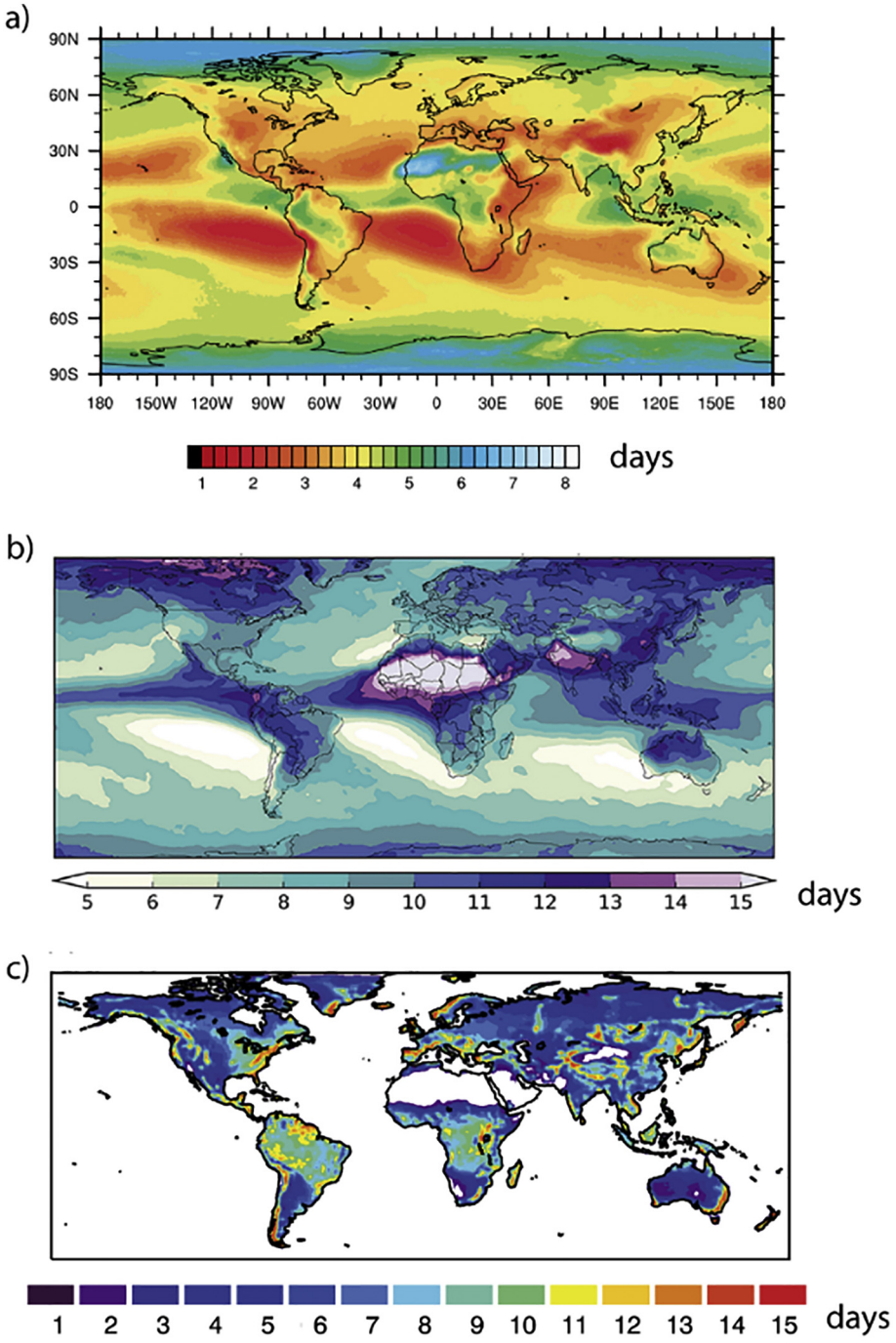

Fig. 2. Annual average of values of residence time in days using ERA-I dataset for (a) Läderach and Sodemann (2016) for 1979–2013, (b) van Der Ent and Tuinenburg (2017) for 2002–2008, and (c) the optimal integration times over continents for Lagrangian approaches by Nieto and Gimeno (2019) (arid region are neglected and plotted in white) for 1980–2015.

2015). Despite some works having attributed the origin of precipitation over China mainly to oceanic regions (Pan et al., 2017; Wang and Chen, 2012; Bin et al., 2013; Chen et al., 2012), several other studies have highlighted the importance of moisture recycling and external continental sources, considering them to be primary moisture sources, especially over northern and inland regions (Drumond et al., 2011a; Wei et al., 2012; Sun and Wang, 2015; Ma et al., 2018; Hua et al., 2017) and showing their interannual variability (Guo et al., 2018). The influence of the sources varies not only regionally but also seasonally. Despite the Pacific Ocean or the land areas being important contributors throughout the year, the Indian Ocean shows higher moisture contributions in the summer months (Baker et al., 2015; Sun and Wang, 2015).

For northern Asia, only a few analyses of moisture transport are available. Stohl and James (2005) analysed the moisture transport between oceanic regions and river basins, including the north Eurasian Lena, Ob, and Yenisey basins. Their results, realised as an annual mean, identify recycling and continental local evaporation as the main sources for the three basins. Only for the Ob basin does the oceanic contribution from the Atlantic seems to have any influence. A similar analysis for the winter season was undertaken by Gimeno et al. (2015), in which the Atlantic Ocean and the Mediterranean Sea were identified as the main moisture sources, considering the total area of all three river basins.

Over India, the Indian Ocean is found to be one of the main moisture

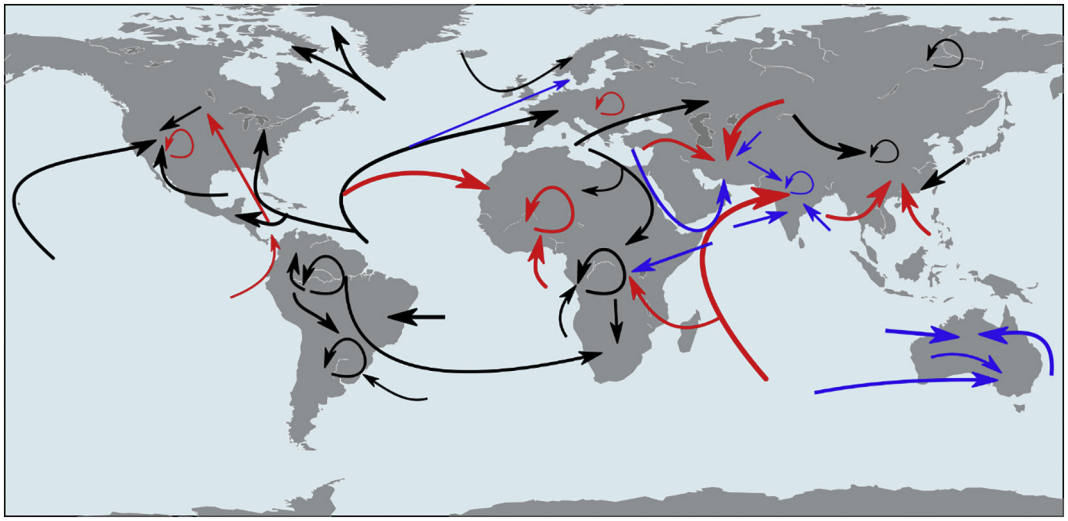

Fig. 3. Links between main regional sinks and sources as found in the literature. Red and Blue arrows represent the moisture transport associated with boreal summer and winter months respectively. Black arrows represent sources that appear in both seasons. A looped arrow represents moisture recycling. (For interpretation of the references to color in this figure legend, the reader is referred to the web version of this article.)

sources, especially in summer, however the source is west of that of China, with the greatest moisture uptake located over the Arabian Sea and the North African coast (Ordóñez et al., 2012; Pathak et al., 2017). This moisture transport path is associated with the Somali Low-Level jet that occurs in summer. The Indian Ocean moisture contribution over India is lower in winter and the moisture uptake is limited to the northern part of the Ocean, including the Arabian Sea and the Bay of Bengal. Recycling is an important source in winter (Ordóñez et al., 2012). According to Pathak et al. (2017), the Ganga river basin is the main continental moisture source in summer; however, continental regions to west of India were found to be important Indian contributors by Ordóñez et al. (2012). Finally, over the Middle East, the contribution of the southern Indian Ocean is decreasing (Heydarizad et al., 2018a; Athar and Ammar, 2016). In the summer months, the moisture contribution from the Indian Ocean is still relevant (Heydarizad et al., 2018a; Athar and Ammar, 2016); however its effect is limited to southern areas over the Arabian Peninsula or southwestern Iran and southern Pakistan (Athar and Ammar, 2016; Ullah and Gao, 2012). For this season, an important continental moisture source was discovered by Heydarizad et al. (2018a) to affect moisture transport over Iran, these results being in agreement with the southwestward moisture flux observed by Athar and Ammar (2016) over the Middle East. In winter, the main moisture sources are located over the oceanic areas close to the region. The Red Sea is an important moisture source for the region, and there is also an important contribution from the Arabian Sea and the Gulf of Persia (Heydarizad et al., 2018a; Athar and Ammar, 2016; Zolina et al., 2017). Some moisture contribution was also observed from the Mediterranian Sea (Heydarizad et al., 2018a; Athar and Ammar, 2016), and recycling was also found to be relevant over Iran (Heydarizad et al., 2018a).

Over Oceania, some authors investigated the moisture transport towards Australia in austral summer, when most of the annual precipitation occurs. Over the northeastern region, most of the moisture reaches Australia from the Coral Sea (Berry et al., 2011; Ackerley et al., 2014). Over the western part, this moisture source is still relevant and is associated with the variability of rainfall; however, for this region, the Indian Ocean was also found to be an important contributor (Berry et al., 2011; Ackerley et al., 2014). Over the southern part, the moisture contribution is linked with transport from the Indian Ocean (Guan et al., 2013; Barras and Simmonds, 2009), being especially associated with frontal systems (Guan et al., 2013). Continental areas were also found to act as moisture sources for the region, associated with synoptic low-pressure and trough systems (Guan et al., 2013)

4.3. North America

Two main source regions were identified for the United States by Vachon et al. (2010), namely the Pacific Ocean and the Gulf of Mexico. Over the Eastern part of the continent, the moisture contribution comes from the Eastern Atlantic and the Gulf of Mexico and is associated with the path of tropical and extratropical cyclones (Xu et al., 2017; Knight and Davis, 2007). However, over higher latitudes such as Greenland or the Canadian Archipelago the main moisture contribution is from nearer oceanic areas from the northern Atlantic Ocean (Sodemann et al., 2008; Kopec et al., 2016). Over the central US in spring and summer, the precipitation is strongly influenced by the Great Plains Low Level Jet (GPLLJ), which provides moisture from the Gulf of Mexico and the Caribbean Sea (Knippertz and Wernli, 2010). In general terms, the Atlantic was found by a number of authors to influence the variability of precipitation over the central US via southerly moisture transport associated with the GPLLJ (Ruiz-Barradas and Nigam, 2005; Wang et al., 2006, 2008; Drumond et al., 2011b), and was also suggested to contribute to moisture transport towards the eastern US (Drumond et al., 2011b).

On the west coast of the United States, the main source of moisture is the Pacific Ocean for all seasons, but especially in winter. In the other seasons, the contributions from the Gulf of Mexico, the Gulf of California, and land areas are more important (Bracken et al., 2015). Over the Southwestern United States, summer precipitation is especially important given that it provides most of the annual rainfall (Carleton et al., 1990) and that this precipitation is strongly linked with the North American monsoon (NAM) (Ropelewski et al., 2005). The moisture contributions from these three sources in summer over the western US was found by several authors to be associated with the monsoon (Ordoñez et al., 2019; Higgins et al., 2004; Dominguez et al., 2016). Hu and Dominguez (2015) found that continental regions provide more than 40% of the moisture contribution to the NAM precipitation, and the importance of evapotranspiration sources was also noted by Bohn and Vivoni (2016). In winter, the origin of precipitation over western North America was suggested to be associated with extratropical cyclones and ARs from tropical and subtropical regions (Ralph et al., 2004; Roberge et al., 2009; Lavers and Villarini, 2015; Bao et al., 2006). A tropical moisture source near Hawaii was found to affect precipitation over the western United States and Canada, associated

with ARs (Knippertz and Wernli, 2010; Roberge et al., 2009).

4.4. Central and South America

Over Central America and northeastern South America, two main regions are suggested as moisture sources, namely the Caribbean Sea and the equatorial Pacific region (Durán-Quesada et al., 2010, 2012, 2017; Esquivel-Hernández et al., 2019). According to Durán-Quesada et al. (2010), the Caribbean Sea is the main moisture source for the all seasons over Central America, affecting entire region. However, the Pacific contribution only appears in summer and autumn, and its effect is restricted to southern regions of Central America. Despite the lesser effect of the Pacific Ocean on moisture availability for Central America, it has been shown to influence the variability of the precipitation (Durán-Quesada et al., 2017; Gallego et al., 2019). In addition to the Caribbean Sea, the warm waters of the Atlantic (commonly termed the 'warm pool' (WP)) were found to contribute to precipitation over the Caribbean region (Wang et al., 2006, 2008). Furthermore, Arias et al. (2015) found that the tropical Atlantic influences wet-weather events over northern South America. Over northeastern South America, the influence of the Pacific source is greater than over Central America (Durán-Quesada et al., 2012), despite their small contribution (Durán-Quesada et al., 2012; Windhorst et al., 2013). Moreover, for this region, continental sources over South America become relevant for moisture transport (Durán-Quesada et al., 2012; Esquivel-Hernández et al., 2019; Windhorst et al., 2013; Hoyos et al., 2018). In particular, the moisture contribution from the Amazon basin was suggested by several authors (Hoyos et al., 2018; Esquivel-Hernández et al., 2019). In general terms, the moisture transport towards Central and northeastern South America was associated with a regional LLJ (Durán-Quesada et al., 2017; Sakamoto et al., 2011; Arias et al., 2015; Gallego et al., 2019; Esquivel-Hernández et al., 2019; Hoyos et al., 2018) and the ENSO was also shown to influence the transport (Silva et al., 2009).

Over the Amazon region, the tropical Atlantic is the main moisture source all year round (Drumond et al., 2014; Satyamurty et al., 2013a). This source shows seasonal variability, being the greatest contributor to the tropical North Atlantic in austral summer and showing a greater contribution to the south in the remaining seasons (Drumond et al., 2014; Durán-Quesada et al., 2012). Recycling from the Amazon basin was also found to be relevant over the region. Satyamurty et al. (2013a) found that recycling contributes around 37 and 16% to the moisture over the region in wet (October to April) and dry (May to September) seasons, respectively. Their results are in agreement with other findings (e.g., Drumond et al., 2014; Bosilovich and Chern, 2006; Burde et al., 2006). The evapotranspiration over the Amazon region also provides moisture for recycling.

The Amazon region was found to be an important source of moisture for several regions over South America; especially over the La Plata river basin and adjacent regions (Zemp et al., 2014; Martinez and Dominguez, 2014; Drumond et al., 2014), or as previously highlighted, over northern regions of South America. Over the La Plata river basin, the Amazon was found to be the second highest continental contributor for mean annual precipitation by Martinez and Dominguez (2014), with local recycling over the La Plata basin being the main source. Over this region, continental areas were found to be the main sources by several authors (Drumond et al., 2008; Martinez and Dominguez, 2014). Moreover, external sources from the southern Pacific and the Tropical Atlantic are also found to contribute to precipitation in the basin (Drumond et al., 2008; Martinez and Dominguez, 2014). Drumond et al. (2008) highlighted the influence of the tropical Atlantic Ocean, which varies seasonally from the northern regions in austral summer months to southern ones in winter, when the oceanic contribution is higher (Martinez and Dominguez, 2014).

4.5. Africa

Over Africa, the movement of the ITCZ and the monsoon each govern the precipitation cycle (Hagos and Cook, 2007). Over western Africa and the Sahel, the wet season occurs between March and September and is characterised by the seasonal wind shift produced by the heat contrast between the Sahara and the Atlantic Ocean (Peyrillé et al., 2007; Thorncroft et al., 2011). Several studies have found that most of the low level moisture transport associated with the wet season over the Sahel (July to September) comes from the Gulf of Guinea; the eastern part of Atlantic Ocean is also identified as an important source of moisture for the region (eg Lélé and Leslie, 2016; Lélé et al., 2015; Thorncroft et al., 2011; Sorí et al., 2017a). Despite the higher moisture transport from the Gulf of Guinea, the westerly transport associated with the LLJ has a clear influence on the rainfall pattern over western Africa (Mera et al., 2014; Fontaine et al., 2003; Grams et al., 2010), being highly correlated with the Sahelian variability of precipitation (Pu and Cook, 2012). The flux from the ocean towards western Africa becomes clear when Eulerian approaches are applied (e.g., Lélé et al., 2015; Thorncroft et al., 2011). However, Lagrangian experiments have also highlighted the continental and recycling contributions over this area. Nieto et al. (2006), for example, stated that recycling over the Sahelian region is greater than the contribution from external moisture sources, and it was furthermore found to be a relevant moisture source over the Niger river basin by Sorí et al. (2017a).

Over the northern coast of Africa (north of 25°N), the influence of moisture from the Gulf of Guinea disappears altogether. Over the western part, the main source is the eastern Atlantic Ocean; however, this influence diminishes with longitude as the Mediterranean Sea gains in importance, and the Mediterranean is the main source over Eastern North Africa (Gómez-Hernández et al., 2013; Drumond et al., 2011c). The moisture contribution from the Mediterranean Sea to Africa as a whole was also demonstrated in several studies, not only over Northern Africa but also further south. Analysis of not only the boundary layer but also the total tropospheric moisture flux shows that the moisture contribution from the Mediterranean Sea is significantly higher over the Sahelian region and western Africa (Fontaine et al., 2003). Fontaine et al. (2003) found that most of the atmospheric moisture over this region has a northerly origin if the total flux in the 1000–300 hPa layer is integrated; they concluded that the transport from the Mediterranean is especially relevant for low-level convergence over the Sahelian belt. Nieto et al. (2006) also identified this Sea as the main moisture source for the Sahel if recycling is not taken into consideration.

Moisture flow from the Mediterranean Sea was also observed over Central Eastern Africa including Ethiopia; however, over this region the contribution from the Indian Ocean, the Congo Basin, and the Red Sea was shown to have a greater impact on Ethiopian precipitation (Viste and Sorteberg, 2013a, 2013b). Sorí et al. (2017b) investigated the moisture transport over the Congo, in western Central Africa, finding that recycling is the main moisture source here. Other important moisture contributors include the Atlantic Ocean. Despite the fact that some important moisture uptake was found over the Red Sea and the Indian Ocean towards the region, results indicate that these sources have little effect.

Over southern Africa, it is traditionally the southwestern and tropical Indian Ocean that is identified as the main moisture source (Washington and Preston, 2006), with the tropical flow being especially associated with wet austral summer events (Cook et al., 2004; Hart et al., 2010). Moreover, the Atlantic Ocean was also found to be an important contributor over this region (Vigaud et al., 2006, 2009), with this source being especially relevant over the western part of South Africa in winter (Reason and Jagadheesha, 2005; Ramos et al., 2019). In winter, most of the precipitation is associated with cyclonic activity across the Atlantic Ocean (Reason and Rouault, 2005; Stager et al., 2012). Recently, Ramos et al. (2019) pointed out the contribution from South America to precipitation in southern Africa during winter,

associated with ARs. Although most studies of South African precipitation have identified the main sources as external oceanic ones, continental sources from northern parts of Africa were also found to contribute to precipitation here (Jack, 2012).

5. Atmospheric moisture transport and extreme events: anomalies of moisture transport linked to droughts and floods

The source-sink relationship for atmospheric water vapour can be used to assess the causes of strong precipitation events and floods, as well as the longer-term variability of rainfall and drought (Gimeno, 2013). The past decade has seen a growing number of studies that have employed different methods and techniques to try to achieve this goal for various regions worldwide.

5.1. Atmospheric moisture transport and drought

The term drought refers to a prolonged dry period in the natural climate cycle, initially caused by a lack of rainfall, which can occur anywhere in the world (WMO, 2012), and which propagates through the hydrological cycle. It is a complex phenomenon that is difficult to predict and one of the most important natural disasters to affect the planet. To explain the role of the atmospheric branch of the hydrological cycle during the most severe meteorological drought events for 27 reference regions identified by the Intergovernmental Panel on Climate Change (IPCC) for 1980–2015, Drumond et al. (2019) applied a Lagrangian model to track air parcels along their trajectories in order to compute the moisture contribution to precipitation *((E – P) < 0)* over each region from the climatological moisture sources. Their results are contained in a catalogue, in which quantitative values allow a clear evaluation of possible relationships and permit inter-comparisons to be made between global climatic regions. The approach implemented is represented in Fig. 4, which shows each of the steps involved, yielding the moisture contribution from each climatological source during a drought episode in the Amazon region. In this way, according to the relative entropy calculated at each point between the evaporative source averaged over the three driest years in the period 1979–2005 (based on GPCP precipitation), when arid and semiarid regions suffer from drought, there are large changes in the patterns of evaporative moisture sources (Dirmeyer et al., 2014). The same approach as that used by Drumond et al. (2019) and initially proposed by Stohl and James (2004, 2005) has been used in modelling studies for similar purposes, at a regional scale and for almost all continents (Table 1).

5.1.1. Europe

For record-breaking droughts affecting western and central Europe from July 2016 to June 2017, the reduction in moisture transport from the Atlantic had an effect in the northern part (García-Herrera et al., 2019). A coherent reduction in moisture contribution from the Mediterranean Sea to central-eastern Europe and the eastern Mediterranean was also noted by Drumond et al. (2017) during the most severe summer and winter droughts from 1980 to 2012. The Mediterranean Sea, and also the North Atlantic Ocean, are found to be key regions from which a reduction in moisture transport to the European region is associated with the most severe drought episodes over the last few decades in this region (Stojanovic et al., 2017, 2018a, 2018b). In these studies, the authors agree that the efficiency of the moisture supply from the sources to the European region depends on large-scale atmospheric circulation, atmospheric blocking, and dynamical conditions. A reduction on the moisture release from the tropics has been also associated with dry extremes (e.g. in 2005) in the Loire River basin in France (Lu and Hao, 2017), when there is significantly insufficient supply of moisture.

5.1.2. Asia and Oceania

In Asia, monsoons are the most important atmospheric systems in the modulation of precipitation during the rainy season. If the onset of the monsoon in the Arabian Sea and the Bay of Bengal is signalled by a change in the direction of the wind and the integrated moisture transport, the summer monsoon then starts earlier in the Bay of Bengal than in the Arabian Sea, and the phase difference is likely to be the cause of pre-monsoon drought in India (Liu and Xie, 2017). Severe and extreme drought conditions in major river basins such as the Indus, Ganges and Brahmaputra during 1980–2017 were directly related to a reduction in the contribution to precipitation from their climatological moisture sources (the Indian region, the basins themselves, the Indian Ocean (Arabian Sea, Bay of Bengal) (Sorí et al., 2017c)). In south-western China, the recent decrease in dry-season precipitation and severe droughts have coincided with a decline in southwestern moisture transport, in addition to mid-latitude changes in circulation (Xin-Gang et al., 2015). In further analysis, Zhang et al. (2017) used a Water Accounting Model to reveal that the decline in June-August-September precipitation over south-western China is principally triggered by a change in the seasonal-mean component rather than the transient

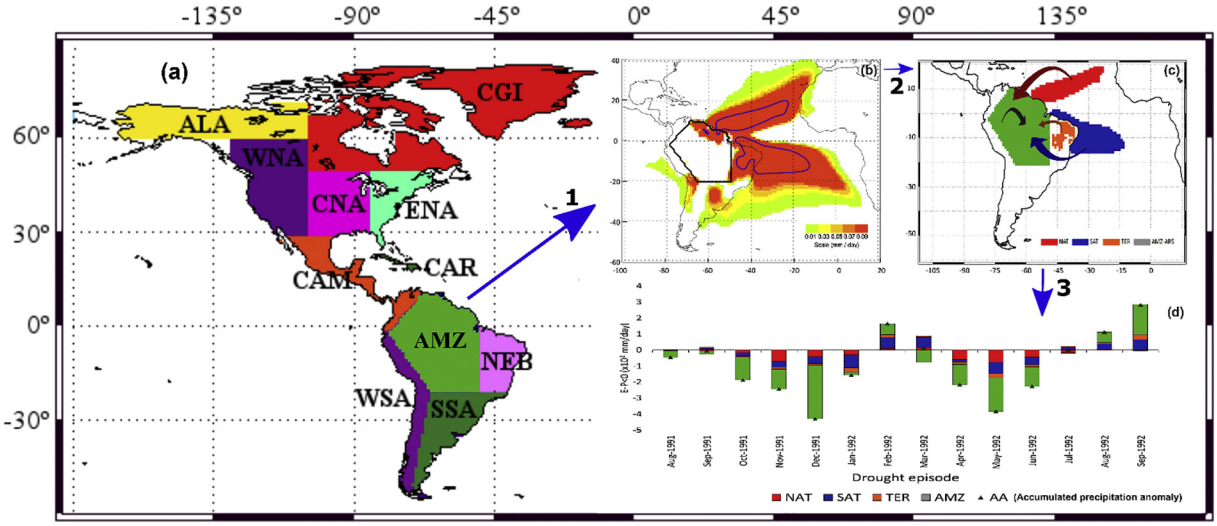

Fig. 4. Schematic representation of: 1- Identification of the Amazon (AMZ) (a) annual climatological moisture sources obtained by computing (E − P) along paths of air masses backwards in time from AMZ (b) 2 – Delimitation of the most important regions acting as sources of moisture (c) 3 – Forward tracking of air masses from each source and computation of (E − P) < 0 over AMZ (d) Adapted from Drumond et al. (2019).

Table 1
Descriptive information on drought events and the relationship with atmospheric moisture.

Affected region	Event/Date	Related to	Technique applied	Reference
Worldwide				
Worldwide IPCC regions	Extreme drought events from 1980 to 2014	Anomalous moisture supply from climatological moisture sources	Lagrangian	Drumond et al. (2019)
Semiarid and arid regions worldwide	Three driest years/in the period 1979–2005	Where precipitable moisture often has a relatively long path, generally have more distant sources during droughts than wet periods	Lagrangian	Dirmeyer et al. (2014)
Europe				
Northern Europe	Extreme year: July 2016 to June 2017	Anomalous moisture contribution from the North Atlantic ocean	Lagrangian	García-Herrera et al. (2019)
Central-eastern Europe and the eastern Mediterranean	Most severe summer and winter droughts from 1980 to 2012	Anomalous moisture contribution from the Mediterranean Sea	Lagrangian	Drumond et al. (2017)
Danube River basin and Central Europe	Drought events (1989/1990 and 2003) in the Danube River basin; 51 meteorological drought episodes; most severe in 2003	Anomalous moisture supply from climatological moisture sources	Lagrangian	Stojanovic et al. (2017, 2018a, 2018b)
Loire River basin	Year 2005	Anomalous tropical moisture export from different cluster of trajectories	Lagrangian	Lu and Hao (2017)
Asia				
Indogangetic region	Pre-monsoon drought	Change of wind and vertically integrated moisture flux directions	Eulerian	Liu and Xie (2017)
Indus, Ganges and Brahmaputra River basins	Severe and extremely dry conditions/period 1980–2017	Anomalous moisture contribution from the Indian Ocean (the Arabian Sea, Bay of Bengal), surrounding continental sources and the basins themselves	Lagrangian	Sorí et al. (2017c)
South-western China	Severe dry seasons/2009–2013	A decline in southwest moisture transport, in addition to mid-latitude changes in circulation	Eulerian	Xin-Gang et al. (2015)
North China	Higher frequency of droughts in North China/after the 1990s	decreasing moisture flux from South to North China	Eulerian	Zhang et al. (2011)
North America				
Central US	Severe drought episode/in 2012	Reduction in the moisture contribution from local and continental climatological moisture sources (mainly from June to October) and from the mid-latitude Pacific, and the tropical Atlantic	Lagrangian; Eulerian	Drumond et al. (2016); Roy et al. (2019)
North America	Drought propagation/1980–2016	Decreased moisture transport from land areas upwind	Lagrangian	Herrera-Estrada et al. (2019)
South America				
Negro and Madeira River basins	Driest episodes/1980–2016	Reduction in moisture lost over the basins from air masses arriving from Tropical North and South Atlantic and continental sources	Lagrangian	Sorí et al. (2018)
North East Brazil	Extreme droughts/2010 and 2016	Warm surface water in the tropical North Atlantic, which favoured an anomalously northward migration of the ITCZ and a reduction in moisture transport from the tropical North Atlantic to the region	Eulerian	Marengo et al. (2016a, 2016b)
Africa				
Fertile Crescent	Drought episodes/1998–2000 and 2007–2009	The drastic decline in moisture supply from the eastern Mediterranean Sea and the Fertile Crescent itself;	Lagrangian	Salah et al. (2018)
Niger River Basin	Dry conditions/1981–2017	Reduction of moisture lost over the basin on air masses arriving from the South Atlantic Ocean and the Sahel	Lagrangian	Sorí et al. (2019)
Northern Ethiopian highlands	Driest summer months/July–August 1998–2008	Reduced moisture income from the south (Gulf of Guinea, CEA)	Lagrangian	Viste and Sorteberg (2013a)

Table 2
Summary information of intense precipitation events and floods associated with atmospheric moisture.

Affected region	Event/Date	Related to	Technique applied	Reference
Europe				
Northwest Italy	Extraordinary annual rainfall events/ 1938–2002	Moisture evaporated in the North Atlantic Ocean	Lagrangian, Eulerian	Pinto et al. (2013)
North-western Mediterranean	50 strongest precipitation events /1989–2009	Substantial moisture from the Mediterranean Sea, North Atlantic (in autumn and winter) and evapotranspiration from the European land mass (in summer)	Lagrangian	Winschall et al. (2014b).
Mediterranean region	Five years that exhibit the greatest precipitation during the period 1980–2015	Increased moisture supply from the Mediterranean Sea	Lagrangian	Ciric et al. (2018b)
Danube River Basin	Longer precipitation events 1981–2015	Anomalous moisture supplies from the Mediterranean	Lagrangian	Ciric et al. (2018a)
Danube River Basin (Central Europe)	rainfall event 23 September 1996	Anomalous moisture supply from the Mediterranean Sea, Black Sea, and North Atlantic Ocean	Lagrangian	Ciric et al. (2017)
Europe, (Mediterranean region)	2002	Strong evaporation from the Mediterranean Sea, and from the land.	Lagrangian	Stohl and James (2004)
Eastern Europe	Flood event May 2010	Continental evapotranspiration, the Mediterranean Sea and the North Atlantic Ocean contributes to precipitation under cyclonic conditions	Lagrangian/ Eulerian	Winschall et al. (2014a)
Central Europe	Severe heavy precipitation and flooding, June 2013	Continental moisture recycling	Lagrangian	Grams et al. (2014) and Kelemen et al. (2016)
Loire River basin	Flood events during December/1982 to January/1983	Enhanced tropical moisture export from three cluster of trajectories	Lagrangian	Lu and Hao (2017)
Asia				
South China	103 winter intense precipitation events 1979–2013	Major moisture transport from oceanic sources 68% with the remaining 32% from continental	Lagrangian	Huang et al. (2018a)
Southeastern Tibetan Plateau	Extreme precipitation events between 1979 and 2016	80% of moisture supply from continental areas over India subcontinent.	Lagrangian/ Eulerian	Huang et al. (2018b)
South of East China	Rainstorms between 1961 and 2010	Strength of meridional moisture flux during the monsoon season	Lagrangian/ Eulerian	Zhao et al. (2016)
Northeastern China	Extreme precipitation days in winter between 1979 and 2016	70% contribution from cyclones associated with increased moisture contribution from East China Sea, Sea of Japan and East Asia.	Lagrangian	Lin et al. (2019)
Central India	Extreme precipitation events between 1950 and 2015	Major moisture supply from the Arabian Sea and local recycling	Lagrangian	Roxy et al. (2017)
Nepal	Extreme precipitation events between 1979–2010	Moisture flux coming from the Arabian Sea and continuing along the Himalayas to the east	Lagrangian	Bohlinger and Sorteberg (2018)
Brahmaputra and Ganges River basins	Extreme wet conditions between 1981 and 2015	Reduced moisture loss on air masses from climatological moisture sources	Lagrangian	Sorí et al. (2018).
Indian subcontinent	395 rainstorms 1951–2015	Colder sea surface temperature anomalies over the eastern equatorial Indian Ocean and associated moisture divergent flow and strong moisture convergence over the Indian landmass and the Bay of Bengal	Eulerian	Karuna Sagar et al. (2017)
North America				
Mississippi River basin	River flood in 1927	Anomalously large water vapour flux from the Gulf of Mexico	Eulerian	Smith and Baeck (2015)
Ohio basin	20 extreme spring floods/1901–2008	Sustained advection of low-level moisture from the tropical Atlantic Ocean and the Gulf of Mexico	Eulerian	Nakamura et al. (2013)
Midwestern United States	Extremely high precipitation May–July from 1979 to 2007	Enhanced anomalous moisture transport following evaporation from the GM, eastern Mexico, but also from the Caribbean Sea	Lagrangian	Dirmeyer and Kinter (2010)
Mississippi river basin	Study cases by clusters of trajectories between 1979 and 2013	Enhanced tropical moisture export from the Pineapple Express, the Great Plain (i.e., from Gulf of Mexico), Gulf Stream and West Pacific regions.	Lagrangian	Lu and Hao (2017)
Northern California	Extreme precipitation events. Period: November to March from 1979 to 2013	Enhanced tropical moisture export from the Pineapple Express region	Lagrangian	Steinschneider and Lall (2015b)
Missouri River Basin	Floods from 1966 to 2014	Enhanced tropical moisture export from the Pineapple Express, the Great Plain (i.e., from Gulf of Mexico), Gulf Stream and West Pacific regions.	Lagrangian/ Eulerian	Najibi et al. (2019)
Canada	90,000 extreme precipitation events from 1949 to 2012	Terrestrial evapotranspiration and moisture sources from the Pacific and the Arctic oceans (Atlantic Ocean).	Lagrangian	Tan et al. (2018)
South America				
Northern South America (Colombia, Venezuela, Guyanas)	Anomalously strong wet season 2010–2012	Moisture transport from the Pacific Ocean and Caribean Sea associated with the westerly flow of the Chocó LLJ and the weakening of the CLLJ respectively.	Eularian/ Lagrangian	Arias et al., 2015

(*continued on next page*)

Table 2 (*continued*)

Affected region	Event/Date	Related to	Technique applied	Reference
Eastern Amazonia and Northeast Brazil	Flood event 2009	Moisture transport from the tropical North Atlantic, along with an uncommonly intense Chaco low and an anomalous southward migration of the Intertropical Convergence Zone	Eulerian	Marengo et al. (2012)
Amazonia	Flood event 2012	Abundant moisture transport flux from the tropical North Atlantic and the Caribbean Sea toward the north-western Amazon (active phase of La Niña)	Eulerian	Marengo et al. (2013), Espinoza et al. (2012), Satyamurty et al. (2013b)
		Moisture contribution from northern South America	Eulerian/ Lagrangian	Arias et al. (2015)
South-western Amazonia	2014	Abundant moisture transport flux from the tropical South Atlantic	Eulerian	Espinoza et al. (2014)
Africa				
Northern Ethiopian highlands	Wet summer months	Increased moisture from the Gulf of Guinea, CEA, and the Indian Ocean	Lagrangian	Viste and Sorteberg (2013a)
Northern Africa	Wetter conditions	Spatial expansion of the climatological moisture sources located in the European Mediterranean region and the Atlantic	Lagrangian	Drumond et al. (2011c)

component of the moisture transport over this region. Reduced moisture transport from South to North China is also the major cause of frequent droughts in North China, a decrease that is directly associated with more intense and higher frequency droughts after the 1990s (Zhang et al., 2011).

5.1.3. North America

A Lagrangian diagnostic scheme was used to show that the well-known severe drought episode over the central US in 2012 was associated with some reduction in the moisture contribution from the local and continental climatological moisture sources, mainly from June to October (Drumond et al., 2016), as well as the mid-latitude Pacific, and the tropical Atlantic (Roy et al., 2019). The drought event of 2011 in Texas was more specifically associated with a reduction in moisture advection from the tropical and mid-latitude Atlantic (Roy et al., 2019). The reduced moisture transport was also crucial for drought propagation in 1980–2016 in North America, and agricultural droughts in many sub-regions of North America may be amplified by decreased moisture transport from land areas upwind of them, linked to reduced evapotranspiration and dry soil moisture from these areas (Herrera-Estrada et al., 2019).

5.1.4. Central and South America

In South America, the hydrological variability and warming trend seen in Amazonia affect one of the most important ecosystems on the planet. This is a particular hotspot because of the observed and expected impacts on environmental and socioeconomic development (Chaudhari et al., 2019; Bathiany et al., 2018). The atmospheric response to the interannual variability of the tropical North and South Atlantic Sea Surface Temperature variability is typically analysed through the moisture flux and its divergence over the continent (De sousa et al., 2018). The extreme droughts of 2010 and 2016 in Northeast Brazil were associated with warm surface water in the tropical North Atlantic, which favoured an anomalous northward migration of the ITCZ and a reduction in the moisture transport from the tropical North Atlantic to the region (Marengo et al., 2016a, 2016b). Other methodologies have also quantified the reduction of moisture from these oceanic regions and the Amazonia itself during very dry events (in the Negro and Madeira River basins (Sorí et al., 2018), revealing the clear importance of regional recycling in the modulation of rainfall in the continent.

5.1.5. Africa

The hydroclimatology of Africa is very diverse. The study of Salah et al. (2018) of an important ecological region, namely the Fertile Crescent in northern Africa, confirms the relationship between a drastic decline in moisture supply from the eastern Mediterranean Sea and the rainfall in the Fertile Crescent during the droughts of 1998–2000 and 2007–2009. West Africa contains the Niger River basin, where dry conditions in rainfall climatological zones are directly related to a reduction in the loss of moisture over the basin for air masses arriving from the South Atlantic Ocean and the Sahel (Sorí et al., 2019). For East Africa, Viste and Sorteberg (2013a) associated the causes of wet/dry summer months in the northern Ethiopian highlands with increased/reduced moisture income from the south (Gulf of Guinea, Central Equatorial Africa). Central Equatorial Africa contains the Congo River basin, an ecosystem of global importance. The driest years in this basin are associated with less moisture loss here as computed for air masses arriving from both the Atlantic and the Indian Oceans as well as from the surrounding continental regions (Sorí et al., 2017b).

5.2. Extreme precipitation and floods associated with atmospheric moisture transport

As for atmospheric moisture and connected patterns of drought, there are a number of recent studies in which attempts have been made

to assess the same relationship but for extreme precipitation events (Table 2). In the scientific literature the expression: 'extreme precipitation event' is considered to be the occurrence of heavy precipitation.

5.2.1. Europe

Extreme precipitation events in Europe (including the Mediterranean region) are known to be related to enhanced atmospheric moisture transport from the North Atlantic Ocean and the Mediterranean Sea. For example, extreme rainfall events over the last 50 years in northwest Italy are clearly related to moisture evaporated from the North Atlantic Ocean (Pinto et al., 2013). The development of Storm Klaus (an exceptional winter storm that struck Europe on 23–24 January 2009) was also supported by an extraordinary tropical moisture export from the whole of the central and western tropical Atlantic (Liberato et al., 2011). Both the North Atlantic Ocean and the Mediterranean Sea supplied substantial amounts of moisture for the 50 strongest precipitation events in the north-western Mediterranean during 1989–2009, for which evapotranspiration from the European landmass during summer also played a key role (Winschall et al., 2014b). However, according to Ciric et al. (2018a), while the Mediterranean Sea is not an important source of climatological precipitation for some European regions, it is during extreme precipitation years. Contrary to previous findings, Ulbrich et al. (2009) suggested that additional moisture advected from the North Atlantic into the Mediterranean Basin plays a major role in the magnitude of extreme precipitation events. Apart from the two oceanic sources, continental evapotranspiration was also an important source of moisture in 2002 and 2010 for the summer floods in Europe in these years (Stohl and James, 2004; Winschall et al., 2014a), and also in 2013 in Central Europe (Kelemen et al., 2016; Grams et al., 2014). By applying a Lagrangian model, Ciric et al. (2017) found that in addition to the Mediterranean Sea and the North Atlantic Ocean, moisture from the Black Sea was related to an intense rainfall event detected on 23 September 1996 in the Danube River Basin. Among 100 extreme precipitation events observed in this basin (during 1981–2015), those with longer durations are more influenced by extreme anomalous moisture supply from the Mediterranean than those of shorter durations. However, it is during these shorter events that the Mediterranean Sea contributes more moisture (Ciric et al., 2018b). Revisiting several previous publications, Krichak et al. (2016) also restated the importance of anomalously intense transports of moist air from the tropical and subtropical Atlantic Ocean in the occurrence of cold-season extreme precipitation events in the European Mediterranean region. Moisture release from the tropics has been also linked to flood events in the Loire River basin (Lu and Hao, 2017). Export of moisture from the tropics is an important driver of extreme events in the midlatitudes.

5.2.2. Asia

Various authors have identified the primary moisture sources for intense precipitation events and floods in Asia. Using a Lagrangian method, Huang et al. (2018a) found that for 103 extreme winter precipitation events over South China for the period 1979–2013, oceanic moisture sources provided on average about 68% of the moisture (South China Sea 30.9%, the western North Pacific 20.2%, East China Sea 14.9%), while the remaining 32% came from terrestrial sources (South China itself 14.6%, south-eastern Asia 11.5%). For the South-eastern Tibetan Plateau, however, the land areas over the Indian subcontinent were found to contribute almost 80% of the moisture supply in wintertime extreme precipitation events (Huang et al., 2018b). Torrential rainfall in southern China in the Sichuan Basin between 2009 and 2013 also received moisture from the Arabian Sea, the Bay of Bengal, the Indo-China Peninsula, and the Sichuan Basin itself. A little further north, in the southern part of East China, the frequency of summer rainstorms between 1961 and 2010 was characterized by a decadal variation that was statistically significantly related to the strength of meridional moisture flux during the monsoon season (Zhao et al., 2016). Over northern East China cyclone activity was found to contribute about 70% of the extreme precipitation days (Lin et al., 2019). The cyclones associated with extreme precipitation days show increased moisture contribution from the Sea of Japan, East China Sea and East Asia. The hydroclimatology of the Indogangetic region has been also widely investigated. Roxy et al. (2017) used a dynamic recycling model to study the role of sources of moisture for extreme precipitation events over the period 1950–2015 in central India, finding that approximately 36% of the total moisture for these extreme events comes from the Arabian Sea, while only 26% can be traced to the Bay of Bengal, and just 9% to the central Indian Ocean. Meanwhile, local recycling contributes about 29% of the moisture. Abundant moisture transport along the Himalayan foothills from the Bay of Bengal to northern Pakistan was one of the causes of the 2010 flood in Pakistan (Lau and Kim, 2012; Houze et al., 2011). The computed moisture sources for extreme precipitation events in Nepal match the pattern of moisture flux from the Arabian Sea, continuing along the Himalayas to the east (Bohlinger and Sorteberg, 2018). The Bay of Bengal was also shown to be linked with extreme wet conditions in the Brahmaputra and Ganges River basins (Sorí et al., 2017c). To the east, the strong convergence of integrated water vapour transported from the Arabian Sea becomes more important for rainfall events in western and Southern India (Ordóñez et al., 2012), and extreme wet conditions in the Ganges and Indus River Basins (Sorí et al., 2017c; Pathak et al., 2017). Moisture from both the Bay of Bengal and the Arabian Sea also affects significantly the duration of intense precipitation events over the Indian subcontinent (Karuna Sagar et al., 2017).

Lagrangian analysis reveals that as a moisture source the Arabian Sea has a dominating influence on both wet conditions and river discharges in the Shiraz and Mashhad regions of Iran, in the Middle East, during wet periods (Heydarizad et al., 2018b). Eulerian and Lagrangian analyses have revealed moisture transport from nearby and remote tropical regions, leading to above-normal tropospheric moisture over Saudi Arabia prior to the occurrence of extreme precipitation events in Saudi Arabia in autumn (November 2009), winter (January 2005), and spring (April–May 2013) (Vries et al., 2016).

5.2.3. North America

With regard to North America, Smith and Baeck (2015) investigated the 1927 Mississippi River flood and related this event to an anomalously large water vapour flux from the Gulf of Mexico, with anomalous conditions in the Pacific that controlled the development of baroclinic disturbances over the central United States. Nakamura et al. (2013) investigated 20 extreme spring floods in the Ohio basin (in the northeastern United States) for the period 1901–2008, and discovered that all these floods were associated with a similar pattern of sustained advection of low-level moisture and warm air from the tropical Atlantic Ocean and the Gulf of Mexico. Not only the Gulf of Mexico but also the Gulf of California were identified by Erlingis et al. (2019) as moisture for the flash floods over the United States in a study that investigated a total number of 19253 events. The extremely high precipitation that occurred during the period May–July from 1979 to 2007 over the Midwestern region of the United States was also related to be an enhanced anomalous moisture transport that followed evaporation from the Gulf of Mexico and eastern Mexico, but also from the Caribbean Sea (Dirmeyer and Kinter, 2010). In addition, soil moisture models for the summer flood of 1993 confirm a feedback mechanism, consisting of an increase in soil moisture leading to higher evapotranspiration and precipitation and lower temperature, primarily over the Midwest and the Great Plains (Saini et al., 2016).

Through machine learning techniques have been shown that tropical moisture exports help to explain dominant modes of total precipitation variability across the eastern United States (Steinschneider and Lall, 2015a), the occurrence of extreme precipitation in the Mississippi River basin (Lu and Hao, 2017) and Northern California

(Steinschneider and Lall, 2015b), and the inference and prediction of flood duration at the Missouri River Basin (Najibi et al., 2019). A complete detailed study Schlef et al. (2019) summarizes the synoptic-scale atmospheric circulation patterns, and the tropical moisture export associated with extreme floods across the United States. The moisture sources for over 90 000 extreme precipitation events in Canada were identified by Tan et al. (2018) using the HYSPLIT model, permitting the identification of terrestrial evapotranspiration as a source that provides moisture for many extreme precipitation events in Canada for all four seasons during 1949–2012, especially for inland regions. For western and central (eastern) Canada, extreme precipitation events were mainly fed by moisture sources from the Pacific and the Arctic oceans (Atlantic Ocean).

5.2.4. South America

For South America, multiple studies have focused on the Amazon River basin, the largest in the world. An unusually early start to the rainy season in the North and North-western Amazon during May–June 2009 and abundant precipitation in large parts of eastern Amazonia and Northeast Brazil from May to July 2009 was due to moisture transport from the tropical North Atlantic, along with an uncommonly intense Chaco low and an anomalous southward migration of the Intertropical Convergence Zone (ITCZ) (Marengo et al., 2012). The period 2010–2012 was charecterised by one of the strongest wet seasons over northern South America (Arias et al., 2015). According to Arias et al. (2015), this period is characterized by increased moisture contribution from the Pacific Ocean (via westerly transport form the Chocó LLJ linked with ENSO variability) and the Caribbean Sea (caused by the weakening on the Caribbean Low Level Jet (CLLJ). In 2012, the Amazon basin experienced a record flood for the previous 50 years, which according to Marengo et al. (2013) and Espinoza et al. (2012) was associated with both La Niña and warm conditions in the tropical South Atlantic. Satyamurty et al. (2013b) analysed the moisture flux during this event and found an anomalously warm tropical North Atlantic accompanied by a colder-than-normal South Atlantic and a moisture flux convergence 38% higher than the extreme precipitation normally seen in the Amazon basin. An extraordinarily warm Subtropical South Atlantic together with warm conditions in the western Pacific-Indian Ocean favoured moisture transport over Southwestern Amazonia during extreme precipitation and floods over south-western Amazonia, especially in the Andean countries (Bolivia and Southern Peru), and over western Brazilian Amazonia (Espinoza et al., 2014). Arias et al. (2015) also observed a southward transport form norther South America into the northeastern Amazon in 2012 being this region a potential source of moisture to activate convection in the Amazon.

5.2.5. Africa

Compared with other regions, for Africa there are fewer recent studies relating extreme precipitation to atmospheric moisture transport. For wetter conditions in northern Africa, it appears that there is a spatial expansion of the climatological moisture sources located in the European-Mediterranean region and the Atlantic (Drumond et al., 2011c). Unseasonal extreme precipitation events in tropical West Africa have been associated with extratropical disturbances via a decrease in surface pressure over the Sahara/Sahel and a subsequent inflow of moist air from the Gulf of Guinea (Davis et al., 2013). To the east, the wet summer months in the northern Ethiopian highlands in July–August 1998–2008 were associated with an increased release of moisture in the region by air masses arriving from the Gulf of Guinea and enhanced southerlies along the coast of East Africa, increasing transport from the Indian Ocean (Viste and Sorteberg, 2013a; Table 2).

6. The role of meteorological structures at planetary scale in the moisture transport: Low-Level Jets, Atmospheric Rivers and monsoons

At the global scale, Atmospheric Rivers (ARs) and Low-Level Jet systems (LLJs) are the two major mechanisms of moisture transport (Gimeno et al., 2016). Global climate change is causing important modifications to patterns of moisture transport. Over a relatively short time scale, variations in the regions of occurrence, frequency, intensity, and amount of moisture transported by these large-scale meteorological structures is having an ongoing significant socioeconomic impact. On the one hand, it is well known that according to the Clausius-Clapeyron equation, an increase in temperature favours an increased amount of water vapour available in the atmosphere, which suggests enhanced moisture transport. This in turn can lead to the intensification of extreme rainfall, and therefore to an increased flood risk. On the other hand, changes in atmospheric circulation trigger variations in regions of occurrence and in the frequency of particular moisture transport mechanisms, which affects the balance of regional availability of water.

Although the literature has grown over the last few decades, precipitation linked with ARs and LLJs is not well quantified and could be underestimated at a regional scale (Gimeno et al., 2016). In general, reanalysis studies are a reasonable representation of the structure of LLJs. However, they underestimate the frequency of occurrence of LLJs, and therefore their contribution to the total transport of moisture (e.g., Berg et al., 2015). LLJs and ARs are widely recognised for their key roles in the regional and global water cycle. Both mechanisms have a particular importance for hydrometeorological extremes due to the greater ability of these structures for moisture transport (floods) or the lack thereof (droughts). In a previous review, Gimeno et al. (2012) emphasised the importance of these mechanisms of moisture transport and their relationship with hydroclimatic extremes. An intensification (or reduction) of moisture transport related to these meteorological structures could lead to flood (or drought) scenarios. Thus, future changes in moisture transport and their frequency and intensity under global warming have become a critical issue for short- and medium-term planning for national and regional strategies for adaptation and mitigation.

Major LLJs are frequently associated with monsoon circulation (Gimeno et al., 2016), and are responsible for most of the moisture transport from remote regions, which then results in precipitation over continental monsoonal regions. In light of the intense interest in this topic, many papers have been published on the sources of moisture associated with monsoons.

6.1. Atmospheric Rivers

The relatively narrow and elongated atmospheric pathways along which large amounts of water vapour are transported from the subtropics to the midlatitudes are known as Atmospheric Rivers (ARs). These structures are usually located within the warm conveyor belt in the pre-cold-frontal region of extratropical cyclones and are characterised by high water vapour contents and strong low-level winds (Ralph et al., 2004, 2017b , Lavers and Villarini, 2013b; Cordeira et al., 2013; Gimeno et al., 2014; Waliser and Guan, 2017). Eiras-Barca et al. (2018b) reported that ARs are a phenomenon generally linked with explosive cyclogenesis over the North Atlantic and North Pacific basins.

It is common for up to five or six ARs to occur simultaneously in each hemisphere. Although these systems cover less than 10% of the Earth's surface, more than 90% of the poleward atmospheric moisture transport in the midlatitudes is transported along concentrated pathways by ARs (Zhu and Newell, 1998). In rough terms, the ratio of moisture transport by ARs is similar to the transport of water in the largest continental rivers. Nevertheless, continental rivers follow the same pathway regardless of the volume of water they transport, while ARs show strong temporal variation and their flows can cover much

wider areas. Although there is currently some consensus in designating these structures 'Atmospheric Rivers', some authors refer to systems with similar phenomenology as Aerial Rivers (Arraut et al., 2012; Poveda et al., 2014), Tropospheric Rivers (Newell et al., 1992), or Tropical moisture exports (Knippertz and Wernli, 2010; Knippertz et al., 2013; Lu and Lall, 2016). At a regional scale, ARs are also known by their local name, i.e., "Pineapple Express" (Dettinger et al., 2011) or "Maya Express" (Dirmeyer and Kinter, 2009).

The AMS definition for ARs tries to summarize the knowalge that we have so far about these phenoma: "A long, narrow, and transient corridor of strong horizontal water vapor transport that is typically associated with a low-level jet stream ahead of the cold front of an extratropical cyclone. The water vapor in Atmospheric Rivers is supplied by tropical and/or extratropical moisture sources. ARs frequently lead to heavy precipitation where they are forced upward—for example, by mountains or by ascent in the warm conveyor belt. Horizontal water vapor transport in the midlatitudes occurs primarily in ARs and is focused in the lower troposphere. Atmospheric Rivers are the largest "rivers" of fresh water on Earth, transporting on average more than double the flow of the Amazon River."

There are two main approaches for detecting ARs. The first is based on an analysis of the integrated water vapour column (IWV) (e.g., Guan et al., 2010; Dettinger et al., 2011); the second uses the integrated vapour transport fields (IVTs) computed between 1000 and 300 hPa (e.g., Lavers et al., 2012, 2013; Guan and Waliser, 2015, 2017; Ramos et al., 2015). According to the definition of an AR, some authors have established geometric requirements and minimum water vapour contents in an attempt to identify them as such. For example, Guan and Waliser (2015) defined AR events using the 85th percentile specific to each season; In addition, they checked the geometrical conditions of length, width, or the ratio between them, among other methods to identify objectively the structure of ARs. The main methodologies used in the detection and general characteristics of ARs were summarised by Gimeno et al. (2014).

Although the values of IWV are greater in summer, the analysis of the contribution of ARs to extreme precipitation events has been studied mainly only in winter. This responds to the fact that the stream flow is stronger in the cold season due to the strong flows associated with extratropical cyclones. Thus, a region affected by extratropical cyclones is a potential area of occurrence of ARs. There is more and more evidence that ARs play a relevant role in intense precipitation events around the world: on the western US (e.g., Hughes et al., 2014, Backes et al., 2015, Ralph et al., 2016,); central US (e.g., Nayak et al., 2014; Nayak and Villarini, 2017); Europe (Lavers et al., 2012, 2018; Lavers and Villarini, 2013b; Sodemann and Stohl, 2013; Eiras-Barca et al., 2016); Madeira Island (Couto et al., 2015); New Zealand (Kingston et al., 2016); South America (Zandonadi Moura and Lima, 2018; Viale et al., 2018); Bay of Bengal (Yang et al., 2018); Nepal (Thapa et al., 2018); and South Africa (Blamey et al., 2017). On the other hand, ARs play an important role as a precursor to extreme winter floods (Lavers et al., 2011; Liberato et al., 2013; Ramos et al., 2015; Pereira et al., 2016).

Moisture transport from the North Atlantic Ocean towards Europe occurs through ARs, which are one of the main mechanisms of moisture transport in this region. ARs supply water vapour, bringing large amounts of moisture and often contributing to extreme precipitation events, triggering heavy floods in Europe (Liberato et al., 2013; Lavers and Villarini, 2013a). In particular, in the northwest of the Iberian Peninsula, persistent ARs effectively cause a doubling of the precipitation during flood events (Ramos et al., 2015, 2018; Eiras-Barca et al., 2018a). The behaviour of ARs in regions with strong topography favours an increase in precipitation (Champion et al., 2015; Valenzuela and Kingsmill, 2015; Kingston et al., 2016; Rössler et al., 2014). Lavers and Villarini (2013a) studied extreme precipitation events in Europe. They reported that the heaviest rainfall events are linked with AR systems, and that orographic lifting plays a significant role in rainfall in Western Europe. Orographic blocking acts as a barrier to inland penetration of moisture and it has also been reported to be a critical factor in triggering heavy floods in the Western US (Neiman et al., 2011; Hughes et al., 2014).

ARs are capable of transporting large amounts of moisture from tropical reservoirs (e.g., Eiras-Barca et al., 2017). The large moisture sources for ARs are located in subtropical oceans. Ramos et al. (2016a) identified the major ARs that affect the western European coast in winter and then applied a Lagrangian methodology to calculate the anomalous uptakes of moisture for those ARs. The subtropical Atlantic is the main source of moisture for AR events. Although the main anomalous areas of moisture uptake are located between 20 and 40°N, there is some local transport from extratropical areas near the continental sink (Ramos et al., 2016a). Nevertheless, according to Dacre et al. (2015), ARs are not necessarily fed by long distance moisture transport from the tropics/subtropics, but are rather a consequence of sources of moisture exported from extratropical cyclones as they travel towards the high latitudes.

Researchers have focused special attention on ARs that reach the west coast of the US, which is a very sensitive area in terms of the availability of water resources (Rutz and Steenburgh, 2012; Rutz et al., 2013, 2015; Rivera et al., 2013; Dettinger et al., 2011; Ralph and Dettinger, 2011; Payne and Magnusdottir, 2016). Although ARs are related to the generation of heavy floods that cause heavy damage, precipitation linked with ARs is also essential for water resources in California (Dettinger et al., 2011). Ryoo et al. (2015) used a model of back-trajectories to characterise the origin of the moisture of AR events on the US west coast. Trajectories of tropical and extratropical origin are closely associated with AR events, which then identify the subtropical Pacific as a source of moisture for ARs that reach the west coast.

The connection between ARs and heavy precipitation and subsequent flooding has been also identified over the central and Midwestern US (Lavers and Villarini, 2015). The most extreme Midwest floods of 1993 and 2008 were linked to ARs (Lavers and Villarini, 2013b; Nayak and Villarini, 2017). The region of maximum moisture located within the Great Plains Low-Level Jet is an AR, known locally as the "Maya Express" (Dirmeyer and Kinter, 2009, 2010); this transports a large amount of moisture from the Gulf of Mexico and the Caribbean Sea, which are the main source regions for this structure (Moore et al., 2012; Nakamura et al., 2013).

Considering the relevance of the northward advection of moisture by ARs, Vázquez et al. (2018) reported the sources of moisture for ARs that reach the Arctic domain. The main source of moisture for ARs that reach the Arctic extends over the oceans of the North Atlantic and North Pacific. In addition, there is a local maximum of moisture located in the region of maximum occurrence of ARs. However, in summer, the moisture has a continental origin, appearing in parts of North America and Eurasia (Vázquez et al., 2018). Although the increase of moisture in the Arctic may have different effects (Gimeno et al., 2019), events of heavy accumulation of snow in February 2009 and 2011 were associated with the entry of moisture from ARs (Gorodetskaya et al., 2014). On the other hand, the fact that ARs are associated with extratropical cyclones plays a decisive factor in the entry of moisture to the Arctic (Gimeno et al., 2019). Therefore, within the context of global warming, the variabilities of cyclone frequency and intensity are key factors in the transport of moisture towards the Arctic.

ARs and LLJs are generally studied as independent structures. Despite this, Ramos et al. (2019) reported a combination of ARs that made landfall in South Africa, associated with a particular phase of the South American Low-Level Jet (SALLJ). They indicated that the SALLJ that occurs in a No Chaco Jet event (NCJE) phase transports moisture from the South American continent (a region that includes the Paraná River Basin and southern Amazon River Basin) to the western and central South Atlantic basin. This moisture is then transported by ARs to the west coast of South Africa. An anomalous moisture sink for the

NCJE days and IVT anomalies for the ARs days have been detected, confirming the existence of this link (Ramos et al., 2019). Thus, the two margins of the South Atlantic Ocean appear to be connected by a combination of the two most important meteorological structures for moisture transport, LLJs and ARs.

The evaluation of future projections of moisture transport points to an enhanced frequency and intensity of ARs, with an increase in the length of the season in which these systems occur, and an increase in water vapour transported by them (Dettinger et al., 2011; Lavers et al., 2011; Gao et al., 2016; Warner et al., 2014; Ramos et al., 2016b), all of which confirms an intensification of the hydrological cycle, and in particular an intensification of the hydrological extremes (Allan et al., 2014). The fact that most of these changes have a thermodynamic origin reinforces the hypothesis of an anthropogenic origin of global warming. However, the global analysis of future projections indicates a slight decrease in the frequency of ARs and an increase in the flow of ARs, with a consequently greater associated moisture transport (Espinoza et al., 2018). At smaller scales, changes in frequency indicate both an increase in the AR flows that make landfall, and an increase in moisture transport according to the greater amount of water vapour available in the atmosphere due to climate warming. Lavers et al. (2013) documented an increase in the frequency of ARs landfalling in Great Britain. In the European sector, an increase in the annual number of days of ARs is related to changes in the circulation of the Jet Stream (Gao et al., 2016). Increased frequencies of ARs were also found for the western US (Dettinger et al., 2011; Warner et al., 2014).

6.2. Low-Level Jets

Another key mechanism associated with the transport of large amounts of water vapour is the Low-Level Jet (LLJ). These are elongated wind corridors located in the lower troposphere, where the maximum of wind speed is within the first kilometre above ground level. More definitions of LLJs may be found in Nicholson (2016). It is common for the core of the jet to be 300–700 m above ground level. The fact that the strongest winds are found at low levels mean that LLJ structures are systems that have the potential to transport large amounts of moisture (Gimeno et al., 2016).

In contrast to ARs, which are mostly confined to extratropical regions (Gimeno et al., 2014), LLJs have been described in several regions around the world (Stensrud, 1996; Rife et al., 2010). Although they occur throughout the year, LLJs have a marked seasonal component associated with the warm season, when they are generally more frequent and intense (Bonner, 1968). Many LLJs have a diurnal cycle, and exhibit maximum wind speeds at night. Termed Nocturnal or Night Low-Level Jet (NLLJ), they are formed by the decoupling of the planetary boundary layer after sunset.

There are two main methods for detecting LLJs. The first is based on criteria of wind speed and height, which are not entirely objective, and is one of the most widely accepted. The Bonner criterion (Bonner, 1968) is based on the magnitude and vertical shear of the wind, where the wind speed must exceed 12 m/s and decrease by at least 6 m/s to the next higher-level minimum or to the 3 km level, whichever is the lower. Some authors have tried to reduce subjectivity in the detection of LLJs. Montini et al. (2019), for example, established the seasonal 75th percentile as a wind speed threshold, in order to use fixed wind speeds to identify events relating to the South American Low-Level Jet. In the second method, Rife et al. (2010) proposed a global index of NLLJ activity based on the vertical structure of the temporal variation of the wind for detecting NLLJs. According to this method, in order to detect a NLLJ event, two criteria must be satisfied simultaneously, namely (i) the wind speed must be greater at the surface than at height and (ii) the wind speed must be greater at noon than at midnight.

Employing this last method at a global scale, Rife et al. (2010) reported and characterised twenty-one continental regions where NLLJs occur frequently, including several regions that had not been previously identified. Most NLLJs were detected in the Northern hemisphere near the coast, where there is a strong land-sea contrast. In a companion paper, Monaghan et al. (2010) investigated the linkages between nocturnal precipitation extremes and NLLJs detected previously by means of a statistical approach. They reported a strong relationship between the occurrence of NLLJs and nocturnal rainfall extremes in at least ten regions around the world. Oceans and coastal regions near NLLJs play an important role in their contribution to extreme rainfall.

One of the best documented LLJ is the Great Plains Low-Level Jet (GPLLJ), which is reported to bring considerable moisture to the continental United States (Pu et al., 2016; Algarra et al., 2019). Located in the central eastern US, the GPLLJ plays a critical role in the hydrological cycle, modulating the entry of moisture from the Gulf of Mexico. Numerous authors have documented the linkage between the GPLLJ and heavy flooding in the American Midwest (Patricola et al., 2015; Dong et al., 2011; Moore et al., 2012; Nakamura et al., 2013; Lackmann, 2013). Harding and Snyder (2015) indicated that the negative phase of the Pacific-North American (PNA) teleconnection pattern is related to strong GPLLJ events and enhanced precipitation over the north-central US. The Gulf of Mexico and the Caribbean Sea are the main sources of moisture for the GPLLJ, which transports a large amount of moisture to the interior of the US. During the heavy floods of 1993 and 2008 in the Midwest, an AR named locally as the “Maya Express” spread along the Caribbean Sea to the US, transporting large amounts of moisture. The “Maya Express” was fed from moisture in the GPLLJ, triggering major floods in the southeastern US. (Dirmeyer and Kinter, 2009, 2010).

The impact of short-term flooding related to the transport of large amounts of water vapour can be a significant hazard. However, the continued absence of rainfall, linked with a change in the position or amount of moisture transported by the GPLLJ induces drought events that also have significant socioeconomic impacts (Cook and Vizy, 2010; Harding and Snyder, 2014). Barandiaran et al. (2013) reported that the GPLLJ in spring has strengthened and expanded northwards over the last few decades. This northward migration of the GPLLJ decreased the precipitation over the Southern Plains and has increased the risk of droughts in this area. Nevertheless, areas located in the Northern Plains have seen increased rainfall and have thus become more susceptible to flooding. Considering future scenarios, Harding and Snyder (2014) found an increase in rainfall for April-July and an increase in extreme rainfall in the central US, related to a strengthening of the GPLLJ. However, they also found an increased incidence of drought in August-September over the North Central US, which was associated with a slight weakening of the GPLLJ.

One further example is the Caribbean Low-Level Jet (CLLJ), which is located in the Caribbean Sea and transports moisture towards Central America, crossing the Panamá isthmus and reaching the western Pacific. The CLLJ is the main transport moisture mechanism from the Caribbean Sea for Central America (Durán-Quesada et al., 2010). However, the position of the CLLJ has a strong seasonal cycle. During the warm season, it moves northwards to reach the central US and becomes a Southern branch of the GPLLJ (Cook and Vizy, 2010). Nevertheless, during the cold season, the northeast trade winds divide when crossing central America, and one part merges with the Chorro del Occidente Colombiano (hereafter, Chocó LLJ). The strong land-sea temperature contrast causes a southern flow to develop parallel to the western Chilean Andes, known as the Chocó LLJ (Poveda and Mesa, 2000). When it reaches the Colombian Andes, due to the influence of westerly winds the Chocó becomes a westerly LLJ and penetrates as far as the Colombian coast, causing increased rainfall in this region (Sakamoto et al., 2011; Poveda et al., 2014).

Durán-Quesada et al. (2017) analysed the sources of moisture for Central America and the role of the main mechanisms of moisture transport. At a regional scale, Central American precipitation is controlled by LLJs. The role of the Caribbean Sea as a source of moisture in Central America is observed all year round thanks to the CLLJ, which

acts as an inter-basin transport mechanism. Moreover, the contribution to precipitation of the Chocó LLJ from the eastern tropical Pacific is particularly relevant during boreal summer and autumn, when the winds penetrate southern Central America (Durán-Quesada et al., 2017). In northern parts of South America, particularly in Colombia, 2010 and 2011 were characterised as the wettest years since records began. Moisture transport to northern South America during the anomalously wet event of 2010–2012 was analysed by Arias et al. (2015). The weakening CLLJ led to a larger moisture input into western Colombia from the Caribbean Sea. Moreover, it was identified that the main source of moisture associated with this wet episode was the eastern Pacific through the westerly flow of the Chocó LLJ. The convergence of the two LLJs over the eastern Pacific-western Colombia contributes to the explanation of the region's world record rainfall (Poveda et al., 2014; Hoyos et al., 2019).

The South American Low-Level Jet (SALLJ) is the main mechanism that modulates moisture transport in the South American continent (e.g., do Nascimento et al., 2016; Montini et al., 2019). In particular, during the wet season, the northeast trade winds, replete with moisture from the tropical Atlantic, penetrate northern South America as an LLJ structure, transporting large amounts of moisture along the eastern border of the Andes to southern part of the Amazon basin and the La Plata River Basin. Numerous authors have reported the potential evapotranspiration from the Amazon Basin as a source of moisture for the southern regions of South America, given its location on the pathway of the SALLJ. Using water vapor tracers, Yang and Dominguez (2019) find that the contribution of Amazonian moisture to precipitation in southeastern South America via the SALLJ is about 16%, which is less than previous studies using simple analytical recycling models. Nevertheless, the widespread conversion of natural forest into grassland, which has been ongoing for several decades, affects the water cycle, decreasing the evapotranspiration ratio and hence the moisture transported by the SALLJ (Zemp et al., 2014). Any reduction in the evapotranspiration ratio in the Amazon basin due to anthropogenic activities can reduce its significance as a moisture source region. This scenario then leads to a decrease in moisture transport by the SALLJ and an increased risk of hydroclimatic extremes, such as drought due to lack of rainfall (Marengo and Espinoza, 2016). According to its orientation, two major SALLJ configurations are possible: the Chaco jet event (CJE) in which the SALLJ transports moisture to southern South America and the La Plata River Basin, and the no Chaco jet event (NCJE), which is more frequent during the austral summer and the path of SALLJ from 25°S is more zonal with an easterly component (Salio et al., 2002; Nicolini and Saulo, 2006). This latter phase (NCJE) is related to the transport of moisture to the South Atlantic, which can then feed ARs that reach the west coast of South Africa (Ramos et al., 2018).

6.3. Monsoons

Although the current suite of models has improved understanding of ocean-continent-atmosphere coupling, some uncertainty remains in relation to the beginning and end of the monsoon season (Sperber et al., 2017). A better understanding of the processes that govern moisture transport could improve the prediction of monsoon precipitation. The fact that monsoon regimes often occur in developing countries that are particularly vulnerable to climate variability and climate change implies that the impact of these climatic systems is even more intense. Usually, monsoons affect densely populated areas and can both have devastating impacts on human lives and cause economic damage. Monsoon regions present a marked seasonal cycle with heavy precipitation in summer in response to strong atmosphere-ocean-land interactions as the climate system undergoes annual variations in insolation. Monsoons occur mainly near tropical and subtropical oceans, in North America, India, Australia, and Africa (Zhisheng et al., 2015).

Over the last few years, sources of moisture associated with the western North American monsoon have been widely investigated. In a recent study, Ordoñez et al. (2019) differentiated between continental and oceanic moisture sources. Their results show that during the western North American monsoon season, recycling is the main source of moisture, followed by an oceanic source located in the Gulf of California. Nevertheless, in the days leading up to rainfall events, Ordoñez et al. (2019) reported a remarkable increase in moisture flow from the Caribbean Sea to the Monsoon region. Precipitation from recycling is an important factor in monsoon intensity. The importance of continental evaporation as a source of moisture was reported using different methodologies (Bosilovich, 2003; Hu and Dominguez, 2015; Dominguez et al., 2016). Dominguez et al. (2016) reported that local recycling is the second most important source of moisture for the North American monsoon after the transport of moisture at low-level from the Gulf of California. Oceanic sources for the monsoon contribute to the transport of moisture at different levels. Low-level moisture transport from the Gulf of California is the source of moisture for the Monsoon, while the Gulf of Mexico transports moisture mostly at medium levels (above 800 mb).

The Western and Southern India (WSI) summer monsoon provides a large amount of summer rainfall to densely populated areas in eastern Asia. Using a Lagrangian methodology, Ordóñez et al. (2012) identified the main sources of moisture during the WSI. Oceanic sources from the Arabian Sea and the Indian Ocean are more intense during the monsoon season, linked to the Somali Low-Level Jet (SLLJ); the northwestern continental source of WSI is more intense during the boreal summer; recycling in the WSI region occurs at the end of the Monsoon season when the SLLJ is less relevant in the transport of moisture. A fourth and less important source of moisture is the Bay of Bengal, which is active during the winter months but becomes a sink region in summer. The role of the SLLJ is closely linked to the active phase of the WSI and is an important mechanism of moisture transport (Sagalgile et al., 2018; Syed and Hannachi, 2018).

The West African monsoon (WAM) modulates rainfall in West Africa. Lélé et al. (2015) assessed moisture transport in West Africa and found that in spring (April-June) the transport of moisture to the Gulf of Guinea is associated more with an Atmospheric River. However, during the monsoon peak season (July-September) the strengthening of the West African westerly jet (WAWJ) makes the moisture flow more zonal and the transport of moisture to the west increases. The WAWJ transports moisture from the eastern tropical Atlantic to West Africa; variations in the WAWJ are significantly positively correlated with variations in precipitation in the Sahel region (Pu and Cook, 2012). Although the WAWJ and the monsoon flow contribute to the transport of moisture and consequently to rainfall in western Africa, they are physically separate meteorological systems governed by different dynamics (Pu and Cook, 2010, 2012). The position of the Atlantic Intertropical Convergence Zone (ITCZ) favours the establishment of zonal acceleration and is dynamically associated with the formation of the WAWJ (Pu and Cook, 2012). Seasonal analysis shows that the zonal pattern contributes more to the transport of moisture to the Sahel, while the land pattern is such that it contributes more to the coast of Guinea (Lélé et al., 2015). Similar results were reported by Pu and Cook (2012), who revealed that strong anomalous WAWJ was associated with higher moisture transport towards the west and heavy rainfall in the Sahel. The influence of recycling and transport of moisture from the Mediterranean basin have also been identified as sources of moisture for the WAM (e.g., Nieto et al., 2006).

In northern Australia, precipitation is mainly related to the monsoon regime. The monsoon is responsible for heavy rainfall in northern Australia. The wet season is characterised by persistent winds from the west below 700 mb, which transport moisture from the northeast Indian Ocean to the north of Australia. During the last few decades the monsoon in the north of Australia has been strengthened, with more intense and longer-lasting precipitation (Catto et al., 2012; Gallego et al., 2017). The increase in rainfall in north and northwest Australia may be linked to an enhanced transport of moisture associated with

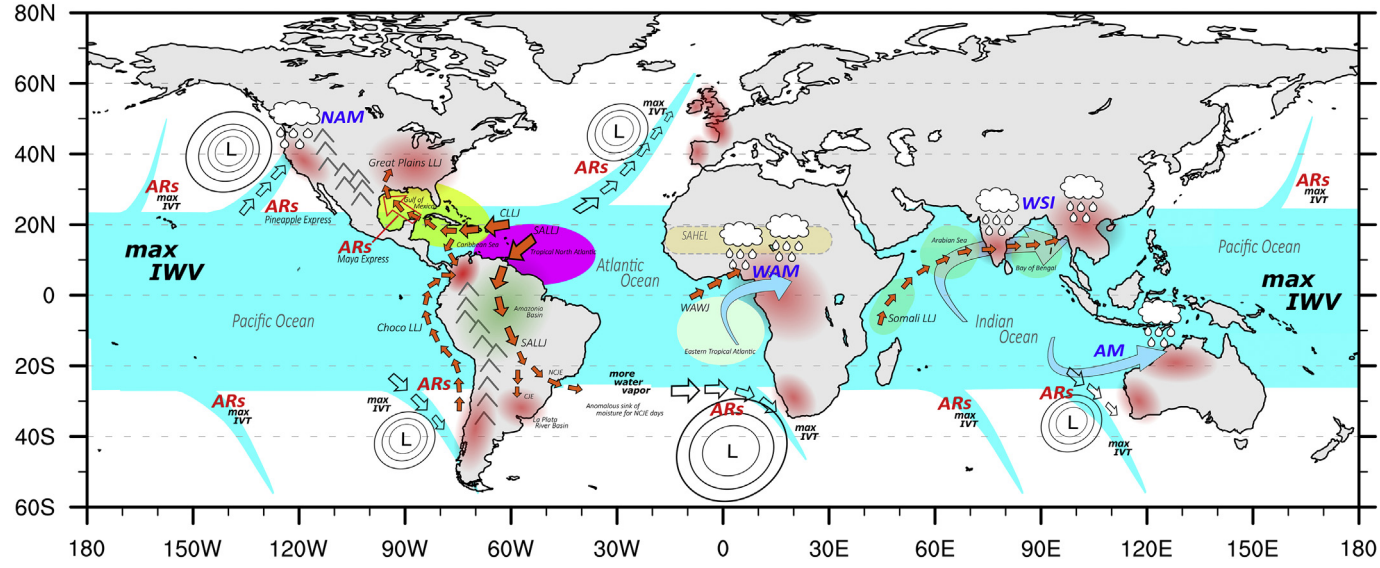

Fig. 5. Major mechanisms of moisture transport at the global scale: Low-level Jet (LLJ), Atmospheric Rivers (ARs) and Monsoon systems. The region of maximum IWV is indicated in blue. Regions affected by the main mechanisms of moisture transport are summarised in red. Black arrows show the AR landfall regions. The local names of some ARs are shown: The Pineapple Express and The Maya Express. Orange arrows indicate the trajectory and position of some LLJs. The names of the LLJs are shown: The Great Plains Low-Level Jet (GPLLJ), The Chocó Low-Level Let (ChocoLLJ), the South American Low-Level Jet (SALLJ), the Caribbean Low-Level Jet (CLLJ), the West African Westerly Jet (WAWJ), and the Somali Low-Level Jet (Somali LLJ). The two-phase nature of the SALLJ is indicated: The Chaco jet event (CJE) and the no Chaco event (NCJE). Blue arrows indicate the trajectory of the main monsoon regimes. The names of the monsoon regimes are indicated: North American Monsoons (NAM), West African Monsoon (WAM), Western and Southern India (WSI), and Australian Monsoon (AM). The main sources of moisture are indicated. (For interpretation of the references to color in this figure legend, the reader is referred to the web version of this article.)

changes in synoptic weather systems (Berry et al., 2011; Clark et al., 2018).

A schematic view of the major mechanisms of moisture transport at the global scale together with their main sources of moisture are displayed in Fig. 5.

7. Future challenges

Over the next few years, further progress in the general area of atmospheric moisture transport is essential, and will require advances in the assessment of moisture sources, improvement in the approaches used to find the source-sink relationships, or better understanding of the role of moisture transport on rainfall distribution, and how the moisture is transported by atmospheric structures at the planetary scale, such as by Atmospheric Rivers or Low-Level Jet systems. We propose the following non-exhaustive list of seven challenges, which we believe to be essential in future research efforts.

Challenge 1: Regarding stable water isotopes, recent advances in measurement and modelling have been extensively discussed in literature. Nevertheless, the amount of isotopic data is still minimal compared with other climate data. A rapid increase in the number of satellite sensors, together with a dense network of in-situ measurements, may help to provide a global budget of the phenomena of interest, along with their inclusion in cloud microphysical analyses and validation of water vapour tracer models.

Challenge 2: Regarding analytical, Lagrangian, and Eulerian dispersion models, the scale of achievements has been somewhat constrained by computational limitations, especially in the latter. Advances in computational sciences could provide greater capabilities for atmospheric sciences, allowing us to derive global and climatological conclusions from tools that are nowadays used only at mesoscale and in very time-limited frameworks.

Challenge 3: Regarding residence/integration times, the consensus ranges from 8 to 10 days but is restricted to a global average as the time of residence has been determined to be constrained by the effect of local scale, with vegetation coverage playing a key role as a modulator of surface fluxes. A question that remains unanswered is whether the coarse resolution of the model-derived products (compared to the local scale of evapotranspiration) is suitable for assessing residence time of moisture in complex terrains, which applies for most of the tropics in which the greatest amount of atmospheric moisture is contained. Moreover, warming conditions pose a challenging scenario in that the residence time of atmospheric moisture is sensitive to temperature, hence warming may lead to an increase in the lifetime of moisture (see e.g., Stier et al., 2019).

Challenge 4: For the identification of moisture sources, beyond the identification of the sources of moisture and the discussion on how the results may differ depending on the approach used, of particular importance is the impact of the moisture origin on rainfall patterns. Knowledge of whether the dominant process that defines a given moisture source is evaporation from a water body or moisture recycling, for example, has specific implications on the distribution and intensity of the rainfall. Where the latter is the origin, this implies a partial constraint to the development of the production of rain, influencing aspects such as area, intensity, persistence, and even diurnal cycling. There is a need to improve the assessment of moisture sources, which is limited mainly due to the grid scale of the model outputs.

Challenge 5: As far as drought events are concerned, at the global scale, droughts are becoming both more frequent and more destructive. Multiple processes drive droughts; therefore, in the present and over the long term, the challenge of coping with this phenomenon may be addressed in hydrometeorology by determining possible strong links between changes in ocean and land evaporation for climatological moisture sources, and possible changes on the moisture supply from these regions as a precursor to the decline in rainfall over continental target regions. Considering that drought is caused initially by a decrease in rainfall, moisture transport from climatological source regions might have potential as an input to statistical models to predict the onset, persistence or recovery of drought episodes.

Challenge 6: Regarding heavy precipitation events, this phenomenon is usually linked to variations in the amount of atmospheric moisture transport at different time scales by mesoscale (e.g., local storms) and

synoptic systems (e.g., Low Level Jets, Atmospheric Rivers, cyclones). Considering that the frequency of extreme precipitation events is projected to increase under a warming climate, there is a need to better identify and delimit the sources of moisture supplying local and regional anomalous intense precipitation, and to evaluate independently the role of oceanic and continental moisture sources in providing moisture during these events, as well as to improve the assimilation of water vapour flux data in the model simulations, thus permitting us to improve the monitoring and forecasting of mesoscale and synoptic systems that generate heavy rainfall events.

Challenge 7: Regarding the major modes of moisture transport and their role in extreme precipitation events, it is necessary to improve the quantification of moisture transported by ARs and LLJ systems. Current tools are not able to quantify the transport of moisture, so they sometimes overestimate or neglect the moisture transported by these systems. Therefore, new techniques are needed to quantify the moisture transported by these mechanisms more precisely. Furthermore, accurate assessments are needed of how global warming will affect the main mechanisms of moisture transport. Changes in the regions of occurrence, in their frequencies and in the amount of moisture transported by ARs and LLJs will occur as a result of global warming. Detailed analyses are necessary to understand these changes in moisture transport patterns.

Funding

The present work was funded by the Spanish government within the LAGRIMA (RTI2018-095772-B-I00) and EVOCAR (CGL2015-65141-R) projects, funded by Ministerio de Ciencia, Innovación y Universidades, Spain, which are also funded by FEDER (European Regional Development Fund, ERDF). Marta Vázquez, Jorge Eiras-Barca and Rogert Sorí are supported by the Xunta de Galicia (Galician Regional Government) under grants ED481B 2018/062, ED481B 2018/069 and ED481B 2019/070. Iago Algarra was financially supported by the Spanish Government (MINECO) under grant CGL2015-65141-R. Jorge Eiras-Barca is also supported by the Fulbright Program (US Department of State). Milica Stojanovic is supported by the FCT-Portugal project “Weather Extremes in the Euro Atlantic Region: Assessment and Impacts-WEx-Atlantic” (PTDC/CTA-MET/29233/2017). Alexandre M. Ramos was supported by the Scientific Employment Stimulus 2017 from Fundação para a Ciência e Tecnologia (FCT, CEECIND/00027/2017). Francina Dominguez is supported by National Science Foundation (NSF) CAREER Award AGS 1454089. Partial support was also obtained from the Xunta de Galicia under the Project ED431C 2017/64-GRC “Programa de Consolidación e Estructuración de Unidades de Investigación Competitivas (Grupos de Referencia Competitiva)” and Consellería de Educación e Ordenación Universitaria Xunta de Galicia cofunding from the ERDF, in the framework of the Operational Program Galicia 2014-2020 “A way to build Europe”.

Declaration of competing interest

I confirm that there is no conflict of interest.

References

Ackerley, D., Berry, G., Jakob, C., Reeder, M.J., 2014. The roles of diurnal forcing and large-scale moisture transport for initiating rain over Northwest Australia in a GCM. Q. J. R. Meteorol. Soc. 140, 2515–2526. https://doi.org/10.1002/qj.2316.

Algarra, I., Eiras-Barca, J., Miguez-Macho, G., Nieto, R., Gimeno, L., 2019. On the assessment of the moisture transport by the Great Plains low-level jet. Earth Syst. Dynam. 10, 107–119. https://doi.org/10.5194/esd-10-107-2019.

Allan, R.P., Liu, C., Zahn, M., Lavers, D.A., Koukouvagias, E., Bodas-Salcedo, A., 2014. Physically consistent responses of the global atmospheric hydrological cycle in models and observations. Surv. Geophys. 35 (3), 533–552. https://doi.org/10.1007/s10712-012-9213-z.

Allen, S.T., Keim, R.F., Barnard, H.R., McDonnell, J.J., Renée Brooks, J., 2017. The role of stable isotopes in understanding rainfall interception processes: a review. Water 4 (1), e1187. https://doi.org/10.1002/wat2.1187.

Arias, P.A., Martínez, J.A., Vieira, S.C., 2015. Moisture sources to the 2010–2012 anomalous wet season in Northern South America. Clim. Dyn. 45, 2861–2884. https://doi.org/10.1007/s00382-015-2511-7.

Arnault, J., Knoche, R., Wei, J., Kunstmann, H., 2016. Evaporation tagging and atmospheric water budget analysis with WRF: a regional precipitation recycling study for West Africa. Water Resour. Res. 52, 1544–1567. https://doi.org/10.1002/2015WR017704.

Arraut, J.M., Nobre, C., Barbosa, H.M.J., Obregon, G., Marengo, J., 2012. Aerial rivers and lakes: looking at large-scale moisture transport and its relation to amazonia and to subtropical rainfall in South America. J. Clim. 25 (2), 543–556. https://doi.org/10.1175/2011JCLI4189.1.

Athar, H., Ammar, K., 2016. Seasonal characteristics of the large-scale moisture flux transport over the Arabian Peninsula. Theor. Appl. Climatol. 124, 565–578. https://doi.org/10.1007/s00704-015-1437-7.

Backes, T.M., Kaplan, M.L., Schumer, R., Mejia, J.F., 2015. A climatology of the vertical structure of water vapor transport to the Sierra Nevada in cool season atmospheric river precipitation events. J. Hydrometeorol. 16 (3), 1029–1047. https://doi.org/10.1175/jhm-d-14-0077.1.

Baer, D.S., Paul, J.B., Gupta, M., O'Keefe, A., 2002. Sensitive absorption measurements in the near-infrared region using off-axis integrated-cavity-output spectroscopy. Appl. Phys. B Lasers Opt. 75 (2–3), 261–265. https://doi.org/10.1007/s00340-002-0971-z.

Baker, A.J., Sodemann, H., Baldini, J.U.L., Breitenbach, S.F.M., Johnson, K.R., van Hunen, J., Zhang, P., 2015. Seasonality of westerly moisture transport in the East Asian summer monsoon and its implications for interpreting precipitation δ 18 O. J. Geophys. Res. Atmos. 120 (12), 5850–5862. https://doi.org/10.1002/2014JD022919.

Bao, J.-W., Michelson, S.A., Neiman, P.J., Ralph, F.M., Wilczak, J.M., 2006. Interpretation of enhanced integrated water vapor bands associated with extratropical cyclones: their formation and connection to tropical moisture. Mon. Weather Rev. 134, 1063–1080. https://doi.org/10.1175/MWR3123.1.

Barandiaran, D., Wang, S.-Y., Hilburn, K., 2013. Observed trends in the Great Plains low-level jet and associated precipitation changes in relation to recent droughts. Geophys. Res. Lett. 40 (23), 6247–6251. https://doi.org/10.1002/2013GL058296.

Barras, V., Simmonds, I., 2009. Observation and modeling of stable water isotopes as diagnostics of rainfall dynamics over southeastern Australia. J. Geophys. Res. 114, 23308. https://doi.org/10.1029/2009JD012132.

Bathiany, S., Dakos, V., Scheffer, M., Lenton, T.M., 2018. Climate models predict increasing temperature variability in poor countries. Sci. Adv. 4 (5), eaar5809. https://doi.org/10.1126/sciadv.aar5809.

Berg, L.K., Riihimaki, L.D., Qian, Y., Yan, H., Huang, M., 2015. The low-level jet over the southern great plains determined from observations and reanalyses and its impact on moisture transport. J. Clim. 28 (17), 6682–6706. https://doi.org/10.1175/JCLI-D-14-00719.1.

Berry, G., Reeder, M.J., Jakob, C., 2011. Physical mechanisms regulating summertime rainfall over northwestern Australia. J. Clim. 24 (14), 3705–3717. https://doi.org/10.1175/2011JCLI3943.1.

Bin, C., Xiang-De, X., Tianliang, Z., 2013. Main moisture sources affecting lower yangtze river basin in boreal summers during. Int. J. Climatol. 33, 1035–1046. https://doi.org/10.1002/joc.3495.

Bisselink, B., Dolman, A.J., 2008. Precipitation recycling: moisture sources over Europe using ERA-40 data. J. Hydrometeorol. 9 (5), 1073–1083. https://doi.org/10.1175/2008JHM962.1.

Blamey, R.C., Ramos, A.M., Trigo, R.M., Tomé, R., Reason, C.J.C., 2017. The influence of atmospheric rivers over the South Atlantic on winter rainfall in South Africa. J. Hydrometeorol. 19 (1), 127–142. https://doi.org/10.1175/jhm-d-17-0111.1.

Boesch, H., Deutscher, N.M., Warneke, T., Byckling, K., Cogan, A.J., Griffith, D.W.T., Parker, R.J., Wang, Z., 2013. HDO/H2O ratio retrievals from GOSAT. Atmos. Meas. Tech. 6, 599–612. https://doi.org/10.5194/amt-6-599-2013.

Bohlinger, P., Sorteberg, A., 2018. A comprehensive view on trends in extreme precipitation in Nepal and their spatial distribution. Int. J. Climatol. 38, 1833–1845. https://doi.org/10.1002/joc.5299.

Bohn, T.J., Vivoni, E.R., 2016. Process-based characterization of evapotranspiration sources over the North American monsoon region. Water Resour. Res. 52 (1), 358–384. https://doi.org/10.1002/2015WR017934.

Bonner, W.D., 1968. Climatology of the low level jet. Mon. Weather Rev. 96 (12), 833–850. https://doi.org/10.1175/1520-0493(1968)096<0833:COTLLJ>2.0.CO;2.

Bosilovich, M.G., 2003. Numerical simulation of the large-scale North American monsoon water sources. J. Geophys. Res. 108 (D16), 1–14. https://doi.org/10.1029/2002jd003095.

Bosilovich, M.G., Chern, J.-D., 2006. Simulation of water sources and precipitation recycling for the MacKenzie, Mississippi, and Amazon River Basins. J. Hydrometeorol. 7 (3), 312–329. https://doi.org/10.1175/JHM501.1.

Bosmans, J.H.C., van Beek, L.P.H., Sutanudjaja, E.H., Bierkens, M.F.P., 2017. Hydrological impacts of global land cover change and human water use. Hydrol. Earth Syst. Sci. 21, 5603–5626. https://doi.org/10.5194/hess-21-5603-2017.

Bracken, C., Rajagopalan, B., Alexander, M., Gangopadhyay, S., 2015. Spatial variability of seasonal extreme precipitation in the Western United States. J. Geophys. Res. Atmos. 120 (10), 4522–4533. https://doi.org/10.1002/2015JD023205.

Burde, G.I., Gandush, C., Bayarjargal, Y., 2006. Bulk recycling models with incomplete vertical mixing. Part II: precipitation recycling in the Amazon Basin. J. Clim. 19 (8), 1473–1489. https://doi.org/10.1175/JCLI3688.1.

Carleton, A.M., Carpenter, D.A., Weser, P.J., 1990. Mechanisms of interannual variability of the southwest United states summer rainfall maximum. J. Clim. 3 (9), 999–1015. https://doi.org/10.1175/1520-0442(1990)003<0999:MOIVOT>2.0.CO;2.

Catto, J.L., Jakob, C., Nicholls, N., 2012. The influence of changes in synoptic regimes on

north Australian wet season rainfall trends. J. Geophys. Res. Atmos. 117 (10), 1–9. https://doi.org/10.1029/2012JD017472.
Champion, A.J., Allan, R.P., Lavers, D.A., 2015. Atmospheric rivers do not explain UK summer extreme rainfall. J. Geophys. Res. 120 (14), 6731–6741. https://doi.org/10.1002/2014JD022863.
Chaudhari, S., Pokhrel, Y., Moran, E., Miguez-Macho, G., 2019. Multi-decadal hydrologic change and variability in the amazon river basin: understanding terrestrial water storage variations and drought characteristics. Hydrol. Earth Syst. Sci. 23, 2841–2862. https://doi.org/10.5194/hess-23-2841-2019.
Chen, B., Xu, X.-D., Yang, S., Zhang, W., 2012. On the origin and destination of atmospheric moisture and air mass over the Tibetan Plateau. Theor. Appl. Climatol. 110 (3), 423–435. https://doi.org/10.1007/s00704-012-0641-y.
Chen, G., Norris, J., Neelin, J.D., Lu, J., Leung, L.R., Sakaguchi, K., 2019. Thermodynamic and dynamic mechanisms for hydrological cycle intensification over the full probability distribution of precipitation events. J. Atmos. Sci. 76, 497–516. https://doi.org/10.1175/JAS-D-18-0067.1.
Ciric, D., Stojanovic, M., Drumond, A., Nieto, R., Gimeno, L., 2016. Tracking the origin of moisture over the Danube River Basin using a lagrangian approach. Atmosphere 7 (12), 162. https://doi.org/10.3390/atmos7120162.
Ciric, D., Nieto, R., Ramos, A.M., Drumond, A., Gimeno, L., 2017. Wet spells and associated moisture sources anomalies across Danube River basin. Water 9, 615. https://doi.org/10.3390/w9080615.
Ciric, D., Nieto, R., Ramos, A.M., Drumond, A., Gimeno, L., 2018a. Contribution of moisture from mediterranean sea to extreme precipitation events over Danube River basin. Water 10 (9), 1182. https://doi.org/10.3390/w10091182.
Ciric, D., Nieto, R., Losada, L., Drumond, A., Gimeno, L., 2018b. The mediterranean moisture contribution to climatological and extreme monthly continental precipitation. Water 10 (4), 519. https://doi.org/10.3390/w10040519.
Clark, S., Reeder, M.J., Jakob, C., 2018. Rainfall regimes over northwestern Australia. Q. J. R. Meteorol. Soc. 144 (711), 458–467. https://doi.org/10.1002/qj.3217.
Cook, K.H., Vizy, E.K., 2010. Hydrodynamics of the Caribbean low-level jet and its relationship to precipitation. J. Clim. 23 (6), 1477–1494. https://doi.org/10.1175/2009JCLI3210.1.
Cook, C., Reason, C.J.C., Hewitson, B.C., 2004. Wet and dry spells within particularly wet and dry summers in the South African summer rainfall region. Clim. Res. 26, 17–31. https://doi.org/10.3354/cr026017.
Cordeira, J.M., Ralph, F.M., Moore, B.J., 2013. The development and evolution of two atmospheric rivers in proximity to western North Pacific tropical cyclones in October 2010. Mon. Weather Rev. 141, 4234–4255. https://doi.org/10.1175/MWR-D-13-00019.
Cosgrove, W.J., Loucks, D.P., 2015. Water management: current and future challenges and research directions. Water Resour. Res. 51, 4823–4839. https://doi.org/10.1002/2014WR016869.
Couto, F.T., Salgado, R., Costa, M.J., Prior, V., 2015. Precipitation in the Madeira Island over a 10-year period and the meridional water vapour transport during the winter seasons. Int. J. Climatol. 35 (13), 3748–3759. https://doi.org/10.1002/joc.4243.
Craig, H., 1961. Isotopic variations in meteoric waters. Science 133 (3465), 1702–1703. https://doi.org/10.1126/science.133.3465.1702.
Crosson, E.R., Ricci, K.N., Richman, B.A., Chilese, F.C., Owano, T.G., Provencal, R.A., Todd, M.W., Glasser, J., Kachanov, A.A., Paldus, B.A., Spence, T.G., Zare, R.N., 2002. Stable isotope ratios using cavity ring-down spectroscopy: determination of 13C/12C for carbon dioxide in human breath. Anal. Chem. 74 (9), 2003–2007. https://doi.org/10.1021/ac025511d.
Dacre, H.F., Clark, P.A., Martinez-Alvarado, O., Stringer, M.A., Lavers, D.A., 2015. How do atmospheric rivers form? Bull. Am. Meteorol. Soc. 96 (8), 1243–1255. https://doi.org/10.1175/BAMS-D-14-00031.1.
Dansgaard, W., 1954. The O18-abundance in fresh water. Geochim. Cosmochim. Acta 6 (5–6), 241–260. https://doi.org/10.1016/0016-7037(54)90003-4.
Dansgaard, W., 1964. Stable isotopes in precipitation. Tellus 16 (4), 436–468. https://doi.org/10.3402/tellusa.v16i4.8993.
Davis, J., Knippertz, P., Fink, A.H., 2013. The predictability of precipitation episodes during the West African dry season. Q. J. R. Meteorol. Soc. 139, 1047–1058. https://doi.org/10.1002/qj.2014.
De Leeuw, J., Methven, J., Blackburn, M., 2017. Physical factors influencing regional precipitation variability attributed using an airmass trajectory method. J. Clim. 30 (18), 7359–7378. https://doi.org/10.1175/JCLI-D-16-0547.1.
De sousa, A.C., Candido, L.A., Andreoli, R.V., 2018. Variabilidade interanual da precipitação e fluxo de umidade sobre a amazônia usando o QTCM. Rev. Bras. Meteorol. 33 (1), 41–56. https://doi.org/10.1590/0102-7786331015.
Dee, S., Noone, D., Buenning, N., Emile-Geay, J., Zhou, Y., 2015. SPEEDY-IER: a fast atmospheric GCM with water isotope physics. J. Geophys. Res. Atmos. 120 (1), 73–91. https://doi.org/10.1002/2014JD022194.
Dettinger, M.D., Ralph, F.M., Das, T., Neiman, P.J., Cayan, D.R., 2011. Atmospheric rivers, floods and the water resources of California. Water 3 (2), 445–478. https://doi.org/10.3390/w3020445.
Dettinger, M., Ralph, F.M., Lavers, D., 2015. Setting the stage for a global science of atmospheric rivers. Eos 96. https://doi.org/10.1029/2015EO038675, 2015.
Ding, Y., Sun, Y., Wang, Z., Zhu, Y., Song, Y., 2009. Inter-decadal variation of the summer precipitation in China and its association with decreasing Asian summer monsoon part II: possible causes. Int. J. Climatol. 29 (13), 1926–1944. https://doi.org/10.1002/joc.1759.
Dirmeyer, P.A., Kinter, J.L., 2009. The "Maya Express": floods in the U.S. Midwest. Eos (Washington, DC) 90 (12), 101–102. https://doi.org/10.1029/2009EO120001.
Dirmeyer, P.A., Kinter, J.L., 2010. Floods over the U.S. Midwest: a regional water cycle perspective. J. Hydrometeorol. 11, 1172–1181. https://doi.org/10.1175/2010JHM1196.1.
Dirmeyer, P.A., Wei, J., Bosilovich, M.G., Mocko, D.M., 2014. Comparing evaporative sources of terrestrial precipitation and their extremes in MERRA using relative entropy. J. Hydrometeorol. 15, 102–116. https://doi.org/10.1175/JHM-D-13-053.1.
do Nascimento, M.G., Herdies, D.L., Oliveira de Souza, D., 2016. The South American water balance: the influence of low-level jets. J. Clim. 29, 1429–1449. https://doi.org/10.1175/JCLI-D-15-0065.1.
Dominguez, F., Kumar, P., Liang, X., Ting, M., 2006. Impact of atmospheric moisture storage on precipitation recycling. J. Clim. 19, 1513–1530. https://doi.org/10.1175/JCLI3691.1.
Dominguez, F., Miguez-Macho, G., Hu, H., 2016. WRF with water vapor tracers: a study of moisture sources for the North American monsoon. J. Hydrometeorol. 17, 1915–1927. https://doi.org/10.1175/JHM-D-15-0221.1.
Dong, X., Xi, B., Kennedy, A., Feng, Z., Entin, J.K., Houser, P.R., Schiffer, R.A., L'Ecuyer, T., Olson, W.S., Hsu, K., Liu, W.T., Lin, B., Deng, Y., Jiang, T., 2011. Investigation of the 2006 drought and 2007 flood extremes at the Southern Great Plains through an integrative analysis of observations. J. Geophys. Res. 116 (D3), D03204. https://doi.org/10.1029/2010JD014776.
Drumond, A., Nieto, R., Gimeno, L., Ambrizzi, T., 2008. A lagrangian identification of major sources of moisture over central Brazil and La Plata Basin. J. Geophys. Res. 113 (D14), D14128. https://doi.org/10.1029/2007JD009547.
Drumond, A., Nieto, R., Gimeno, L., 2011a. Sources of moisture for China and their variations during drier and wetter conditions in 2000 − 2004: a lagrangian approach. Clim. Res. 50 (2), 215–225. https://doi.org/10.3354/cr01043.
Drumond, A., Nieto, R., Gimeno, L., 2011b. On the contribution of the tropical western hemisphere warm pool source of moisture to the northern hemisphere precipitation through a Lagrangian approach. J. Geophys. Res. Atmos. 116 (D21). https://doi.org/10.1029/2010JD015397.
Drumond, A., Nieto, R., Hernández, E., Gimeno, L., 2011c. A Lagrangian analysis of the variation in moisture sources related to drier and wetter conditions in regions around the Mediterranean Basin. Nat. Hazards Earth Syst. Sci. 11 (8), 2307–2320. https://doi.org/10.5194/nhess-11-2307-2011.
Drumond, A., Marengo, J., Ambrizzi, T., Nieto, R., Moreira, L., Gimeno, L., 2014. The role of the Amazon Basin moisture in the atmospheric branch of the hydrological cycle: a lagrangian analysis. Hydrol. Earth Syst. Sci. 18, 2577–2598. https://doi.org/10.5194/hess-18-2577-2014.
Drumond, A., Nieto, R., Gimeno, L., 2016. A Lagrangian approach for investigating anomalies in the moisture transport during drought episodes. Cuad. Investig. Geogr. 42 (1), 113–125. https://doi.org/10.18172/cig.2925.
Drumond, A., Gimeno, L., Nieto, R., Trigo, R.M., Vicente-Serrano, S., Gimeno, L., 2017. Drought episodes in the climatological sinks of the Mediterranean moisture source: the role of moisture transport. Glob. Planet. Chang. 151, 4–14. https://doi.org/10.1016/j.gloplacha.2016.12.004.
Drumond, A., Stojanovic, M., Nieto, R., Vicente-Serrano, S., Gimeno, L., 2019. Linking anomalous moisture transport and drought episodes in the IPCC reference regions. Bull. Amer. Meteor. Soc. https://doi.org/10.1175/BAMS-D-18-0111.1.
Durán-Quesada, A.M., Gimeno, L., Amador, J.A., Nieto, R., 2010. Moisture sources for central America: identification of moisture sources using a Lagrangian analysis technique. J. Geophys. Res. 115 (D5), D05103. https://doi.org/10.1029/2009JD012455.
Durán-Quesada, A.M., Reboita, M., Gimeno, L., 2012. Precipitation in tropical America and the associated sources of moisture: a short review. Hydrol. Sci. J. 57. https://doi.org/10.1080/02626667.2012.673723.
Durán-Quesada, A.M., Gimeno, L., Amador, J., 2017. Role of moisture transport for central American precipitation. Earth Syst. Dynam 8, 147–161. https://doi.org/10.5194/esd-8-147-2017.
Dyroff, C., FŘtterer, D., Zahn, A., 2010. Compact diode-laser spectrometer ISOWAT for highly sensitive airborne measurements of water-isotope ratios. Appl. Phys. B Lasers Opt. 98 (2–3), 537–548. https://doi.org/10.1007/s00340-009-3775-6.
Eiras-Barca, J., Brands, S., Miguez-Macho, G., 2016. Seasonal variations in North Atlantic atmospheric river activity and associations with anomalous precipitation over the Iberian Atlantic Margin. J. Geophys. Res. Atmos. 121 (2), 931–948. https://doi.org/10.1002/2015JD023379.
Eiras-Barca, J., Dominguez, F., Hu, H., Garaboa-Paz, D., Miguez-Macho, G., 2017. Evaluation of the moisture sources in two extreme landfalling atmospheric river events using an Eulerian WRF tracers tool. Earth Syst. Dynam. 8, 1247–1261. https://doi.org/10.5194/esd-8-1247-2017.
Eiras-Barca, J., Lorenzo, N., Taboada, J., Robles, A., Miguez-Macho, G., 2018a. On the relationship between atmospheric rivers, weather types and floods in Galicia (NW Spain). Nat. Hazards Earth Syst. Sci. 18 (6), 1633–1645. https://doi.org/10.5194/nhess-18-1633-2018.
Eiras-Barca, J., Ramos, A.M., Pinto, J.G., Trigo, R.M., Liberato, M.L.R., Miguez-Macho, G., 2018b. The concurrence of atmospheric rivers and explosive cyclogenesis in the North Atlantic and North Pacific basins. Earth Syst. Dyn. 9 (1), 91–102. https://doi.org/10.5194/esd-9-91-2018.
Erlingis, J.M., Gourley, J.J., Basara, J.B., 2019. Diagnosing moisture sources for flash floods in the United States. Part II: terrestrial and oceanic sources of moisture. J. Hydrometeorol. 20, 1511–1531. https://doi.org/10.1175/JHM-D-18-0120.1.
Espinoza, J.C., Ronchail, J., Frappart, F., Lavado, W., Santini, W., Guyot, J.L., 2012. The major floods in the Amazonas River and tributaries (Western Amazon Basin) during the 1970–2012 period: a focus on the 2012 flood. J. Hydrometeorol. 14, 1000–1008. https://doi.org/10.1175/JHM-D-12-0100.1.
Espinoza, J.C., Marengo, J.A., Ronchail, J., Molina, J., Noriega, L., Guyot, J.L., 2014. The extreme 2014 flood in South-Western Amazon basin: the role of tropical-subtropical South Atlantic SST gradient. Environ. Res. Lett. 9, 124007. https://doi.org/10.1088/1748-9326/9/12/124007.
Espinoza, V., Waliser, D.E., Guan, B., Lavers, D.A., Ralph, F.M., 2018. Global analysis of

climate change projection effects on Atmospheric Rivers. Geophys. Res. Lett. 4299–4308. https://doi.org/10.1029/2017GL076968.
Esquivel-Hernández, G., Mosquera, G.M., Sánchez-Murillo, R., Quesada-Román, A., Birkel, C., Crespo, P., Célleri, R., Windhorst, D., Breuer, L., Boll, J., 2019. Moisture transport and seasonal variations in the stable isotopic composition of rainfall in Central American and Andean Páramo during El Niño conditions (2015–2016). Hydrol. Process. 13438. https://doi.org/10.1002/hyp.13438.
FAO, 2011. The State of the World's Land and Water Resources for Food and Agriculture (SOLAW) – Managing Systems at Risk. Food and Agriculture Organization of the United Nations, Rome and Earthscan, London.
Fontaine, B., Roucou, P., Trzaska, S., 2003. Atmospheric water cycle and moisture fluxes in the West African monsoon: mean annual cycles and relationship using NCEP/NCAR reanalysis. Geophys. Res. Lett. 30 (3), 1117. https://doi.org/10.1029/2002GL015834.
Frankenberg, C., Wunch, D., Toon, G., Risi, C., Scheepmaker, R., Lee, J.E., Wennberg, P., Worden, J., 2013. Water vapor isotopologue retrievals from high-resolution GOSAT shortwave infrared spectra. Atmos. Meas. Tech. 6 (2), 263–274. https://doi.org/10.5194/amt-6-263-2013.
Galewsky, J., Rabanus, D., 2016. A stochastic model for diagnosing subtropical humidity dynamics with stable isotopologues of water vapor. J. Atmos. Sci. 73 (4), 1741–1753. https://doi.org/10.1175/JAS-D-15-0160.1.
Galewsky, J., Steen-Larsen, H.C., Field, R.D., Worden, J., Risi, C., Schneider, M., 2016. Stable isotopes in atmospheric water vapor and applications to the hydrologic cycle. Rev. Geophys. 54 (4), 809–865. https://doi.org/10.1002/2015RG000512.
Gallego, D., García-Herrera, R., Peña-Ortiz, C., Ribera, P., 2017. The steady enhancement of the Australian Summer Monsoon in the last 200 years. Sci. Rep. 7 (1), 16166. https://doi.org/10.1038/s41598-017-16414-1.
Gallego, D., García-Herrera, R., Gómez-Delgado, F.D.P., Ordoñez-Perez, P., Ribera, P., 2019. Tracking the moisture transport from the Pacific towards Central and northern South America since the late 19th century. Earth Syst. Dynam 10, 319–331. https://doi.org/10.5194/esd-10-319-2019.
Gao, Y., Lu, J., Leung, L.R., 2016. Uncertainties in projecting future changes in atmospheric rivers and their impacts on heavy precipitation over Europe. J. Clim. 29 (18), 6711–6726. https://doi.org/10.1175/JCLI-D-16-0088.1.
García-Herrera, R., Garrido-Pérez, J.M., Barriopedro, D., Ordóñez, C., Vicente-Serrano, S.M., Nieto, R., Gimeno, L., Sorí, R., Yiou, P., 2019. The European 2016/2017 drought. J. Clim. 32 (11), 3169–3187. https://doi.org/10.1175/JCLI-D-18-0331.1.
Gimeno, L., 2013. Grand challenges in atmospheric science. Front. Earth Sci. 1, 1–5. https://doi.org/10.3389/feart.2013.00001.
Gimeno, L., Nieto, R., Trigo, R.M., Vicente-Serrano, S.M., López-Moreno, J.I., 2010. Where does the Iberian Peninsula moisture come from? An answer based on a Lagrangian approach. J. Hydrometeorol. 11 (2), 421–436. https://doi.org/10.1175/2009JHM1182.1.
Gimeno, L., Stohl, A., Trigo, R.M., Dominguez, F., Yoshimura, K., Yu, L., Drumond, A., Durán-Quesada, A.M., Nieto, R., 2012. Oceanic and terrestrial sources of continental precipitation. Rev. Geophys. 50 (4). https://doi.org/10.1029/2012RG000389.
Gimeno, L., Nieto, R., Vázquez, M., Lavers, D.A., 2014. Atmospheric rivers: a mini-review. Front. Earth Sci. 2, 2. https://doi.org/10.3389/feart.2014.00002.
Gimeno, L., Vázquez, M., Nieto, R., Trigo, R.M., 2015. Atmospheric moisture transport: the bridge between ocean evaporation and arctic ice melting. Earth Syst. Dynam. 6, 583–589. https://doi.org/10.5194/esd-6-583-2015.
Gimeno, L., Dominguez, F., Nieto, R., Trigo, R., Drumond, A., Reason, C.J.C., Taschetto, A.S., Ramos, A.M., Kumar, R., Marengo, J., 2016. Major mechanisms of atmospheric moisture transport and their role in extreme precipitation events. Annu. Rev. Environ. Resour. 41, 117–141. https://doi.org/10.1146/annurev-environ-110615-085558.
Gimeno, L., Vázquez, M., Eiras-Barca, J., Sorí, R., Algarra, I., Nieto, R., 2019. Atmospheric moisture transport and the decline in Arctic Sea ice. Wiley Interdiscip. Rev. Clim. Chang. 1–12. https://doi.org/10.1002/wcc.588.
Gimeno-Sotelo, L., Nieto, R., Vázquez, M., Gimeno, L., 2019. The role of moisture transport for precipitation in the inter-annual and inter-daily fluctuations of the Arctic sea ice extension. Earth Syst. Dynam. 10, 121–133. https://doi.org/10.5194/esd-10-121-2019.
Giorgi, F., Raffaele, F., Coppola, E., 2019. The response of precipitation characteristics to global warming from climate projections. Earth Syst. Dynam. 10, 73–89. https://doi.org/10.5194/esd-10-73-2019.
Goessling, H., Reick, C.H., 2013. On the" well-mixed" assumption and numerical 2-D tracing of atmospheric moisture. Atmos. Chem. Phys. 13, 5567–5585. https://doi.org/10.5194/acp-13-5567-2013.
Gómez-Hernández, M., Drumond, A., Gimeno, L., Garcia-Herrera, R., 2013. Variability of moisture sources in the Mediterranean region during the period. Water Resour. Res. 49, 6781–6794. https://doi.org/10.1002/wrcr.20538.
Gorodetskaya, I.V., Tsukernik, M., Claes, K., Ralph, M.F., Neff, W.D., van Lipzig, N.P.M., 2014. The role of atmospheric rivers in anomalous snow accumulation in East Antarctica. Geophys. Res. Lett. 41 (17), 6199–6206. https://doi.org/10.1002/2014GL060881.
Grams, C.M., Jones, S.C., Marsham, J.H., Parker, D.J., Haywood, J.M., Heuveline, V., 2010. The Atlantic inflow to the Saharan heat low: observations and modelling. Q. J. R. Meteorol. Soc. 136, 125–140. https://doi.org/10.1002/qj.429.
Grams, C.M., Binder, H., Pfahl, S., Piaget, N., Wernli, H., 2014. Atmospheric processes triggering the central European floods in June 2013. Nat. Hazards Earth Syst. Sci. 14, 1691–1702. https://doi.org/10.5194/nhess-14-1691-2014.
Guan, B., Waliser, D.E., 2015. Detection of atmospheric rivers: evaluation and application of an algorithm for global studies. J. Geophys. Res. Atmos. 120 (24), 12514–12535. https://doi.org/10.1002/2015JD024257.
Guan, B., Waliser, D.E., 2017. Atmospheric rivers in 20 year weather and climate simulations: a multimodel, global evaluation. J. Geophys. Res. 122 (11), 5556–5581. https://doi.org/10.1002/2016JD026174.
Guan, B., Molotch, N.P., Waliser, D.E., Fetzer, E.J., Neiman, P.J., 2010. Extreme snowfall events linked to atmospheric rivers and surface air temperature via satellite measurements. Geophys. Res. Lett. 37 (20), 2–7. https://doi.org/10.1029/2010GL044696.
Guan, H., Zhang, X., Skrzypek, G., Sun, Z., Xu, X., 2013. Deuterium excess variations of rainfall events in a coastal area of South Australia and its relationship with synoptic weather systems and atmospheric moisture sources. J. Geophys. Res. Atmos. 118 (2), 1123–1138. https://doi.org/10.1002/jgrd.50137.
Guo, L., Klingaman, N.P., Demory, M.-E., Vidale, P.L., Turner, A.G., Stephan, C.C., 2018. The contributions of local and remote atmospheric moisture fluxes to East Asian precipitation and its variability. Clim. Dyn. 51, 4139–4156. https://doi.org/10.1007/s00382-017-4064-4.
Gustafsson, M., Rayner, D., Chen, D., 2010. Extreme rainfall events in Southern Sweden: where does the moisture come from? Tellus Ser. A Dyn. Meteorol. Oceanogr. 62, 605–616. https://doi.org/10.1111/j.1600-0870.2010.00456.x.
Hagos, S.M., Cook, K.H., 2007. Dynamics of the West African monsoon jump. J. Clim. 20 (21), 5264–5284. https://doi.org/10.1175/2007JCLI1533.1.
Harding, K.J., Snyder, P.K., 2014. Examining future changes in the character of Central U.S. warm-season precipitation using dynamical downscaling. J. Geophys. Res. Atmos. 119 (23), 13116–13136. https://doi.org/10.1002/2014JD022575.
Harding, K.J., Snyder, P.K., 2015. The relationship between the Pacific-North American teleconnection pattern, the great plains low-level jet, and North Central U.S. heavy rainfall events. J. Clim. 28 (17), 6729–6742. https://doi.org/10.1175/JCLI-D-14-00657.1.
Hart, N.C.G., Reason, C.J.C., Fauchereau, N., 2010. Tropical–extratropical interactions over Southern Africa: three cases of heavy summer season rainfall. Mon. Weather Rev. 138 (7), 2608–2623. https://doi.org/10.1175/2010MWR3070.1.
Held, I.M., Soden, B.J., 2006. Robust responses of the hydrological cycle to global warming. J. Clim. 19, 5686–5699. https://doi.org/10.1175/JCLI3990.1.
Herrera-Estrada, J.E., Martinez, J.A., Dominguez, F., Findell, K.L., Wood, E.F., Sheffield, J., 2019. Reduced moisture transport linked to drought propagation across North America. Geophys. Res. Lett. 46, 1–11. https://doi.org/10.1029/2019GL082475.
Heydarizad, M., Raeisi, E., Sori, R., Gimeno, L., 2018a. The identification of Iran's moisture sources using a lagrangian particle dispersion model. Atmosphere 9 (10), 408. https://doi.org/10.3390/atmos9100408.
Heydarizad, M., Raeisi, E., Sorí, R., Gimeno, L., Nieto, R., 2018b. The role of moisture sources and climatic teleconnections in Northeastern and South-Central Iran's Hydroclimatology. Water. 10 (11), 1550. https://doi.org/10.3390/w10111550.
Higgins, R.W., Shi, W., Hain, C., 2004. Relationships between Gulf of California moisture surges and precipitation in the southwestern United States. J. Clim. 17 (15), 2983–2997. https://doi.org/10.1175/1520-0442(2004)017<2983:RBGOCM>2.0.CO;2.
Houze, R.A., Rasmussen, K.L., Medina, S., Brodzik, S.R., Romatschke, U., 2011. Anomalous atmospheric events leading to the summer 2010 floods in Pakistan. Bull. Amer. Meteor. Soc. 92, 291–298. https://doi.org/10.1175/2010BAMS3173.1.
Hoyos, I., Dominguez, F., Cañón-Barriga, J., Martínez, J.A., Nieto, R., Gimeno, L., Dirmeyer, P.A., 2018. Moisture origin and transport processes in Colombia, Northern South America. Clim. Dyn. 50 (3–4), 971–990. https://doi.org/10.1007/s00382-017-3653-6.
Hoyos, I., Cañón-Barriga, J., Arenas-Suárez, T., Dominguez, F., Rodríguez, B.A., 2019. Variability of regional atmospheric moisture over Northern South America: patterns and underlying phenomena. Clim. Dyn. 52 (1–2), 893–911. https://doi.org/10.1007/s00382-018-4172-9.
Hu, H., Dominguez, F., 2015. Evaluation of oceanic and terrestrial sources of moisture for the North American Monsoon using numerical models and precipitation stable isotopes. J. Hydrometeorol. 16 (1), 19–35. https://doi.org/10.1175/JHM-D-14-0073.1.
Hu, Q., Jiang, D., Lang, X., Xu, B., 2018. Moisture sources of the Chinese Loess Plateau during 1979–2009. Palaeogeogr. Palaeoclimatol. Palaeoecol. 509, 156–163. https://doi.org/10.1016/J.PALAEO.2016.12.030.
Hua, L., Zhong, L., Ma, Z., 2017. Decadal transition of moisture sources and transport in northwestern China during summer from 1982 to 2010. J. Geophys. Res. Atmos. 122 (23), 12522–12540. https://doi.org/10.1002/2017JD027728.
Huang, W., He, X., Yang, Z., Qiu, T., Wright, J.S., Wang, B., Lin, D., 2018a. Moisture sources for wintertime extreme precipitation events over South China during 1979–2013. J. Geophys. Res. Atmos. 123, 6690–6712. https://doi.org/10.1029/2018JD028485.
Huang, W., Qiu, T., Yang, Z., Lin, D., Wright, J.S., Wang, B., He, X., 2018b. On the formation mechanism for wintertime extreme precipitation events over the southeastern Tibetan Plateau. J. Geophys. Res. Atmos. 123, 12692–12714. https://doi.org/10.1029/2018JD028921.
Hughes, M., Mahoney, K.M., Neiman, P.J., Moore, B.J., Alexander, M., Ralph, F.M., 2014. The landfall and inland penetration of a flood-producing Atmospheric River in Arizona. Part II: sensitivity of modeled precipitation to terrain height and atmospheric river orientation. J. Hydrometeorol. 15 (5), 1954–1974. https://doi.org/10.1175/JHM-D-13-0176.1.
Hurley, J.V., Galewsky, J., Worden, J., Noone, D., 2012. A test of the advection-condensation model for subtropical water vapor using stable isotopologue observations from Mauna Loa Observatory, Hawaii. J. Geophys. Res. Atmos. 117 (D19). https://doi.org/10.1029/2012JD018029.
Insua-Costa, D., Miguez-Macho, G., 2018. A new moisture tagging capability in the Weather Research and Forecasting model: formulation, validation and application to the 2014 Great Lake-effect snowstorm. Earth Syst. Dynam. 9, 167–185. https://doi.org/10.5194/esd-9-167-2018.
IPCC, 2014. Climate Change. 2014. Synthesis Report. Contribution of Working Groups I,

II and III to the Fifth Assessment Report of the Intergovernmental Panel on Climate Change. [Core Writing Team, R.K. Pachauri and L.A. Meyer (eds.)]. IPCC, Geneva, Switzerland 151 pp.
Jack, C., 2012. A Lagrangian Moisture Source Attribution Model and Analysis of Southern Africa. University of Cape Town.
Jouzel, J., Delaygue, G., Landais, A., Masson-Delmotte, V., Risi, C., Vimeux, F., 2013. Water isotopes as tools to document oceanic sources of precipitation. Water Resour. Res. 49 (11), 7469–7486. https://doi.org/10.1002/2013WR013508.
Karuna Sagar, S., Rajeevan, M., Viajaya Bhaskara Rao, S., 2017. On increasing monsoon rainstorms over India. Nat. Hazards 85, 1743–1757. https://doi.org/10.1007/s11069-016-2662-9.
Kelemen, F.D., Ludwig, P., Reyers, M., Ulbrich, S., Pinto, J.G., 2016. Evaluation of moisture sources for the Central European summer flood of May/June 2013 based on regional climate model simulations. Tellus A Dyn. Meteorol. Oceanogr. 68, 29288. https://doi.org/10.3402/tellusa.v68.29288.
Keune, J., Sulis, M., Kollet, S., Siebert, S., Wada, Y., 2018. Human water use impacts on the strength of the continental sink for atmospheric water. Geophys. Res. Lett. 45, 4068–4076. https://doi.org/10.1029/2018GL077621.
Keys, P.W., Wang-Erlandsson, L., Gordon, L.J., 2016. Revealing invisible water: moisture recycling as an ecosystem service. PLoS One 11 (3), e0151993. https://doi.org/10.1371/journal.pone.0151993.
Kingston, D.G., Lavers, D.A., Hannah, D.M., 2016. Floods in the Southern Alps of New Zealand: the importance of atmospheric rivers. Hydrol. Process. 30 (26), 5063–5070. https://doi.org/10.1002/hyp.10982.
Knight, D.B., Davis, R.E., 2007. Climatology of tropical cyclone rainfall in the Southeastern United States. Phys. Geogr. 28 (2), 126–147. https://doi.org/10.2747/0272-3646.28.2.126.
Knippertz, P., Wernli, H., 2010. A Lagrangian climatology of tropical moisture exports to the Northern Hemispheric extratropics. J. Clim. 23 (4), 987–1003. https://doi.org/10.1175/2009JCLI3333.1.
Knippertz, P., Wernli, H., Gläser, G., 2013. A global climatology of tropical moisture exports. J. Clim. 26 (10), 3031–3045. https://doi.org/10.1175/JCLI-D-12-00401.1.
Knoche, H.R., Kunstmann, H., 2013. Tracking atmospheric water pathways by direct evaporation tagging: a case study for West Africa. J. Geophys. Res. Atmos. 118 (22), 12–345. https://doi.org/10.1002/2013JD019976.
Kopec, B.G., Feng, X., Michel, F.A., Posmentier, E.S., 2016. Influence of sea ice on Arctic precipitation. Proc. Natl. Acad. Sci. U. S. A. 113 (1), 46–51. https://doi.org/10.1073/pnas.1504633113.
Krichak, S.O., Feldstein, S.B., Alpert, P., Gualdi, S., Scoccimarro, E., Yano, J.I., 2016. Discussing the role of tropical and subtropical moisture sources in cold season extreme precipitation events in the Mediterranean region from a climate change perspective. Nat. Hazards Earth Syst. Sci. 16, 269–285. https://doi.org/10.5194/nhess-16-269-2016.
Lackmann, G.M., 2013. The south-central U.S. flood of May 2010: present and future. J. Clim. 26 (13), 4688–4709. https://doi.org/10.1175/JCLI-D-12-00392.1.
Läderach, A., Sodemann, H., 2016. A revised picture of the atmospheric moisture residence time. Geophys. Res. Lett. 43 (2), 924–933. https://doi.org/10.1002/2015GL067449.
Landsberg, J., Romanini, D., Kerstel, E., 2014. Very high finesse optical-feedback cavity-enhanced absorption spectrometer for low concentration water vapor isotope analyses. Opt. Lett. 39 (7), 1795–1798. https://doi.org/10.1364/OL.39.001795.
Lau, W.K.M., Kim, K.M., 2012. The 2010 Pakistan flood and Russian heat wave: teleconnection of hydrometeorological extremes. J. Hydrometeorol. 13, 392–403. https://doi.org/10.1175/JHM-D-11-016.1.
Lavers, D.A., Villarini, G., 2013a. The nexus between atmospheric rivers and extreme precipitation across Europe. Geophys. Res. Lett. 40 (12), 3259–3264. https://doi.org/10.1002/grl.50636.
Lavers, D.A., Villarini, G., 2013b. Atmospheric rivers and flooding over the central United States. J. Clim. 26 (20), 7829–7836. https://doi.org/10.1175/JCLI-D-13-00212.1.
Lavers, D.A., Villarini, G., 2015. The contribution of atmospheric rivers to precipitation in Europe and the United States. J. Hydrol. 522, 382–390. https://doi.org/10.1016/J.JHYDROL.2014.12.010.
Lavers, D.A., Allan, R.P., Wood, E.F., Villarini, G., Brayshaw, D.J., Wade, A.J., 2011. Winter floods in Britain are connected to atmospheric rivers. Geophys. Res. Lett. 38 (23), 1–8. https://doi.org/10.1029/2011GL049783.
Lavers, D.A., Villarini, G., Allan, R.P., Wood, E.F., Wade, A.J., 2012. The detection of atmospheric rivers in atmospheric reanalyses and their links to British winter floods and the large-scale climatic circulation. J. Geophys. Res. Atmos. 117 (D20). https://doi.org/10.1029/2012JD018027.
Lavers, D.A., Allan, R.P., Villarini, G., Lloyd-Hughes, B., Brayshaw, D.J., Wade, A.J., 2013. Future changes in atmospheric rivers and their implications for winter flooding in Britain. Environ. Res. Lett. 8. https://doi.org/10.1088/1748-9326/8/3/034010.
Lavers, D.A., Richardson, D.S., Ramos, A.M., Zsoter, E., Pappenberger, F., Trigo, R.M., 2018. Earlier awareness of extreme winter precipitation across the western Iberian Peninsula. Meteorol. Appl. 25 (4), 622–628. https://doi.org/10.1002/met.1727.
Lélé, M.I., Leslie, L.M., 2016. Intraseasonal variability of low-level moisture transport over West Africa. Clim. Dyn. 47 (11), 3575–3591. https://doi.org/10.1007/s00382-016-3334-x.
Lélé, M.I., Leslie, L.M., Lamb, P.J., 2015. Analysis of low-level atmospheric moisture transport associated with the West African Monsoon. J. Clim. 28 (11), 4414–4430. https://doi.org/10.1175/JCLI-D-14-00746.1.
Liberato, M.L., Pinto, J.G., Trigo, I.F., Trigo, R.M., 2011. Klaus—an exceptional winter storm over northern Iberia and southern France. Weather 66 (12), 330–334. https://doi.org/10.1002/wea.755.
Liberato, M.L.R., Ramos, A.M., Trigo, R.M., Trigo, I.F., Durán-Quesada, A.M., Nieto, R., Gimeno, L., 2013. Moisture sources and large-scale dynamics associated with a flash flood event. In: Lin, J., Brunner, D., Gerbig, C., Stohl, A., Luhar, A., Webley, P. (Eds.), Lagrangian Modeling of the Atmosphere, https://doi.org/10.1029/2012GM001244.
Lin, D., Huang, W., Yang, Z., He, X., Qiu, T., Wang, B., Wright, J.S., 2019. Impacts of wintertime extratropical cyclones on temperature and precipitation over northeastern China during 1979–2016. J. Geophys. Res. Atmos. 124, 1514–1536. https://doi.org/10.1029/2018JD029174.
Liu, W.T., Xie, X., 2017. Premonsoon drought in India observed from space. J. Hydrometeorol. 18, 683–692. https://doi.org/10.1175/JHM-D-16-0014.1.
Lu, M., Hao, X., 2017. Diagnosis of the tropical moisture exports to the mid-latitudes and the role of atmospheric steering in the extreme precipitation. Atmosphere 8 (12), 256.
Lu, M., Lall, U., 2016. Tropical moisture exports, extreme precipitation and floods in Northeastern US. Hydrol. Earth Syst. Sci. Discuss. https://doi.org/10.5194/hess-2016-403.
Ma, Y., Lu, M., Chen, H., Pan, M., Hong, Y., 2018. atmospheric moisture transport versus precipitation across the Tibetan Plateau: a mini-review and current challenges. Atmos. Res. 209, 50–58. https://doi.org/10.1016/J.ATMOSRES.2018.03.015.
Madakumbura, G.D., Kim, H., Utsumi, N., Shiogama, H., Fischer, E.M., Seland, Ø., Scinocca, J.F., Mitchell, D.M., Hirabayashi, Y., Oki, T., 2019. Event-to-event intensification of the hydrologic cycle from 1.5 °C to a 2 °C warmer world. Sci. Rep. 9, 3483. https://doi.org/10.1038/s41598-019-39936-2.
Marengo, J.A., Espinoza, J.C., 2016. Extreme seasonal droughts and floods in Amazonia: causes, trends and impacts. Int. J. Climatol. 36 (3), 1033–1050. https://doi.org/10.1002/joc.4420.
Marengo, J.A., Tomasella, J., Soares, W.R., Alves, L.M., Nobre, C.A., 2012. Extreme climate events in the Amazon basin. Theor. Appl. Climatol. 107, 73–85. https://doi.org/10.1007/s00704-011-0465-1.
Marengo, J.A., Alves, L.M., Soares, W.R., Rodriguez, D.A., Camargo, H., Riveros, M.P., Pabló, A.D., 2013. Two contrasting severe seasonal extremes in tropical south america in 2012: flood in Amazonia and drought in northeast brazil. J. Clim. 26 (22), 9137–9154. https://doi.org/10.1175/JCLI-D-12-00642.1.
Marengo, J.A., Espinoza, J.C., Ronchail, J., Alves, L.M., 2016a. Tropical South America east of the Andes, in State of the climate in 2015. Bull. Am. Meteorol. Soc. 97 (8), S184–S185.
Marengo, J.A., Torres, R.R., Alves, L.M., 2016b. Drought in Northeast Brazil—past, present, and future. Theor. Appl. Climatol. 129, 1189–1200. https://doi.org/10.1007/s00704-016-1840-8.
Martinez, J.A., Dominguez, F., 2014. Sources of atmospheric moisture for the La Plata River basin*. J. Clim. 27 (17), 6737–6753. https://doi.org/10.1175/JCLI-D-14-00022.1.
Mera, R., Laing, A.G., Semazzi, F., 2014. Moisture variability and multiscale interactions during Spring in West Africa. Mon. Weather Rev. 142 (9), 3178–3198. https://doi.org/10.1175/MWR-D-13-00175.1.
Methven, J., 1997. Offline trajectories: calculation and accuracy. U.K. universities global atmospheric modelling programme. Tech. Rep. 44 18 pp.
Monaghan, A.J., Rife, D.L., Pinto, J.O., Davis, C.A., Hannan, J.R., 2010. Global precipitation extremes associated with diurnally varying low-level jets. J. Clim. 23, 5065–5084. https://doi.org/10.1175/2010JCLI3515.1.
Montini, T.L., Jones, C., Carvalho, L.M.V., 2019. The South American low-level jet: a new climatology, variability, and changes. J. Geophys. Res. Atmos. 124 (3), 1200–1218. https://doi.org/10.1029/2018JD029634.
Moore, B.J., Neiman, P.J., Ralph, F.M., Barthold, F.E., 2012. Physical processes associated with heavy flooding rainfall in Nashville, Tennessee, and vicinity during 1–2 May 2010: the role of an atmospheric river and mesoscale convective systems*. Mon. Weather Rev. 140 (2), 358–378. https://doi.org/10.1175/MWR-D-11-00126.1.
Najibi, N., Devineni, N., Lu, M., Perdigão, R.A.P., 2019. Coupled flow accumulation and atmospheric blocking govern flood duration. npj Clim Atmos Sci 2, 19. https://doi.org/10.1038/s41612-019-0076-6.
Nakamura, J., Lall, U., Kushnir, Y., Robertson, A.W., Seager, R., 2013. Dynamical structure of extreme floods in the U.S. Midwest and the UK. J. Hydrometeorol. 14, 485–504. https://doi.org/10.1175/JHM-D-12-059.1.
Nayak, M.A., Villarini, G., 2017. A long-term perspective of the hydroclimatological impacts of atmospheric rivers over the central United States. Water Resour. Res. 53 (2), 1144–1166. https://doi.org/10.1002/2016WR019033.
Nayak, M.A., Villarini, G., Lavers, D.A., 2014. On the skill of numerical weather prediction models to forecast atmospheric rivers over the central United States. Geophys. Res. Lett. 41 (12), 4354–4362. https://doi.org/10.1002/2014GL060299.
Neiman, P.J., Schick, L.J., Ralph, F.M., Hughes, M., Wick, G.A., 2011. Flooding in western Washington: the connection to atmospheric rivers*. J. Hydrometeorol. 12 (6), 1337–1358. https://doi.org/10.1175/2011jhm1358.1.
Newell, R.E., Newell, N.E., Zhu, Y., Scott, C., 1992. Tropospheric rivers? – A pilot study. Geophys. Res. Lett. 19 (24), 2401–2404. https://doi.org/10.1029/92GL02916.
Nicholson, S., 2016. The Turkana low-level jet: mean climatology and association with regional aridit. Int. J. Climatol. 36 (6), 2598–2614. https://doi.org/10.1002/joc.4515.
Nicolini, M., Saulo, A.C., 2006. Modeled Chaco low-level jets and related precipitation patterns during the 1997–1998 warm season. Meteorog. Atmos. Phys. 94 (1–4), 129–143. https://doi.org/10.1007/s00703-006-0186-7.
Nieto, R., Gimeno, L., 2019. A database of optimal integration times for Lagrangian studies of atmospheric moisture sources and sinks. Scientific Data 6, 59. https://doi.org/10.1038/s41597-019-0068-8.
Nieto, R., Gimeno, L., Trigo, R.M., 2006. A Lagrangian identification of major sources of Sahel moisture. Geophys. Res. Lett. 33 (18). https://doi.org/10.1029/2006GL027232.
Nieto, R., Gimeno, L., Drumond, A., Hernandez, E., 2010. A Lagrangian identification of the main moisture sources and sinks affecting the Mediterranean area. WSEAS Trans.

Environ. Dev. 5, 6.
Nieto, R., Castillo, R., Drumond, A., Gimeno, L., 2014. A catalog of moisture sources for continental climatic regions. Water Resour. Res. 50, 5322–5328. https://doi.org/10.1002/2013WR013901.
Ordóñez, P., Ribera, P., Gallego, D., Peña-Ortiz, C., 2012. Major moisture sources for Western and Southern India and their role on synoptic-scale rainfall events. Hydrol. Process. 26, 3886–3895. https://doi.org/10.1002/hyp.8455.
Ordoñez, P., Nieto, R., Gimeno, L., Ribera, P., Gallego, D., Ochoa-Moya, C.A., Quintanar, A.I., 2019. Climatological moisture sources for the Western North American Monsoon through a Lagrangian approach: their influence on precipitation intensity. Earth Syst. Dynam. 10, 59–72. https://doi.org/10.5194/esd-10-59-2019.
Pan, C., Zhu, B., Gao, J., Kang, H., 2017. Source apportionment of atmospheric water over East Asia-a source tracer study in CAM5.1. Geosci. Model Dev. 10, 673–688. https://doi.org/10.5194/gmd-10-673-2017.
Pathak, A., Ghosh, S., Martinez, J.A., Dominguez, F., Kumar, P., 2017. Role of oceanic and land moisture sources and transport in the seasonal and interannual variability of Summer Monsoon in India. J. Clim. 30, 1839–1859. https://doi.org/10.1175/JCLI-D-16-0156.1.
Patricola, C.M., Chang, P., Saravanan, R., 2015. Impact of Atlantic SST and high frequency atmospheric variability on the 1993 and 2008 Midwest floods: regional climate model simulations of extreme climate events. Clim. Chang. 129 (3–4), 397–411. https://doi.org/10.1007/s10584-013-0886-1.
Payne, A.E., Magnusdottir, G., 2016. Persistent landfalling atmospheric rivers over the west coast of North America. J. Geophys. Res. 121 (22), 13287–13300. https://doi.org/10.1002/2016JD025549.
Pereira, S., Ramos, A.M., Zêzere, J.L., Trigo, R.M., Vaquero, J.M., 2016. Spatial impact and triggering conditions of the exceptional hydro-geomorphological event of December 1909 in Iberia. Nat. Hazards Earth Syst. Sci. 16 (2), 371–390. https://doi.org/10.5194/nhess-16-371-2016.
Pérez-Munuzuri, V., Garaboa-Paz, D., 2016. Mixing of spherical bubbles with time-dependent radius in incompressible flows. Phys. Rev. E 93 (2), 023107. https://doi.org/10.1103/PhysRevE.93.023107.
Pérez-Muñuzuri, V., Eiras-Barca, J., Garaboa-Paz, D., 2018. Tagging moisture sources with Lagrangian and inertial tracers: application to intense atmospheric river events. Earth Syst. Dynam. 9, 785–795. https://doi.org/10.5194/esd-9-785-2018.
Peyrillé, P., Lafore, J.-P., Redelsperger, J.L., 2007. An idealized two-dimensional framework to study the West African Monsoon. Part I: validation and key controlling factors. J. Atmos. Sci. 64 (8), 2765–2782. https://doi.org/10.1175/JAS3919.1.
Pfahl, S., Wernli, H., Yoshimura, K., Dubey, M.K., 2012. The isotopic composition of precipitation from a winter storm—a case study with the limited-area model COSMO iso. Atmos. Chem. Phys. 12, 1629–1648. https://doi.org/10.5194/acp-12-1629-2012.
Pinto, J.G., Ulbrich, S., Parodi, A., Rudari, R., Boni, G., Ulbrich, U., 2013. Identification and ranking of extraordinary rainfall events over Northwest Italy: the role of Atlantic moisture. J. Geophys. Res. Atmos. 118 (5), 2085–2097. https://doi.org/10.1002/jgrd.50179.
Poveda, G., Mesa, O.J., 2000. On the existence of Lloró (the rainiest locality on Earth): enhanced ocean-land-atmosphere interaction by a low-level jet. Geophys. Res. Lett. 27 (11), 1675–1678. https://doi.org/10.1029/1999GL006091.
Poveda, G., Jaramillo, L., Vallejo, L.F., 2014. Seasonal precipitation patterns along pathways of South American low-level jets and aerial rivers. Water Resour. Res. 50 (1), 98–118. https://doi.org/10.1002/2013WR014087.
Pu, B., Cook, K.H., 2010. Dynamics of the West African westerly jet. J. Clim. 23 (23), 6263–6276. https://doi.org/10.1175/2010JCLI3648.1.
Pu, B., Cook, K.H., 2012. Role of the West African westerly jet in Sahel rainfall variations. J. Clim. 25 (8), 2880–2896. https://doi.org/10.1175/JCLI-D-11-00394.1.
Pu, B., Dickinson, R.E., Fu, R., 2016. Dynamical connection between Great Plains low-level winds and variability of central Gulf States precipitation. J. Geophys. Res. Atmos. 121 (7), 3421–3434. https://doi.org/10.1002/2015JD024045.
Ralph, F.M., Dettinger, M.D., 2011. Storms, floods, and the science of atmospheric rivers. EOS Trans. Am. Geophys. Union 92 (32), 2009–2011. https://doi.org/10.1029/2011EO320001.
Ralph, F.M., Neiman, P.J., Wick, G.A., 2004. Satellite and CALJET aircraft observations of atmospheric rivers over the eastern North Pacific Ocean during the winter of 1997/98. Mon. Weather Rev. 132, 1721–1745. https://doi.org/10.1175/1520-0493(2004)132<1721:SACAOO>2.0.CO;2.
Ralph, F.M., Cordeira, J.M., Neiman, P.J., Hughes, M., 2016. Landfalling atmospheric rivers, the Sierra barrier jet, and extreme daily precipitation in Northern California's Upper Sacramento River watershed. J. Hydrometeorol. 17, 1905–1914. https://doi.org/10.1175/JHM-D-15-0167.1.
Ralph, F.M., Dettinger, M., Lavers, D., Gorodetskaya, I.V., Martin, A., Viale, M., White, A.B., Oakley, N., Rutz, J., Spackman, J.R., Wernli, H., Cordeira, J., 2017a. Atmospheric rivers emerge as a global science and applications focus. Bull. Amer. Meteor. Soc. 98, 1969–1973. https://doi.org/10.1175/BAMS-D-16-0262.1.
Ralph, F.M., Iacobellis, S., Neiman, P., Cordeira, J., Spackman, J., Waliser, D., Wick, G., White, A., Fairall, C., 2017b. Dropsonde observations of total water vapor transport within North Pacific atmospheric rivers. J. Hydrometeorol. 18, 2577–2596. https://doi.org/10.1175/JHM-D-17-0036.
Ramos, A.M., Trigo, R.M., Liberato, M.L.R., Tomé, R., 2015. Daily precipitation extreme events in the Iberian Peninsula and its association with atmospheric rivers*. J. Hydrometeorol. 16 (2), 579–597. https://doi.org/10.1175/JHM-D-14-0103.1.
Ramos, A.M., Nieto, R., Tomé, R., Gimeno, L., Trigo, R.M., Liberato, M.L.R., Lavers, D.A., 2016a. Atmospheric rivers moisture sources from a Lagrangian perspective. Earth Syst. Dyn. 7 (2), 371–384. https://doi.org/10.5194/esd-7-371-2016.
Ramos, A.M., Tomé, R., Trigo, R.M., Liberato, M.L.R., Pinto, J.G., 2016b. Projected changes in atmospheric rivers affecting Europe in CMIP5 models. Geophys. Res. Lett. 43, 9315–9323. https://doi.org/10.1002/2016GL070634.
Ramos, A.M., Martins, M.J., Tomé, R., Trigo, R.M., 2018. Extreme precipitation events in summer in the Iberian Peninsula and its relationship with atmospheric rivers. Front. Earth Sci. 6, 110. https://doi.org/10.3389/feart.2018.00110.
Ramos, A.M., Blamey, R.C., Algarra, I., Nieto, R., Gimeno, L., Tomé, R., Reason, C.J.C., Trigo, R.M., 2019. From Amazonia to southern Africa: atmospheric moisture transport through low-level jets and atmospheric rivers. Ann. N. Y. Acad. Sci. 1436 (1), 217–230. https://doi.org/10.1111/nyas.13960.
Rasmusson, E.M., Mo, K.C., 1996. Large-scale atmospheric moisture cycling as evaluated from NMC global analysis and forecast products. J. Clim. 9 (12), 3276–3297. https://doi.org/10.1175/1520-0442(1996)009<3276:LSAMCA>2.0.CO;2.
Reason, C.J.C., Jagadheesha, D., 2005. Relationships between South Atlantic SST variability and atmospheric circulation over the South African region during austral winter. J. Clim. 18 (16), 3339–3355. https://doi.org/10.1175/JCLI3474.1.
Reason, C.J.C., Rouault, M., 2005. Links between the Antarctic Oscillation and winter rainfall over western South Africa. Geophys. Res. Lett. 32 (7). https://doi.org/10.1029/2005GL022419.
Rife, D.L., Pinto, J.O., Monaghan, A.J., Davis, C.A., Hannan, J.R., 2010. Global distribution and characteristics of diurnally varying low-level jets. J. Clim. 23 (19), 5041–5064. https://doi.org/10.1175/2010JCLI3514.1.
Rios-Entenza, A., Soares, P.M., Trigo, R.M., Cardoso, R.M., Miguez-Macho, G., 2014. Moisture recycling in the Iberian Peninsula from a regional climate simulation: spatiotemporal analysis and impact on the precipitation regime. J. Geophys. Res. Atmos. 119 (10), 5895–5912. https://doi.org/10.1002/2013JD021274.
Rivera, E.R., Dominguez, F., Castro, C.L., 2013. Atmospheric rivers and cool season extreme precipitation events in the Verde River basin of Arizona. J. Hydrometeorol. 15 (2), 813–829. https://doi.org/10.1175/jhm-d-12-0189.1.
Roberge, A., Gyakum, J.R., Atallah, E.H., 2009. Analysis of intense poleward water vapor transports into high latitudes of western North America. Weather Forecast. 24 (6), 1732–1747. https://doi.org/10.1175/2009WAF2222198.1.
Ropelewski, C.F., Gutzler, D.S., Higgins, R.W., Mechoso, C.R., 2005. The North American monsoon system. The global monsoon system: research and forecast. WMO Tech. Doc. 1266, 207–218.
Rössler, O., Froidevaux, P., Börst, U., Rickli, R., Martius, O., Weingartner, R., 2014. Retrospective analysis of a nonforecasted rain-on-snow flood in the Alps – a matter of model limitations or unpredictable nature? Hydrol. Earth Syst. Sci. 18, 2265–2285. https://doi.org/10.5194/hess-18-2265-2014.
Roxy, M.K., Ghosh, S., Pathak, A., Athulya, R., Mujumdar, M., Murtugudde, R., Terray, P., Rajeevan, M., 2017. A threefold rise in widespread extreme rain events over central India. Nat. Commun. 8, 708. https://doi.org/10.1038/s41467-017-00744-9.
Roy, T., Martinez, J.A., Herrera-Estrada, J.E., Zhang, Y., Dominguez, F., Berg, A., Ek, M., Wood, E.F., 2019. Role of moisture transport and recycling in characterizing droughts: perspectives from two recent US droughts and the CFSv2 system. J. Hydrometeorol. 20, 139–154. https://doi.org/10.1175/JHM-D-18-0159.1.
Ruiz-Barradas, A., Nigam, S., 2005. Warm season rainfall variability over the U.S. great plains in observations, NCEP and ERA-40 reanalyses, and NCAR and NASA atmospheric model simulations. J. Clim. 18 (11), 1808–1830. https://doi.org/10.1175/JCLI3343.1.
Rutz, J.J., Steenburgh, W.J., 2012. Quantifying the role of atmospheric rivers in the interior western United States. Atmos. Sci. Lett. 13 (4), 257–261. https://doi.org/10.1002/asl.392.
Rutz, J.J., Steenburgh, W.J., Ralph, F.M., 2013. Climatological characteristics of atmospheric rivers and their inland penetration over the western United States. Mon. Weather Rev. 142 (2), 905–921. https://doi.org/10.1175/mwr-d-13-00168.1.
Rutz, J.J., Steenburgh, W.J., Ralph, F.M., 2015. The inland penetration of atmospheric rivers over western North America: a Lagrangian analysis. Mon. Weather Rev. 143, 1924–1944. https://doi.org/10.1175/MWR-D-14-00288.1.
Ryoo, J., Waliser, D.E., Waugh, D.W., Wong, S., Fetzer, E.J., Fung, I., 2015. Classification of atmospheric river events on the U.S. West Coast using a trajectory model. J. Geophys. Res. Atmos. 120 (8), 3007–3028. https://doi.org/10.1002/2014JD022023.
Sagalgile, A.P., Chowdary, J.S., Srinivas, G., Gnanaseelan, C., Parekh, A., Attada, R., Singh, P., 2018. Indian summer monsoon sub-seasonal low-level circulation predictability and its association with rainfall in a coupled model. Pure Appl. Geophys. 175 (1), 449–463. https://doi.org/10.1007/s00024-017-1702-z.
Saini, R., Wang, G., Pal, J.S., 2016. Role of soil moisture feedback in the development of extreme summer drought and flood in the United States. J. Hydrometeorol. 17, 2191–2207. https://doi.org/10.1175/JHM-D-15-0168.1.
Sakamoto, M.S., Ambrizzi, T., Poveda, G., 2011. Moisture sources and life cycle of convective systems over Western Colombia. Adv. Meteorol. 1–11. https://doi.org/10.1155/2011/890759.
Salah, Z., Nieto, R., Drumond, A., Gimeno, L., Vicente-Serrano, S.M., 2018. A Lagrangian analysis of the moisture budget over the Fertile Crescent during two intense drought episodes. J. Hydrol. 560, 382–395. https://doi.org/10.1016/j.jhydrol.2018.03.021.
Salio, P., Nicolini, M., Saulo, A.C., 2002. Chaco low-level jet events characterization during the austral summer season. J. Geophys. Res. 107 (D24), 4816. https://doi.org/10.1029/2001JD001315.
Satyamurty, P., da Costa, C.P., Manzi, A.O., 2013a. Moisture source for the Amazon Basin: a study of contrasting years. Theor. Appl. Climatol. 111, 195–209. https://doi.org/10.1007/s00704-012-0637-7.
Satyamurty, P., da Costa, C.P., Manzi, A.O., Candido, L.A., 2013b. A quick look at the 2012 record flood in the Amazon Basin. Geophys. Res. Lett. 40, 1396–1401. https://doi.org/10.1002/grl.50245.
Schlef, K.E., Moradkhani, H., Lall, U., 2019. Atmospheric circulation patterns associated with extreme United States floods identified via machine learning. Sci. Rep. 9, 7171. https://doi.org/10.1038/s41598-019-43496-w.
Schneider, M., Borger, C., Wiegele, A., Hase, F., García, O.E., Sepúlveda, E., Werner, M.,

2017. MUSICA MetOp/IASI {H2O,δD} pair retrieval simulations for validating tropospheric moisture pathways in atmospheric models. Atmos. Meas. Tech. 10, 507–525. https://doi.org/10.5194/amt-10-507-2017.
Silva, G.A.M., Ambrizzi, T., Marengo, J.A., 2009. Observational evidences on the modulation of the South American low level jet east of the Andes according the ENSO variability. Ann. Geophys. 27, 645–657. https://doi.org/10.5194/angeo-27-645-2009.
Singh, H.A., Bitz, C.M., Nusbaumer, J., Noone, D.C., 2016. A mathematical framework for analysis of water tracers: Part 1: development of theory and application to the pre-industrial mean state. J. Adv. Model. Earth Syst. 8 (2), 991–1013. https://doi.org/10.1002/2016MS000649.
Smith, J.A., Baeck, M.L., 2015. "Prophetic vision, vivid imagination": the 1927 Mississippi River flood. Water Resour. Res. 51, 9964–9994. https://doi.org/10.1002/2015WR017927.
Sodemann, H., Stohl, A., 2013. Moisture origin and meridional transport in atmospheric rivers and their association with multiple cyclones. Mon. Weather Rev. 141 (8), 2850–2868. https://doi.org/10.1175/MWR-D-12-00256.1.
Sodemann, H., Zubler, E., 2009. Seasonal and inter-annual variability of the moisture sources for Alpine precipitation during 1995–2002. Int. J. Climatol. 30 (7). https://doi.org/10.1002/joc.1932.
Sodemann, H., Schwierz, C., Wernli, H., 2008. Interannual variability of Greenland winter precipitation sources: Lagrangian moisture diagnostic and North Atlantic Oscillation influence. J. Geophys. Res. 113 (D3), D03107. https://doi.org/10.1029/2007JD008503.
Sorí, R., Nieto, R., Drumond, A., Gimeno, L., 2017a. The Niger River basin moisture sources: a Lagrangian analysis. Atmosphere 8 (12), 38. https://doi.org/10.3390/atmos8020038.
Sorí, R., Nieto, R., Vicente-Serrano, S.M., Drumond, A., Gimeno, L., 2017b. A Lagrangian perspective of the hydrological cycle in the Congo River basin. Earth Syst. Dynam. 8, 653–675. https://doi.org/10.5194/esd-8-653-2017.
Sorí, R., Nieto, R., Vicente-Serrano, S.M., Drumond, A., Gimeno, L., 2017c. The atmospheric branch of the hydrological cycle over the Indus, Ganges, and Brahmaputra river basins. Hydrol. Earth Syst. Sci. 21, 6379–6399. https://doi.org/10.5194/hess-21-6379-2017.
Sorí, R., Marengo, J.A., Nieto, R., Drumond, A., Gimeno, L., 2018. The atmospheric branch of the hydrological cycle over the Negro and Madeira River basins in the Amazon Region. Water 10 (6), 738. https://doi.org/10.3390/w10060738.
Sorí, R., Nieto, R., Drumond, A., Stojanovic, M., Gimeno, L., 2019. On the connection between atmospheric moisture transport and dry conditions in rainfall climatological zones of the Niger River basin. Water 11 (3), 622. https://doi.org/10.3390/w11030622.
Sperber, K.R., Cusiner, E., Kitoh, A., Mechoso, C.R., Moise, A., Moufouma-Okia, W., Schiro, K., Turner, A.G., 2017. Modelling monsoons. In: Chang, C.-P., Kuo, H.-C., Lau, N.-C., Johnson, R.H., Wang, B., Wheeler, M.C. (Eds.), The Global Monsoon System: Research and Forecast, 3rd edition. 9. World Scientific, Singapore, pp. 79–101. https://doi.org/10.1142/9789813200913_0007. World Scientific Series on Asia-Pacific Weather and Climate.
Stager, J.C., Mayewski, P.A., White, J., Chase, B.M., Neumann, F.H., Meadows, M.E., King, C.D., Dixon, D.A., 2012. Precipitation variability in the winter rainfall zone of South Africa during the last 1400 yr linked to the austral westerlies. Clim. Past Discuss. 7, 4375–4399. https://doi.org/10.5194/cp-8-877-2012.
Steinschneider, S., Lall, U., 2015a. Daily precipitation and tropical moisture exports across the Eastern United States: an application of archetypal analysis to identify spatiotemporal structure. J. Clim. 28, 8585–8602. https://doi.org/10.1175/JCLI-D-15-0340.1.
Steinschneider, S., Lall, U., 2015b. A hierarchical Bayesian regional model for nonstationary precipitation extremes in Northern California conditioned on tropical moisture exports. Water Resour. Res. 51, 1472–1492. https://doi.org/10.1002/2014WR016664.
Stensrud, D.J., 1996. Importance of low-level jets to climate: a review. J. Clim. 9 (8), 1698–1711. https://doi.org/10.1175/1520-0442(1996)009<1698:IOLLJT>2.0.CO;2.
Stephens, G.L., Hakuba, M.Z., Webb, M.J., Lebsock, M., Yue, Q., Kahn, B.H., Hristova-Veleva, S., Rapp, A.D., Stubenrauch, C.J., Elsaesser, G.S., Slingo, J., 2018. Regional intensification of the tropical hydrological cycle during ENSO. Geophys. Res. Lett. 45, 4361–4370. https://doi.org/10.1029/2018GL077598.
Stier, P., Hodnebrog, Ø., Myhre, G., Samset, B.H., Alterskjær, K., Andrews, T., Boucher, O., Faluvegi, G., Fläschner, D., Forster, P.M., Kasoar, M., 2019. Increased water vapour lifetime due to global warming. Atmos. Chem. Phys. Discuss. https://doi.org/10.5194/acp-2019-121.
Stohl, A., James, P., 2004. A Lagrangian analysis of the atmospheric branch of the global water cycle. Part I: method description, validation, and demonstration for the August 2002 flooding in central Europe. J. Hydrometeorol. 5, 656–678. https://doi.org/10.1175/1525-7541(2004)005<0656:ALAOTA>2.0.CO;2.
Stohl, A., James, P., 2005. A Lagrangian analysis of the atmospheric branch of the global water cycle. Part II: moisture transports between Earth's ocean basins and river catchments. J. Hydrometeorol. 6, 961–984. https://doi.org/10.1175/JHM470.1.
Stojanovic, M., Drumond, A., Nieto, R., Gimeno, L., 2017. Moisture transport anomalies over the Danube river basin during two drought events: a Lagrangian analysis. Atmosphere 8 (10), 193. https://doi.org/10.3390/atmos8100193.
Stojanovic, M., Drumond, A., Nieto, R., Gimeno, L., 2018a. Anomalies in moisture supply during the 2003 drought event in Europe: a Lagrangian analysis. Water 10 (4), 467. https://doi.org/10.3390/w10040467.
Stojanovic, M., Drumond, A., Nieto, R., Gimeno, L., 2018b. Variations in moisture supply from the Mediterranean Sea during meteorological drought episodes over central Europe. Atmosphere 9 (7), 278. https://doi.org/10.3390/atmos9070278.
Sun, B., Wang, H., 2014. Moisture sources of semiarid grassland in China using the Lagrangian particle model FLEXPART. J. Clim. 27 (6), 2457–2474. https://doi.org/10.1175/JCLI-D-13-00517.1.
Sun, B., Wang, H., 2015. Analysis of the major atmospheric moisture sources affecting three sub-regions of East China. Int. J. Climatol. 35 (9), 2243–2257. https://doi.org/10.1002/joc.4145.
Syed, F., Hannachi, A., 2018. Inter-annual variability of moisture transport over the northern Indian Ocean and South Asian summer monsoon. Clim. Res. 75 (1), 23–31. https://doi.org/10.3354/cr01506.
Tan, X., Gan, T.Y., Chen, Y.D., 2018. Moisture sources and pathways associated with the spatial variability of seasonal extreme precipitation over Canada. Clim. Dyn. 50, 629–640. https://doi.org/10.1007/s00382-017-3630-0.
Thapa, K., Endreny, T.A., Ferguson, C.R., 2018. Atmospheric rivers carry nonmonsoon extreme precipitation into Nepal. J. Geophys. Res. Atmos. 123 (11), 5901–5912. https://doi.org/10.1029/2017JD027626.
Thorncroft, C.D., Nguyen, H., Zhang, C., Peyrillé, P., 2011. Annual cycle of the West African monsoon: regional circulations and associated water vapour transport. Q. J. R. Meteorol. Soc. 137 (654), 129–147. https://doi.org/10.1002/qj.728.
Tuinenburg, O.A., van der Ent, R.J., 2019. Land surface processes create patterns in atmospheric residence time of water. J. Geophys. Res. Atmos. 124 (2), 583–600. https://doi.org/10.1029/2018JD028871.
Ulbrich, S., Pinto, J.G., Rudari, R., Parodi, A., 2009. The role of moisture advection from the North Atlantic basin to extreme precipitation events over the Western Mediterranean. EMS Annu. Meet. Abstr. 6 EMS2009-260.
Ullah, K., Gao, S., 2012. Moisture transport over the Arabian Sea associated with summer rainfall over Pakistan in 1994 and 2002. Adv. Atmos. Sci. 29 (3), 501–508. https://doi.org/10.1007/s00376-011-0200-y.
Vachon, R.W., Welker, J.M., White, J.W.C., Vaughn, B.H., 2010. Monthly precipitation isoscapes (d 18 O) of the United States: connections with surface temperatures, moisture source conditions, and air mass trajectories. J. Geophys. Res. 115, 21126. https://doi.org/10.1029/2010JD014105.
Valenzuela, R.A., Kingsmill, D.E., 2015. Orographic precipitation forcing along the coast of Northern California during a landfalling winter storm. Mon. Weather Rev. 143 (9), 3570–3590. https://doi.org/10.1175/mwr-d-14-00365.1.
Van der Ent, R.J., Savenije, H.H.G., 2011. Length and time scales of atmospheric moisture recycling. Atmos. Chem. Phys. 11 (5), 1853–1863. https://doi.org/10.5194/acp-11-1853-2011.
van der Ent, R.J., Savenije, H.H.G., 2013. Oceanic sources of continental precipitation and the correlation with sea surface temperature. Water Resour. Res. 49, 3993–4004. https://doi.org/10.1002/wrcr.20296.
van Der Ent, R.J., Tuinenburg, O.A., 2017. The residence time of water in the atmosphere revisited. Hydrol. Earth Syst. Sci. 21, 779–790. https://doi.org/10.5194/hess-21-779-2017.
van der Ent, R.J., Savenije, H.H.G., Schaefli, B., Steele-Dunne, S.C., 2010. Origin and fate of atmospheric moisture over continents. Water Resour. Res. 46https://doi.org/10.1029/2010WR009127. W09525.
van der Ent, R.J., Wang-Erlandsson, L., Keys, P.W., Savenije, H.H.G., 2014. Contrasting roles of interception and transpiration in the hydrological cycle – part 2: moisture recycling. Earth Syst. Dynam. 5, 471–489. https://doi.org/10.5194/esd-5-471-2014.
Vázquez, M., Algarra, I., Eiras-Barca, J., Ramos, A.M., Nieto, R., Gimeno, L., 2018. Atmospheric rivers over the Arctic: Lagrangian characterisation of their moisture sources. Water 11 (1), 1–14. https://doi.org/10.3390/w11010041.
Viale, M., Valenzuela, R., Garreaud, R.D., Ralph, F.M., 2018. Impacts of atmospheric rivers on precipitation in southern South America. J. Hydrometeorol. 19, 1671–1687. https://doi.org/10.1175/JHM-D-18-0006.1.
Vigaud, N., Richard, Y., Rouault, M., Fauchereau, N., 2006. Water vapour transport from the tropical Atlantic and summer rainfall in tropical southern Africa. Clim. Dyn. 28 (2–3), 113–123. https://doi.org/10.1007/s00382-006-0186-9.
Vigaud, N., Richard, Y., Rouault, M., Fauchereau, N., 2009. Moisture transport between the South Atlantic Ocean and Southern Africa: relationships with summer rainfall and associated dynamics. Clim. Dyn. 32 (1), 113–123. https://doi.org/10.1007/s00382-008-0377-7.
Viste, E., Sorteberg, A., 2013a. The effect of moisture transport variability on Ethiopian summer precipitation. Int. J. Climatol. 33, 3106–3123. https://doi.org/10.1002/joc.3566.
Viste, E., Sorteberg, A., 2013b. Moisture transport into the Ethiopian highlands. Int. J. Climatol. 33, 249–263. https://doi.org/10.1002/joc.3409.
Vries, A.J., Feldstein, S.B., Riemer, M., Tyrlis, E., Sprenger, M., Baumgart, M., Fnais, M., Lelieveld, J., 2016. Dynamics of tropical–extratropical interactions and extreme precipitation events in Saudi Arabia in autumn, winter and spring. Q. J. R. Meteorol. Soc. 142 (697), 1862–1880. https://doi.org/10.1002/qj.2781.
Waliser, D., Guan, B., 2017. Extreme winds and precipitation during landfall of atmospheric rivers. Nat. Geosci. 10 (3), 179–183. https://doi.org/10.1038/ngeo2894.
Wang, H., Chen, H., 2012. Climate control for southeastern China moisture and precipitation: Indian or East Asian monsoon? J. Geophys. Res. Atmos. 117 (D12). https://doi.org/10.1029/2012JD017734.
Wang, C., Enfield, D.B., Lee, S.-K., Landsea, C.W., 2006. Influences of the Atlantic warm pool on Western Hemisphere summer rainfall and Atlantic hurricanes. J. Clim. 19 (12), 3011–3028. https://doi.org/10.1175/JCLI3770.1.
Wang, C., Lee, S.-K., Enfield, D.B., 2008. Climate response to anomalously large and small Atlantic warm pools during the summer. J. Clim. 21 (11), 2437–2450. https://doi.org/10.1175/2007JCLI2029.1.
Wang, N., Zeng, X., Zheng, Y., Zhu, J., Jiang, S., 2018. The atmospheric moisture residence time and reference time for moisture tracking over China. J. Hydrometeorol. 19, 1131–1147. https://doi.org/10.1175/JHM-D-17-0204.1.
Warner, M.D., Mass, C.F., Salathé, E.P., 2014. Changes in winter atmospheric rivers along

the North American west coast in CMIP5 climate models. J. Hydrometeorol. 16 (1), 118–128. https://doi.org/10.1175/jhm-d-14-0080.1.
Washington, R., Preston, A., 2006. Extreme wet years over southern Africa: role of Indian Ocean sea surface temperatures. J. Geophys. Res. 111 (D15), D15104. https://doi.org/10.1029/2005JD006724.
Wei, J., Dirmeyer, P.A., Bosilovich, M.G., Wu, R., 2012. Water vapor sources for Yangtze River Valley rainfall: climatology, variability, and implications for rainfall forecasting. J. Geophys. Res. Atmos. 117 (D5). https://doi.org/10.1029/2011JD016902.
Wei, J., Knoche, H.R., Kunstmann, H., 2015. Contribution of transpiration and evaporation to precipitation: an ET-Tagging study for the Poyang Lake region in Southeast China. J. Geophys. Res. Atmos. 120 (14), 6845–6864. https://doi.org/10.1002/2014JD022975.
Windhorst, D., Waltz, T., Timbe, E., Frede, H.-G., Breuer, L., 2013. Impact of elevation and weather patterns on the isotopic composition of precipitation in a tropical montane rainforest. Hydrol. Earth Syst. Sci. 17, 409–419. https://doi.org/10.5194/hess-17-409-2013.
Winschall, A., Pfahl, S., Sodemann, H., Wernli, H., 2014a. Comparison of Eulerian and Lagrangian moisture source diagnostics – the flood event in eastern Europe in May 2010. Atmos. Chem. Phys. 14, 6605–6619. https://doi.org/10.5194/acp-14-6605-2014.
Winschall, A., Sodemann, H., Pfahl, S., Wernli, H., 2014b. How important is intensified evaporation for Mediterranean precipitation extremes? J. Geophys. Res. Atmos. 119 (9), 5240–5256. https://doi.org/10.1002/2013JD021175.
WMO (World Meteorological Organization) No. 385, 2012. International Glossary of Hydrology. (ISBN 978-92-63-03385-8).
Worden, J., Kulawik, S., Frankenberg, C., Payne, V., Bowman, K., Cady-Peirara, K., Wecht, K., Lee, J.-E., Noone, D., 2012. Profiles of CH4, HDO, H2O, and N2Owith improved lower tropospheric vertical resolution from aura TES radiances. Atmos. Meas. Tech. 5, 397–411. https://doi.org/10.5194/amt-5-397-2012.
Xin-Gang, D., Ye, L., Ping, W., 2015. Warm–dry collocation of recent drought in southwestern China tied to moisture transport and climate warming. Chinese Physics B 24. https://doi.org/10.1088/1674-1056/24/4/049201.
Xu, G., Osborn, T.J., Matthews, A.J., 2017. Moisture transport by Atlantic tropical cyclones onto the North American continent. Clim. Dyn. 48 (9–10), 3161–3182. https://doi.org/10.1007/s00382-016-3257-6.
Yanai, M., Tomita, T., 1998. Seasonal and interannual variability of atmospheric heat sources and moisture sinks as determined from NCEP–NCAR reanalysis. J. Clim. 11 (3), 463–482. https://doi.org/10.1175/1520-0442(1998)011<0463:SAIVOA>2.0.CO;2.
Yang, Z., Dominguez, F., 2019. Investigating land surface effect on the moisture transport over South America with a moisture tagging model. J. Clim. https://doi.org/10.1175/JCLI-D-18-0700.1.
Yang, Y., Zhao, T., Ni, G., Sun, T., 2018. Atmospheric rivers over the Bay of Bengal lead to northern Indian extreme rainfall. Int. J. Climatol. 38 (2), 1010–1021. https://doi.org/10.1002/joc.5229.
Yoshimura, K., 2015. Stable water isotopes in climatology, meteorology, and hydrology: a review. J. Meteorol. Soc. Jpn. Ser. II 93 (5), 513–533. https://doi.org/10.2151/jmsj.2015-036.
Zandonadi Moura, L., Lima, C.H.R., 2018. Analysis of atmospheric moisture transport to the Upper Paraná River basin. Int. J. Climatol. 38 (14), 5153–5167. https://doi.org/10.1002/joc.5718.
Zemp, D.C., Schleussner, C.-F., Barbosa, H.M.J., van der Ent, R.J., Donges, J.F., Heinke, J., Sampaio, G., Rammig, A., 2014. On the importance of cascading moisture recycling in South America. Atmos. Chem. Phys. 14 (23), 13337–13359. https://doi.org/10.5194/acp-14-13337-2014.
Zhang, Z., Zhang, Q., Chen, X., Zhang, J., Zhou, J., 2011. Statistical properties of moisture transport in East Asia and their impacts on wetness/dryness variations in North China. Theor. Appl. Climatol. 104, 337–347. https://doi.org/10.1007/s00704-010-0346-z.
Zhang, L., Wu, L., Gan, B., 2013. Modes and mechanisms of global water vapor variability over the twentieth century. J. Clim. 26, 5578–5593. https://doi.org/10.1175/JCLI-D-12-00585.1.
Zhang, C., Tang, Q., Chen, D., Li, L., Liu, X., Cui, H., 2017. Tracing changes in atmospheric moisture supply to the drying Southwest China. Atmos. Chem. Phys. 17, 10383–10393. https://doi.org/10.5194/acp-17-10383-2017.
Zhang, F., Li, G., Yue, J., 2019. The moisture sources and transport processes for a sudden rainstorm associated with double low-level jets in the Northeast Sichuan basin of China. Atmosphere 10, 160. https://doi.org/10.3390/atmos10030160.
Zhao, Y., Xu, X.D., Zhao, T.L., Xu, H.X., Mao, F., Sun, H., Wang, Y.H., 2016. Extreme precipitation events in East China and associated moisture transport pathways. Sci. China Earth Sci. 59 (9), 1–19. https://doi.org/10.1007/s11430-016-5315-7.
Zhisheng, A., Guoxiong, W., Jianping, L., Youbin, S., Yimin, L., Weijian, Z., Yanjun, C., Anmin, D., Li, L., Jiangyu, M., Hai, C., Zhengguo, S., Liangcheng, T., Hong, Y., Hong, A., Hong, C., Juan, F., 2015. Global monsoon dynamics and climate change. Annu. Rev. Earth Planet. Sci. 43, 29–77. https://doi.org/10.1146/annurev-earth-060313-054623.
Zhong, L., Hua, L., Luo, D., 2018. Local and external moisture sources for the Arctic warming over the Barents–Kara Seas. J. Clim. 31, 1963–1982. https://doi.org/10.1175/JCLI-D-17-0203.1.
Zhu, Y., Newell, R.E., 1998. A proposed algorithm for moisture fluxes from atmospheric rivers. Mon. Weather Rev. 126 (3), 725–735. https://doi.org/10.1175/1520-0493(1998)126<0725:apafmf>2.0.co;2.
Zolina, O., Dufour, A., Gulev, S.K., Stenchikov, G., 2017. Regional hydrological cycle over the red sea in ERA-interim. J. Hydrometeorol. 18 (1), 65–83. https://doi.org/10.1175/JHM-D-16-0048.1.

Atmospheric Research 229 (2019) 39–59

Contents lists available at ScienceDirect

Atmospheric Research

journal homepage: www.elsevier.com/locate/atmosres

Invited review article

Global climatology of nocturnal low-level jets and associated moisture sources and sinks

Iago Algarra[a,*], Jorge Eiras-Barca[a,b], Raquel Nieto[a], Luis Gimeno[a]

[a] EPhysLab (Environmental Physics Laboratory), CIM-UVigo, Universidade de Vigo, Ourense, Spain
[b] Department of Atmospheric Sciences, University of Illinois at Urbana-Champaign, Urbana, IL, United States

A B S T R A C T

Low-level jets (LLJs) are defined as regions of anomalously high wind speeds occurring within the first kilometre of the troposphere. They are filamentous structures that are usually strongly related to moisture transport. This study analysed the moisture transport associated with LLJs, and the role of LLJs in precipitation events that occasionally lead to extreme precipitation and major floods. A daily climatology dataset of nocturnal LLJs was developed and moisture transport was studied by analysing the source and sink regions. A nocturnal LLJ index based on the vertical structure of temporal wind variations was applied, and a total of 33 nocturnal LLJs were identified and characterised. The FLEXPART Lagrangian model was then used to simulate jet behaviour and to identify major source and sink regions during the period from 1980 to 2016. Differences between days with LLJs and days with no LLJs were subsequently calculated for each LLJ on a global scale with respect to moisture transport for the sources and sinks of moisture. Finally, each LLJ was analysed in terms of its associated socioeconomic impact and relationship with water scarcity.

1. Introduction

Low-level jets (LLJs) are common global meteorological phenomena and they are considered a major global mechanism of moisture transport, together with atmospheric rivers. As such, they are receiving an increasing attention in analyses of local precipitation in the regions in which they occur (Gimeno et al., 2016). In fact, LLJs generally occur in specific regions of the world, and tend to be semi-stationary seasonal events. Simplistically, they can be defined as filamentous regions or corridors of anomalously high wind speeds that are located within the first kilometre of the troposphere (Jiang et al., 2006; Nicholson, 2016). Several dynamic conditions are responsible for triggering and maintaining the structures of these LLJs, which can be essentially summarised as follows: (i) thermal gradients generated by topography, (ii) oscillations of the Planetary Boundary Layer (PBL), and (iii) characteristics of the Earth's surface. As an example, the Intra-Americas low-level jet (IALLJ) shows clear seasonal behaviour in response to thermal contrasts during the summer season (Amador, 2008). During the boreal summer, the IALLJ is divided into two branches: one that moves to the north, and another that crosses Central America and reaches the Pacific Ocean. However, in winter, one branch of the IALLJ turns to the south after crossing the Isthmus of Panama. Although LLJ systems occur throughout the year, they tend to be more strongly associated with the warm season (Bonner, 1968), and are more stable during the night (Blackadar, 1957). For these two reasons, this study focuses on nocturnal LLJs that begin to develop after sunset, reach a maximum at midnight, dissipate with the onset of daytime convective mixing, and are assumed to be caused by the nocturnal decoupling of the PBL (e.g. Jiang et al., 2007).

An initial theory on the development of LLJs was presented in a seminal paper by Blackadar (1957), who proposed that LLJs are the result of inertial oscillation of the ageostrophic wind triggered by a sudden decay of turbulence in the boundary layer after sunset, due to radiative cooling of the land's surface. However, this theory cannot explain the occurrence of certain LLJ structures, such as the Great Plains LLJ (GPLLJ). A subsequent theory proposed by Holton (1967) emphasised the importance of the role of thermal forcing in the diurnal oscillation of the boundary layer wind (as a consequence of sloping terrain), which affects the strength of LLJs. More recently, although the formation of these structures and their dominant mechanism are not yet well understood, a combination of the Blackadar mechanism and the thermal wind balance produced by sloping terrain are assumed to lead to the generation of these nocturnal LLJs (Parish and Oolman, 2010; Shapiro et al., 2016; Parish, 2017). For example, Wexler (1961) proposed that the origin of the GPLLJ is related to blocking of the easterly trade winds by the Rocky Mountains, and topography is thus an important trigger for the formation of such LLJ structures. Terrain characteristics can significantly deviate the direction of the wind at low levels and canalise it. Another example of this is the South American LLJ (SALLJ), whose flow intensifies when channelled through the

* Corresponding author.
E-mail address: ialgarra@uvigo.es (I. Algarra).

https://doi.org/10.1016/j.atmosres.2019.06.016
Received 15 February 2019; Received in revised form 21 June 2019; Accepted 22 June 2019
Available online 24 June 2019

eastern Andes (Salio et al., 2002). Furthermore, models of general circulation (Ting and Wang, 2006; Jiang et al., 2007) and experiments with terrain and terrain suppression (Pan et al., 2004) have suggested that topography is an essential factor in maintaining LLJs.

Climatological interest in LLJs is increasing because they are considered to be the main mechanisms for (sub)tropical moisture transport (Gimeno et al., 2016). Furthermore, their key role in transporting moisture suggests that they are strongly associated with precipitation patterns. It is therefore expected that changes in the behaviour of LLJs will lead to modifications in local (and even global) hydrological cycles (e.g. Pan et al., 2004; Gimeno et al., 2016). As with atmospheric rivers, a clear connection with the behaviour of nocturnal LLJs and extreme precipitation has been determined, and Gimeno et al. (2016) (and references therein) show that anomalies in the behaviour of LLJs, in regions that are strongly affected by them, are strongly related to the occurrence of droughts or floods. In addition, Monaghan et al. (2010) showed that nocturnal precipitation in at least ten different regions worldwide is clearly led by these jets.

LLJs are not a new phenomenon in the literature, and numerous studies have described and analysed their occurrence in specific regions. In particular, continental areas affected by monsoon regimes have received special attention. These areas have a common characteristic: the LLJ plays a key role in transporting large amounts of seasonal moisture in areas where adjacent oceanic regions act as dominant moisture sources. Studies presenting this aspect have been conducted on the North American Monsoon (NAM, Higgins et al., 1997b; Higgins et al., 1997a, b; Mo and Berbery, 2004) and in an analysis of the South American Monsoon (SAM, e.g. Vera et al., 2006). Furthermore, Xavier et al. (2018) and Wang et al. (2012) obtained similar conclusions with respect to monsoonal LLJs over India and China, respectively.

Studies have also been conducted on other aspects of LLJs. For example, Stensrud (1996) summarised in a review paper the most likely regions for LLJ occurrence. Rife et al. (2010) identified continental regions where nocturnal LLJs occur using an objective methodology based on the wind's vertical-structure index over a short period (1985–2005). Twenty-one potential LLJ regions were identified in their analysis during the summer period, including two LLJs that had not been previously identified (the Tarim Pendi and the Ethiopian LLJs).

One of the most studied LLJs is perhaps the GPLLJ (e.g. Bonner, 1968; Whiteman et al., 1997). It is located on the Great Plains, and has been previously associated with precipitation anomalies over the entire eastern US (e.g. Higgins et al., 1997a,b; Mo and Berbery, 2004; Algarra et al., 2019). Together with the GPLLJ, the mechanism of the South American LLJ (SALLJ) has also been well-documented in the literature (e.g. Marengo et al., 2004; Vera et al., 2006). The SALLJ flows parallel to the east of the Andes and has an important geostrophic component; it is considered to be the main mechanism contributing to moisture transport that reaches the La Plata River basin, and it carries moisture from the Amazon throughout the South American continent (Vera et al., 2006; van der Ent et al., 2010).

The bulk of the literature has been based on Bonner criteria (Bonner, 1968) for identifying LLJ events (e.g. Whiteman et al., 1997; Saulo et al., 2000; Marengo, 2002; Marengo et al., 2004; Salio et al., 2002). These criteria are based on the magnitude, horizontal extent, and vertical profile of the wind speed. However, Oliveira et al. (2018) modified the criteria when identifying the SALLJ by increasing the depth of the layer, and these changes have enabled the identification of a broader spectrum of LLJs. In addition, Montini et al. (2019) recently used the 75th percentile of wind speed as a threshold when identifying SALLJ events, rather than using a fixed threshold. Another method of identification of LLJ events, used in this work, is that proposed by Rife et al. (2010). Differently from the Bonner criteria, the Rife methodology allows to establish an intensity index of LLJ, reducing the subjectivity of the Bonner method by not having to establish fixed thresholds. More details on the methodology based on Rife et al. (2010) can be consulted in the Data and Methods section.

Despite the increasing interest in the connection between LLJs and extreme rainfall, and the associated increased understanding, a lack of high-resolution data and long-term observations have hampered global-perspective analyses. In addition, classical approaches used in such studies are based on Eulerian formalisms (e.g. Marengo et al., 2004) and do not allow for global identification of source and sink regions, which is a particularity of Lagrangian approaches. Furthermore, the total amount of precipitable water, or precipitation, associated with each LLJ has not yet been quantified well, and it is likely to be larger than the amount currently considered (Gimeno et al., 2016).

This paper provides a detailed analysis of source and sink regions of each LLJ, with the aim of understanding and better-predicting present and future impacts on the hydrological cycle. This is especially relevant within the context of global warming, where an intensification of the hydrological cycle is foreseen (Gimeno et al., 2010, 2012, 2013). The goals of this research are to 1) objectively identify the most relevant LLJs worldwide, and to characterise their dynamical structure (both horizontally and vertically) together with their typical time evolution; and 2) detect their associated moisture sources and sink regions and their potential impacts on social-economy. The structure of the article is as follows: Section 2 presents the methodologies used in this work; Section 3 presents the results in terms of the impacts from both physical and socioeconomical perspectives; and Section 4 includes both a discussion of the results and the conclusions that can be derived from them.

2. Data and methods

2.1. Rainfall, population and water scarcity datasets

Socioeconomic impacts associated with LLJs have been estimated from rainfall, population, and water scarcity datasets. Information on rainfall was retrieved from the Multi-Source Weighted-Ensemble Precipitation (MSWEP) dataset, which is a high-resolution (0.25°) gauge-satellite-reanalyses-based dataset available at a 3 h time step that has become a very reliable precipitation tool used in hydrological analyses (Beck et al., 2017). Information on population was obtained from the Socioeconomic Data and Applications Center (SEDAC, http://sedac.ciesin.columbia.edu). In particular, the Gridded Population of the World (GPWv4) dataset, which provides an estimation of human population using a combination of national censuses and population registers, was applied using the year 2015 as the representative year. Finally, water scarcity datasets were obtained from waterfootprint.org at a resolution of 0.5°. This dataset covers the period from 1996 to 2005. Water scarcity is calculated as the ratio of the local blue water footprint to the total blue water availability. More information on this can be found in Mekonnen and Hoekstra (2016).

2.2. Nocturnal low-level jet index

In this study, period from 1980 to 2016 were analysed. A 37-year output of 6 h ERA-Interim reanalysis data (Dee et al., 2011) with a 0.25° horizontal resolution was obtained from the European Centre for Medium-Range Weather Forecast (ECMWF) and was used to calculate the nocturnal low-level jet index (NLLJI). Since these LLJs are mostly associated with the warm season, this study focuses on the months of January and July for the southern and northern hemispheres, respectively (as in Rife et al., 2010). To take into account the particularities of the terrain, sigma levels have been used on which an interpolation has been carried out to obtain hourly outputs.

The methodology applied to calculate the NLLJI was obtained from Rife et al. (2010) and is based on the time evolution of the vertical wind structure and the diurnal-nocturnal variation of wind fields. By calculating the NLLJI at each grid point on a global scale, this index aims to detect LLJs that are more intense at midnight. The index is calculated as

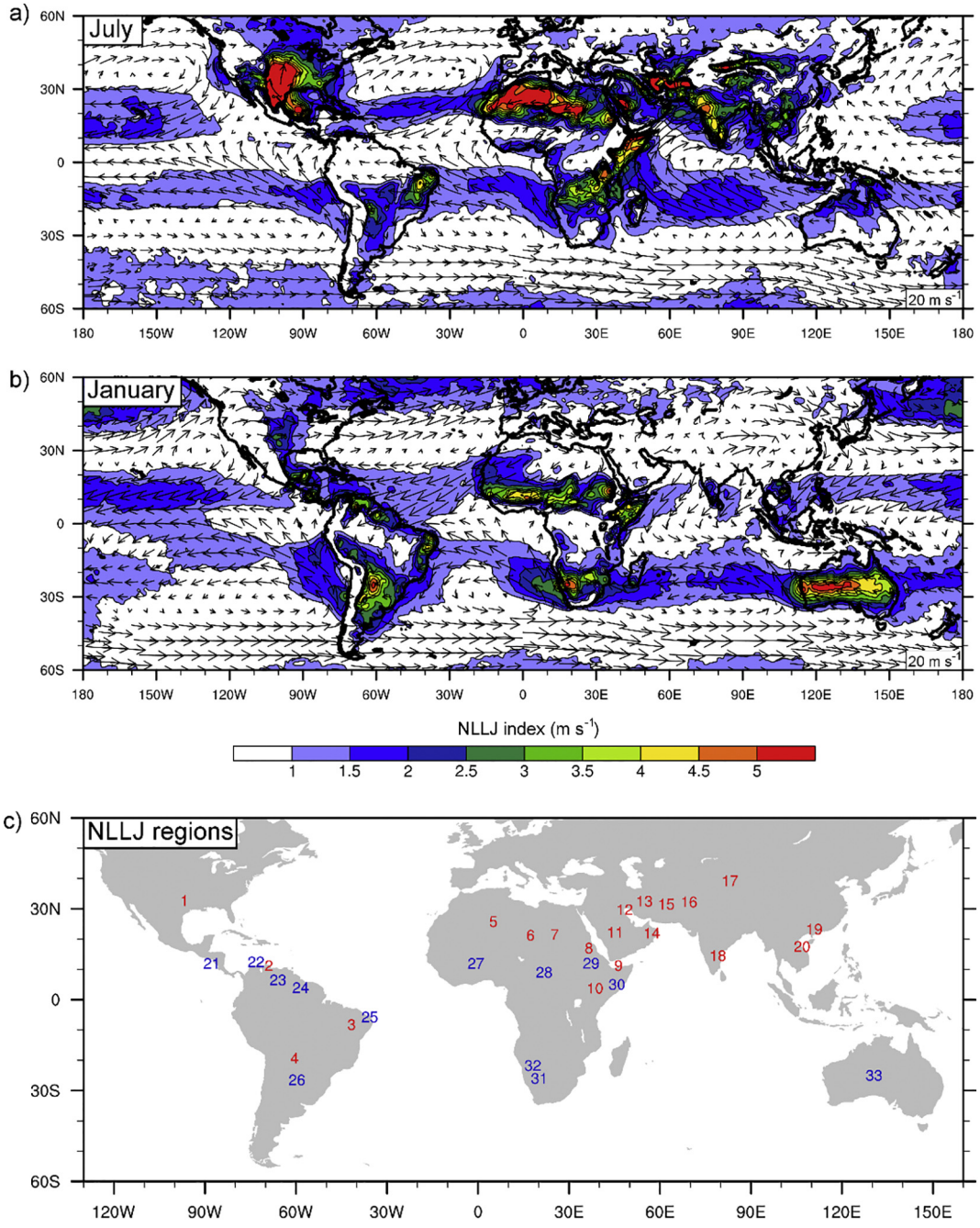

Fig. 1. Nocturnal Low-Level Jet Index (NLLJI, shaded, in $m{\cdot}s^{-1}$) and near-surface winds (arrows) calculated for (a) July and (b) January throughout the period 1980–2016 at the local midnight from ERA-Interim reanalysis data at 0.25° resolution in both longitude and latitude. Panel (c) shows locations of main LLJs worldwide identified in (a) and (b) for January (blue) and July (red). (For interpretation of the references to colour in this figure legend, the reader is referred to the web version of this article.)

shown in Eq. (1):

$$NLLJI = \lambda\varphi\sqrt{[(u_{00}^{L1} - u_{00}^{L2}) - (u_{12}^{L1} - u_{12}^{L2})]^2 + [(v_{00}^{L1} - v_{00}^{L2}) - (v_{12}^{L1} - v_{12}^{L2})]^2} \quad (1)$$

where u and v are the zonal and meridional components of the wind field, 00 and 12 are midnight and noon solar time, respectively, and $L1$ and $L2$ represent the near-to-surface level (53 sigma level) and height level (42 sigma level), respectively. The difference between both levels varies between 3000 m and 3800 m above sea level as a function of topography. Globally averaged, sigma level 53 has an average height of 550 m, whereas sigma level 42 has an average height of 4000 m.

Moreover, λ (Eq. (2)) and φ (Eq. (3)) are two binary operators which guarantee that the index exists only if the wind module is greater at L1 than at L2, and greater at 00 than at 12, and are used to preserve the nocturnal and low-level restricted character of the detected systems,

$$\lambda = \begin{cases} 0, & ws_{00}^{L1} \leq ws_{12}^{L1} \\ 1, & ws_{00}^{L1} > ws_{12}^{L1} \end{cases} \quad (2)$$

$$\varphi = \begin{cases} 0, & ws_{00}^{L1} \leq ws_{00}^{L2} \\ 1, & ws_{00}^{L1} > ws_{00}^{L2} \end{cases} \quad (3)$$

2.3. Identification of moisture sources: FLEXPART model

The Lagrangian model, FLEXPART (FLEXible PARTicle dispersion model) version 9.0 (Stohl et al., 2005), was used in backward mode to identify moisture sources associated with each detected NLLJ. ERA-Interim datasets, which are proven to be reliable tools for reproducing the hydrological cycle, were used to provide initial and boundary conditions to the model. FLEXPART has been successfully applied in the analysis of the atmospheric branch of the hydrological cycle (e.g. Nieto et al., 2008; Sodemann et al., 2008; Sodemann and Stohl, 2009; Gimeno et al., 2010; Drumond et al., 2014; Hu et al., 2018; Chen et al., 2017; Ramos et al., 2016) and has been proven capable of adequately locating the origin of precipitation associated with diverse dynamical systems (e.g. Gimeno et al., 2012).

The global experiment FLEXPART makes a homogenous division of the atmosphere from a certain number of parcels/particles (approximately 2 million) and allows such particles to be advected in the wind field, which enables them to be individually tracked. It also provides diagnostic variables of interest, such as the date, position, specific humidity and temperature. In this study, simulations were performed for the 1980–2016 period at a 1° horizontal resolution on 61 vertical levels (covering the entire troposphere) with an interpolated 3 h time step. A complete description as well as the configuration of the model can be found in the FLEXPART technical note by Stohl et al. (2005).

The transport time of the trajectories was integrated for 10 days, as this is the average water vapour lifetime in the atmosphere (Numaguti, 1999). The moisture changes associated with each particle were obtained using a general equation that analyses infinitesimal changes in specific humidity (q) with time (Eq. (4)), where m is the constant mass of the particle, and e - p depicts the water flux associated with the particle,

$$e - p = m\frac{dq}{dt} \tag{4}$$

The total surface freshwater flux budget (E – P: evaporation minus precipitation per unit area) is obtained when all particles at each grid position are considered (Eq. (5)), where K is the total number of particles in the atmospheric column and A is the area of the atmospheric column,

$$E - P = \frac{\sum_{k=1}^{K}(e - p)}{A} \tag{5}$$

Following the methodology of Stohl and James (2004, 2005), in a backward experiment, regions where evaporation exceeds precipitation ($E - P > 0$) are defined as moisture sources of the initially tagged area. In contrast, in a forward experiment, regions where precipitation exceeds evaporation ($E - P < 0$) are defined as moisture sinks. In our study, the tagged area corresponds to regions where the value of the NLLJI is above the 75th percentile.

3. Results

Fig. 1a and b show the average daily NLLJI calculated for the period 1980–2016 in the months of July and January, respectively, together with the mean wind fields at 00 solar local time at the near-surface level (53 sigma level). The 95th percentile of the NLLJI was used as the threshold to detect the main regions of occurrence. In total, 33 regions of NLLJ occurrence were identified on a global scale, and are summarised in Fig. 1c, where blue and red numbers show LLJs identified in the austral summer (a total of 13), and in the boreal summer (a total of 20), respectively.

Table 1 presents the main characteristics of each of the detected NLLJ, where the main core location, mean wind speed and direction at the height of the jet's core, and its duration during the day are displayed. The orientation of each jet is based on the eight principal directions of the wind-rose within its core, according to which most jets (60%) have a westerly orientation. Most of the detected NLLJs are confined between 30°N and 30°S, with the exception of five jets located at a latitude > 30°N: the Tarim Pendi LLJ (site 17), which is the jet located furthest away from the equator (39.25°N), the Great Plains LLJ (site 1, at 32.75°N), the Iran LLJ (site 13, at 32.5°N), the Afghanistan LLJ (site 15, at 31.5°N), and the Pakistan LLJ (site 16, at 32.25°N).

The duration of LLJs during the day was determined using the 75th percentile wind value at the level of the jet's core on the jet core level, where the maximum wind velocity is found. Jets are normally initiated at sunset, although in some cases they can be delayed until around midnight. However, the timing of their ending is more variable. In some cases, it usually occurs at dawn; however, all jets stop with sunrise. The temporal hourly evolution of wind speed calculated for the NLLJ maximum is shown for all LLJs in the supplementary material (Fig. S1).

Fig. 1a and b show that the strongest jets are found in the northern hemisphere, where the greater continental extension tends to produce an earth-ocean contrast that has a greater intensity on a larger scale than in the southern hemisphere, and the more-intense temperature gradient causes the development of stronger NLLJs. Another common characteristic of most NLLJs is that they have a maximum intensity over large land areas. In addition, some are close to continental borders, as in the case of the Ethiopia LLJ in north-western Africa (site 29), or the Maracaibo LLJ in northern South America (sites 2 and 22), which is identified in both January and July, at 12.5°N and 11.25°N, respectively. The Maracaibo LLJ (sites 2 and 22) and the South American LLJ (SALLJ, sites 4 and 26) are detected both in January and July, but they have greater intensities in the warm season, as expected. Thus, throughout the results, we will refer to Maracaibo-Jul and SALLJ-Jul for the LLJ that occur in July (i.e., boreal summer), and Macaraibo-Jan and SALLJ-Jan for the LLJ that occur in January (i.e., austral summer). North-eastern Brazil has different jets in the two seasons: Piaui LLJ (site 3) in July and the Rio Grande do Norte LLJ (RGN, site 25) in January (denoted by the name of the region over which it occurs). The NLLJ occurs over the Gulf of Aden (site 9) and can be considered to be a continental fingerprint of the branch of the Somali LLJ (site 14), which is identified over the Gulf of Oman; it flows parallel to the shore and reaches the Indian Peninsula where the Monsoon LLJ (site 18) is also located. The Turkana LLJ (site 30) is also detected both in warm and cold seasons, and there is a remarkable difference between the wind components of the two seasons.

The vertical wind profile was calculated for all LLJ-days within each region identified in Fig. 1c (Fig. 2). LLJs detected over America (Fig. 2a and d), Africa (Fig. 2b and e) and Europe, Asia and Oceania (Fig. 2c and f) are presented separately and for each season. It is evident that the maximum wind speed occurs at near-surface levels. For instance, the Piaui LLJ (site 3) has a maximum wind speed at the highest level (49 sigma level), while the Namibia LLJ (site 32) is detected at the lowest level (55 sigma level). The supplementary material shows wind vertical profiles for the days with no LLJs (Fig. S2).

Fig. 3 shows the frequency distribution of NLLJIs over each detected LLJ area for both January and July. NLLJIs are evaluated at the local midnight and at the mean height of the jet's core. Even when a no-fit analyses was applied, most of the distributions are Weibull-like and the maximum frequencies are between 5 and 15 m/s. In particular, remarkable is the case of the South American LLJ, where many events above 15 m/s (with relatively long tails) occur in both January and July.

With respect to the number of jet days, Fig. 4 shows the percentage number of days for NLLJs events. Regions under a NLLJ influence rarely have < 70% of days during which an NLLJ occurs. During the analysed months, LLJs are a common local climatological feature. In particular, the South American LLJ occurs on > 45% of days in the cold season, and others such as the Afghanistan LLJ (96%) and the Piaui LLJ (98%) stand out with respect to their high coincidence ratios.

The methodology proposed by Bonner (1968) establishes fixed thresholds of wind speed and vertical shear. Although the use of these

Table 1
Mean characteristics of all NLLJs shown in Fig. 1. LST: Local Solar Time; asterisk: NLLJ occurring during the austral summer (January).

Site No.	Name	Location of jet core	Mean wind speed and direction in jet core (m/s)	UTC and LST time of max	Time of onset and cessation (LST)	Bonner category	Height of jet core (sigma level)
1	Great Plains	32.75°N, 99°W	12.7–225° (SW)	06, 23	22–03	1	53
2	Maracaibo-Jul	11.25°N, 70.75°W	12.8–270° (W)	06, 01	19–01	1	53
3	Piaui	8.25°S, 43.5°W	9.7–315° (NW)	06, 03	19–03	1	51
4	South American-Jul	19.25°S, 62.25°W	16.8–180° (S)	06, 02	23–05	2	50
5	Algeria	25.75°N, 3.25°E	12.4–270° (W)	00, 00	23–04	1	53
6	Libya	21.25°N, 15.5°E	13.2–225° (SW)	00, 01	22–03	1	54
7	Egypt	21.5°N, 23.5°E	10.5–225° (SW)	00, 02	00–05	1	55
8	Sudan	17°N, 34.75°E	11.8–45° (NE)	00, 02	01–06	1	54
9	Gulf of Aden	12.25°N, 44.50°E	15.9–45° (NE)	00, 03	23–04	2	53
10	Lake Turkana	3.75°N, 36.75°E	13.6–315° (NW) (NW)	00, 02	22–03	1	53
11	Arabia Saudi	22.25°N, 43°E	12.0–135° (SE)	00, 03	00–05	1	54
12	Persian Gulf	29.75°N, 48.5°E	12.3–135° (SE)	00, 02	22–03	1	54
13	Iran	32.5°N, 53°E	12.3–270° (W)	18, 22	20–01	1	53
14	Somali	22°N, 55.5°E	12.4–45° (NE)	00, 04	23–05	1	54
15	Afghanistan	31.5°N, 60.25°E	20.2–180° (S)	00, 04	23–04	3	54
16	Pakistan	32.25°N, 67.75°E	10.2–90° (E)	18, 22	19–00	1	54
17	Tarim Pendi	39.25°N, 81.25°E	9.2–225° (SW)	00, 06	00–06	1	54
18	India Monsoon	14.5°N, 77.25°E	12.8–90° (E)	00, 05	02–07	1	51
19	China Monsoon	23.25°N, 109°E	10.3–0° (N)	18, 02	01–06	1	52
20	SE Asia Monsoon	17.5°N, 105°E	8.6–45° (NE)	18, 01	23–04	1	52
21	Caribbean*	12°N, 87°W	13.6–225° (SW)	06, 00	00–06	1	51
22	Maracaibo-Jan*	12.5°N, 74°W	10.6–270° (W)	06, 01	18–01	1	53
23	Llanos*	6.5°N, 67.5°W	10.9–225° (SW)	06, 02	00–05	1	52
24	Guyana*	4°N, 60.25°W	10.7–225° (SW)	06, 02	01–06	1	52
25	Rio G. Norte*	5.75°S, 38°W	10.3–270° (W)	00, 21	19–01	1	54
26	South American-Jan*	26.5°S, 61.5°W	9.9–180° (S)	06, 02	00–05	1	52
27	Ivory Coast*	12°N, 2.5°W	10.7–225° (SW)	06, 06	01–06	1	54
28	Bodélé*	9°N, 20°E	9.7–225° (SW)	06, 07	02–07	1	53
29	Ethiopia*	13.25°N, 35.5°E	10.3–180° (S)	00, 02	23–04	1	54
30	Turkana*	6°N, 42.75°E	10.5–270° (W)	00, 03	01–06	1	53
31	Botswana*	26°S, 18°E	9.0–270° (W)	00, 02	00–05	1	54
32	Namibia*	21.75°S, 16.25°E	9.9–0° (N)	18, 19	16–21	1	55
33	Australia*	25°S, 128.75°E	12.5–270° (W)	18, 02	00–05	1	54

fixed thresholds may be subjective, the Bonner methodology has been widely used in the identification of LLJs, particularly of SALLJ events (e.g., Salio et al., 2002; Marengo et al., 2004). Recent works have modified these thresholds by seasonal percentiles of wind speed reducing the subjectivity in the identification (Montini et al., 2019). Bonner's classic method defines three increasingly stringent requirements: that the wind speed is > 12, 16, 20 m/s within 1.5 km from the ground, and that the wind speed decreases by at least 6 m/s to the next higher-level minimum or to the 3 km level, whichever is lower. The categories for the LLJs are shown in Table 1.

3.1. Sources and sinks of moisture

Once regions of NLLJ occurrence were properly detected, simulations using trajectory outputs from FLEXPART enabled the identification of the major moisture sources and sinks associated with each jet (as explained in the methodology section). Regions within the 75th percentile of the NLLJI (green coloured contours in Figs. 5–16) were used to analyse moisture transport. To identify moisture source regions associated with the areas of interest, the model was run in backward mode to show regions where (E - P) > 0, and in forward mode to identify regions where (E - P) < 0, which are considered moisture sinks. The procedure was repeated for all NLLJs, and results are discussed in the regional analysis in the following sub-sections.

Systematic regionalisation was conducted to enable a better description of LLJ moisture transport, focusing firstly on North America followed by Central and South America, Africa (from north to south), Asia, and Australia. As discussed in the Data and Methods section, FLEXPART method is not able to compute evaporation and precipitation separately. Thus, throughout the discuss of the results, "precipitation" actually refers to the contribution of moisture to precipitation.

3.1.1. North America

The seasonality of rainfall in North America is strongly influenced by the Great Plains LLJ (GPLLJ). Fig. 5a shows the moisture climatology for July (from 1980 to 2016; related to regions contained within the green contour, as explained in the previous section). The reddish colours relate to the source of moisture, characterised by (E - P) > 0 values in the backward mode computed from FLEXPART outputs, and the bluish colours relate to sink regions characterised by (E - P) < 0 in the forward mode. The vector field represents the global wind velocity climatology for July 1980–2016, which is expected to converge from the source to the sink. Main source regions for the GPLLJ belong to both continental and oceanic domains, extending from the Caribbean Sea to the area of the maximum NLLJI itself. Moisture sinks are mostly continental, and cover the vast majority of North America's east and northeast regions.

Fig. 5b shows a comparison between moisture sources and sinks for days on which jets are detected, and for those on which jets are not detected. This plot is composed using the difference between (E - P) < 0 values for jet days and (E - P) < 0 for no-jet days for the moisture sinks, and the difference between (E - P) > 0 values for jet days and no-jet days for the moisture sources. The two fields of differences are plotted together, and the results can be interpreted as follows: a) reddish colours show regions that are more active as moisture sources on jet days compared to non-jet days; b) blueish colours show regions that are more active as moisture sinks on jet days; and c) greenish colours are regions that are more active as moisture sinks on non-jet days. Vectors refer to the wind climatology only for those days with jets plotted at surface level. To ensure clarity, regions that are more active as sinks on non-jet days are not shown. The results

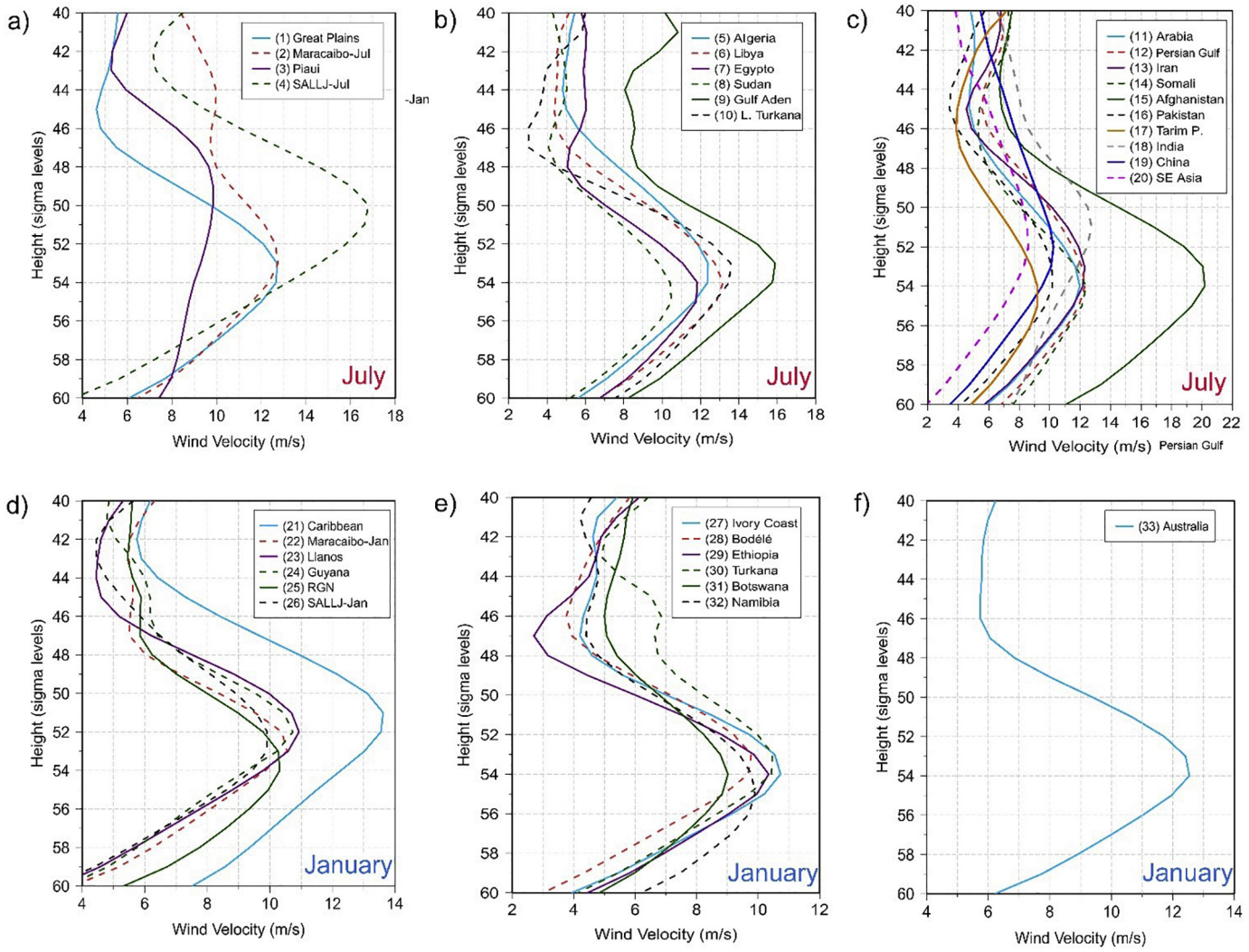

Fig. 2. Frequency distributions for the NLLJ regions identified in Fig. 1 for January (a, b, c) and July (d, e, f). Jet locations were divided into three mains regions for better visualisation: America (a, d) including North America and South America, Africa (b, e), and Europe-Asia-Oceania (c, f).

show that the regions where most of the moisture advected by the GPLLJ originate are the southern Gulf of Mexico and the Caribbean Sea, but also extend eastward over the Atlantic Ocean (reddish colours). This moisture transport is highly influenced by the orography, which plays a key role in the upward forcing of the GPLLJ (Parish and Clark, 2017) and it is the trigger for the instability and consequent precipitation. The Rocky Mountains also block the circulation to the west, creating a channelling effect that forces the moisture to flow north and eastward, which then contributes to North America's central, east and north-eastern precipitation (blueish colours). During no-jet days, the moisture sink region and precipitation are positioned southward (greenish colours).

3.1.2. Central and South America

The moisture transport for Central and South America is strongly modulated by several LLJs. In general, the Tropical North Atlantic Ocean (TNA) is the major source of moisture in relation to the regime of trade winds linked with the southern branch of the north Atlantic subtropical high. The Caribbean Low-Level Jet (CLLJ) is a permanent LLJ, and there is a marked semi-annual cycle influenced by this easterly wind (Amador, 2008; Muñoz et al., 2008): during the boreal summer, the CLLJ peaks in zonal wind intensity and splits into two branches, one crosses Central America and the other one recurves northward forming the GPLLJ (Cook and Vizy, 2010), which contributes to the increased moisture penetrating into North America. In contrast, during the austral summer, the maximum winds of the CLLJ move towards the south, and the moisture transport is advected from the tropical Atlantic into the Caribbean Sea and crossing into Central America, and a marked flow penetrates South America forming an essential component of the South American Monsoon and the South America LLJ (SALLJ) (Amador, 2008; Poveda et al., 2014).

With respect to the focus of this study (i.e., NLLJIs), only one LLJ was detected over Central America during January (site 21, Fig. 1). Fig. 6a shows that moisture is advected by the CLLJ to Central America, where it crosses the land to the western Pacific coast. The main sink for this moisture is positioned over the Pacific Ocean. However, less moisture is associated with this than with its northern branch to the Great Plains during summer (see Fig. 5a). During jet days the moisture source over the Atlantic is intensified, but intensification of precipitation over the continent is not observed (Fig. 6b).

The Maracaibo low-level jet (positioned over the Maracaibo brackish tidal bay) is a semi-permanent LLJ present in both July and January (sites 2 and 22, respectively, Fig. 1) that is located in northern South America. As the Maracaibo LLJ is a fingerprint of the CLLJ southern branch, it is influenced by the position and intensity of easterly trade winds, and it has a marked zonal component: the major sinks of moisture are located over on the Pacific coast of Colombia and Ecuador during austral summer (Fig. 6e), but more northward over

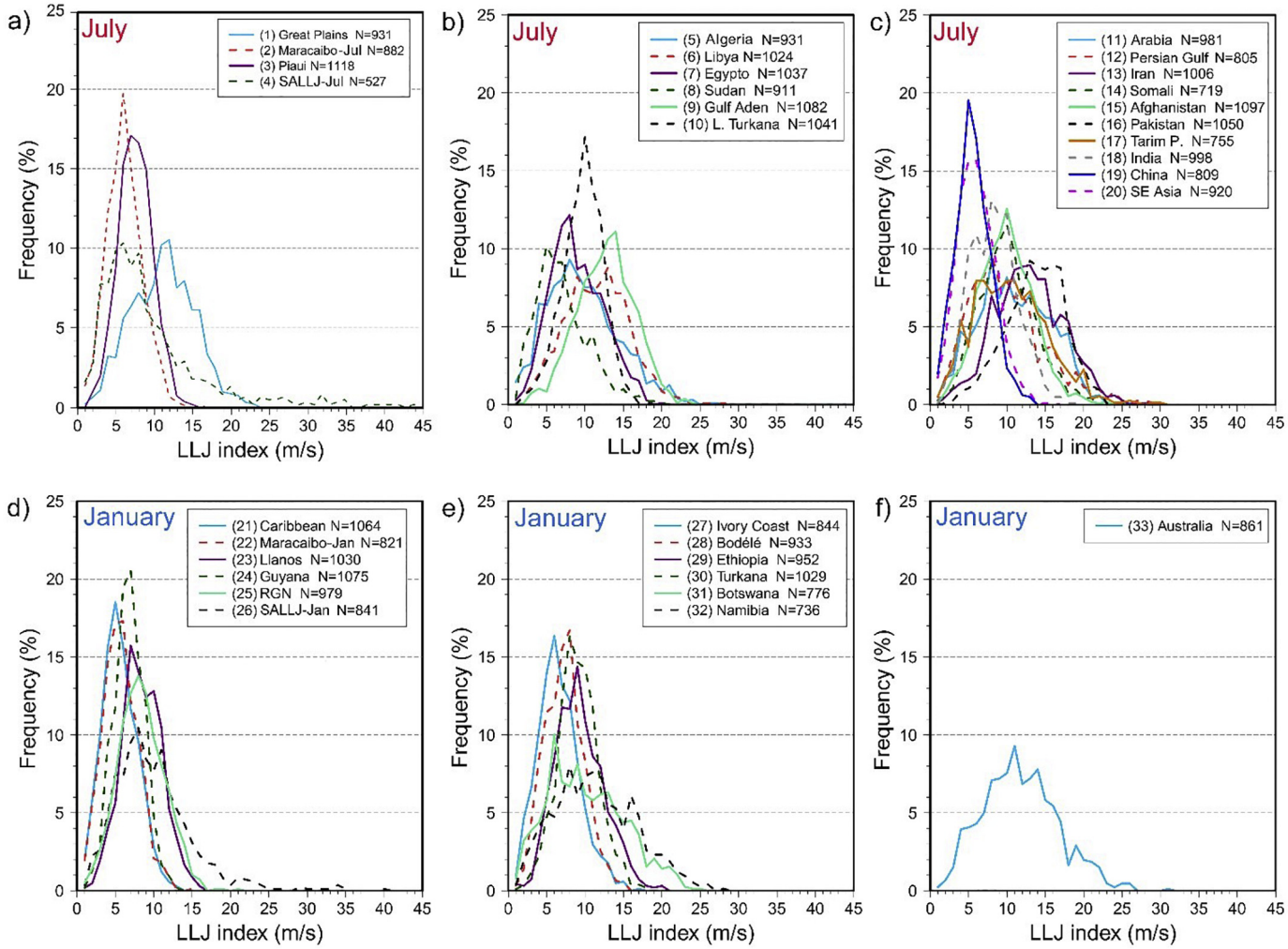

Fig. 3. Wind vertical profile (in m/s) over the maximum point of the index for each region identified in Fig. 1c. Each profile relates to the local midnight (LST in Table 1). Representations were grouped by LLJ locations into three main regions for better visualisation: America (a, d) including North America and South America, Africa (b, e), and Europe-Asia-Oceania (c, f).

Central America (Costa Rica and Panamá) during the boreal summer (Fig. 6c) and extending over the Pacific Ocean due to intensification of the trade winds. During jet days (Fig. 6d and f) precipitation is intensified over the same climatological sink areas (blueish colours), although there is an associated reduction over northern Colombia (green colour).

Also located in the north of South America, Los Llanos LLJ (site 23, Fig. 1) and Guyana LLJ (site 24, Fig. 1) are considered to be parts of the northern branch of another large atmospheric structure, known as the semi-permanent South American low-level jet (SALLJ), which is associated with the continental entrance of the trade wind. As previously noted, the SALLJ is key to South America's climate. During the warm-wet season, the southward flux of moisture east of the Andes is an important regional feature of South America, and similar to the Rocky Mountains with the GPLLJ, the north–south orientation of the Andes Mountains influences regional circulations that are conducive to channelling moisture transport from the tropics to high latitudes. Moisture sinks for both LLJs are located in central South America over the western Amazon River basin, with a larger sink extension for the Guyana LLJ because of the greater quantity of moisture transported from the TNA source (Fig. 6g and i). During jet days, an intensification is observed over the source of moisture located in the TNA. This structure transports higher amounts of moisture to the sink regions of Ecuador and Peru, where more precipitation is expected on LLJ days. On non-LLJ days, moisture is not advected as far as during jet days, and the sink is located north-eastward over southern Venezuela and the northern Amazon basin (Fig. 6h and j).

Further south, the LLJ detected over Argentina (known as the SALLJ) is present throughout the year (sites 4 and 26 in Fig. 1, for austral winter and summer, respectively), although it is much more intense during the warm season. Fig. 7a and c shows that the main source of moisture for the SALLJ is located in the south of the Amazon, where intense recycling processes, and the moisture transported by the northern branch of this structure, contribute to the increased availability of moisture for the SALLJ (Drumond et al., 2010; Martinez et al., 2014; Marengo and Espinoza, 2016). The moisture sinks are positioned predominantly over the western La Plata river Basin (the second largest drainage basin in South America after the Amazon) and over its river mouth. During jet days, moisture for precipitation is increased over their climatological sinks (Fig. 7b and d). It is interesting that this increase is more intense and focused over the central part of the climatological sink during jet days in July, and there is less precipitation around it (Fig. 7b). In January, precipitation is reduced during jet days on both sides of the maximum NLLJI area (Fig. 7d).

Another semi-permanent low-level jet is located in the northeast region of Brazil. It is known as the Rio Grande do Norte low-level jet (RGN) when it occurs in January (site 25, Fig. 1), and as the Piaui low-level jet in July (site 3, Fig. 1). Both of them are associated with the easterly trade winds of the southern hemisphere. Fig. 7e and g show that while both LLJs share a moisture source, which is located eastward

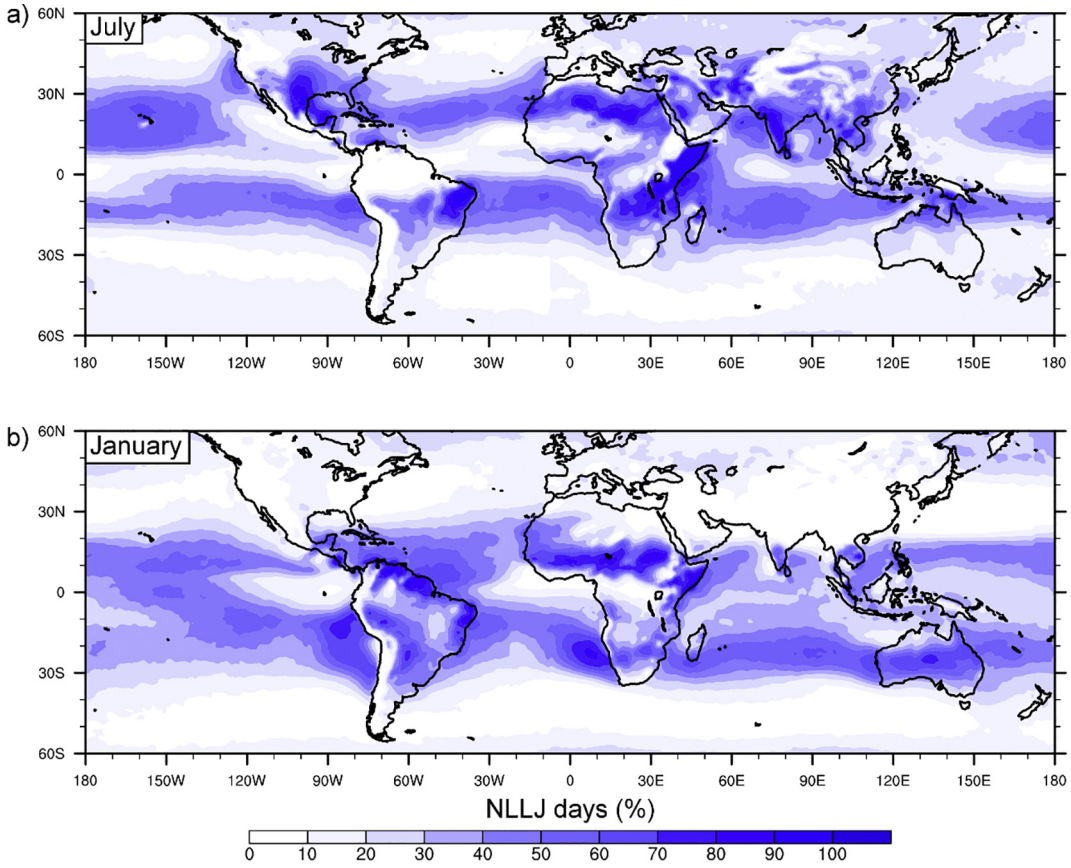

Fig. 4. Mean percentage number of days on which NLLJ was detected for both (a) July and (b) January.

in the Tropical South Atlantic region (but which is more evaporative during July), the moisture sink associated with the Rio Grande do Norte LLJ (Fig. 7g) is located over the closer westward areas of maximum LLJ intensity within the northeast region itself (characterised by a semiarid climate). In addition, the moisture sinks associated with the Piaui LLJ (Fig. 7e) are split in two branches: one is located southward over the La Plata River Basin, and the other northward over the western Amazon basin. It is shown that during jet days in January (Fig. 7h) the areas near the LLJ core receive less moisture for precipitation (greenish colours) and moisture that produces precipitation is increased in the southernmost area. In contrast, during jet days in July (Fig. 7f), the central Amazon River basin receives less moisture for precipitation, whereas moisture is highly increased over the La Plata River Basin (blueish colours). Conversely, during no-jet days, precipitation moves mostly towards the north of South America in July over Colombia and eastern Venezuela (greenish colours in Fig. 7f), whereas it remains near

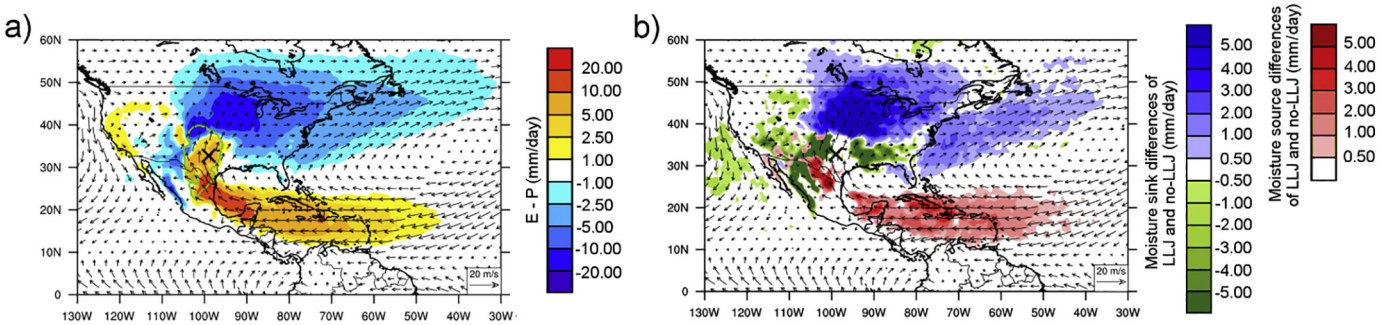

Fig. 5. Outline of socio-economic impacts for both July and January (a and b, respectively). Grey boxes show mean values together with minimum and maximum values of precipitation in 1980–2016 for each region involved (in mm/month). Green and blue dots represent the population and the water scarcity index, respectively. a) Mean climatology of the (E - P) field for regions surrounded by a green contour (75th percentile of the NLLJ index value) for July 1980–2016. Blueish colours indicate regions where (E - P) $<$ 0 in the forward simulation and are considered to be moisture sinks (i.e., the precipitation is larger than the evaporation), whereas reddish colours indicate regions where (E - P) $>$ 0 in the backward simulation, are considered to be moisture sources (i.e., the evaporation is larger than precipitation). The black cross indicates the point of maximum NLLJ intensity. The vectors relate to wind climatology for July (1980–2016) at the surface level near the maximum LLJ intensity level. b) Differences between the (E - P) field during jet days and the (E - P) field on non-jet days. Blueish and greenish colours indicate a positive and negative differences, respectively, for sinks of moisture; in blue colour are regions more active as moisture sinks on jet days while in green colour are regions that are more active as moisture sinks on non-jet days. Reddish colours indicate a positive difference for the source of moisture; in red colour are regions that are more active as moisture source on jet days compared to non-jet days. In this case, vectors refer to the wind climatology only for those jet days, and are plotted for the surface level. (For interpretation of the references to colour in this figure legend, the reader is referred to the web version of this article.)

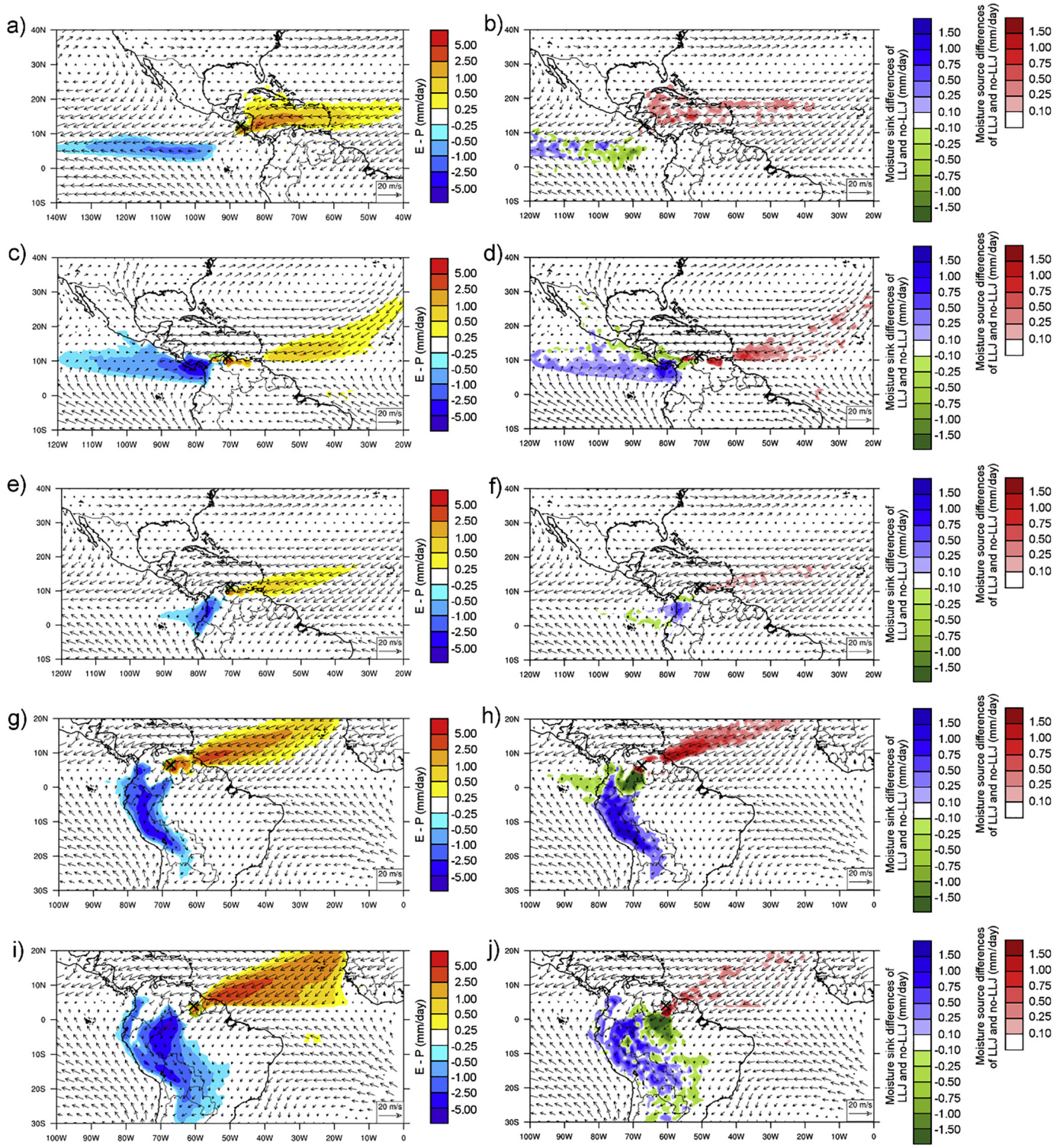

Fig. 6. As in Fig. 5 but for: (a, b) Caribbean LLJ in January; (c, d)Maracaibo LLJ in July and (e, f) in January; (g, h) Llanos LLJ in January; and (i, h) Guyana LLJ in January.

the jet core in January (Fig. 7h).

3.1.3. Africa

Four main areas of LLJ occurrence are identified in Africa: the central Sahara, the Sahel, and the areas around the Horn of Africa and southern Africa. It is known that LLJs in Africa are most frequently embedded in either the south-westerly monsoon flow or the dry north-easterly Harmattan flow (Schepanski et al., 2017), and this orientation means that the Mediterranean Sea acts as an important source of moisture for NLLJs detected in inner areas of north Africa over the central Sahara (Fiedler et al., 2013) and the Sahelian region (Nieto et al., 2006, 2016; Salih et al., 2015). In central Sahara (Fig. 8) the Algeria LLJ (site 5, Fig. 1), Libya LLJ (site 6, Fig. 1) and the Egypt LLJ (site 7, Fig. 1) can be considered to be local maxima of the same dynamic structure. They are the fingerprints of the north-easterlies that transport moisture from the central Mediterranean Sea to the Sahel

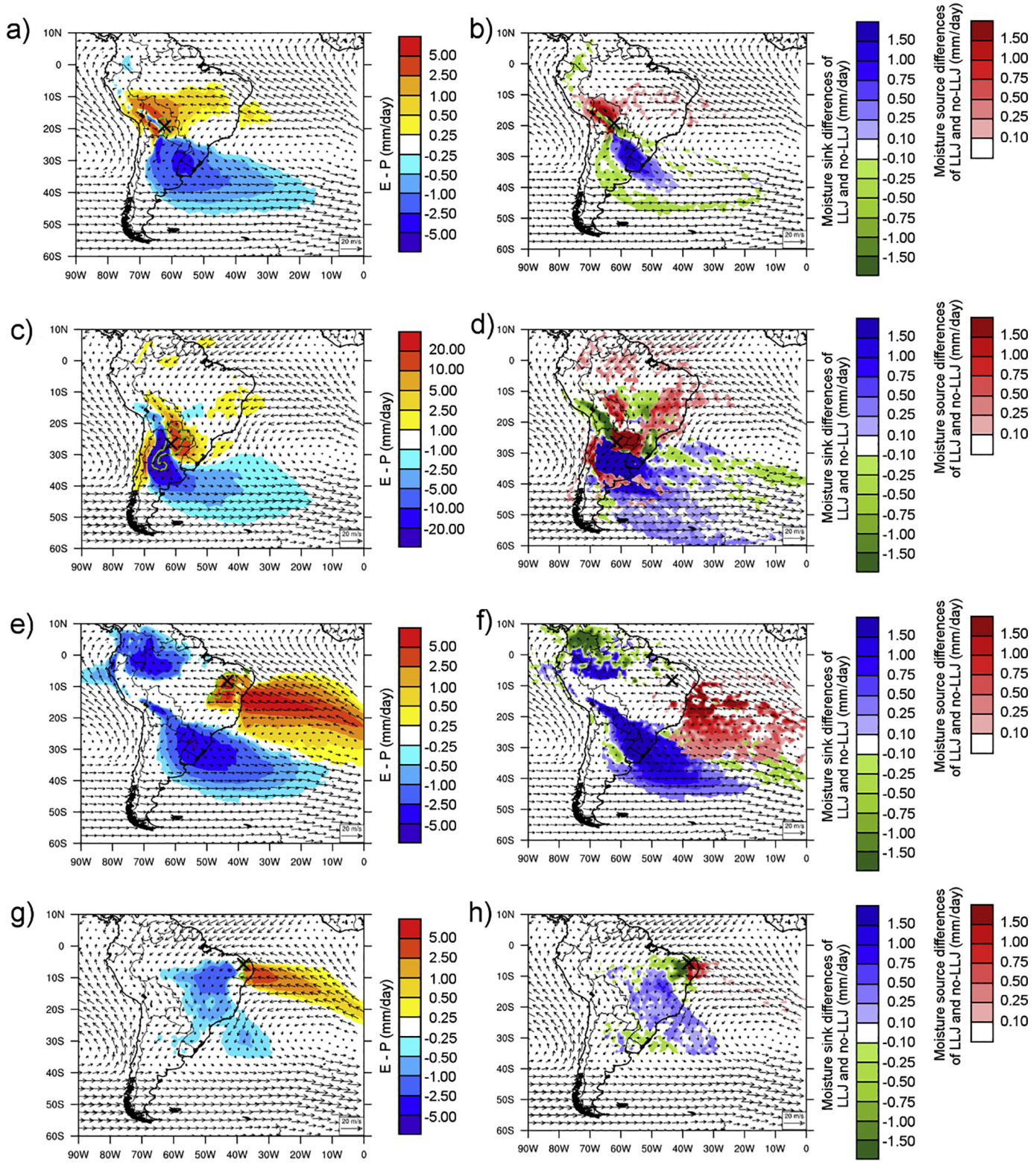

Fig. 7. As in Fig. 5 but for: (a, b) SALLJ in July and (c, d) in January; (e, f) Piaui LLJ; and (g, h) Rio Grande do Norte LLJ.

region (Fig. 8a, c, and e), and they are also controlled by the position of the Saharan Heat Low (Allen and Washington, 2014). The moisture transport for precipitation is not highly associated with the LLJs in the region (blueish colours in Fig. 8a, and c), but it appears to be important for the Egypt LLJ (Fig. 8e), and it effects a latitudinal band over central Africa (from Cameroon to Ethiopia) and is reinforced during jet days (bluish colours in Fig. 8f).

For the Sahel region during January, the Ivory Coast low-level jet (site 27, Fig. 1), which is located in the western Sahel region, transports moisture to the Atlantic Ocean that reaches part of the northern South American continent (Fig. 9a). The intense source of moisture associated with the Ivory Coast LLJ area is the consequence of intense recycling over the region (Savenije, 1995). During jet days, the role of the Mediterranean basin as a source of moisture is intensified (reddish

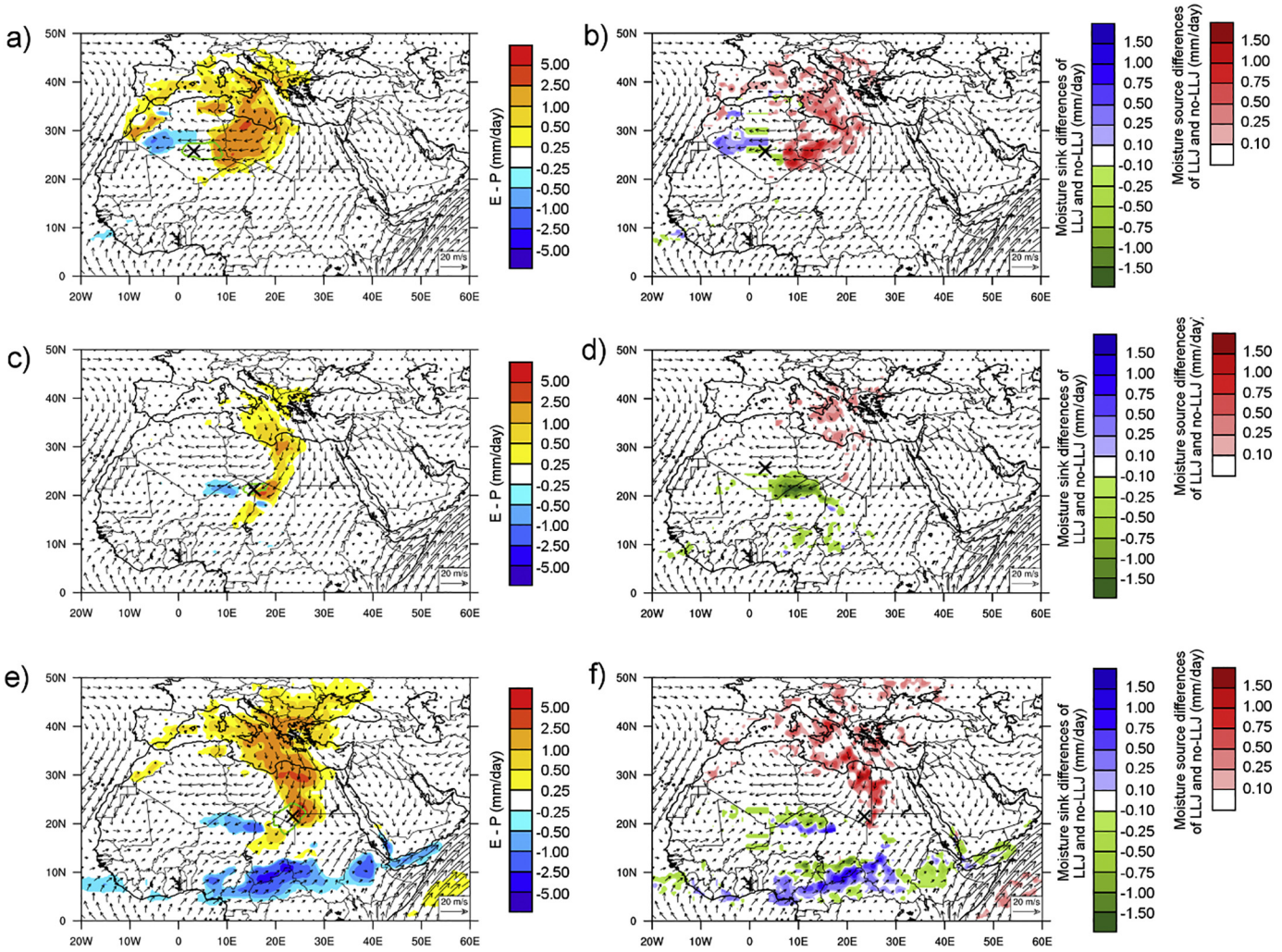

Fig. 8. As in Fig. 5 but for: (a, b) Algeria LLJ; (c, d) Libya LLJ; and (e, f) Egypt LLJ.

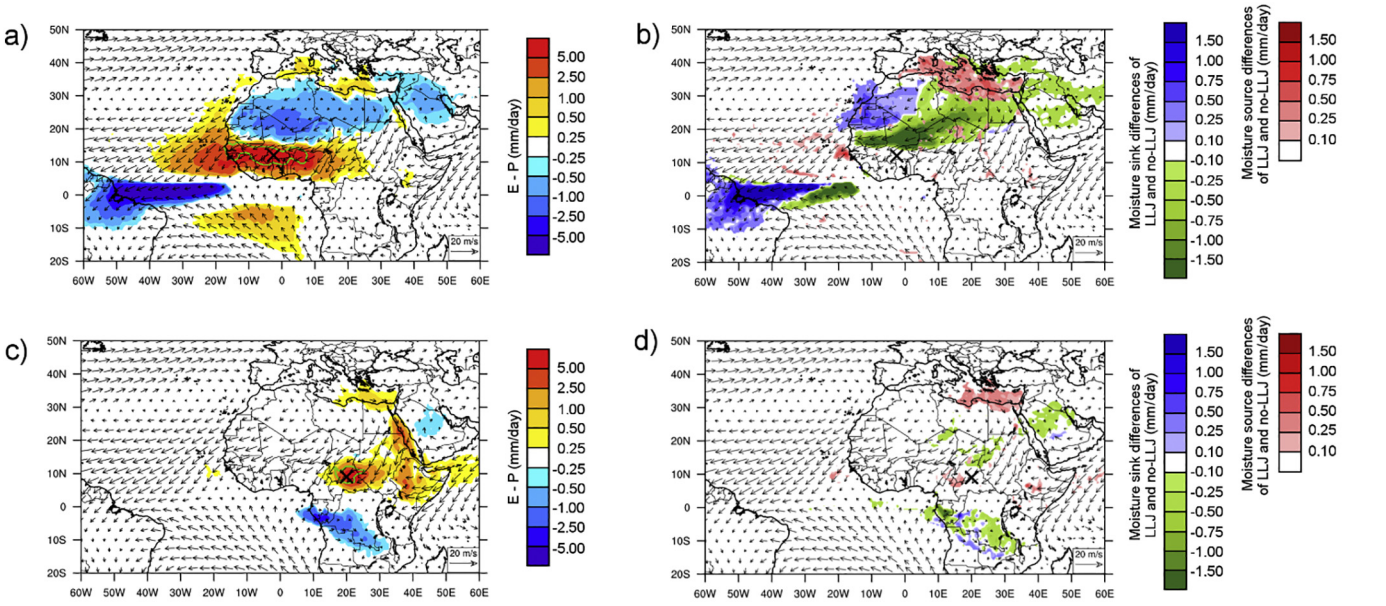

Fig. 9. As in Fig. 5 but for: (a, b) Ivory Coast LLJ; and (c, d) Bodélé LLJ. (For interpretation of the references to colour in this figure legend, the reader is referred to the web version of this article.)

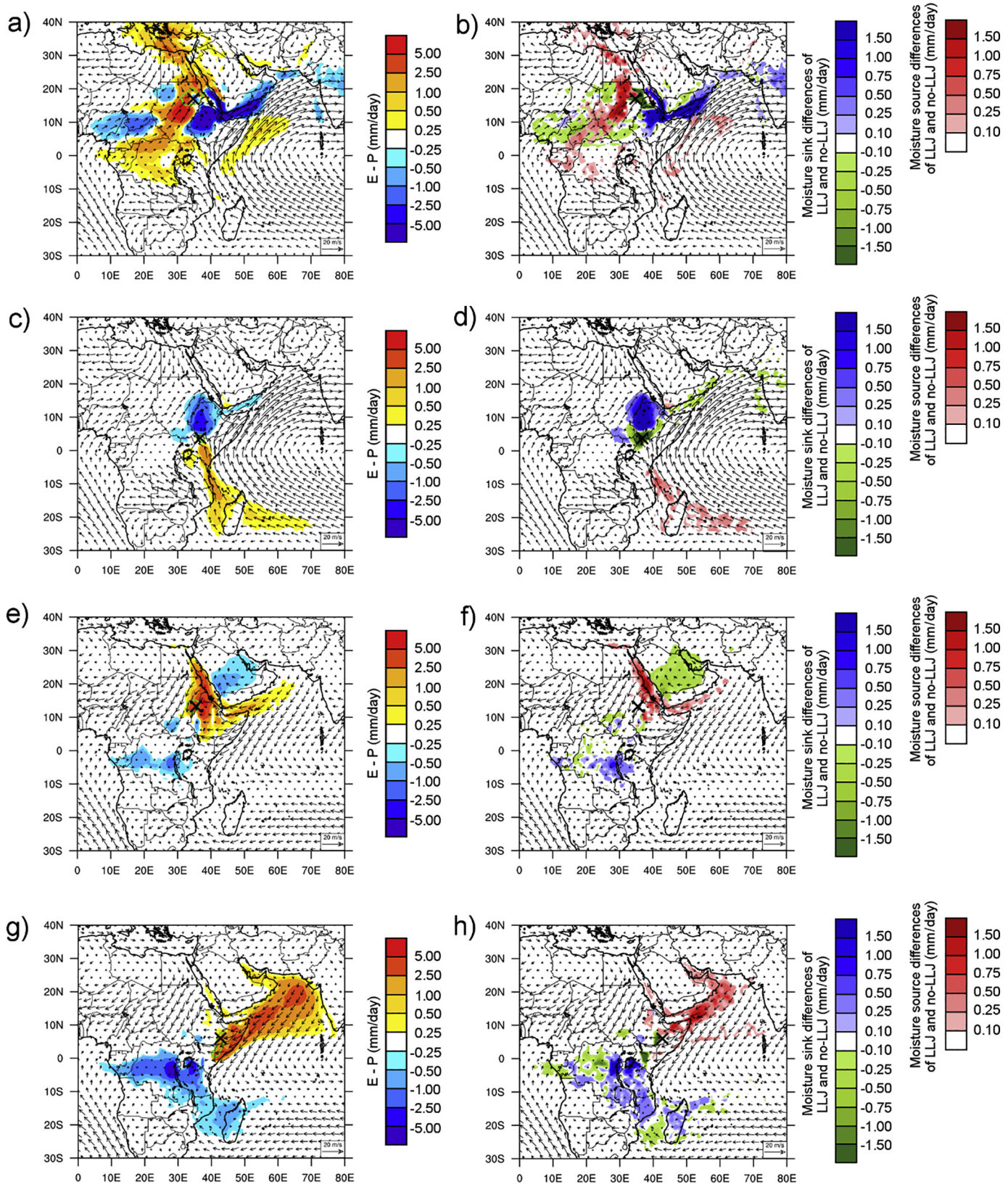

Fig. 10. As in Fig. 5 but for: (a, b) Sudan LLJ; (c, d) Lake Turkana LLJ; (e, f) Ethiopia LLJ; (g, h) Turkana LLJ.

colours in Fig. 9b), the moisture reaches the northeast of South America (blueish colours), and more moisture is available for precipitation over north-western Africa. However, on no-jet days, a weakening of wind intensity causes the sink of moisture to be located in the north of Sahel region (greenish in Fig. 9b); on the contrary, during jet days there is less moisture available for precipitation to northern Sahel, and even to the Arabian Peninsula.

The Bodélé LLJ (site 28 in Fig. 1) is also located in the Sahel strip.

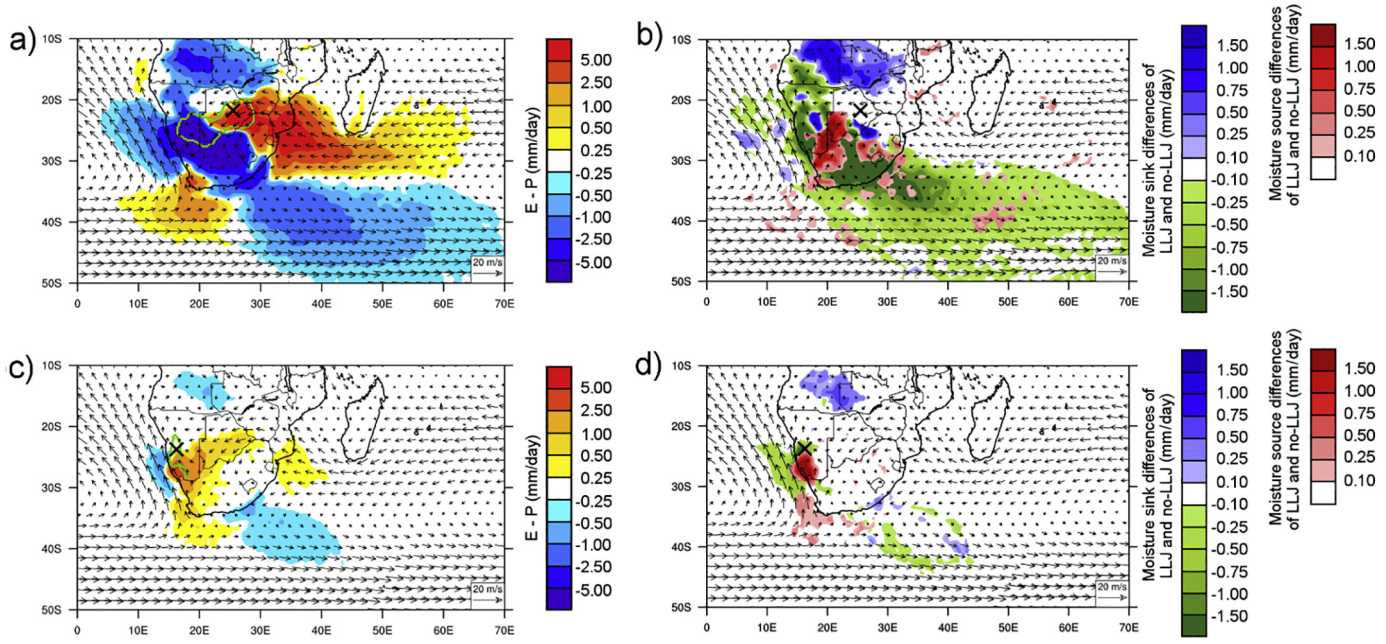

Fig. 11. As in Fig. 5 but for: (a, b) Botswana LLJ; and (c, d) Namibia LLJ.

Despite the large atmospheric transport of dust that is commonly linked with this NLLJ (Knippertz and Todd, 2012; Fiedler et al., 2013), part of the Red Sea and the Horn of Africa are identified as associated moisture sources and there is intense local recycling (Fig. 9c). The climatological sink of moisture is located in central-southwestern Africa (Fig. 9c). The difference in the E - P field between LLJ days and no-LLJ days is negligible, but there is a slight increase in moisture transported from the southern Mediterranean basin during jet days (Fig. 9d).

Four LLJs are located over the Horn of Africa (see Fig. 10). During the boreal summer, the Sudan low-level jet (site 8, Fig. 1) uptakes moisture from the Mediterranean Sea and from the centre of Africa, due to convergence of north and south wind flows to the jet region, and the Gulf of Aden and coastal areas around it act as the main sink areas of moisture (Fig. 10.

a). On jet days, these climatological sources and sinks are intensified (reddish and blueish colours in Fig. 10b), where the moisture sink is located over the continental centre of Africa on no-jet days (greenish colours in Fig. 10). The Lake Turkana LLJ (site 10, Fig. 1) transports moisture from the Mozambique Channel to the north (Fig. 10c). During jet days, the strengthening wind intensity causes an intensification of moisture available for precipitation over Ethiopia (blueish colours in Fig. 10d), but during no-jet days, the moisture does not move so far north and is mainly localised in the north of Kenya. However, the wind patterns change from south to north during the austral summer. The Ethiopia low level jet (site 29, Fig. 1) is associated with north-easterlies and uptakes moisture from the Red Sea, Aden Gulf and part of the east continental area and transports -it to the continental interior of Africa (Fig. 10e). On jet days, the sources and sinks are reinforced (Fig. 10f). The Arabian Peninsula is shown to be linked with the behaviour of this LLJ, as the region acts as a climatological sink of moisture (Fig. 10e), but only during no-jet days (greenish colours in Fig. 10f), and transport is inhibited during jet days. Finally, for the Turkana LLJ (site 30, Fig. 1) in January, the Arabian Sea acts as the main source transporting moisture for precipitation over a broad band, from the Equator latitudes reaching Madagascar (Fig. 10g). On jet days, moisture advection intensifies in the region near the Gulf of Aden, and the moisture is displaced towards the north of Kenya and northwest of the Congo (blueish colours in Fig. 10h), whereas during no-jet days, the Congo River basin acts as a sink (greenish colours in Fig. 10 h).

The last African region we have analysed is Southern Africa (Fig. 11). Here, during the austral summer, the moisture supply tends to be associated with an inflow from the Indian Ocean via the Botswana low-level jet (site 31, Fig. 1), which converges in the continental area of southern Africa, and moisture inflows from the tropical southeast Atlantic via the Namibia low-level jet (site 32, Fig. 1) (Cook et al., 2004). Our results show that the Botswana LLJ uptakes moisture mainly from southern Madagascar over the south west Indian Ocean and continental areas over south-eastern Africa. Climatologically, the moisture is transported to the southwest, mainly over South Africa and Namibia (Fig. 11a), but a northward branch also transports it to the Congo River Basin. During jet days, this river basin sink is reinforced; while on no-jet days, the moisture sink is located in the Southern Africa (blueish and greenish colours respectively in Fig. 11b). The Namibia LLJ is located on the south-eastern coast of Africa and is the continental fingerprint of the Benguela low-level coastal jet (BLLCJ). It is a coastal jet developed in a region of high upwelling that increases the thermal contrast between land and ocean. It favours the development of the LLJ, as does the presence of the mountain chain and a semi-permanent high-pressure centre (Patricola and Chang, 2017; Nicholson, 2010). This LLJ uptakes moisture on the west coast of South Africa, and the sink is positioned over Angola (Fig. 11c and d).

3.1.4. Asia and Australia

Three regions with low-level jet occurrence are identified in western Asia during the boreal summer. Firstly, the Persian Gulf low-level jet (site 12, Fig. 1) is a thermal phenomenon located in the north of the Persian Gulf. Commonly known as the Shamal Wind or the Persian Gulf of Summer low-level jet, it is a northerly to north-westerly wind that is oriented parallel to the Zagros Mountains (Govinda Rao and Hatwar, 2003; Giannakopoulou and Toumi, 2012). The Persian Gulf LLJ uptakes moisture (Fig. 12a) from the eastern Mediterranean Sea, the Black Sea, and the Fertile Crescent. On the other hand, this LLJ does not have a well-defined climatological moisture sink pattern. Following the southward wind flow, the sink is mainly positioned over the Arabian Peninsula and Ethiopia (Fig. 12a). An intensification in the moisture source is observed during jet days, and this is transported towards the south of the Arabian Peninsula (blueish colours in Fig. 12b). However, during no-jet days, moisture for precipitation is mostly concentrated over northern Saudi Arabia (Fig. 12b). Another low-level jet is identified over the Arabian Peninsula (tagged as the Arabia low-level jet in

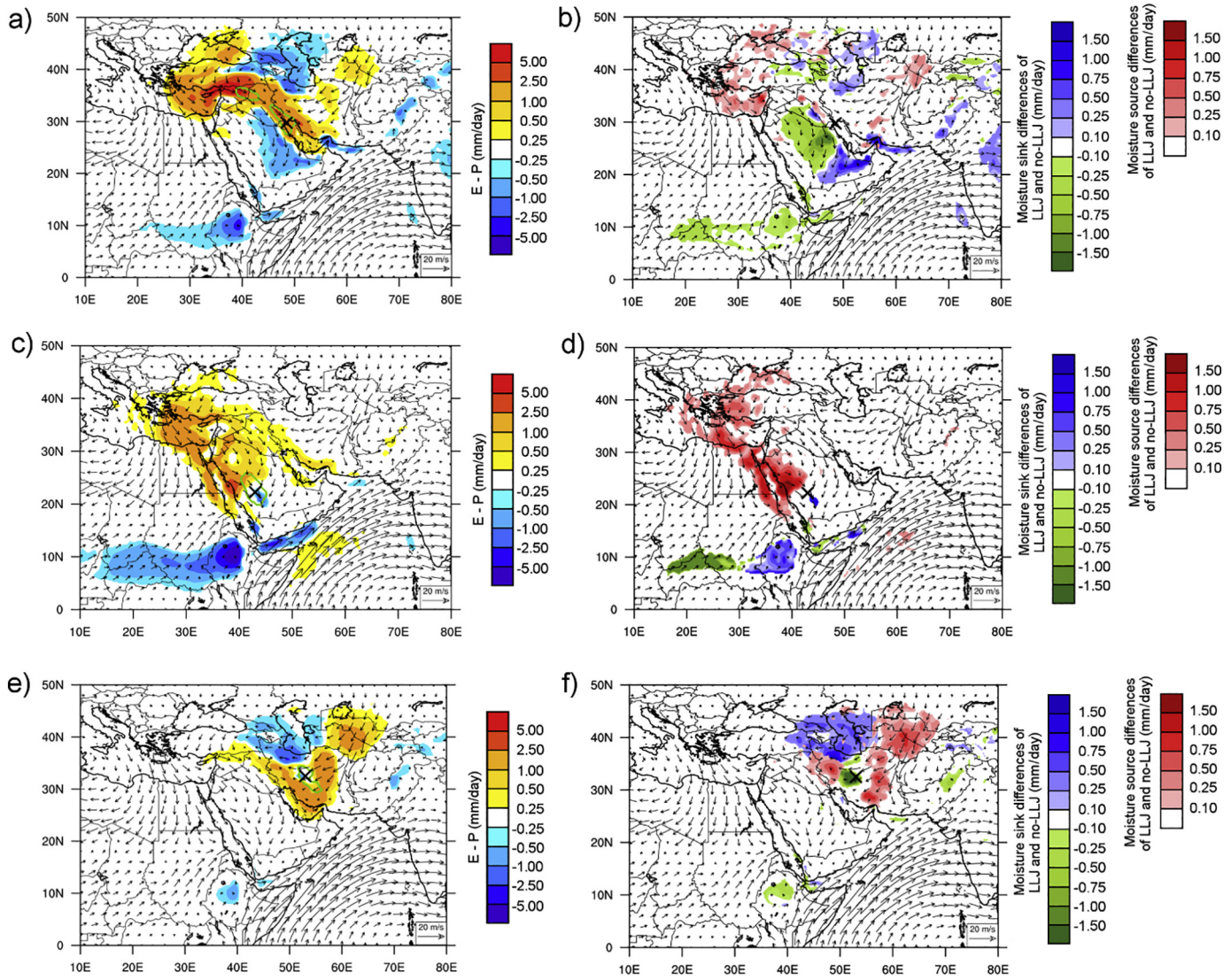

Fig. 12. As in Fig. 5 but for: (a, b) Arabia Saudi LLJ; (c, d) Iran LLJ; and (e, f) Persian Gulf LLJ.

Fig. 1, site 11); this is associated with northerly winds, and it also uptakes moisture (Fig. 12c) from the eastern Mediterranean Sea and from the north of the Arabian Peninsula to the Middle East. The Arabia LLJ contributes to intensifying moisture over the sink located from Ethiopia to the west, which conforms the western Sahelian region. The moisture uptake is enhanced during jet days, and the sink is mainly positioned over Ethiopia, while during no-jet days it is located westward over Chad and Sudan (Fig. 12d).

Finally, the Iran low-level jet (site 13, Fig. 1) is located south of the Caspian Sea and is associated with north-eastern winds. It uptakes moisture from the surrounding continental areas, and during jet days the loss of moisture associated with this structure is enhanced northward around the Caspian Sea (Fig. 12e). On jet days, as in other cases, the source and sink are intensified. However, on no-jet days, moisture for precipitation is constricted over the maximum occurrence area of the LLJ (Fig. 12f).

Two regions of LLJ occurrence are detected in central Asia. One region shows two maximum cores for the INLLJ: one is the Afghanistan low-level jet (site 15, Fig. 1), which is a jet that develops in the channel east of the Seistan Mountains along the border between Iran and Afghanistan, and the other occurs over Pakistan (site 16, Fig. 1). They play key roles in generating dust (Alizadeh-Choobari et al., 2014) and both carry minimal moisture (Fig. 13a and c). Another characteristic is that they are the first LLJs associated with north winds that turn towards an eastern component and contribute to the availability of atmospheric moisture for precipitation over the Pakistan region. The difference in the E - P field between jet days and no-jet days is not remarkable; however, there is a light intensification of moisture transported towards the east (Fig. 13b and d). Another LLJ over this area is the Tarim Pendi LLJ (site 17, Fig. 1). It is located on the north side of the Tarim Basin, is associated with westerly winds, and is the main source of moisture is the region of the occurrence of LLJ and westwards areas. The sink region is mostly located in eastern China (Fig. 13e). The E - P differences for jet days and no-jet days have a dipole arrangement: during jet days the moisture is transported north of locations where the core of the LLJ is located (blueish colours), while during no-jet days, moisture available for precipitation is localised to the south (greenish colours, Fig. 13f).

One of the most outstanding features of the Asian climate is the summer monsoon. The Somali low-level jet is an important component of the monsoonal Indian system, and it plays a crucial role in its temporal variability (Webster et al., 1998; Narayanan et al., 2016). In addition, the equatorial flows associated with the jet play a role in the advection of moisture towards the Indian subcontinent. In our work, we detected the continental fingerprint of this main flow, and this is the reason why three individual LLJs were reported. However, they

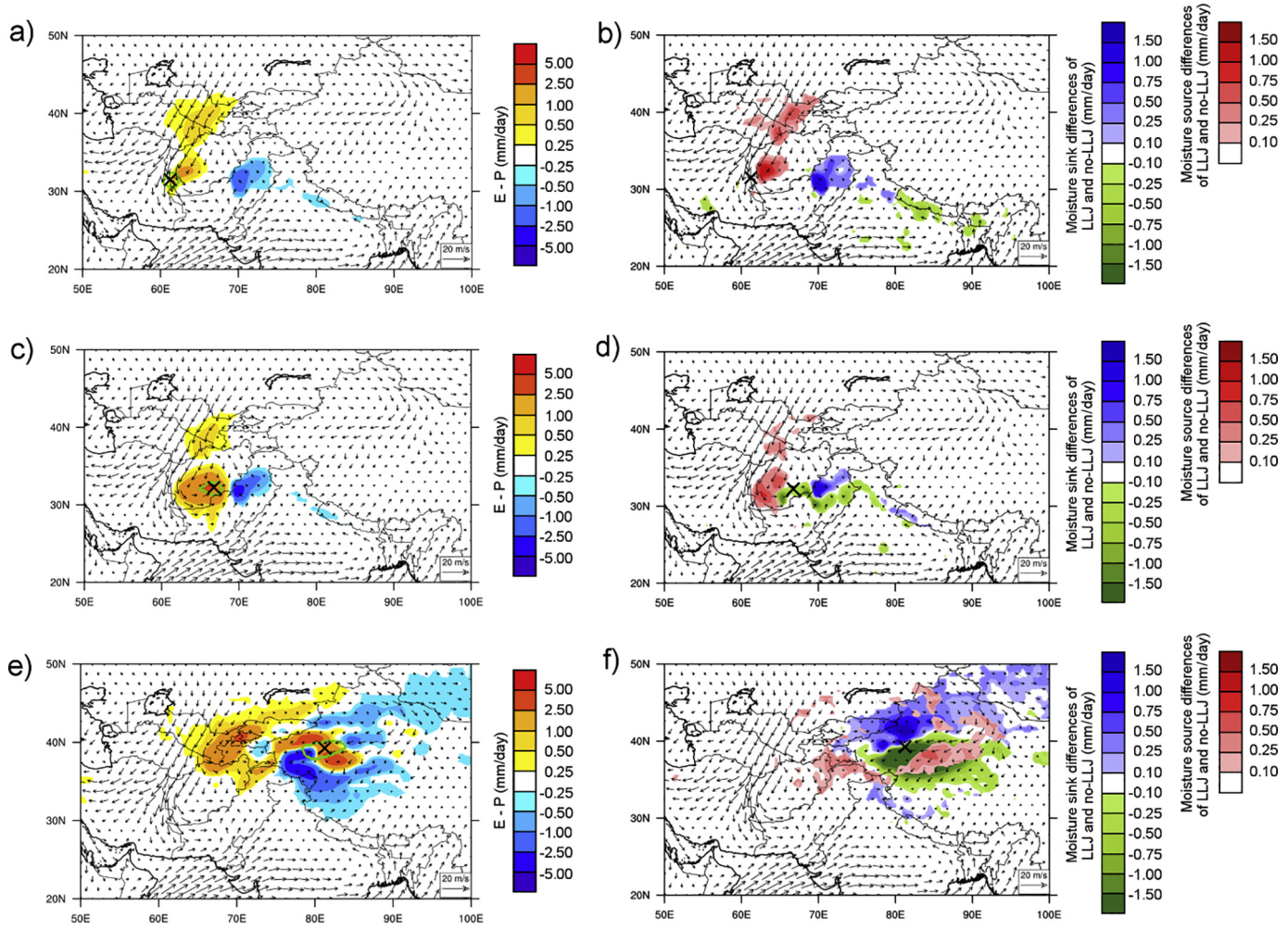

Fig. 13. As in Fig. 5 but for: (a, b) Afghanistan LLJ; (c, d) Pakistan LLJ; and (e, f) Tarim Pendi LLJ.

ultimately have the same structure, and Fig. 14 should be interpreted in this way. Two LLJs are detected over the east coast of Africa at two points and are named the Somali LLJ (site 14, Fig. 1) and the Gulf of Aden LLJ (site 9, Fig. 1), whereas the India Monsoon Low- Level Jet (IMLLJ; site 18, Fig. 1) over the Indian peninsula has the highest signal. The complete system of this LLJ uptakes moisture from the western Indian Ocean, which acts as the main source, and is transported by the LLJ parallel to the coast. The Arabian Sea also contributes to increasing the amount of moisture before it reaches the Indian and Thailand peninsulas and south-eastern Asia, which are the climatological moisture sinks (Fig. 14a, c, and e). A prominent pattern can be seen when the difference between jet days and no-jet days is shown: moisture for precipitation is transported far away to the east during jet days but is more restricted over the Indian subcontinent during no-jet days (Fig. 14f).

Further east over Asia, the China (site 19, Fig. 1) and Southeast Asian LLJ (site 20, Fig. 1) are detected; both are structures associated with monsoonal flows and both uptake moisture from the Arabian Sea and Bengal Bay and transport it to southeast China (Fig. 15a and c), although the China LLJ transports moisture for precipitation with greater intensity. During jet days, an increase in moisture uptake is observed in source regions, and intense associated precipitation occurs over eastern Asia, while during no-jet days, moisture for precipitation is concentrated over central Asia and the southern Asia region (blueish and greenish colours, respectively, in Fig. 15b and d).

Finally, the Australia LLJ fingerprint (site 33, Fig. 1) is detected in our study over the western-central region and is modified by, and strongly related to, the Asian monsoon during summer (Gu et al., 2010; May, 1995). It is associated with easterly winds and moisture uptake along the continent of Australia from the eastern part (including part of the Coral Sea) to the western coast. The climatological continental moisture sinks are located in the south of Australia (Fig. 16a). During jet days there is an intensification of local moisture uptake, including from the Great Australian Bight, and precipitation remains there. On the contrary, during no-jet days, the sink for precipitation moves eastward to the Tasman Sea and its influence reaches New Zealand (Fig. 16b).

4. Discussion and conclusions

A global distribution of nocturnal low-level jets (NLLJ) associated with warm seasons for both hemispheres is obtained in this work by employing a nocturnal index, based on the vertical distribution and time evolution of winds (Rife et al., 2010), and fed with ERA-Interim data from 1980 to 2016. A total of 33 NLLJ regions are identified and characterised: 20 in the northern hemisphere and 13 in the southern hemisphere. Some new NLLJs in the easternmost region of Brazil and the western region of Asia are documented here. With respect to the wind speed vertical profile, the jet core tends to be localised between sigma levels of 54–52, that is, close to surface; with the exception of the South American Low-Level Jet during austral winter, where the maximum winds are located close to 50 sigma level.

Not only does this work identify the central position of global LLJs, but it also provides the locations of main moisture sinks and sources

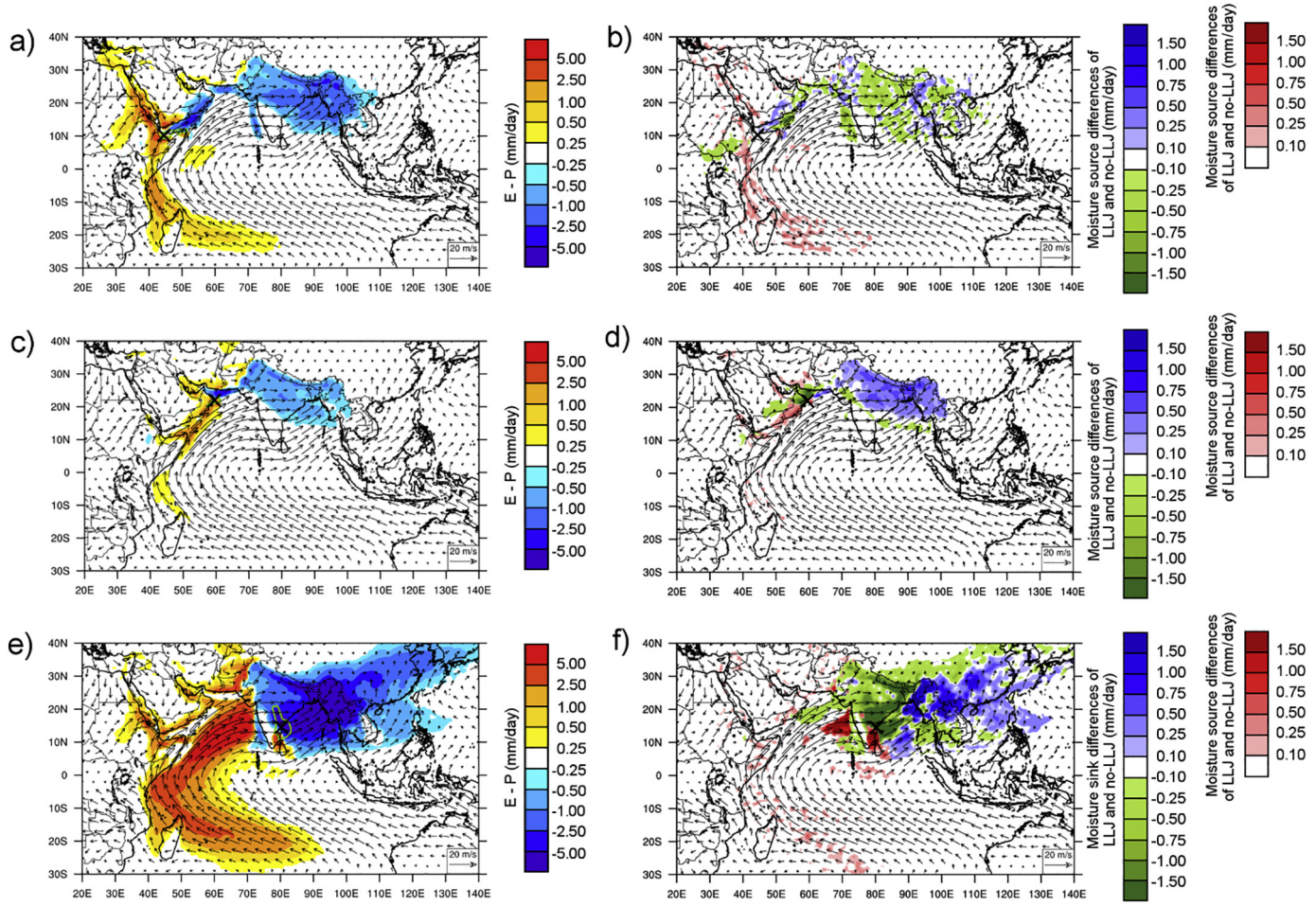

Fig. 14. As in Fig. 5 but for: (a, b) Gulf of Aden LLJ; (c, d) Somali LLJ; and (e, f) India Monsoon LLJ.

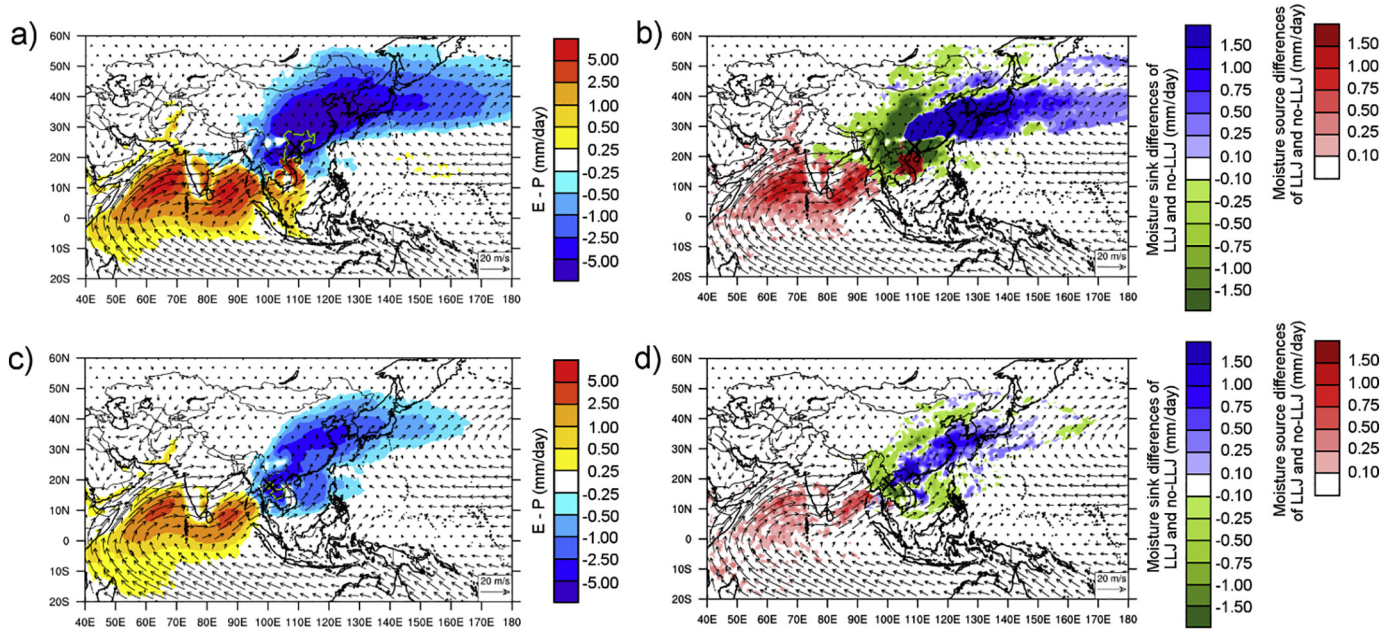

Fig. 15. As in Fig. 5 but for: (a, b) China Monsoon LLJ; and (c, d) India Monsoon LLJ.

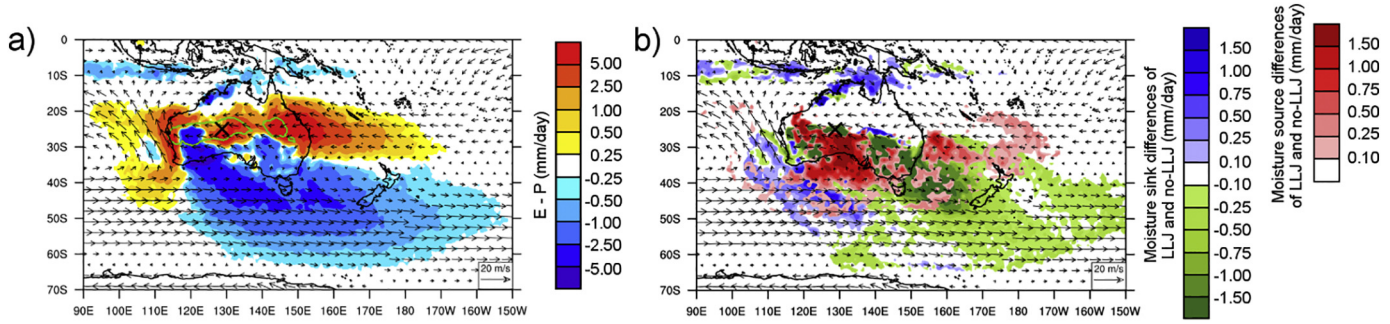

Fig. 16. As in Fig. 5 but for: (a, b) Australia LLJ.

associated with each LLJ as calculated by the Lagrangian model FLEXPART. These are discussed in the Results section. The cases of North and South America are particularly interesting. For instance, moisture transported by the GPLLJ plays a decisive role in the hydrological cycle of North America and is key to the generation of rainfall during the summer (Stensrud, 1996; Schubert et al., 1998). Some authors have identified the Caribbean Sea and the Gulf of Mexico as moisture sources for rainfall over the US (Brubaker et al., 2001; Bosilovich and Schubert, 2002). For instance, Helfand and Schubert (1995) estimated that at least one third of the moisture provided to the North American continent throughout May and June is transported by the GPLLJ. Algarra et al. (2019) quantified that > 80% of moisture transported by the GPLLJ originates from the Gulf of Mexico. The Lagrangian methodology used in this study objectively evidences the role of the Gulf of Mexico and the Caribbean Sea as sources of moisture for the GPLLJ, and the areas where associated precipitation occurs during jet days. Published works have already recognised that enhanced precipitation occurring over the north central United States and the Great Plains are associated with LLJ days and decreased precipitation over the Gulf of Mexico and East Coast (Higgins et al., 1996; Mo and Berbery, 2004). The nocturnal mesoscales convective systems play a key role over the Great Plains and are associated with increased night time precipitation (Pu et al., 2014); the maximum intensity of the GPLLJ during boreal summer enhances nocturnal precipitation over the Great Plains (25% more than during the day; Higgins et al., 1996).

The moisture transport in South America is highly modulated by several LLJs. The Caribbean Sea behaves as a regional moisture conveyor for the Caribbean LLJ, which modulates precipitation over Costa Rica and Nicaragua (Amador, 2008). However, the South American LLJ is the most relevant transport mechanism in this continent. The SALLJ is an easterly trade wind from the tropical North Atlantic Ocean that penetrates northern South America and is closely related to La Plata River Basin. When crossing the Amazon, the flow of wind decreases and the moisture content increases due to evaporative processes in the basin that play a key role in the contribution of moisture transported by the SALLJ. Lagrangian results show that during the wet season, the moisture is exported from the Amazon basin and transported via the SALLJ east of the Andes, thereby contributing to precipitation over southern Amazonia and the La Plata River Basin (as also explained in Marengo et al., 2004; and Drumond et al., 2014). The amount of atmospheric moisture transported by the SALLJ is comparable to the discharge of the Amazon River (Arraut et al., 2012). In addition, changes in land use (particularly deforestation, which affected the Amazon basin during the last few decades) are also altering the rate of evapotranspiration and affecting the water cycle (Zemp et al., 2014).

The reduction in regional moisture available from the tropical North Atlantic supply may have important consequences for the stability of the Amazonian rainforests and also for other southern regions that depend on the Amazon rainforest as a moisture source. It is necessary to point out that between 60% and 70% of the average annual precipitation in the La Plata River Basin derives from evapotranspiration occurring in the South American continent (Dirmeyer et al., 2007; van der Ent et al., 2010; Martinez et al., 2014). Local transpiration is as important as oceanic evaporation in this region: it is evident that if the wide Amazon basin receives significantly less precipitation and becomes drier than usual, extreme drought would potentially be induced in regions that depend on Amazonian moisture, such as the La Plata River Basin (e.g. Spracklen et al., 2012), which was determined by Lagrangian analysis as the climatological sink of moisture, and which would undergo changes in the precipitation pattern (whether associated with LLJ presence or not).

The climate of Africa is mainly dominated by the position of the Intertropical Convergence Zone (ITCZ) and the monsoonal regimes which strongly modulate the seasonality of rainfall. In Africa, low-level jet structures are common features in desert regions, where they are associated with mineral dust emissions and have an important control on the diurnal dust distribution variations (Heinold et al., 2013; Knippertz and Todd, 2012). To the east of central Africa, the Bodélé depression is widely known to be the main source of mineral dust emissions globally (Prospero et al., 2002; Washington and Tood, 2003), and numerous studies have studied the role of the Bodélé low-level jet and its relationship with the transport of mineral dust (Washington and Tood, 2005; Washington et al., 2006). Although the Mediterranean Sea basin and the Red Sea region have a significant influence on the moisture content available to the low-level jet located in the African continent, the moisture content transported by these structures is much lower than LLJs whose sources of moisture are located in oceanic regions in tropical latitudes. Despite the large amount of dust associated with it, the African Easterly Jet (AEJ) has a role in the transport of moisture and is associated with easterly winds. Furthermore, the Mediterranean Sea is a main source of moisture for jets located in northern Africa. It appears that the west African monsoon is not related to an LLJ structure.

In contrast, low-level jet structures are strongly associated with monsoon regimes in the Asia and Australia region and are key atmospheric structures for transporting moisture. In particular, the gulf of Bengal and the Indian Ocean behave as main sources of moisture for the India Monsoon LLJ, the Southeast Asia Monsoon LLJ, and the China Monsoon LLJ during the rainy season, and changes in the LLJ regime affect the precipitation pattern over the Asian continent.

It is crucial to understand the possible socioeconomic impacts of changes in LLJs, with respect to their role as atmospheric branches of the hydrological cycle (Sivapalan et al., 2012), and associated changes that could occur in precipitation over particular regions. It has been shown that LLJs are key in modulating precipitation patterns via sinks of moisture related to each jet. Such variables linked to rainfall are obviously affected by temporal changes, and can affect the water available for drinking, agriculture, or for ecosystems. New dimensions in hydrological studies show that, for instance, the heterogeneity of moisture recycling is affected according to each country's social characteristics (Keys and Wang-Erlandsson, 2018). To assist with socio-climatology exploration, we discuss each of the detected LLJs moisture

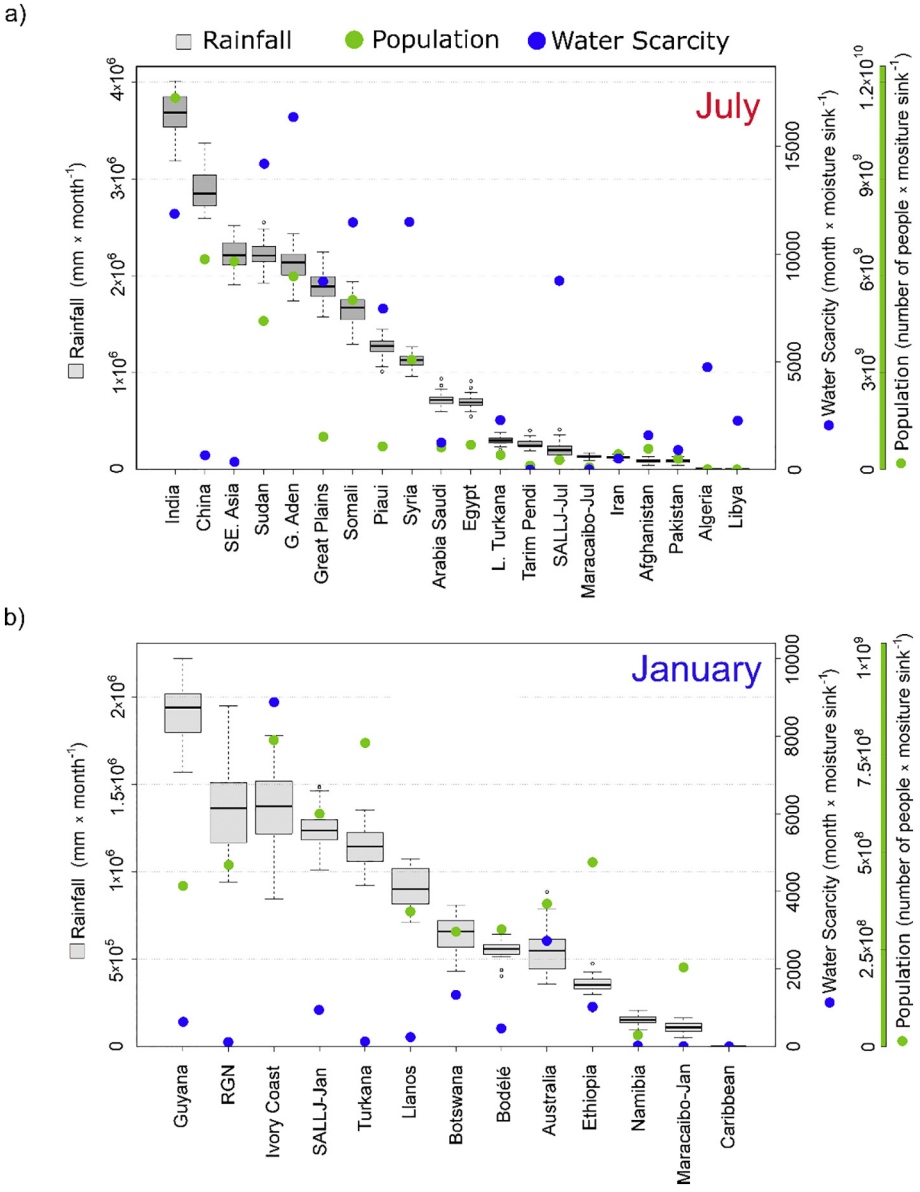

Fig. 17. Outline of socio-economic impacts for both July and January (a and b, respectively). Grey boxes show mean values together with minimum and maximum values of precipitation in 1980–2016 for each region involved (in mm/month). Green and blue dots represent the population and the water scarcity index, respectively.

sinks with respect to precipitation, and the information provided can be used to determine water scarcity (the lack of fresh water to meet water demands) in accordance with population density. It is essential to associate these structures with socioeconomic impacts to highlight the importance of these low-level jets. This is particularly important within the current context of climate change, in which an intensification of the LLJ events is foreseen. As previously commented, NLLJs tend to modulate the rainfall in regions where they occur, and changes in their intensity or frequency can have a direct impact in the availability of water resources. Some of these regions are characterised by great sensibility in terms of water resources, and consequently LLJs have an important socio-economic impact on the lives of local people. In addition, it is expected that LLJs will increase in frequency and intensity in the future (Cook et al., 2008; Harding and Snyder, 2014), and such mechanisms are thus expected to become more important.

LLJ are particularly important at hydroclimatic extremes due to their great ability to transport moisture. The intensification (in terms of wind intensity or frequency), absence, or changes in the LLJ occurrence position can trigger heavy floods or drought events causing severe socioeconomic impact. Sinks regions linked to LLJs are of special interest, as changes in the transport of moisture to these regions can have a great socioeconomic impact, especially in those regions that are most vulnerable in terms of water scarcity. Fig. 17 shows rainfall (grey boxes), population (green dots), and water scarcity (blue dots) calculated for moisture sinks associated with the LLJs presented in this work. Rainfall, population, and water scarcity datasets are calculated independently for each sink region associated with each LLJ.

Higher amounts of precipitation from LLJs are identified in the overpopulated regions of Asia under the influence of the monsoon regimes (areas affected by the Indian Monsoon LLJ, the China and the Southeast Asia LLJ), followed by regions with sinks located on the eastern coast of Africa. However, although the total number of people living in both areas is high, the amount of water available differs. It is the arid regions of north Africa and the Horn of Africa where water is scarcer, and this shows that a minimal change in the amount of precipitation (that has a direct bearing on freshwater availability) would have a knock-on effect.

This type of analysis can be used to assist politicians, economists, and social-agriculture developers in making smart choices with respect to water policies.

Overall, the results obtained here are in agreement with those of several previous studies. Even though different datasets have been used to identify the position of jets, differences in the frequency distribution or vertical profiles observed are negligible. By identifying the moisture sources and sinks for peak activity months of LLJs (the warm season) and including fingerprints for days both with and without jets, this work provides a unique and useful insight on a global scale. The identification of areas affected by precipitation (and its variability) associated with each LLJ can also be used in social-climatology analyses and when making hydrological decisions, as most main river basins throughout the world are rainfall sinks in this respect. However, such work would require an analysis of the entire annual cycle associated with each jet, and an exhaustive analysis of associated extreme drought and flood events. Although such features have been widely analysed for some relevant jets, such as the GPLLJ or the SALLJ, this is not the case for most of the jets, and as such will be the subject of future analyses.

Author contributions

RN and LG had the initial idea. IA carried out the calculations and data analysis. IA wrote the original draft, and IA and JEB reviewed the subsequent versions. RN, LG, IA, and JEB commented and reviewed the manuscript before submission.

Competing interests

The authors declare that they have no conflict of interest.

Acknowledgments

Iago Algarra was financially supported by the Spanish Government (MINECO, CGL2015-65141-R). Jorge Eiras-Barca was financially supported by the EDB481B 2018/069 grant from the Xunta de Galicia, Spain and the Fulbright Commission, US. This work is part of the LAGRIMA project funded by Ministerio de Ciencia, Innovación y Universidades, Spain. This work was also partially supported by Xunta de Galicia, Spain under Project ED431C 2017/64-GRC “Programa de Consolidación e Estructuración de Unidades de Investigación Competitivas (Grupos de Referencia Competitiva)”.

Appendix A. Supplementary data

Supplementary data to this article can be found online at https://doi.org/10.1016/j.atmosres.2019.06.016.

References

Algarra, I., Eiras-Barca, J., Miguez-Macho, G., Nieto, R., Gimeno, L., 2019. On the assessment of the moisture transport by the Great Plains low-level jet. Earth Syst. Dynam. 10, 107–119. https://doi.org/10.5194/esd-10-107-2019.

Alizadeh-Choobari, O., Zawar-Reza, P., Sturman, A., 2014. The “wind of 120days” and dust storm activity over the Sistan Basin. Atmos. Res. 143, 328–341. https://doi.org/10.1016/j.atmosres.2014.02.001.

Allen, C.J.T., Washington, R., 2014. The low-level jet dust emission mechanism in the Central Sahara: Observations from Bordj-Badji Mokhtar during the June 2011 Fennec Intensive Observation Period. J. Geophys. Res. Atmos. 119, 2990–3015. https://doi.org/10.1002/2013JD020594.

Amador, J.A., 2008. The Intra-Americas Sea low-level jet: Overview and future research. Ann. N. Y. Acad. Sci. 1146, 153–188. https://doi.org/10.1196/annals.1446.012.

Arraut, J.M., Nobre, C., Barbosa, H.M.J., Obregon, G., Marengo, J., Arraut, J.M., Nobre, C., Barbosa, H.M.J., Obregon, G., Marengo, J., 2012. Aerial Rivers and Lakes: looking at Large-Scale Moisture Transport and its Relation to Amazonia and to Subtropical Rainfall in South America. J. Clim. 25, 543–556. https://doi.org/10.1175/2011JCLI4189.1.

Beck, H.E., Van Dijk, A.I.J.M., Levizzani, V., Schellekens, J., Miralles, D.G., Martens, B., De Roo, A., 2017. MSWEP: 3-hourly 0.25° global gridded precipitation (1979-2015) by merging gauge, satellite, and reanalysis data. Hydrol. Earth Syst. Science 21, 589–615. https://doi.org/10.5194/hess-21-589-2017.

Blackadar, A.K., 1957. Boundary layer wind maxima and their significance for the growth of nocturnal inversions. Bull. Amer. Meteor. Soc. 38, 283–290.

Bonner, W.D., 1968. Climatology of the low level jet. Mon. Weather Rev. 96, 833–850. https://doi.org/10.1175/1520-0493(1968)096<0833:COTLLJ>2.0.CO;2.

Bosilovich, M.G., Schubert, S.D., 2002. Water Vapor Tracers as Diagnostics of the Regional Hydrologic Cycle. J. Hydrometeorol. 3, 149–165. https://doi.org/10.1175/1525-7541(2002)003<0149:WVTADO>2.0.CO;2.

Brubaker, K.L., Dirmeyer, P.A., Sudradjat, A., Levy, B.S., Bernal, F., Brubaker, K.L., Dirmeyer, P.A., Sudradjat, A., Levy, B.S., Bernal, F., 2001. A 36-yr climatological description of the evaporative sources of warm-season precipitation in the Mississippi River Basin. J. Hydrometeorol. 2, 537–557. https://doi.org/10.1175/1525-7541(2001)002<0537:AYCDOT>2.0.CO;2.

Chen, B., De Xu, X., Zhao, T.L., 2017. Quantifying oceanic moisture exports to mainland China in association with summer precipitation. Clim. Dyn. 51, 1–16. https://doi.org/10.1007/s00382-017-3925-1.

Cook, K.H., Vizy, E.K., 2010. Hydrodynamics of the Caribbean low-level jet and its relationship to precipitation. J. Clim. 23, 1477–1494. https://doi.org/10.1175/2009JCLI3210.1.

Cook, C., Reason, C., Hewitson, B., 2004. Wet and dry spells within particularly wet and dry summers in the south African summer rainfall region. Clim. Res. 26, 17–31. https://doi.org/10.3354/cr026017.

Cook, K.H., Vizy, E.K., Launer, Z.S., Patricola, C.M., 2008. Springtime intensification of the great plains low-level jet and midwest precipitation in GCM Simulations of the twenty-first century. J. Clim. 21, 6321–6340. https://doi.org/10.1175/2008JCLI2355.1.

Dee, D.P., Uppala, S.M., Simmons, A.J., Berrisford, P., Poli, P., Kobayashi, S., Andrae, U., Balmaseda, M.A., Balsamo, G., Bauer, P., Bechtold, P., Beljaars, A.C.M., van de Berg, L., Bidlot, J., Bormann, N., Delsol, C., Dragani, R., Fuentes, M., Geer, A.J., Haimberger, L., Healy, S.B., Hersbach, H., Hólm, E.V., Isaksen, L., Kållberg, P., Köhler, M., Matricardi, M., McNally, A.P., Monge-Sanz, B.M., Morcrette, J.-J., Park, B.-K., Peubey, C., de Rosnay, P., Tavolato, C., Thépaut, J.-N., Vitart, F., 2011. The ERA-Interim reanalysis: configuration and performance of the data assimilation system. Q. J. R. Meteorol. Soc. 137, 553–597. https://doi.org/10.1002/qj.828.

Dirmeyer, P.A., Brubaker, K.L., Dirmeyer, P.A., Brubaker, K.L., 2007. Characterization of the global hydrologic cycle from a back-trajectory analysis of atmospheric water vapor. J. Hydrometeorol. 8, 20–37. https://doi.org/10.1175/JHM557.1.

Drumond, A., Nieto, R., Trigo, R., Ambrizzi, T., Souza, E., Gimeno, L., 2010. A lagrangian identification of the main sources of moisture affecting northeastern Brazil during its pre-rainy and rainy seasons. PLoS One 5, 1–8. https://doi.org/10.1371/journal.pone.0011205.

Drumond, A., Marengo, J., Ambrizzi, T., Nieto, R., Moreira, L., Gimeno, L., 2014. The role of the Amazon Basin moisture in the atmospheric branch of the hydrological cycle: a Lagrangian analysis. Hydrol. Earth Syst. Sci. 18, 2577–2598. https://doi.org/10.5194/hess-18-2577-2014.

van der Ent, R.J., Savenije, H.H.G., Schaefli, B., Steele-Dunne, S.C., 2010. Origin and fate of atmospheric moisture over continents. Water Resour. Res. 46. https://doi.org/10.1029/2010WR009127.

Fiedler, S., Schepanski, K., Heinold, B., Knippertz, P., Tegen, I., 2013. Climatology of nocturnal low-level jets over North Africa and implications for modeling mineral dust emission. J. Geophys. Res. Atmos. 118, 6100–6121. https://doi.org/10.1002/jgrd.50394.

Giannakopoulou, E.M., Toumi, R., 2012. The Persian Gulf summertime low-level jet over sloping terrain. Q. J. R. Meteorol. Soc. 138, 145–157. https://doi.org/10.1002/qj.901.

Gimeno, L., Drumond, A., Nieto, R., Trigo, R.M., Stohl, A., 2010. On the origin of continental precipitation. Geophys. Res. Lett. 37https://doi.org/10.1029/2010GL043712. n/a-n/a.

Gimeno, L., Stohl, A., Trigo, R.M., Dominguez, F., Yoshimura, K., Yu, L., Drumond, A., Durán-Quesada, A.M., Nieto, R., 2012. Oceanic and terrestrial sources of continental precipitation. Rev. Geophys. 50, RG4003. https://doi.org/10.1029/2012RG000389.

Gimeno, L., Nieto, R., Drumond, A., Castillo, R., Trigo, R., 2013. Influence of the intensification of the major oceanic moisture sources on continental precipitation. Geophys. Res. Lett. 40, 1443–1450. https://doi.org/10.1002/grl.50338.

Gimeno, L., Dominguez, F., Nieto, R., Trigo, R., Drumond, A., Reason, C.J.C., Taschetto, A.S., Ramos, A.M., Kumar, R., Marengo, J., 2016. Major Mechanisms of Atmospheric Moisture Transport and their Role in Extreme Precipitation events. Annu. Rev. Environ. Resour. https://doi.org/10.1146/annurev-environ-110615-085558.

Govinda Rao, P., Hatwar, H.R., Al-Sulaiti, Mohammed Hassan, Al-Mulla, Ali Hamid, 2003. Summer shamals over the Arabian Gulf. Weather 58, 466–471. https://doi.org/10.1002/wea.6080581206.

Gu, D., Li, T., Ji, Z., Zheng, B., 2010. On the phase relations between the western North Pacific, Indian, and Australian monsoons. J. Clim. 23, 5572–5589. https://doi.org/10.1175/2010JCLI2761.1.

Harding, K.J., Snyder, P.K., 2014. Examining future changes in the character of central u.S. warm-season precipitation using dynamical downscaling. J. Geophys. Res. 119, 13,113–116,136. https://doi.org/10.1002/2014JD022575.

Heinold, B., Knippertz, P., Marsham, J.H., Fiedler, S., Dixon, N.S., Schepanski, K., Laurent, B., Tegen, I., 2013. The role of deep convection and nocturnal low-level jets for dust emission in summertime West Africa: Estimates from convection-permitting simulations. J. Geophys. Res. Atmos. 118 (10), 4385–4400. https://doi.org/10.1002/jgrd.50402.

Helfand, H.M., Schubert, S.D., 1995. Climatology of the simulated Great Plains low-level jet and its contribution to the continental moisture budget of the United States. J. Clim. https://doi.org/10.1175/1520-0442(1995)008<0784:COTSGP>2.0.CO;2.

Higgins, R.W., Mo, K.C., Schubert, S.D., 1996. The moisture budget of the central United

States in spring as evaluated in the NCEP/NCAR and the NASA/DAO reanalyses. Mon. Weather Rev. 124, 939–963. https://doi.org/10.1175/1520-0493(1996)124<0939:TMBOTC>2.0.CO;2.
Higgins, R.W., Yao, Y., Wang, X.L., 1997a. Influence of the North American monsoon system on the U.S. summer precipitation regime. J. Clim. 10, 2600–2622. https://doi.org/10.1175/1520-0442(1997)010<2600:IOTNAM>2.0.CO;2.
Higgins, R.W., Yao, Y., Yarosh, E.S., Janowiak, J.E., Mo, K.C., 1997b. Influence of the great plains low-level jet on summertime precipitation and moisture transport over the Central United States. J. Clim. 10, 481–507. https://doi.org/10.1175/1520-0442(1997)010<0481:IOTGPL>2.0.CO;2.
Holton, J.R., 1967. The diurnal boundary layer wind oscillation above sloping terrain. Tellus 19, 200–205. https://doi.org/10.3402/tellusa.v19i2.9766.
Hu, Q., Jiang, D., Lang, X., Xu, B., 2018. Moisture sources of the Chinese Loess Plateau during 1979–2009. Palaeogeogr. Palaeoclimatol. Palaeoecol. 509, 156–163. https://doi.org/10.1016/j.palaeo.2016.12.030.
Jiang, X., Lau, N.-C., Klein, S.A., 2006. Role of eastward propagating convection systems in the diurnal cycle and seasonal mean of summertime rainfall over the U.S. Great Plains. Geophys. Res. Lett. 33. https://doi.org/10.1029/2006GL027022.
Jiang, X., Lau, N.-C., Held, I.M., Ploshay, J.J., 2007. Mechanisms of the Great Plains Low-Level Jet as simulated in an AGCM. J. Atmos. Sci. 64, 532–547. https://doi.org/10.1175/JAS3847.1.
Keys, P.W., Wang-Erlandsson, L., 2018. On the social dynamics of moisture recycling. Earth Syst. Dyn. 9, 829–847. https://doi.org/10.5194/esd-9-829-2018.
Knippertz, P., Todd, M.C., 2012. Mineral dust aerosols over the Sahara: Meteorological controls on emission and transport and implications for modeling. Rev. Geophys. 50. https://doi.org/10.1029/2011RG000362.
Marengo, J.A., 2002. The South American low-level jet east of the Andes during the 1999 LBA-TRMM and LBA-WET AMC campaign. J. Geophys. Res. 107, 8079. https://doi.org/10.1029/2001JD001188.
Marengo, J.A., Espinoza, J.C., 2016. Extreme seasonal droughts and floods in Amazonia: Causes, trends and impacts. Int. J. Climatol. 36, 1033–1050. https://doi.org/10.1002/joc.4420.
Marengo, J.A., Soares, W.R., Saulo, C., Nicolini, M., Marengo, J.A., Soares, W.R., Saulo, C., Nicolini, M., 2004. Climatology of the low-level jet east of the Andes as derived from the NCEP–NCAR reanalyses: characteristics and temporal variability. J. Clim. 17, 2261–2280. https://doi.org/10.1175/1520-0442(2004)017<2261:COTLJE>2.0.CO;2.
Martinez, J.A., Dominguez, F., Martinez, J.A., Dominguez, F., 2014. Sources of atmospheric moisture for the La Plata River Basin*. J. Clim. 27, 6737–6753. https://doi.org/10.1175/JCLI-D-14-00022.1.
May, P.T., 1995. The Australian nocturnal jet and diurnal variations of boundary-layer winds over Mt. Isa in North-eastern Australia. Q. J. R. Meteorol. Soc. 121, 987–1003. https://doi.org/10.1002/qj.49712152503.
Mekonnen, M.M., Hoekstra, Y.A., 2016. Four billion people experience water scarcity. Sci. Adv. 2, 1–7. https://doi.org/10.1126/sciadv.1500323.
Mo, K.C., Berbery, E.H., 2004. Low-level jets and the summer precipitation regimes over North America. J. Geophys. Res. D Atmos. 109 (D06117), 1–18.
Monaghan, A.J., Rife, D.L., Pinto, J.O., Davis, C.A., Hannan, J.R., 2010. Global precipitation extremes associated with diurnally varying low-level jets. J. Clim. 23, 5065–5084. https://doi.org/10.1175/2010JCLI3515.1.
Montini, T.L., Jones, C., Carvalho, L.M.V., 2019. The South American Low-Level Jet: a New Climatology, Variability, and changes. J. Geophys. Res. Atmos. https://doi.org/10.1029/2018JD029634.
Muñoz, E., Busalacchi, A.J., Nigam, S., Ruiz-Barradas, A., 2008. Winter and summer structure of the Caribbean low-level jet. J. Clim. 21, 1260–1276. https://doi.org/10.1175/2007JCLI1855.1.
Narayanan, S., Kottayil, A., Mohanakumar, K., 2016. Monsoon low-level jet over the gateway of Indian summer monsoon: a comparative study for two distinct monsoon years. Meteorog. Atmos. Phys. 128, 689–696. https://doi.org/10.1007/s00703-016-0459-8.
Nicholson, S.E., 2010. A low-level jet along the Benguela coast, an integral part of the Benguela current ecosystem. Clim. Chang. 99, 613–624. https://doi.org/10.1007/s10584-009-9678-z.
Nicholson, S., 2016. The Turkana low-level jet: mean climatology and association with regional aridity. Int. J. Climatol. 36, 2598–2614. https://doi.org/10.1002/joc.4515.
Nieto, R., Gimeno, L., Trigo, R.M., 2006. A Lagrangian identification of major sources of Sahel moisture. Geophys. Res. Lett. 33, 1–6. https://doi.org/10.1029/2006GL027232.
Nieto, R., Gallego, D., Trigo, R., Ribera, P., Gimeno, L., 2008. Dynamic identification of moisture sources in the Orinoco basin in equatorial South America. Hydrol. Sci. J. 53, 602–617. https://doi.org/10.1623/hysj.53.3.602.
Nieto, R., Vázquez, M., Algarra, I., Gimeno, L., 2016. An analysis of the water cycle in the Sahel through a Lagrangian perspective. In: Proc. 1st Int. Electron. Conf. Atmos. Sci, pp. D004. https://doi.org/10.3390/ecas2016-D004.
Numaguti, A., 1999. Origin and recycling processes of precipitating water over the Eurasian continent: experiments using an atmospheric general circulation model. J. Geophys. Res.-Atmos. 104, 1957–1972. https://doi.org/10.1029/1998JD200026.
Oliveira, M.I., Nascimento, E.L., Kannenberg, C., 2018. A new look at the identification of low-level Jets in South America. Mon. Weather Rev. 146, 2315–2334. https://doi.org/10.1175/MWR-D-17-0237.1.
Pan, Z., Segal, M., Arritt, R.W., 2004. Role of topography in forcing low-level Jets in the central united states during the 1993 flood-altered terrain simulations. Mon. Weather Rev. 132, 396–403. https://doi.org/10.1175/1520-0493(2004)132<0396:ROTIFL>2.0.CO;2.
Parish, T.R., Clark, R.D., 2017. On the initiation of the 20 June 2015 Great Plains low-level jet. J. Appl. Meteorol. Climatol. 56 (7), 1883–1895.
Parish, T.R., Clark, R.D., 2017. On the forcing of the summertime great plains low-level jet. J. Atmos. Sci. 74, 3937–3953. https://doi.org/10.1175/JAS-D-17-0059.1.
Parish, T.R., Oolman, L.D., 2010. On the Role of Sloping Terrain in the Forcing of the Great Plains Low-Level Jet. J. Atmos. Sci. 67, 2690–2699. https://doi.org/10.1175/2010JAS3368.1.
Patricola, C.M., Chang, P., 2017. Structure and dynamics of the Benguela low-level coastal jet. Clim. Dyn. 49, 2765–2788. https://doi.org/10.1007/s00382-016-3479-7.
Poveda, G., Jaramillo, L., Vallejo, L.F., 2014. Seasonal precipitation patterns along pathways of South American low-level jets and aerial rivers. Water Resour. Res. 50, 98–118. https://doi.org/10.1002/2013WR014087.
Pu, B., Dickinson, R.E., 2014. Diurnal Spatial Variability of Great Plains Summer Precipitation Related to the Dynamics of the Low-Level Jet. J. Atmos. Sci. 71 (5), 1807–1817. https://doi.org/10.1175/JAS-D-13-0243.1.
Prospero, J.M., Ginoux, P., Torres, O., Nicholson, S.E., Gill, T.E., 2002. Environmental characterization of global sources of atmospheric soil dust identified with the Nimbus 7 Total Ozone Mapping Spectrometer (TOMS) absorbing aerosol product. Rev. Geophys. 40 (1), 1–31. https://doi.org/10.1029/2000RG000095.
Ramos, A.M., Nieto, R., Tomé, R., Gimeno, L., Trigo, R.M., Liberato, M.L.R., Lavers, D.A., 2016. Atmospheric rivers moisture sources from a Lagrangian perspective. Earth Syst. Dyn. 7, 371–384. https://doi.org/10.5194/esd-7-371-2016.
Rife, D.L., Pinto, J.O., Monaghan, A.J., Davis, C.A., Hannan, J.R., 2010. Global distribution and characteristics of diurnally varying low-level jets. J. Clim. 23, 5041–5064. https://doi.org/10.1175/2010JCLI3514.1.
Salih, A.A.M., Zhang, Q., Tjernström, M., 2015. Lagrangian tracing of Sahelian Sudan moisture sources. J. Geophys. Res. Atmos. 120, 6793–6808. https://doi.org/10.1002/2015JD023238.
Salio, P., Nicolini, M., Saulo, A.C., 2002. Chaco low-level jet events characterization during the austral summer season. J. Geophys. Res. 107, 4816. https://doi.org/10.1029/2001JD001315.
Saulo, A.C., Nicolini, M., Chou, S.C., 2000. Model characterization of the South American low-level flow during the 1997-1998 spring-summer season. Clim. Dyn. 16, 867–881. https://doi.org/10.1007/s003820000085.
Savenije, H.H.G., 1995. New definitions for moisture recycling and the relationship with land-use changes in the Sahel. J. Hydrol. 167, 57–78. https://doi.org/10.1016/0022-1694(94)02632-L.
Schepanski, K., Heinold, B., Tegen, I., 2017. Harmattan, Saharan heat low, and West African monsoon circulation: Modulations on the Saharan dust outflow towards the North Atlantic. Atmos. Chem. Phys. 17, 10223–10243. https://doi.org/10.5194/acp-17-10223-2017.
Schubert, S.D., Helfand, H.M., Wu, C.Y., Min, W., 1998. Subseasonal variations in warm-season moisture transport and precipitation over the central and eastern United States. J. Clim. 11, 2530–2555. https://doi.org/10.1175/1520-0442(1998)011<2530:SVIWSM>2.0.CO;2.
Shapiro, A., Fedorovich, E., Rahimi, S., 2016. A Unified Theory for the Great Plains Nocturnal Low-Level Jet. J. Atmos. Sci. 73, 3037–3057. https://doi.org/10.1175/JAS-D-15-0307.1.
Sivapalan, M., Savenije, H.H.G., Blöschl, G., 2012. Socio-hydrology: a new science of people and water. Hydrol. Process. 26, 1270–1276. https://doi.org/10.1002/hyp.8426.
Sodemann, H., Stohl, A., 2009. Asymmetries in the moisture origin of Antarctic precipitation. Geophys. Res. Lett. 36, 1–5. https://doi.org/10.1029/2009GL040242.
Sodemann, H., Schwierz, C., Wernli, H., 2008. Interannual variability of Greenland winter precipitation sources: Lagrangian moisture diagnostic and North Atlantic Oscillation influence. J. Geophys. Res. Atmos. 113, 1–17. https://doi.org/10.1029/2007JD008503.
Spracklen, D.V., Arnold, S.R., Taylor, C.M., 2012. Observations of increased tropical rainfall preceded by air passage over forests. Nature 489, 282–285. https://doi.org/10.1038/nature11390.
Stensrud, D.J., 1996. Importance of low-level jets to climate: a review. J. Clim. 9, 1698–1711. https://doi.org/10.1175/1520-0442(1996)009<1698:IOLLJT>2.0.CO;2.
Stohl, A., James, P., Stohl, A., James, P., 2004. A lagrangian analysis of the atmospheric branch of the global water Cycle. Part I: method description, validation, and demonstration for the August 2002 flooding in central Europe. J. Hydrometeorol. 5, 656–678. https://doi.org/10.1175/1525-7541(2004)005<0656:ALAOTA>2.0.CO;2.
Stohl, A., James, P., 2005. A Lagrangian Analysis of the Atmospheric Branch of the Global Water Cycle. Part II: Moisture Transports between Earth's Ocean Basins and River Catchments.
Stohl, A., Forster, C., Frank, A., Seibert, P., Wotawa, G., 2005. Technical note: the Lagrangian particle dispersion model FLEXPART version 6.2. Atmos. Chem. Phys. 5, 2461–2474. https://doi.org/10.5194/acp-5-2461-2005.
Ting, M., Wang, H., 2006. The Role of the north American Topography on the Maintenance of the Great Plains Summer Low-Level Jet*. J. Atmos. Sci. 63, 1056–1068. https://doi.org/10.1175/JAS3664.1.
Vera, C., Baez, J., Douglas, M., Emmanuel, C.B., Marengo, J., Meitin, J., Nicolini, M., Nogues-Paegle, J., Paegle, J., Penalba, O., Salio, P., Saulo, C., Silva Dias, M.A., Dias, P.S., Zipser, E., Vera, C., Baez, J., Douglas, M., Emmanuel, C.B., Marengo, J., Meitin, J., Nicolini, M., Nogues-Paegle, J., Paegle, J., Penalba, O., Salio, P., Saulo, C., Dias, M.A.S., Dias, P.S., Zipser, E., 2006. The south american low-level jet experiment. Bull. Am. Meteorol. Soc. 87, 63–78. https://doi.org/10.1175/BAMS-87-1-63.
Wang, B., Liu, J., Kim, H.-J., Webster, P.J., Yim, S.-Y., 2012. Recent change of the global monsoon precipitation (1979–2008). Clim. Dyn. 39, 1123–1135. https://doi.org/10.1007/s00382-011-1266-z.
Washington, R., Todd, M.C., 2005. Atmospheric controls on mineral dust emission from the Bodele Depression, Chad: The role of the low level jet. Geophys. Res. Lett. 32

(17), 1–5.
Washington, R., Todd, M., Goudie, A., Middleton, N., 2003. Global dust storm source areas determined by the total ozone monitoring spectrometer and ground observations. Ann. Assoc. Am. Geogr. 93 (2), 297–313. https://doi.org/10.1111/1467-8306.9302003.
Washington, R., Todd, M.C., Lizcano, G., Tegen, I., Flamant, C., Koren, I., Ginoux, P., Engelstaedter, S., Bristow, C.S., Zender, C.S., Goudie, A.S., Warren, A., Prospero, J.M., 2006. Links between topography, wind, deflation, lakes and dust: The case of the Bodélé Depression, Chad, Geophys. Res. Lett. 33 (9), 1–4. https://doi.org/10.1029/2006GL025827.
Webster, P.J., Magaña, V.O., Palmer, T.N., Shukla, J., Tomas, R.A., Yanai, M., Yasunari, T., 1998. Monsoons: processes, predictability, and the prospects for prediction. J. Geophys. Res. Ocean. 103, 14451–14510. https://doi.org/10.1029/97JC02719.
Wexler, H., 1961. A Boundary Layer Interpretation of the Low-level Jet. Tellus 13, 368–378. https://doi.org/10.1111/j.2153-3490.1961.tb00098.x.
Whiteman, C.D., Bian, X., Zhong, S., 1997. Low-Level Jet Climatology from Enhanced Rawinsonde Observations at a Site in the Southern Great Plains. J. Appl. Meteorol. 36, 1363–1376. https://doi.org/10.1175/1520-0450(1997)036<1363:LLJCFE>2.0.CO;2.
Xavier, A., Kottayil, A., Mohanakumar, K., Xavier, P.K., 2018. The role of monsoon low-level jet in modulating heavy rainfall events. Int. J. Climatol. 38, e569–e576. https://doi.org/10.1002/joc.5390.
Zemp, D.C., Schleussner, C.F., Barbosa, H.M.J., Van Der Ent, R.J., Donges, J.F., Heinke, J., Sampaio, G., Rammig, A., 2014. On the importance of cascading moisture recycling in South America. Atmos. Chem. Phys. 14, 13337–13359. https://doi.org/10.5194/acp-14-13337-2014.

Atmospheric Research 234 (2020) 104733

Contents lists available at ScienceDirect

Atmospheric Research

journal homepage: www.elsevier.com/locate/atmosres

Corrigendum

Corrigendum to "Global climatology of nocturnal low-level jets and associated moisture sources and sinks" [Atmospheric Research (2019) 39–59]

Iago Algarra[a,*], Jorge Eiras-Barca[a,b], Raquel Nieto[a], Luis Gimeno[a]

[a] EPhysLab (Environmental Physics Laboratory), CIM-UVigo, Universidade de Vigo, Ourense, Spain
[b] Department of Atmospheric Sciences, University of Illinois at Urbana-Champaign, Urbana, IL, United States

The authors regret that the caption of Fig. 5 appeared wrongly in the paper. The correct caption is provided below:

Fig. 5. a) Mean climatology of the (E - P) field for regions surrounded by a green contour (75th percentile of the NLLJ index value) for July 1980–2016. Blueish colours indicate regions where (E - P) $<$ 0 in the forward simulation and are considered to be moisture sinks (i.e., the precipitation is larger than the evaporation), whereas reddish colours indicate regions where (E - P) $>$ 0 in the backward simulation, are considered to be moisture sources (i.e., the evaporation is larger than precipitation). The black cross indicates the point of maximum NLLJ intensity. The vectors relate to wind climatology for July (1980–2016) at the surface level near the maximum LLJ intensity level. b) Differences between the (E - P) field during jet days and the (E - P) field on non-jet days. Blueish and greenish colours indicate positive and negative differences, respectively, for sinks of moisture; in blue colour are regions more active as moisture sinks on jet days while in green colour are regions that are more active as moisture sinks on non-jet days. Reddish colours indicate a positive difference for the source of moisture; in red colour are regions that are more active as moisture source on jet days compared to non-jet days. In this case, vectors refer to the wind climatology only for those jet days, and are plotted for the surface level. (For interpretation of the references to colour in this figure legend, the reader is referred to the web version of this article).

The authors would like to apologise for any inconvenience caused.

DOI of original article: https://doi.org/10.1016/j.atmosres.2019.06.016
* Corresponding author.
E-mail address: ialgarra@uvigo.es (I. Algarra).

https://doi.org/10.1016/j.atmosres.2019.104733

Available online 06 November 2019

Earth Syst. Dynam., 10, 107–119, 2019
https://doi.org/10.5194/esd-10-107-2019

Earth System Dynamics
Open Access
EGU

On the assessment of the moisture transport by the Great Plains low-level jet

Iago Algarra[1], Jorge Eiras-Barca[1], Gonzalo Miguez-Macho[2], Raquel Nieto[1], and Luis Gimeno[1]

[1]EPhysLab (Environmental Physics Laboratory), Facultade de Ciencias, Universidade de Vigo, Ourense, Galicia, Spain
[2]Non-Linear Physics Group, Universidade de Santiago de Compostela, Santiago de Compostela, Galicia, Spain

Correspondence: Iago Algarra (ialgarra@uvigo.es)

Received: 16 October 2018 – Discussion started: 29 October 2018
Revised: 23 January 2019 – Accepted: 28 January 2019 – Published: 18 February 2019

Abstract. Low-level jets (LLJs) can be defined as wind corridors of anomalously high wind speed values located within the first kilometre of the troposphere. These structures are one of the major meteorological systems in the meridional transport of moisture on a global scale. In this work, we focus on the southerly Great Plains low-level jet, which plays an important role in the moisture transport balance over the central United States. The Gulf of Mexico is the main moisture source for the Great Plains low-level jet (GPLLJ), which has been identified as a key factor for rainfall modulation over the eastern and central US.

The relationship between moisture transport from the Gulf of Mexico to the Great Plains and precipitation has been well documented in previous studies. Nevertheless, a large uncertainty still remains in the quantification of the moisture amount actually carried by the GPLLJ. The main goal of this work is to address this question. For this purpose, a relatively new tool, the regional atmospheric Weather Research and Forecasting Model with 3-D water vapour tracers (WRF-WVT; Insua-Costa and Miguez-Macho, 2018) is used together with the Lagrangian model FLEXPART to estimate the load of precipitable water advected within the GPLLJ. Both models were fed with data from ERA Interim. From a climatology of jet intensity over a 37-year period, which follows a Gaussian distribution, we select five cases for study, representing the mean and 1 and 2 standard deviations above and below it. Results show that the jet is responsible for roughly 70 %–80 % of the moisture transport occurring in the southern Great Plains when a jet event occurs. Furthermore, moisture transport by the GPLLJ extends to the north-east US, accounting for 50 % of the total in areas near the Great Lakes. Vertical distributions show the maximum of moisture advected by the GPLLJ at surface levels and maximum values of moisture flux about 500 m above, in coincidence with the wind speed profile.

1 Introduction

It is well known that the Great Plains low-level jet (hereafter, GPLLJ) plays an important role in the balance of the moisture transport over the central United States (Stensrud, 1996; Schubert et al., 1998). The atmospheric moisture is transported by the GPLLJ from tropical and subtropical latitudes (particularly the Gulf of Mexico and the Caribbean Sea) into the Great Plains (Helfand and Schubert, 1995; Mo et al., 1997), where the jet is often responsible for nocturnal deep convective activity (Higgins et al., 1997; Pu et al., 2016). In the last decades, a large number of authors have shown the strong influence of the GPLLJ as a modulator of climate and rainfall over this region and even further east (Mo et al., 1995, 1997; Wu and Raman, 1998; Byerle and Paegle, 2003); for instance, throughout May and June it is estimated that at least one-third of the moisture penetrating into the continental US is carried by the GPLLJ (Helfand and Schubert, 1995).

Among the mechanisms which have been proposed as triggers of the GPLLJ are included a combination of inertial oscillations (Blackadar, 1957) and orographic forcing (Wexler, 1961; Byerle and Paegle, 2003; Pan et al.,

2004; Ting and Wang, 2006). In particular, the mechanism of Blackadar (1957) suggests that inertial oscillations near the friction layer can induce the formation of the GPLLJ (Wu and Raman, 1998). Nevertheless, orographic effects are also understood as a key factor in the maintenance of the GPLLJ. In this regard, Ting and Wang (2006) proved that, when the interaction with the orography is removed from numerical simulations, the GPLLJ vanishes, together with an important amount of the summer precipitation over the central and southerly US.

The GPLLJ is a phenomenon confined within the first kilometres of the troposphere and is closely related to the warm season (Bonner, 1968). Moreover, it is characterised by a strong diurnal oscillation, with a peak in strength during night hours (Augustine and Caracena, 1994). A long-term climatology of GPLLJ can be found in the work of Walters et al. (2008). The GPLLJ is a phenomenon extremely localised in time and space, and its role in the continental moisture balance is difficult to study solely from observations.

Nevertheless, a large number of studies have documented the relationship between the major moisture transport and the GPLLJ. Higgins et al. (1996) studied the moisture budget over the central US in May employing NASA/DAO and NCEP/NCAR datasets, together with station observations, to evaluate the limitations of these products. Although both reanalyses overestimate daily mean precipitation rates, they accurately capture the basic temporal and structural characteristics of the GPLLJ. From the data, these authors calculated an increase in atmospheric moisture transport from the Gulf of Mexico during night-time of more than 50 %. In a later work, Higgins et al. (1997) observed a well-defined nocturnal maximum of precipitation over the Great Plains in spring and summer by analysing station data. Linked to low-level jet (LLJ) events, they particularly found an excess of 25 % in the region in nocturnal rainfall during summer when compared with the diurnal precipitation, associated with a rainfall decrease over the Gulf of Mexico. Additionally, Higgins et al. (1997) reported significant differences in precipitation pattern in coincidence (or not) with LLJ events. When an LLJ event occurs, the observations show an enhanced precipitation over the north-central United States and the Great Plains region, together with a decrease along the Gulf of Mexico and the western Atlantic. On the other hand, Mo and Juang (2003) found regional correlation at a distance between evaporation and precipitation, reflected in evaporation anomalies over the Great Plains along the trajectory of the GPLLJ, which are associated with downstream precipitation anomalies.

Otherwise, extreme rainfall events in the central US are related to an increase in moisture convergence downwind of the GPLLJ (Mo et al., 1997). A decisive factor that triggers heavy rains and floods is the presence of moisture advected by the GPLLJ from the Gulf of Mexico and the Caribbean Sea. Moore et al. (2012) reported the physical processes related to the floods in May 2010, when a persistent southerly LLJ associated with an atmospheric river (AR) enhanced the transport of moisture from the Gulf of Mexico into the heavy rainfall region. Thus, important socioeconomic impacts follow enhanced GPLLJ events, which modulates a large percentage of the local extreme precipitation events and flooding in warmer months (Mo et al., 1995, 1997; Beljaars et al., 1996; Trenberth and Guillemot, 1996; Arritt et al., 1997; Nakamura et al., 2013; Nayak et al., 2016). All these results are consistent with the large-scale atmospheric moisture transport and support the marked influence of the GPLLJ over the central-eastern US, which has been shown to trigger more than 60 % of the spring local precipitation over the Great Plains region (Wang and Chen, 2009).

During the last decades, the GPLLJ has experienced a strengthening, accompanied by a northward migration causing a displacement of rainfall in the same direction. As a result, more frequent droughts have been observed in the southern Great Plains (Barandiaran et al., 2013). Moreover, an increase in the number and intensity of GPLLJ events is also forecasted for future projections, which reveal an intensification of the GPLLJ during the spring season associated with global warming (Cook et al., 2008; Tang et al., 2017). As a result, increasing amounts of moisture transport and rainfall are expected, particularly from April to July, over the central US (Harding and Snyder, 2014). The same projections forecast a slight weakening of the GPLLJ from August to December, which could translate into increasing drought conditions.

The knowledge about the GPLLJ, together with the insights on the relationship between the moisture transported by the GPLLJ and local precipitation patterns, has increased considerably during the last decades. However, there are still unanswered questions about the quantification of such water vapour transport and especially about the estimation of the ratio of land to oceanic moisture sources associated with the GPLLJ. This estimate of the oceanic input to the moisture transport associated with the GPLLJ is essential to predict and understand the behaviour of the GPLLJ in future scenarios.

In this work, a new tool, the regional atmospheric Weather Research and Forecasting Model with 3-D water vapour tracer diagnostics (WRF-WVT, Insua-Costa and Miguez-Macho, 2017), is used to quantify the total amount of total precipitable water (TPW) transported by the GPLLJ. To show the differences between the transport of moisture on jet and non-jet days, a 37-year climatology of maximum jet intensity is obtained following the methodology of Rife et al. (2010). The structure of this work is as follows: in Sect. 2 we provide the methodology used, in Sect. 3 we show the results obtained, and finally in Sect. 4 we discuss the conclusions.

2 Data and methods

2.1 Detection of the Great Plains low-level jet

To objectively detect days with LLJ over the Great Plains, we applied the night-time index proposed in Rife et al. (2010), hereafter named NLLJ. This index is based on the temporal variation in the wind's vertical structure and the fact that LLJs are most intense at local midnight. Because both the frequency and intensity of GPLLJ are mostly associated with the warm season, we develop a 37-year climatology for the month of July (representative of the boreal summer). According to the NLLJs characteristics, and with the aim to define the index, two conditions should be met to consider a GPLLJ detection:

1. The wind speed is higher at local midnight than at midday.
2. The local midnight wind speed is higher at the surface (~ 500 m) than above it (~ 4 km).

The index is calculated at each grid point over an area centred over the US using 6-hourly ERA-Interim reanalysis data (Dee et al., 2011) with a 0.25° horizontal resolution. Because the jet core is located within of the first kilometre of the troposphere, it is necessary to take into account the elevation of the land, so sigma coordinates are used. The GPLLJ-climatology is developed for 37 years, from 1980 to 2016, and the NLLJ index can be defined as follows:

$$\mathrm{NLLJ} = \lambda\varphi\sqrt{\left[\left(u_{00}^{\mathrm{L1}} - u_{00}^{\mathrm{L2}}\right) - \left(u_{12}^{\mathrm{L1}} - u_{12}^{\mathrm{L2}}\right)\right]^2 + \left[\left(v_{00}^{\mathrm{L1}} - v_{00}^{\mathrm{L2}}\right) - \left(v_{12}^{\mathrm{L1}} - v_{12}^{\mathrm{L2}}\right)\right]^2}, \quad (1)$$

where u and v are the zonal and meridional wind components, respectively. L1 represents the winds at the surface at the 53 sigma level (elevation near the jet core), approximately 500 m above ground level (a.g.l.), while L2 corresponds to the wind at the 42 sigma level (around 4000 m a.g.l.). Numbers 00 and 12 refer to local midnight and local noon, respectively. λ and φ are binary multipliers representing the temporal and vertical variation in the wind. In particular, λ relates to the daily variation in the wind at 500 m, and φ refers to the wind's vertical variation between 500 m and 4 km at midnight (Rife et al., 2010):

$$\lambda = \begin{cases} 0, \mathrm{ws}_{00}^{\mathrm{L1}} \leq \mathrm{ws}_{12}^{\mathrm{L1}} \\ 1, \mathrm{ws}_{00}^{\mathrm{L1}} > \mathrm{ws}_{12}^{\mathrm{L1}}, \end{cases} \quad (2)$$

$$\varphi = \begin{cases} 0, \mathrm{ws}_{00}^{\mathrm{L1}} \leq \mathrm{ws}_{00}^{\mathrm{L2}} \\ 1, \mathrm{ws}_{00}^{\mathrm{L1}} > \mathrm{ws}_{00}^{\mathrm{L2}}. \end{cases} \quad (3)$$

2.2 Identification of moisture sources associated with the Great Plains low-level jet

For the objective identification of moisture sources associated with the GPLLJ, the Lagrangian backward trajectories from the FLEXPART v9.0 model are used (Stohl et al., 2005a). This model provides a large number of air parcel trajectories from which it is possible to calculate the evaporation minus precipitation budget, tracking all changes in the specific humidity of air parcels.

FLEXPART has been widely and successfully used to track moisture paths for the study of the atmospheric branch of the hydrologic cycle in different parts of the world (e.g. Vázquez et al., 2016; Hu et al., 2018; Sorí et al., 2018). Furthermore, this tool is able to infer the moisture sources for precipitation falling in a target region when backward trajectories are considered (e.g. Stohl et al., 2008; Drumond et al., 2010; Gimeno et al., 2012; Wegmann et al., 2015; Ramos et al., 2016).

In this work we use the outputs of a global experiment in which FLEXPART v9.0 tracks approximately 2 million particles (air parcels) with constant mass distributed on the globe every time step during a 37-year period (1980–2016). These air parcels are advected by the 3-D wind field, and the variables of interest of each particle (position, height, specific humidity and temperature among many others) are saved at each time step. We perform a FLEXPART simulation fed with ERA-Interim reanalysis data at a $1° \times 1°$ horizontal resolution on 61 vertical levels from sea level hPa and 6 h time intervals (00:00, 06:00, 12:00 and 18:00 UTC). The model is run with a 3 h time step, and linear interpolation is used to obtain data with this frequency from ERA-Interim. The backward trajectories are followed for 10 days, which is the average lifetime of water vapour in the atmosphere (Numaguti, 1999).

The changes in specific humidity (q) of each air parcel along its path can be expressed as follows:

$$e - p = m\frac{\mathrm{d}p}{\mathrm{d}t}, \quad (4)$$

where m is the mass of a particle (which remains constant in the simulation), q is the specific humidity, t the time step and $e - p$ (evaporation minus precipitation) represents the water flux associated with the particle. To obtain the instantaneous values of the $E - P$ balance (E denotes evaporation and P the precipitation rate per unit area) in a given area (in this case, over one of $1° \times 1°$ in latitude and longitude), it is necessary to integrate the moisture changes for all particles present in the atmospheric column over such an area (Stohl and James, 2004, 2005b). Thus, following this methodology, in a backward experiment, a moisture source is defined as those regions where $E - P$ is positive $(E - P) > 0$, which implies that evaporation exceeds precipitation, while a moisture sink is defined as a region where $(E - P) < 0$, meaning that precipitation is greater than evaporation.

In our study, backward trajectories were followed from the area composed of points with values of the NLLJ above the 75th percentile to find the main moisture source.

2.3 The regional atmospheric Weather Research and Forecasting Model with 3-D water vapour tracer diagnostics

The mesoscale WRF-WVT (Miguez-Macho et al., 2013; Insua-Costa and Miguez-Macho, 2018) is used to quantify the amount of total precipitable water (TPW) transported by the GPLLJ. In order to analyse the moisture transport associated with the GPLLJ avoiding the effects of other synoptic-scale transport events, we tag the moisture passing northward through a narrow wall located on the northern edge of the moisture source region identified using the FLEXPART model. When a particle of water (whether in liquid, solid or gas state) crosses the wall, it is labelled for further analysis inside the simulation domain. We consider all water traversing the wall to be advected by the GPLLJ.

The horizontal resolution of the simulations is 20 km, and the vertical column is divided into 38 levels. The simulation covers a time window of 11 days, starting 7 days prior to the day of interest. The model parameterisations together with the WRF-WVT are set using the planetary boundary layer (PBL) Yonssei University (YSU) parameterisation (Hu et al., 2013; Shin and Hong, 2011), the Kain–Fritsch schemes for convection (Kain, 2004), the Dudhia one for short-wave radiation (Dudhia, 1989), the Rapid Radiative Transfer Model (RRTM) scheme for long-wave radiation (Mlawer et al., 1997), and the WRF Single-Moment 6-Class Microphysics Scheme (WSM6) (Hong and Lim, 2006).

In addition, we apply spectral nudging of waves longer than 1000 km above the boundary layer, with a relaxation time of 1 h, to avoid the distortion of the large-scale circulation. This configuration has been validated and successfully applied several times with the WRF-WVT in midlatitudes (e.g. Eiras-Barca et al., 2017). Spectral nudging ensures that the large-scale circulation is well captured in the simulations. ERA-Interim data provide lateral boundary and initial conditions for the runs (Dee et al., 2011). The variables of interest for the analysis of the GPLLJ event are computed as follows. Integrated water vapour (IWV), Eq. (5) is obtained by vertical integration of the specific humidity (q) in pressure (p) levels, where g represents the gravitational force. The instant flux of moisture (σ) is calculated as stated in Eq. (6), and the conversion between g and the water vapour mixing ratio obtained from WRF is performed using Eq. (7), where u and v are the horizontal components of the wind field.

$$\mathrm{IWV}_{(i,j)} = \frac{1}{g(k)} \int_{\text{surface}}^{\text{top}} q\,(i,j,k)\,\mathrm{d}p, \tag{5}$$

$$\sigma(i,j,k) = |q \cdot (u,v)|\,, \tag{6}$$

$$q = \frac{w}{w+1}, \text{ with } w \ll 1 \rightarrow q \approx w. \tag{7}$$

Table 1. Case studies objectively selected based on the frequency distribution of the NLLJ index to carry out WRF-WVT simulations. μ is the mean of the distribution and σ its standard deviation. Note: the frequency distribution is calculated at the point of maximum intensity of the NLLJ at 32.75° N, 99° W (black cross in Fig. 1a) using the ERA-Interim reanalysis dataset.

Simulation	Gaussian	NLLJ value	Date	Stat. weight
0		0.00	12 July 2012	0
1	$\mu - 2\sigma$	1.49	19 July 1999	0.0623
2	$\mu - \sigma$	5.54	23 July 1983	0.2445
3	μ	10.19	11 July 1992	0.3864
4	$\mu + \sigma$	14.54	28 July 2002	0.2445
5	$\mu + 2\sigma$	18.89	14 July 2016	0.0623

3 Results

3.1 Characterisation of the Great Plains low-level jet

As previously mentioned, the NLLJ index was calculated at each grid point over the North American region for the month of July over the period 1980–2016. July was found to be the month with maximum LLJ events (Fig. S1 in the Supplement shows the monthly distribution of the GPLLJ days of detection). Figure 1a shows the climatological NLLJ index and the wind field at 500 hPa. The black cross indicates the point of maximum intensity of the index (8.8 m s^{-1}). At this point, located at 32.75° N, 99° W, along the 37-year analysed and for July a total of 931 LLJ days are identified; that is, 81 % of all days have a positive value of the index. At the point of maximum intensity shown in Fig. 1a, Fig. 1b displays the frequency distribution of the NLLJ for the period 1980–2016. A clear peak around 11 m s^{-1} is observed together with Gaussian behaviour (Jarque–Bera test p value = 0.0055, which provides a confidence level close to 99.5 %; red line). The latter has been used to select the five case studies to be analysed with WRF-WVT and listed in Table 1. The five case studies were selected based on the Gaussian adjustment applied to the study. These five events correspond to μ, $\mu \pm 2\sigma$ and $\mu \pm \sigma$ (where μ is the mean of the distribution and σ its standard deviation), and they provide a general perspective of the LLJ's behaviour. Selecting these case studies from the population of LLJ events decreases the computational expense. Since each case study WRF-WVT simulation spans 11 days, a condition of persistence of the index value for at least 2 days after the main jet day is applied. Additionally, we perform a sixth simulation with a non-jet day (simulation 0 in the Table 1). This non-jet day is selected from the developed climatology as the longest non-jet period, in order to avoid overlaps in moisture transport with jet days.

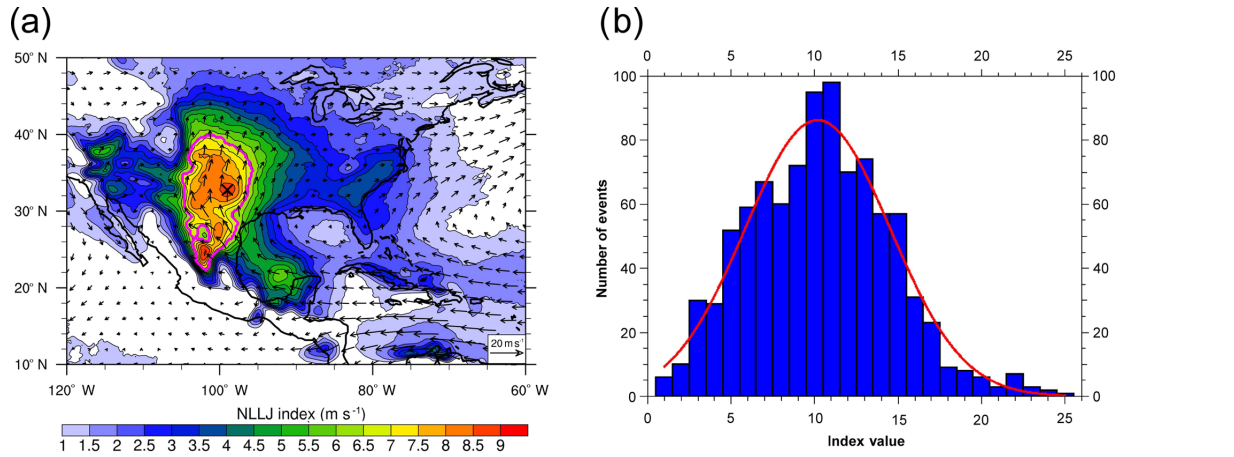

Figure 1. **(a)** Mean NLLJ index (shaded) and 500 m winds (arrows, in m s^{-1}) at local midnight in July (boreal summer) for 1980–2016, calculated from ERA-Interim reanalysis. The black cross at 32.75° N, 99° W shows the point of maximum NLLJ in the climatology. The magenta contour line surrounds the region containing points above the 75th percentile. **(b)** Frequency distributions of the GPLLJ for the months of July from 1980 to 2016 (blue bars). The red curve corresponds to the Gaussian fit (see Table A2). Note: the frequency distributions are calculated at the point of maximum intensity of the NLLJ (at 32.75° N, 99° W; black cross in **a**).

3.2 Moisture transport associated with the Great Plains low-level jet

In order to detect the main climatological oceanic source of moisture for the GPLLJ, we used the FLEXPART trajectories outputs for 1980–2016. The area encompassed in the 75th percentile of the NLLJ index values (magenta line in Fig. 1a) was selected as the target region for the backward experiment (as explained in the methodology). Figure 2 shows the source of moisture in red colour, obtained as the 75th percentile of the $(E-P>0)$ field. This area covers the southern Gulf of Mexico and extends into the Caribbean Sea, between 60–98° W and 12–28° N. Figure S2 in the Supplement shows the individual sources of moisture for each case in study.

Although the flow originating in the source of moisture is advected at low levels as a result of the strong intensity of the trade winds, a 3-D-label wall (at 29–30° N and from 94.5 to 100° W) was used in the WRF-WVT simulations (orange line in Fig. 2). The position of the sentinel wall was selected in the region where oceanic moisture associated with the GPLLJ makes landfall. The wall remained constant in the WRF-WVT simulations. The thin wall was used instead of the entire source regions in order to avoid overlaps in the labelling of moisture caused by secondary, synoptic-scale mechanisms.

Figure 3 shows the ratio of precipitable water transported by the GPLLJ to total precipitable water ($TPW_{tracers} = TPW$) for the six case studies analysed. As mentioned earlier, $TPW_{tracers}$ represents the TPW that has crossed the "wall" highlighted in orange in Fig. 2, which we assume corresponds to moisture advected by the GPLLJ. Following the same behaviour of the GPLLJ itself, the moisture flux is initially in the northward direction and veers east as it penetrates into the Great Plains for all events with positive NLLJ

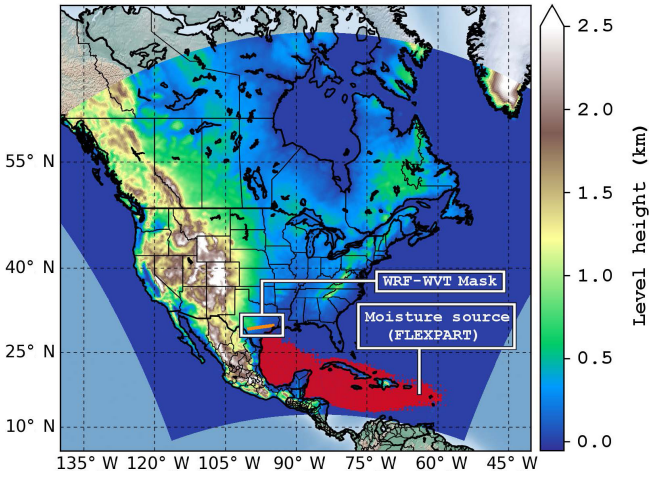

Figure 2. Highlighted in red are moisture sources obtained with FLEXPART from backward trajectories originating in the region outlined in magenta in Fig. 1a. The orange line over the continent marks the position from where precipitable water is tagged in WRF-WVT, corresponding to the northern edge of the FLEXPART source region. All water vapour and condensate crossing through that line is considered as moisture advected by the GPLLJ for further analysis.

index values. As expected, the non-jet event with an NLLJ value equal to zero (Sim 0) does not show significant moisture fluxes. For the jet events, ratios are close to 1 in regions near the tagging wall and extend for hundreds of kilometres northward, with significant values above 60 %. Percentages between 70 % and 80 % are observed in the Great Plains. The large geographical reach of the moisture associated with the GPLLJ is evidenced in this figure, showing that for certain

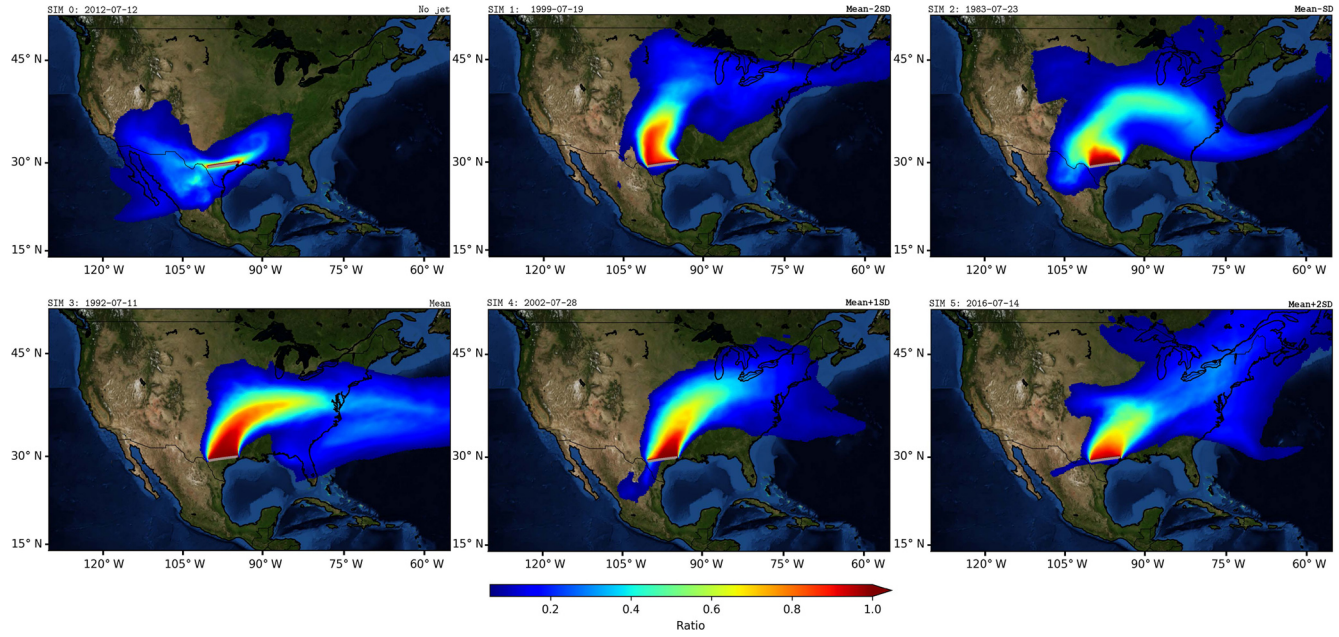

Figure 3. Ratio of tagged precipitable water transported by the GPLLJ to total for the six case studies analysed.

GPLLJ events, it can occasionally explain more than 50 % of TPW even in the north-east US. It is necessary to highlight that higher values in the index do not necessarily mean larger flows of moisture, as can be observed, for example, when Sim 3 and Sim 5 are compared. Figure S3 in the Supplement shows a comparison of accumulated precipitation at 11 days of WRF simulations versus Climate Prediction Center (CPC) gauge-analysis observations (Chen et al., 2008).

As previously stated, the aim of this work is to study the general behaviour of the GPLLJ associated with its moisture transport. In the first simulated case of GPLLJ (Fig. 3 – Sim 1) it is observed that most of the precipitable water is concentrated on the Great Plains, exceeding ratios of 80 % out of the total. In the second GPLLJ event simulated (Fig. 3 – Sim 2), the precipitable water extends north-east of the US and to the south of the Great Lakes and the GPLLJ, where it explains close to the 50 % of precipitable water. The third simulated case corresponds to the average behaviour of the GPLLJ (Fig. 3 – Sim 3) and shows the influence of the GPLLJ in the north-east of the US with ratios near 50 % on the US east coast. Nevertheless, in areas along the path of the GPLLJ, the advection of precipitable water is close to 80 %. In the fourth and fifth simulations of GPLLJ (Fig. 3 – Sim 4 and 5), the plume of precipitable water is concentrated over the Great Plains. However, the water precipitable ratio is reduced as latitude increases, but values are still close to 50 % in the north-eastern areas of the US.

Figure 4 shows the statistically weighted mean of the ratio shown in Fig. 3 for the five case studies with NLLJ > 0 considered in the analysis. The weights associated with each event are stated in the last column of Table 1, and the objective criteria to assign them can be found in Appendix A1. The aim of using weights in the analysis is to give greater importance to the event representing the mean value of the NLLJ and less relevance to the events in the tail of the distribution. Notwithstanding the limited number of simulations used in the analysis, this procedure allows us to interpret Fig. 4 as a "climatology" of the moisture transport associated with the GPLLJ. Roughly 80 %–90 % of the precipitable water in its core zone of influence over the Great Plains, in Texas and Oklahoma, is carried by the GPLLJ when a jet event occurs.

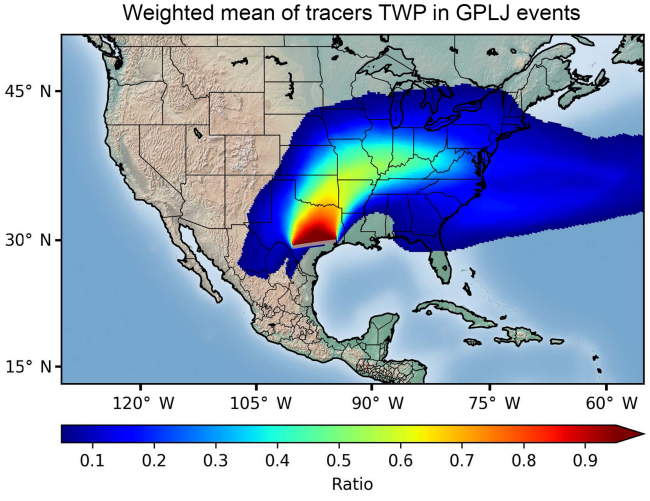

Figure 4. Statistically weighted ratio of precipitable water transported by the GPLLJ for the five case studies with NLLJ > 0 considered in the analysis in Fig. 3. Weights applied are stated in Table 1.

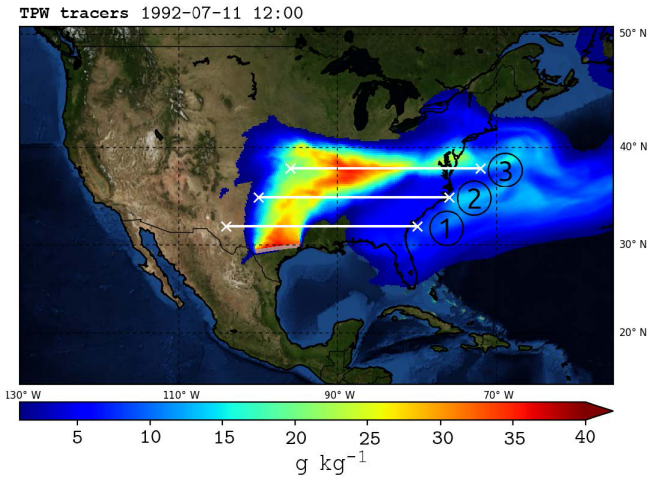

Figure 5. Tracer total precipitable water (TPW, g kg^{-1}) and positions of the cross sections along the central axis of the GPLLJ shown in Figs. 6 and 7, at latitudes 32° N (1), 35° N (2) and 38° N (3) for the main jet event of 11 July 1992.

With increased distance from that area, the ratio of precipitable water transported by the GPLLJ decreases; however, the contribution of moisture from the Gulf of Mexico to TPW is still more than 50 % as far north as the Great Lakes.

Figure 5 shows the TPW and the cross sections for the main GPLLJ event (11 July 1992). Figure 6 shows the vertical distribution of tracer-specific humidity (q_{TR}) and tracer water vapour flux (φ_{TR}) for cross sections at positions depicted in Fig. 5. Tracer moisture (Fig. 6a–c) has a maximum at surface levels, while the moisture flux (Fig. 6d–f) maximises at 500 m a.g.l. where the LLJ core is located. A significant presence of both tracer water vapour and tracer water vapour flux is restricted to the first 2 km a.g.l. Overall, as the latitude increases the water vapour plume from the Gulf of Mexico tends to rise in the vertical column and expand zonally along the GPLLJ path to the east of the US. Equivalent conclusions can be obtained from the remaining events, which are shown in the Supplement (Figs. S4–S7 in the Supplement). Figure 7 shows the water vapour ratio $q_{TR} : q$ for the vertical sections of Fig. 5 for the same event. The moisture pattern behaviour is similar to Fig. 6; for regions close to the Gulf of Mexico the moisture ratio is concentrated mostly at lower levels (Fig. 7a) and extends on the horizontal axis as it moves away from the source of moisture (Fig. 7b). Nevertheless, for remote regions the maximum moisture ratio continues at lower levels (Fig. 7c). The moisture flow has the same pattern: high moisture ratios that remain at low levels despite longitudinal distance (Fig. 7d–f). These results confirm that the GPLLJ transports a great concentrated quantity of moisture.

4 Conclusions and discussions

A combination of Lagrangian and Eulerian methods was used to identify and objectively quantify the moisture transport associated with the GPLLJ. First, the FLEXPART Langrangian model was used to locate the GPLLJ moisture sources for the month of its maximum activity (July) throughout the period 1980–2016. The target region used in the FLEXPART simulation to find the main source of moisture was defined based on the 75th percentile of the GPLLJ index value previously calculated based on the Rife et al. (2010) method. Once the Gulf of Mexico was identified as the main source of moisture ($E - P > 0$) for the GPLLJ, we use a new tool known as Eulerian 3-D WRF-WVT (Insua-Costa and Miguez-Macho, 2018), which was applied to track the moisture advected in six selected GPLLJ events based on the distribution of the GPLLJ index used previously to detect the GPLLJ (Rife et al., 2010). Consequently, this work analysed the behaviour of the GPLLJ during the month of its maximum activity (July) for the period 1980–2016, and we select six representative cases for the WRF-WVT simulation.

The moisture transport analysis reveals the major role played by the GPLLJ in the water cycle of central North America, transporting large amounts of moisture from the Gulf of Mexico as far as the north-east US. In particular, advection by the jet explains more than 80 % of the precipitable water in the southern Great Plains when a jet event occurs, which, in July, is most of the days. The Rocky Mountains block the circulation of GPLLJ and force it to turn to the east of the US, reaching even the eastern coast of the US. The moisture transport associated with the GPLLJ is in a plume of moisture, where the maximum transport occurs in the path of the GPLLJ. As expected, the ratio reduces as latitude increases, but values are still close to 50 % in the north-eastern areas of the US.

We note that the extension of the GPLLJ is dependent on the synoptic conditions or land preconditioning, among other factors, which may alter the ratio of the TPW. For example, the presence of a well-developed high-pressure system at higher latitudes of North America may block the advection of the GPLLJ moisture to this region. Dong et al. (2011) related the drought of 2006 with an anomalous high over the south-western US region and an anomalous low over the Great Lakes. This pattern inhibited the advection of moisture from the Gulf of Mexico, contributing to the extreme dryness, and the lack precipitation was associated with a suppressed cyclonic activity over the south-western US. On the other hand, the 2007 flood events were initially preceded by active synoptic weather patterns, linked to an active moisture transport from the Gulf of Mexico by the GPLLJ. Nevertheless, the analysis of these multiple factors is beyond the scope of this paper.

Higher values in the NLLJ index mean larger differences between winds aloft and at the surface at the reference point, but they do not necessarily mean stronger moisture transport.

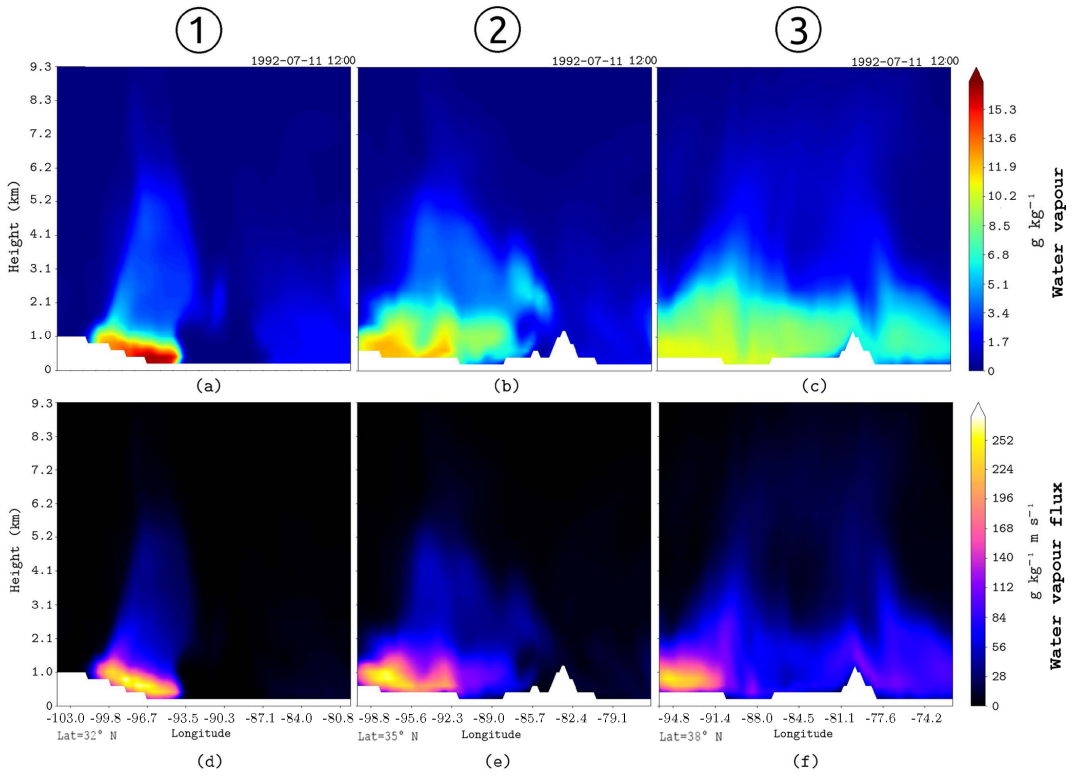

Figure 6. **(a–c)** q_{TR} in g kg^{-1} for the three vertical cross sections at the locations depicted by white lines in Fig. 5. Panels **(d–f)** same as **(a–c)** but for φ_{TR} in g m (kg s)$^{-1}$.

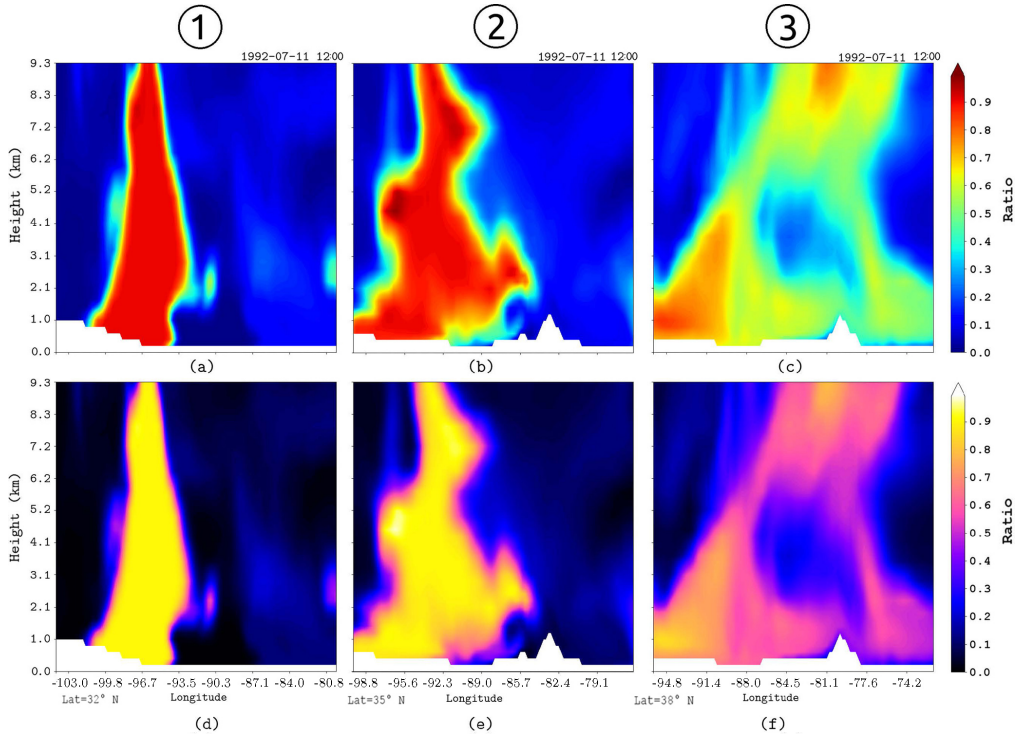

Figure 7. **(a–c)** Ratio of $q_{TR} : q$ for the three vertical cross sections at the locations depicted by white lines in Fig. 5. Panels **(d–f)** same as **(a–c)** but for a ratio of phi$_{TR}$: phi.

These results should be understood as a first approach to the quantification of the large extent of GPLLJ moisture advection and its implications for the water budget in North America. More simulations should be conducted, and other months should be included in FLEXPART backward calculations to extend this work and produce a more comprehensive analysis.

Data availability. No public data are derived from this research. For further information on the WRF-WVT tool, please contact the corresponding author.

Appendix A

Table A1. Statistical weights in the analysis: events.

Simulation	Gaussian point
1	$\mu - 2\sigma$
2	$\mu - \sigma$
3	μ
4	$\mu + \sigma$
5	$\mu + 2\sigma$

Table A2. Gaussian fit $y(x) = y_0 + A \cdot \exp(-\frac{(x-y)^2}{2\sigma^2})$.

Simulation	Gaussian point
y_0	0.03 ± 3.66
A	8.63 ± 4.39
μ	10.19 ± 0.19
σ	4.35 ± 0.30
R^2	0.95

$$\mathrm{StatWeight}_1 = \mathrm{StatWeight}_5 = \frac{\int_{\mu-2.5\sigma}^{\mu-1.5\sigma} y(x)\,\mathrm{d}x}{\int_{\mu-2.5\sigma}^{\mu+2.5\sigma} y(x)\mathrm{d}x} = 0.0623,$$

$$\mathrm{StatWeight}_2 = \mathrm{StatWeight}_4 = \frac{\int_{\mu-1.5\sigma}^{\mu-0.5\sigma} y(x)\,\mathrm{d}x}{\int_{\mu-2.5\sigma}^{\mu+2.5\sigma} y(x)\mathrm{d}x} = 0.2446,$$

$$\mathrm{StatWeight}_3 = \frac{\int_{\mu-1.5\sigma}^{\mu+0.5\sigma} y(x)\,\mathrm{d}x}{\int_{\mu-2.5\sigma}^{\mu+2.5\sigma} y(x)\mathrm{d}x} = 0.38643.$$

Supplement. The supplement related to this article is available online at: https://doi.org/10.5194/esd-10-107-2019-supplement.

Author contributions. IA, RN and LG had the initial idea. GMM developed the WRF-WVT tool. IA and JEB carried out the simulations and data analysis. IA and JEB wrote the original draft and reviewed the subsequent documents. RN, LG and GMM provided suggestions during the revision period.

Competing interests. The authors declare that they have no conflict of interest.

Special issue statement. This article is part of the special issue "The 8th EGU Leonardo Conference: From evaporation to precipitation: the atmospheric moisture transport". It is a result of the 8th EGU Leonardo Conference, Ourense, Spain, 25–27 October 2016.

Acknowledgements. Iago Algarra was financially supported by the Spanish government (MINECO, CGL2015-65141-R). Jorge Eiras-Barca was financially supported by the EDB481B 2018/069 from the Xunta de Galicia and the Fulbright Commission. This work was also partially supported by Xunta de Galicia under Project ED431C 2017/64-GRC "Programa de Consolidación e Estructuración de Unidades de Investigación Competitivas (Grupos de Referencia Competitiva)". This work is part of the LAGRIMA project. The computational part of this work was done in the Supercomputing Center of Galicia, CESGA. Iago Algarra would like to express his gratitude to all the Non-Linear Physics Group for their kind support during his stay at the University of Santiago de Compostela. Finally the authors would like to thank two anonymous referees, who helped to improve the final version of the manuscript.

Edited by: Francina Domínguez
Reviewed by: two anonymous referees

References

Arritt, R. W., Rink, T. D., Segal, M., Todey, D. P., Clark, C. A., Mitchell, M. J., Labas, K. M., Arritt, R. W., Rink, T. D., Segal, M., Todey, D. P., Clark, C. A., Mitchell, M. J., and Labas, K. M.: The Great Plains Low-Level Jet during the Warm Season of 1993, Mon. Weather Rev., 125, 2176–2192, https://doi.org/10.1175/1520-0493(1997)125<2176:TGPLLJ>2.0.CO;2, 1997.

Augustine, J. A. and Caracena, F.: Lower-tropospheric precursors to nocturnal MCS development over the central United States, Weather Forecast., 9, 116–135, https://doi.org/10.1175/1520-0434(1994)009<0116:LTPTNM>2.0.CO;2, 1994.

Barandiaran, D., Wang, S.-Y., and Hilburn, K.: Observed trends in the Great Plains low-level jet and associated precipitation changes in relation to recent droughts, Geophys. Res. Lett., 40, 6247–6251, https://doi.org/10.1002/2013GL058296, 2013.

Beljaars, A. C. M., Viterbo, P., Miller, M. J., and Betts, A. K.: The Anomalous Rainfall over the United States during July 1993: Sensitivity to Land Surface Parameterization and Soil Moisture Anomalies, Mon. Weather Rev., 124, 362–383, https://doi.org/10.1175/1520-0493(1996)124<0362:TAROTU>2.0.CO;2, 1996.

Blackadar, A. K.: Boundary layer wind maxima and their significance for the growth of nocturnal inversions, B. Am. Meteorol. Soc., 38, 283–290, https://doi.org/10.1175/1520-0477-38.5.283, 1957.

Bonner, W. D.: Climatology of the low level jet, Mon. Weather Rev., 96, 833–850, https://doi.org/10.1175/1520-0493(1968)096<0833:COTLLJ>2.0.CO;2, 1968.

Byerle, L. A. and Paegle, J.: Modulation of the Great Plains low-level jet and moisture transports by orography and large-scale circulations, J. Geophys. Res.-Atmos., 108, GCP 6-1–GCP 6-16, https://doi.org/10.1029/2002JD003005, 2003.

Chen, M., Shi, W., Xie, P., Silva, V. B. S., Kousky, V. E., Higgins, R. W., and Janowiak, J. E.: Assessing objective techniques for gauge-based analyses of global daily precipitation, J. Geophys. Res.-Atmos., 113, 1–13, https://doi.org/10.1029/2007JD009132, 2008.

Cook, K. H., Vizy, E. K., Launer, Z. S., and Patricola, C. M.: Springtime intensification of the great plains low-level jet and midwest precipitation in GCM Simulations of the twenty-first century, J. Climate, 21, 6321–6340, https://doi.org/10.1175/2008JCLI2355.1, 2008.

Dee, D. P., Uppala, S. M., Simmons, A. J., Berrisford, P., Poli, P., Kobayashi, S., Andrae, U., Balmaseda, M. A., Balsamo, G., Bauer, P., Bechtold, P., Beljaars, A. C. M., van de Berg, L., Bidlot, J., Bormann, N., Delsol, C., Dragani, R., Fuentes, M., Geer, A. J., Haimberger, L., Healy, S. B., Hersbach, H., Hólm, E. V., Isaksen, L., Kållberg, P., Köhler, M., Matricardi, M., McNally, A. P., Monge-Sanz, B. M., Morcrette, J.-J., Park, B.-K., Peubey, C., de Rosnay, P., Tavolato, C., Thépaut, J.-N., and Vitart, F.: The ERA-Interim reanalysis: configuration and performance of the data assimilation system, Q. J. Roy. Meteor. Soc., 137, 553–597, https://doi.org/10.1002/qj.828, 2011.

Dong, X., Xi, B., Kennedy, A., Feng, Z., Entin, J. K., Houser, P. R., Schiffer, R. A., L'Ecuyer, T., Olson, W. S., Hsu, K. L., Liu, W. T., Lin, B., Deng, Y., and Jiang, T.: Investigation of the 2006 drought and 2007 flood extremes at the Southern Great Plains through an integrative analysis of observations, J. Geophys. Res.-Atmos., 116, D03204, https://doi.org/10.1029/2010JD014776, 2011.

Drumond, A., Nieto, R., Trigo, R., Ambrizzi, T., Souza, E., and Gimeno, L.: A lagrangian identification of the main sources of moisture affecting northeastern Brazil during its pre-rainy and rainy seasons, PLoS One, 5, 1–8, https://doi.org/10.1371/journal.pone.0011205, 2010.

Dudhia, J.: Numerical Study of Convection Observed during the Winter Monsoon Experiment Using a Mesoscale Two-Dimensional Model, J. Atmos. Sci., 46, 3077–3107, https://doi.org/10.1175/1520-0469(1989)046<3077:NSOCOD>2.0.CO;2, 1989.

Eiras-Barca, J., Dominguez, F., Hu, H., Garaboa-Paz, D., and Miguez-Macho, G.: Evaluation of the moisture sources in two extreme landfalling atmospheric river events using an Eulerian WRF tracers tool, Earth Syst. Dynam., 8, 1247–1261, https://doi.org/10.5194/esd-8-1247-2017, 2017.

Gimeno, L., Stohl, A., Trigo, R. M., Dominguez, F., Yoshimura, K., Yu, L., Drumond, A., Durán-Quesada, A. M., and Nieto, R.: Oceanic and terrestrial sources of continental precipitation, Rev. Geophys., 50, RG4003, https://doi.org/10.1029/2012RG000389, 2012.

Harding, K. J. and Snyder, P. K.: Examining future changes in the character of central U.S. warm-season precipitation using dynamical downscaling, J. Geophys. Res., 119, 13113–16136, https://doi.org/10.1002/2014JD022575, 2014.

Helfand, H. M. and Schubert, S. D.: Climatology of the simulated Great Plains low-level jet and its contribution to the continental moisture budget of the United States, J. Climate, 8, 784–806, https://doi.org/10.1175/1520-0442(1995)008<0784:COTSGP>2.0.CO;2, 1995.

Higgins, R. W., Mo, K. C., and Schubert, S. D.: The moisture budget of the central United States in spring as evaluated in the NCEP/NCAR and the NASA/DAO reanalyses, Mon. Weather Rev., 124, 939–963, https://doi.org/10.1175/1520-0493(1996)124<0939:TMBOTC>2.0.CO;2, 1996.

Higgins, R. W., Yao, Y., Yarosh, E. S., Janowiak, J. E., and Mo, K. C.: Influence of the great plains low-level jet on summertime precipitation and moisture transport over the central United States, J. Climate, 10, 481–507, https://doi.org/10.1175/1520-0442(1997)010<0481:IOTGPL>2.0.CO;2, 1997.

Hong, S. and Lim, J.: The WRF single-moment 6-class microphysics scheme (WSM6), J. Korean Meteor. Soc., 42, 129–151, 2006.

Hu, Q., Jiang, D., and Lang, X.: Sources of moisture for different intensities of summer rainfall over the Chinese Loess Plateau during 1979–2009, Int. J. Climatol., 38, e1280–e1287, https://doi.org/10.1002/joc.5416, 2018.

Hu, X. M., Klein, P. M., and Xue, M.: Evaluation of the updated YSU planetary boundary layer scheme within WRF for wind resource and air quality assessments, J. Geophys. Res.-Atmos., 118, 10490–10505, https://doi.org/10.1002/jgrd.50823, 2013.

Insua-Costa, D. and Miguez-Macho, G.: A new moisture tagging capability in the Weather Research and Forecasting model: formulation, validation and application to the 2014 Great Lake-effect snowstorm, Earth Syst. Dynam., 9, 167–185, https://doi.org/10.5194/esd-9-167-2018, 2018.

Kain, J. S.: The Kain–Fritsch Convective Parameterization: An Update, J. Appl. Meteorol., 43, 170–181, https://doi.org/10.1175/1520-0450(2004)043<0170:TKCPAU>2.0.CO;2, 2004.

Miguez-Macho, G., Rios-Entenza, A., and Dominguez, F.: The impact of soil moisture and evapotranspiration fluxes on the spring water cycle in the Iberian Peninsula: A study with moisture tracers in WRF, in: AGU Fall Meeting Abstracts, 2013.

Mlawer, E. J., Taubman, S. J., Brown, P. D., Iacono, M. J., and Clough, S. A.: Radiative transfer for inhomogeneous atmospheres: RRTM, a validated correlated-k model for the longwave, J. Geophys. Res.-Atmos., 102, 16663–16682, https://doi.org/10.1029/97JD00237, 1997.

Mo, K. C. and Juang, H.-M. H.: Relationships between soil moisture and summer precipitation over the Great Plains and the Southwest, J. Geophys. Res.-Atmos., 108, GCP 5-1–GCP 5-17, https://doi.org/10.1029/2002JD002952, 2003.

Mo, K. C., Nogues-Paegle, J., and Paegle, J.: Physical mechanisms of the 1993 summer floods, J. Atmos. Sci., 52, 879–895, https://doi.org/10.1175/1520-0469(1995)052<0879:PMOTSF>2.0.CO;2, 1995.

Mo, K. C., Paegle, J. N., and Higgins, R. W.: Atmospheric processes associated with summer floods and droughts in the central United States, J. Climate, 10, 3028–3046, https://doi.org/10.1175/1520-0442(1997)010<3028:APAWSF>2.0.CO;2, 1997.

Moore, B. J., Neiman, P. J., Ralph, F. M., and Barthold, F. E.: Physical Processes Associated with Heavy Flooding Rainfall in Nashville, Tennessee, and Vicinity during 1–2 May 2010: The Role of an Atmospheric River and Mesoscale Convective Systems, Mon. Weather Rev., 140, 358–378, https://doi.org/10.1175/MWR-D-11-00126.1, 2012.

Nakamura, J., Lall, U., Kushnir, Y., Robertson, A. W., and Seager, R.: Dynamical Structure of Extreme Floods in the U.S. Midwest and the United Kingdom, J. Hydrometeorol., 14, 485–504, https://doi.org/10.1175/JHM-D-12-059.1, 2013.

Nayak, M. A., Villarini, G., Bradley, A. A., Nayak, M. A., Villarini, G., and Bradley, A. A.: Atmospheric Rivers and Rainfall during NASA's Iowa Flood Studies (IFloodS) Campaign, J. Hydrometeorol., 17, 257–271, https://doi.org/10.1175/JHM-D-14-0185.1, 2016.

Numaguti, A.: Origin and recycling processes of precipitating water over the Eurasian continent: Experiments using an atmospheric general circulation model, J. Geophys. Res.-Atmos., 104, 1957–1972, https://doi.org/10.1029/1998JD200026, 1999.

Pan, Z., Segal, M., and Arritt, R. W.: Role of Topography in Forcing Low-Level Jets in the Central United States during the 1993 Flood-Altered Terrain Simulations, Mon. Weather Rev., 132, 396–403, https://doi.org/10.1175/1520-0493(2004)132<0396:ROTIFL>2.0.CO;2, 2004.

Pu, B., Dickinson, R. E., and Fu, R.: Dynamical connection between Great Plains low-level winds and variability of central Gulf States precipitation, J. Geophys. Res.-Atmos., 121, 3421–3434, https://doi.org/10.1002/2015JD024045, 2016.

Ramos, A. M., Nieto, R., Tomé, R., Gimeno, L., Trigo, R. M., Liberato, M. L. R., and Lavers, D. A.: Atmospheric rivers moisture sources from a Lagrangian perspective, Earth Syst. Dynam., 7, 371–384, https://doi.org/10.5194/esd-7-371-2016, 2016.

Rife, D. L., Pinto, J. O., Monaghan, A. J., Davis, C. A., and Hannan, J. R.: Global distribution and characteristics of diurnally varying low-level jets, J. Climate, 23, 5041–5064, https://doi.org/10.1175/2010JCLI3514.1, 2010.

Schubert, S. D., Helfand, H. M., Wu, C. Y., and Min, W.: Subseasonal variations in warm-season moisture transport and precipitation over the central and eastern United States, J. Climate, 11, 2530–2555, https://doi.org/10.1175/1520-0442(1998)011<2530:SVIWSM>2.0.CO;2, 1998.

Shin, H. H. and Hong, S. Y.: Intercomparison of Planetary Boundary-Layer Parametrizations in the WRF Model for a Single Day from CASES-99, Bound.-Lay. Meteorol., 139, 261–281, https://doi.org/10.1007/s10546-010-9583-z, 2011.

Sorí, R., Marengo, J., Nieto, R., Drumond, A., and Gimeno, L.: The Atmospheric Branch of the Hydrological Cycle over the Negro and Madeira River Basins in the Amazon Region, Water, 10, 738, https://doi.org/10.3390/w10060738, 2018.

Stensrud, D. J.: Importance of low-level jets to climate: A review, J. Climate, 9, 1698–1711, https://doi.org/10.1175/1520-0442(1996)009<1698:IOLLJT>2.0.CO;2, 1996.

Stohl, A., James, P., Stohl, A., and James, P.: A Lagrangian Analysis of the Atmospheric Branch of the Global Water Cycle. Part I: Method Description, Validation, and Demonstration for the August 2002 Flooding in Central Europe, J. Hydrometeorol., 5, 656–678, https://doi.org/10.1175/1525-7541(2004)005<0656:ALAOTA>2.0.CO;2, 2004.

Stohl, A. and James, P.: A Lagrangian Analysis of the Atmospheric Branch of the Global Water Cycle. Part II: Moisture Transports between Earth's Ocean Basins and River Catchments, J. Hydrometeorol., 6, 961–984, https://doi.org/10.1175/JHM470.1, 2005a.

Stohl, A., Forster, C., Frank, A., Seibert, P., and Wotawa, G.: Technical note: The Lagrangian particle dispersion model FLEXPART version 6.2, Atmos. Chem. Phys., 5, 2461–2474, https://doi.org/10.5194/acp-5-2461-2005, 2005b.

Stohl, A., Forster, C., and Sodemann, H.: Remote sources of water vapor forming precipitation on the Norwegian west coast at 60° N – A tale of hurricanes and an atmospheric river, J. Geophys. Res.-Atmos., 113, 1–13, https://doi.org/10.1029/2007JD009006, 2008.

Tang, Y., Winkler, J., Zhong, S., Bian, X., Doubler, D., Yu, L., and Walters, C.: Future changes in the climatology of the Great Plains low-level jet derived from fine resolution multi-model simulations, Sci. Rep., 7, 5029, https://doi.org/10.1038/s41598-017-05135-0, 2017.

Ting, M. and Wang, H.: The Role of the North American Topography on the Maintenance of the Great Plains Summer Low-Level Jet, J. Atmos. Sci., 63, 1056–1068, https://doi.org/10.1175/JAS3664.1, 2006.

Trenberth, K. E. and Guillemot, C. J.: Physical processes involved in the 1988 drought and 1993 floods in north America, J. Climate, 9, 1288–1298, https://doi.org/10.1175/1520-0442(1996)009<1288:PPIITD>2.0.CO;2, 1996.

Vázquez, M., Nieto, R., Drumond, A., and Gimeno, L.: Moisture transport into the Arctic: Source-receptor relationships and the roles of atmospheric circulation and evaporation, J. Geophys. Res.-Atmos., 121, 13493–13509, https://doi.org/10.1002/2016JD025400, 2016.

Walters, C. K., Winkler, J. A., Shadbolt, R. P., van Ravensway, J., and Bierly, G. D.: A long-term climatology of southerly and northerly low-level jets for the central United States, Ann. Assoc. Am. Geogr., 98, 521–552, https://doi.org/10.1080/00045600802046387, 2008.

Wang, S. Y. and Chen, T. C.: The late-spring maximum of rainfall over the U.S. central plains and the role of the low-level jet, J. Climate, 22, 4696–4709, https://doi.org/10.1175/2009JCLI2719.1, 2009.

Wegmann, M., Orsolini, Y., Vázquez, M., Gimeno, L., Nieto, R., Bulygina, O., Jaiser, R., Handorf, D., Rinke, A., Dethloff, K., Sterin, A., and Brönnimann, S.: Arctic moisture source for Eurasian snow cover variations in autumn, Environ. Res. Lett., 10, 054015, https://doi.org/10.1088/1748-9326/10/5/054015, 2015.

Wexler, H.: A Boundary Layer Interpretation of the Low-level Jet, Tellus, 13, 368–378, https://doi.org/10.1111/j.2153-3490.1961.tb00098.x, 1961.

Wu, Y. and Raman, S.: The summertime Great Plains low level jet and the effect of its origin on moisture transport, Bound.-Lay. Meteorol., 88, 445–466, https://doi.org/10.1023/A:1001518302649, 1998.

Manuscript Template

On the origin of the anomalous uptake of water vapor by landfalling Atmospheric Rivers

I. Algarra [1]*, R. Nieto[1], L. Gimeno[1]

[1] Environmental Physics Laboratory (EPhysLab), CIM-UVIGO, Universidad de Vigo, Ourense, 32004, Spain. (*) ialgarra@uvigo.es

One of the most robust signals of climate change is the relentless rise in global mean surface temperature, which is linked closely with the water-holding capacity of the atmosphere. A wetter atmosphere leads necessarily to an enhancement of the total transport of moisture via, among other factors, to an intensification of Atmospheric Rivers (ARs), which provide the main mechanism of moisture advection from subtropical to extra-tropical regions. Here we identify those regions of anomalous moisture uptake (AMU) by landfalling ARs and show that on a global scale, the interannual variability of AMU displays a significant increase over the period 1980-2017, close to the Clausius-Clapeyron (CC) scaling, at 7 % per degree of temperature rise. Our results also reveal generalized significant increases in AMU at the regional scale and an asymmetric supply of oceanic moisture, in which the maximum values are located over the region known as the Western Hemisphere Warm Pool (WHWP).

INTRODUCTION

Atmospheric Rivers (ARs) are the main mechanisms by which moisture is transported in extratropical regions *(1, Gimeno et al., 2016)*. These structures are responsible for the horizontal transport of large quantities of water vapor, in up to 3 - 5 different events per hemisphere at any one time, from the subtropics to the mid- and northern latitudes along a relatively narrow (< 1000 km) and elongated (> 2000 km) atmospheric pathway at lower atmospheric levels *(2, Newell et al., 1992; 3, Zhu and Newel, 1998)*. At a synoptic time scale, ARs are generally associated with low-level moisture convergence located in the warm sectors of extra-tropical cyclones, ahead of pre-cold fronts *(4, Ralph et al., 2018)*. Landfalling ARs are therefore often associated with extreme precipitation events and can trigger heavy flooding, especially when subjected to orographic lift over mountainous topography *(5, Dettinger et al., 2011)*. They have been linked to a wide range of socio-economic impacts, affecting the severity and frequency of flooding, and occasionally defining the end of a drought period *(6, Dettinger, 2013)*. Their importance in extreme precipitation events and floods has been analysed in some detail, mostly for the west coast of the United States, where ARs are the primary driver of damage caused by flooding *(7, Corringham et al., 2019)*, and also in western Europe, where intense rainfall is strongly associated with ARs, their persistence being especially relevant as the precursors of winter floods *(8, Lavers et al., 2011; 9, Lavers and Villarini, 2013; 10, Pereira et al., 2018).*

ARs act as bridges or conveyors between oceanic evaporation and continental precipitation *(11, 12, Gimeno et al., 2012, 2020)*, the former being the main origin of water vapor that reaches land masses at extratropical latitudes. The current relentless rise in global mean surface temperature is closely linked to the increase in atmospheric water vapor *(13, Held and Soden, 2006; 14, Bao et al., 2017)*, and the greater availability of water vapor favors a larger transport of moisture, and hence an intensification of extreme precipitation events and floods triggered by ARs *(15, Lavers and Villarini, 2015; 16, Espinoza et al., 2018; 17, Gershunov et al., 2019)*. The water-holding capacity of the atmosphere increases by about 7% per degree of warming *(18, O'Gorman and Muller, 2010)*, leading to an intensification of extreme precipitation events at similar rates. Simulations of climate warming have shown more intense and frequent ARs *(19, Ramos et al., 2016; 16, Espinoza et al., 2018; 20, Massoud et al., 2019; 21, Tan et al., 2020)*, which could lead to higher total rainfall and flooding in mid-latitude land masses. Nevertheless, it remains unclear which areas provide anomalous moisture to the ARs, and whether these show trends linked with global warming. In this study, we performed a global assessment to identify those areas where landfalling ARs (hereafter LARs) receive anomalous moisture, and tried to quantify these effects at regional and global scales in terms of the trends in this supply of moisture.

RESULTS

For the worldwide coastline, and for the period 1980-2017, we first identified the areas of maximum occurrence of LARs **(Fig. 1)** as those in which the number of ARs exceeds 10% of the global total **(see Material and Methods)**. According to the definition, ARs are synoptic systems located in warm sectors of extra-tropical cyclones *(4, Ralph et al., 2018)*, hence we must be careful in selecting regions of maximum occurrence that lack the appropriate structural fingerprint of ARs. This caveat is particularly relevant for tropical areas influenced by monsoon circulation and regions that do not show a relatively deep negative anomaly of mean sea level pressure (MSLP). Thus, initially 24 regions of maximum occurrence of LARs were identified, but only those regions that showed an associated negative wintertime MSLP anomaly **(Fig. S1-S3)**, were considered for moisture uptake analysis. A total of four regions were thus excluded from the study (indicated in red in **Fig. 1**), and our focus was then on the remaining 20 coastal domains. It is important to highlight the requirement of the availability of water vapor in the atmosphere for moisture transport by ARs. Moisture must have evaporated and accumulated in certain areas before its uptake by an AR. The anomalous moisture uptake (herein denoted AMU) for each region over the LARs was identified as those areas where moisture uptake was anomalous during each LAR event using the Lagrangian model FLEXPART v9.0 *(22, Stohl and James 2004; 23, Stohl et al., 2005)* forced by ERA-Interim reanalysis *(24, Dee et al. 2011)* **(see Material and Methods)**. **Fig. 2** shows the 90th percentile of AMU areas for each of the retained 20 regions of maximum occurrence of LAR previously identified in **Fig. 1**. The full values of AMU for each region are given in Figs. S1-3. The AMU regions for LARs are mostly located over large upwind oceanic areas, these positions being highly stable **(Figs. S4-S5** show the weight centroids for the AMU value for each LAR and region). Most regions show a significant increase in AMU for the period 1980-2017, as indicated by the filled areas in **Fig. 2**, while unfilled areas are those with no significant trends **(see individual maps in Fig. S6-S7)**.

We also investigated AMU by LARs at a global scale. **Fig. 3A** shows AMU regions for all LAR events. In general, higher AMU values are found over subtropical oceanic areas, between 25º and 40º in both Hemispheres. Nevertheless, a maximum AMU value for the LARs is seen in the so-called Western Hemisphere Warm Pool (WHWP), a large evaporative region that includes the Gulf of Mexico and the Caribbean Sea, where high sea surface temperatures favor a higher rate of evaporation, providing moisture to the atmosphere and favoring its subsequent transport to other remote regions *(e.g., 25, Drumond et al., 2011)*. The outstanding magnitude of this large AMU maximum results from the oversized importance of the ARs in the northern Atlantic basin when compared to all the other major oceanic basins **(Fig. 2)** and the asymmetric role of ARs in the NH vs SH **(Fig. 3B)**. In fact, this region acts as a large moisture reservoir for ARs that develop in the North Atlantic Ocean and make landfall towards the northern coasts of the west Atlantic basin (American East Coast **(Fig. 2A and Figs. S1G-H)**, Greenland and Iceland **(Fig. 2A and Figs. S2A-B)** and the west coast of Europe **(Fig 2B and Figs. S1C-D-E)**. To a lesser extent, a local input of AMU closer to the landfalling area of ARs is also seen in the mid-latitudes **(Fig. S1-S3)** due to the

local convergence of water vapor along the pathways of ARs *(26, Dettinger et al., 2015)*. Latitudinal variability of AMU is shown in **Fig. 3B,** and this follows a bimodal distribution. Higher values of AMU are located around 40ºN in both hemispheres, and these are twice as high in the Northern Hemisphere, in which the maximum occurrence of LAR was identified. As observed by the shaded grey area in **Fig. 3B**, the interannual variability is rather small implying that there is scarcely any latitudinal variation in the AMU regions from year to year. Nevertheless, by analysing the global interannual variation of AMU **(Fig. 3C)**, a significant increase in AMU can be seen for the period studied, of about 0.9% per decade, which is in accordance with the occurrence of significant increases in AMU for each of the 20 regions of maximum occurrence (trends shown in the supplementary material **Fig. S6-S7**).

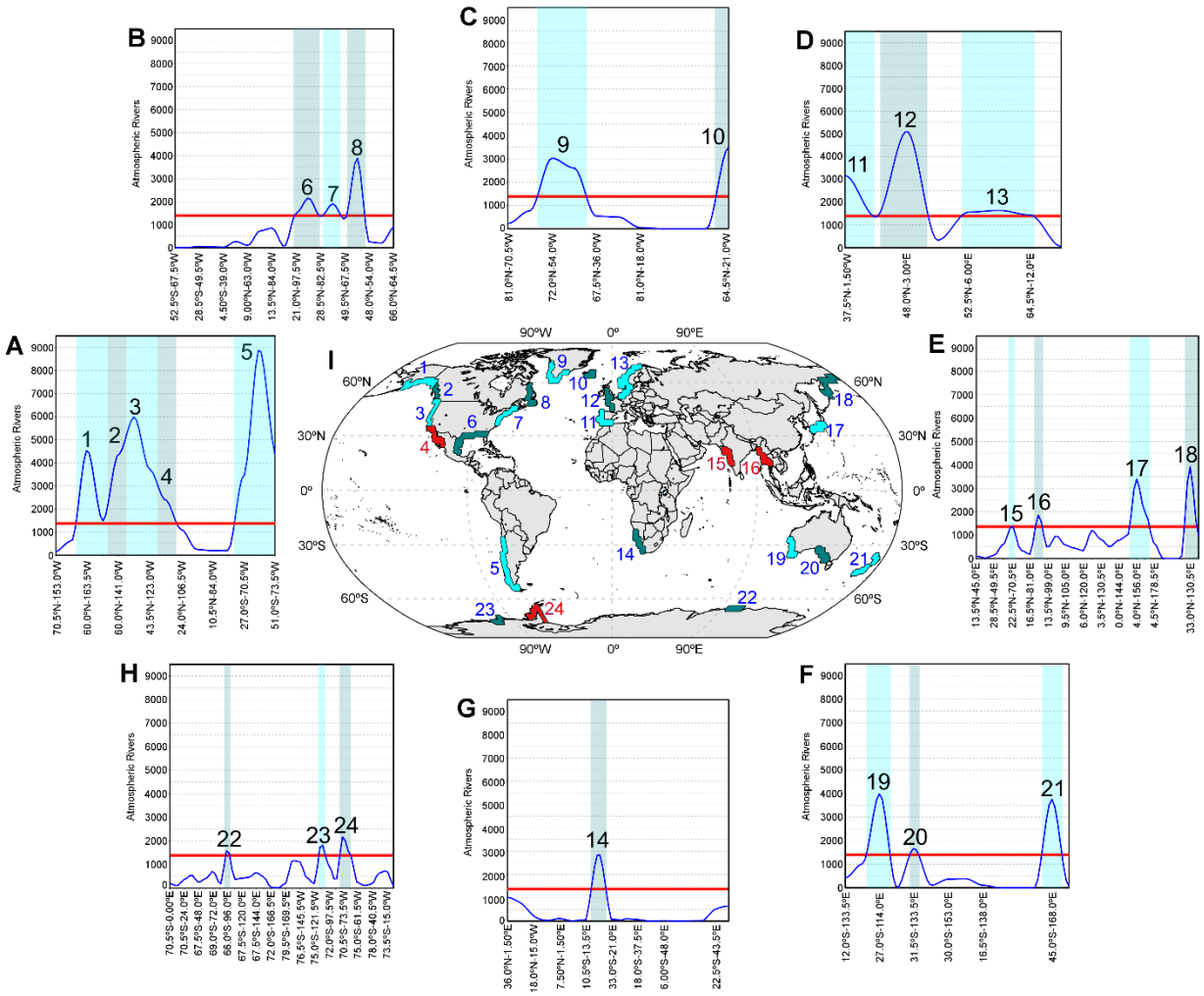

Fig. 1. Regions of maximum occurrence of landfalling AR (LAR). AR frequency over global coastal areas for the period 1980-2017 for: American West Coast **(A)**, American East Coast **(B)**, Greenland and Iceland **(C)**, European West Coast **(D)**, Asian Coast **(E)**, Australian Coast and New Zealand **(F)**, African Coast **(G)**, and Antarctic Coast **(H)**. The blue line shows the number of ARs against coastal longitude and latitude. The red line represents the threshold of 10% of days computed considering all regions. **(I)** Global map showing the 24 LAR regions detected (those not used for the remaining if the study of anomalous moisture uptake are shown in red).

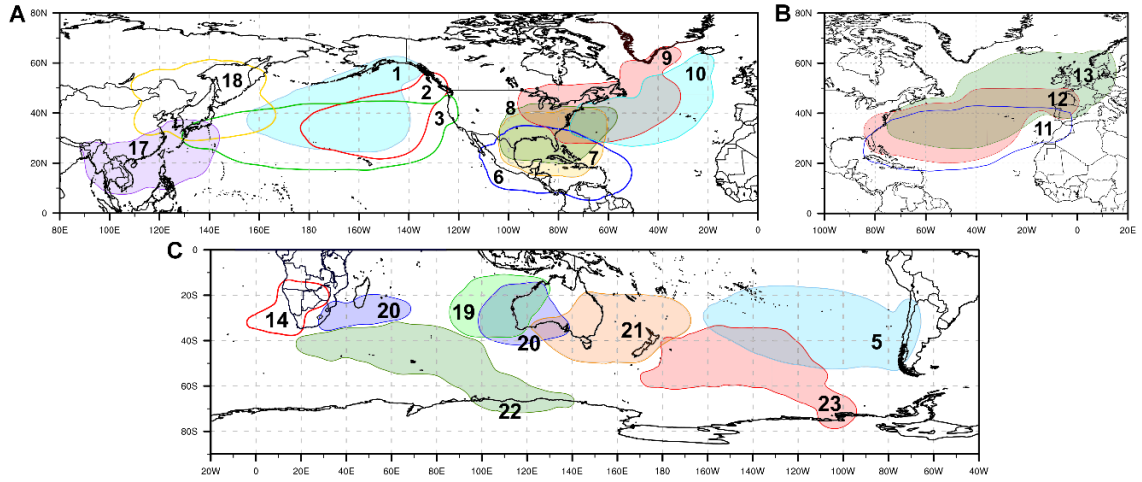

Fig 2. Anomalous moisture uptake (AMU) for regions of maximum occurrence of landfalling ARs (LARs) shown in Fig. 1. 90th percentile of the sum of anomalies of evaporation for each region identified in Fig. 1. (**A**) for north Pacific and North Atlantic Oceans, (**B**) for western Europe and (**C**) for the Southern Hemisphere. Filled areas show a significant increase in evaporation anomalies, while unfilled areas show no significant trend (95% level of significance). The period of study is 1980 - 2017. Trends were calculated using Mann-Kendall test.

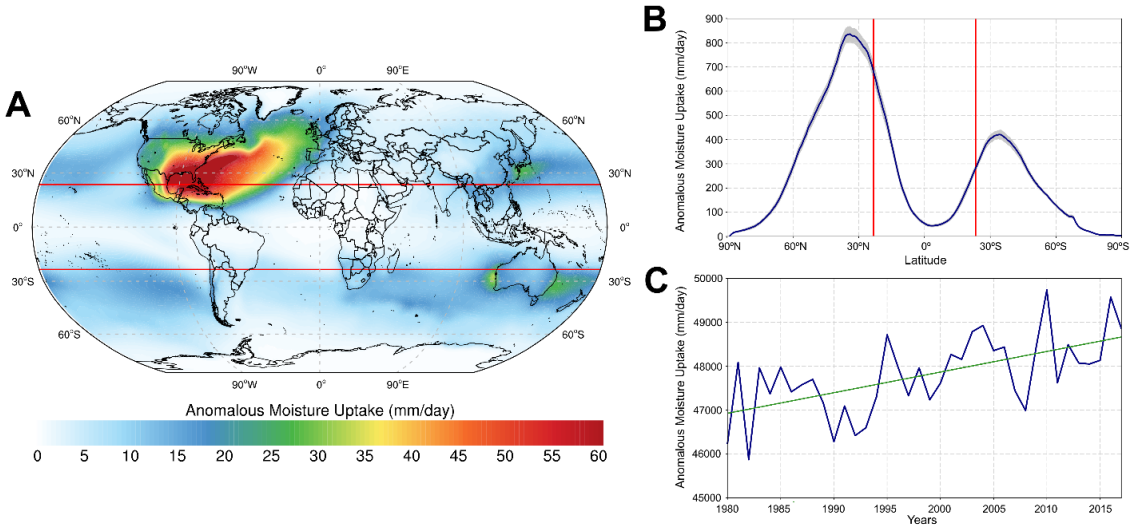

Fig 3. Anomalous moisture uptake of the landfalling AR events (LARs) from 1980-2017. (**A**) Annual sum of positive anomalies of moisture uptake for AR days over the main landfalling regions. The red lines delimit the region between the Tropics of Cancer (23.43ºN) and Capricorn (23.43ºS). The anomalies are calculated over the period 1980-2017. (**B**) Latitudinal sum of AMU (blue line) and its interannual variability (shaded grey area). The vertical red lines delimit the tropical region. (**C**) Worldwide interannual variability of AMU. The green line shows a linear regression.

DISCUSSION

In a warmer climate, ARs are expected to become increasingly intense and to increase in frequency *(27, Dettinger, 2011; 16, Espinoza et al., 2018; 21, Tan et al., 2020)*, likely escalating their socioeconomic impact *(28, Dominguez et al., 2018)*. Although it is not known how the moisture transported by ARs will change, the projected increase of 30 to 40% in the vertically integrated water vapor transport (IVT) in the storm tracks of the Pacific and North Atlantic *(14, Lavers and Villarini, 2015)*, together with the fact that 9 out of 10 liters of the water vapor that reach extra-tropical latitudes do so via ARs *(3, Zhu and Newell, 1998)*, points to an increase in the amount of moisture transport as the temperature rises *(29, Sousa et al., 2019)*. The identification and analysis of the variability and

long-term changes of the regions that provide moisture for these systems has thus become an essential topic for study.

We show a significant increase in the global AMU for landfalling AR events (LARs) in the current climate (about 0.9% per decade for 1980-2017, **Fig. 3C**). We estimate that extreme precipitation events will increase at the same rate as atmospheric moisture following the Clausius-Clapeyron (CC) ratio, in which the overall average amount of water vapor increases at a rate of 7.3%/K with respect to the average global surface air temperature *(14, Bao et al., 2017; 30, Prein et al., 2017)*. Given the critical role of LARs for rainfall and flooding in many regions, their presence can be considered an extreme precipitation event due to the large amount of moisture transported by these systems and the intense rainfall that results when the AR makes landfall *(8, Lavers et al., 2011; 9, Lavers and Villarini, 2013; 31, Ramos et al., 2015; 32, Viale et al., 2018)*. Given that the average warming of the global surface temperature for the period 1980-2016 is closer to 0.5°C *(33, Simmons et al., 2017)*, our results show a significant increase in AMU in the source regions of about 3% over the same period, or about 6% for each degree of temperature increase, following a relationship close to what is expected from the Clausius-Clapeyron ratio.

Although dependent on the latitude of the region in which the AR makes landfall, most AMU maxima are located in areas near tropical latitudes, confirming the subtropical origin of the moisture transported by ARs. An increase (or decrease) in the evaporation rate over these areas leads to a greater (lesser) availability of moisture in the atmosphere, which in turn induces a greater (lesser) transport of moisture by ARs. Our results also reveal a concentration of AMU over the oceans near the areas where AR makes landfall. This is in accordance with the results of previous studies that have revealed how ARs incorporate mid-latitude sources and convergences of local moisture along their paths *(26, Dettinger et al., 2015)*.

Despite the robustness of results, it is necessary to quantify the relative roles of the main drivers of evaporation, sea surface temperature (SST), near-surface wind speed, and near-surface atmospheric specific humidity *(11, Gimeno et al., 2012)* in the anomalous moisture transported by ARs. This will constitute a major challenge in future programs of research.

MATERIALS AND METHODS

Global identification of AR impact regions

In order to detect the main regions of LAR occurrence from 1980 to 2017 over the world's coastlines, we use the AR database developed by *34, Guan and Waliser (2015)*. This database uses the landfall location for ARs at a global scale, at a spatial resolution of 1.5º and a 6 h time step (00.00; 06.00; 12:00; and 18.00 UTC), based on a threshold of IVT intensity, to which geometric conditions are added according to the coherence of AR structures using ERA-Interim reanalysis data from the European Centre for Medium-Range Weather Forecast (ECMWF) *(24, Dee et al., 2011)*. Further details of the AR detection can be found in *34, Guan and Waliser (2015)*.

For the present study, LAR events were counted at a spatial resolution of 12º along each coast. Using this new coarser resolution, we identified those points with a frequency greater than 10% of the total number of days with LARs, i.e., 1388 days, considering these to be the regions of maximum LAR occurrence. To assess whether a LAR event was associated with cyclogenesis, we evaluated the regions identified in terms of wintertime mean sea level pressure (MSLP) anomaly (data obtained from ERA-Interim Reanalysis). Those regions that were not associated with negative anomalies were dismissed.

Given the broad region of occurrence of LARs along the west coast of North America, and in order to obtain a comprehensive assessment in terms of AMU, we considered four different sub-regions (areas numbered by 1, 2, 3, and 4 in Fig.1). This division is somewhat subjective but necessary in order to avoid dealing with ARs reaching California in the same context as those striking British Colombia or even Alaska. Previous studies have classified the trajectories of ARs reaching the West Coast of North America when they penetrate inland in four specific regimes (*35, 36, Rutz et al. (2014; 2015*), this classification being particularly relevant when assessing the role of ARs in terms of precipitation. Nevertheless, in order to be as objective as possible in this regard and focusing on the study of AMU during LAR events, it seems appropriate to establish a regional subdivision in terms of the frequency of LAR events taking the coastal geographical orientation into account. It is important to note that the occurrence of LAR ranges broadly latitude. Starting at the highest latitude, the first region extends along the southern coast of

Alaska, the second and the third extend from 60ºN to 52ºN (based on LAR events with a northwest orientation), then from 36ºN to 52ºN (the region of maximum LAR activity) *(37, Payne and Magnusdottir, 2015; 38, Kim et al., 2019)*, with the fourth and final region extending south of 36ºN (this is not considered in the analysis of moisture anomaly because it does not show a seasonal pattern of negative MSLP anomalies).

FLEXPART model: Anomalous moisture uptake (AMU)

The global FLEXPART model (FLEXible PARTicle dispersion model) version 9.0 *(23, Stohl et al., 2005)* was used to quantify the humidity during AR events. FLEXPART (*22, 39, Stohl and James, 2004; 2005)* is a Lagrangian model that enables us to track atmospheric moisture along each trajectory by following air parcels. The model divides the atmosphere homogeneously into approximately 2.0 million air parcels of constant mass, which are advected by a 3-D wind field. In our simulation, FLEXPART uses ERA-Interim reanalysis data from the ECMWF *(24, Dee et al., 2011)*, which are available at a 6-hour time step (00.00, 06.00, 12.00; and 18.00 UTC) from 1980 to 2017, at a 1º horizontal resolution on 61 vertical levels, from 1000 to 0.1 hPa with approximately 14 model pressure levels below 1500 m and 23 below 5000 m.

To estimate the sources of moisture for AR events, air parcels are tracked backward in time. Thus, changes in the specific humidity along each trajectory by each air parcel can be expressed as (Eq. 1):

$$e - p = m\frac{dq}{dt} \quad (1)$$

where *(e – p)* is the evaporation-minus-precipitation budget, which is the freshwater flux of the particle, *m* represents the mass of each individual air parcel (expressed in kg), *q* represents the specify humidity (measured in g/kg), and *t* is time. The diagnosis of the surface freshwater flux is calculated by integrating (e - p) over the entire atmospheric vertical column for all the resident air parcels (Eq. 2):

$$(E - P) \approx \frac{\sum_{k=1}^{k}(e - p)}{A} \quad (2)$$

where *(E - P)* represents the surface freshwater flux, *K* is the number of air parcels in residence over a specific area, *A*. The backward analysis in time is used to distinguish the origin of the atmospheric moisture in the air masses during LAR events. Thus, a source of moisture can be defined as that region in which the evaporation exceeds the precipitation i.e., (E - P) > 0, and the net moisture budget of the tracked air parcels favors the evaporation from the environment to the particles, where there is a positive contribution of moisture.

A key factor in studies that involve the quantification of the transport of moisture is the residence time of water vapor in the atmosphere. Longer residence times imply the transport of moisture further away from its evaporative source. The water vapor in the atmosphere varies widely spatially and/or seasonally, and it is generally accepted that the residence time of water vapor in the atmosphere is approximately 8-10 days *(40, Numaguti, 1999; 41, van der Ent and Tuinenburg, 2017).* Nevertheless, *42, Nieto and Gimeno (2019*) proposed an optimal time for monthly integrations at a global scale for Lagrangian studies. Here, we have used the mean monthly integration time values for each region of LAR occurrence to compute the individual backward trajectories of air parcels during each LAR event.

In order to identify those regions in which there is an AMU during each LAR event, only positive values of (E - P) are considered. Anomalies of moisture were obtained from the difference between the individual LAR-event moisture uptake and the climatological moisture uptake for the day of the LAR for the entire period 1980-2017. Positive anomalies were calculated by adding the moisture uptake for each individual LAR event. We thus obtain those areas where the LARs gain anomalous moisture along their trajectories.

SUPPLEMENTARY MATERIALS

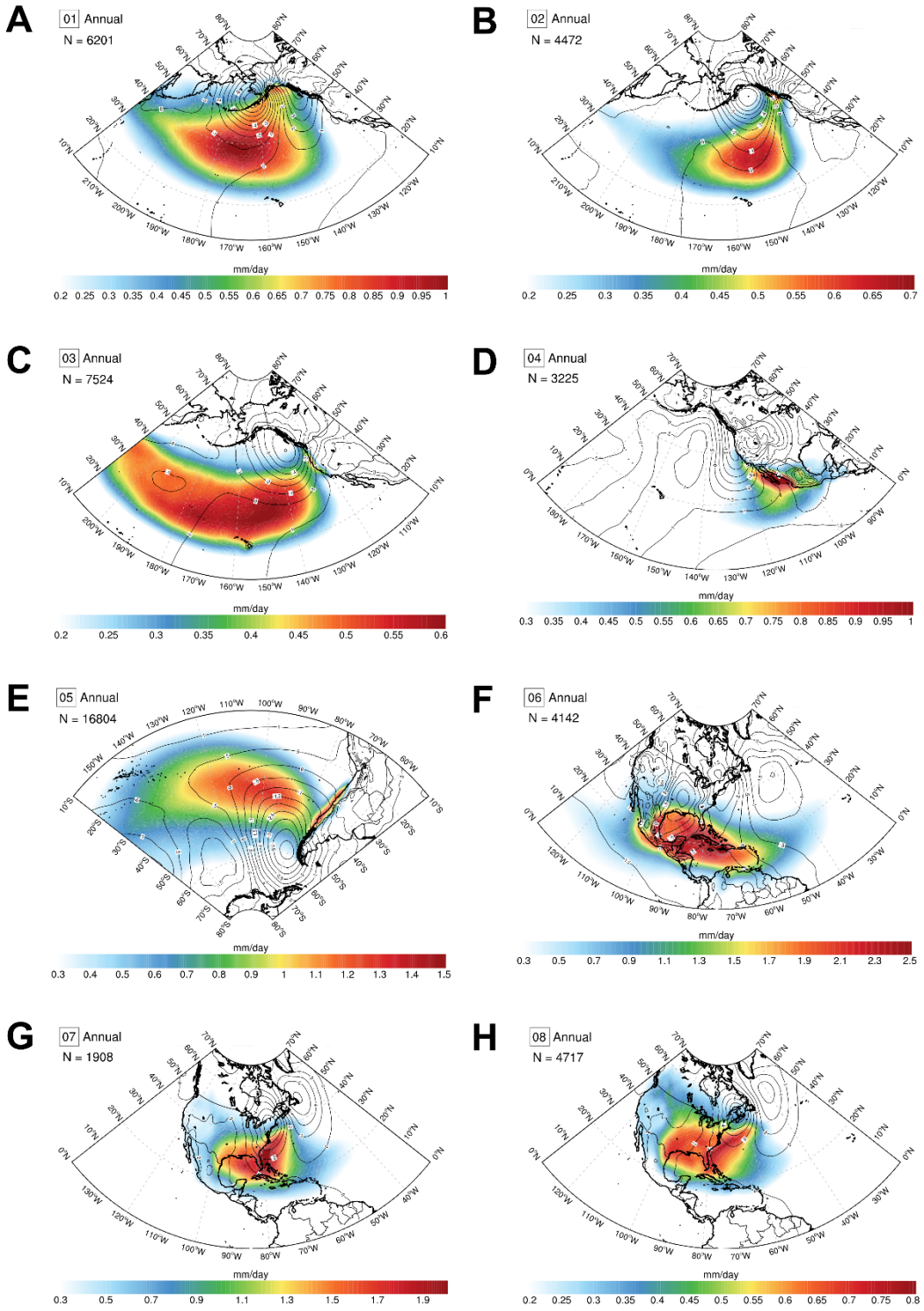

Fig S1. Annual anomalous moisture uptake (AMU) for regions of maximum occurrence of landfalling ARs (LARs) from 1980 to 2017. Spatial pattern of AMU for regions 1 to 8 identified in Fig. 1 (in color, mm/day) and mean sea level pressure anomaly (black isolines, hPa). N denotes the number of LARs over each region.

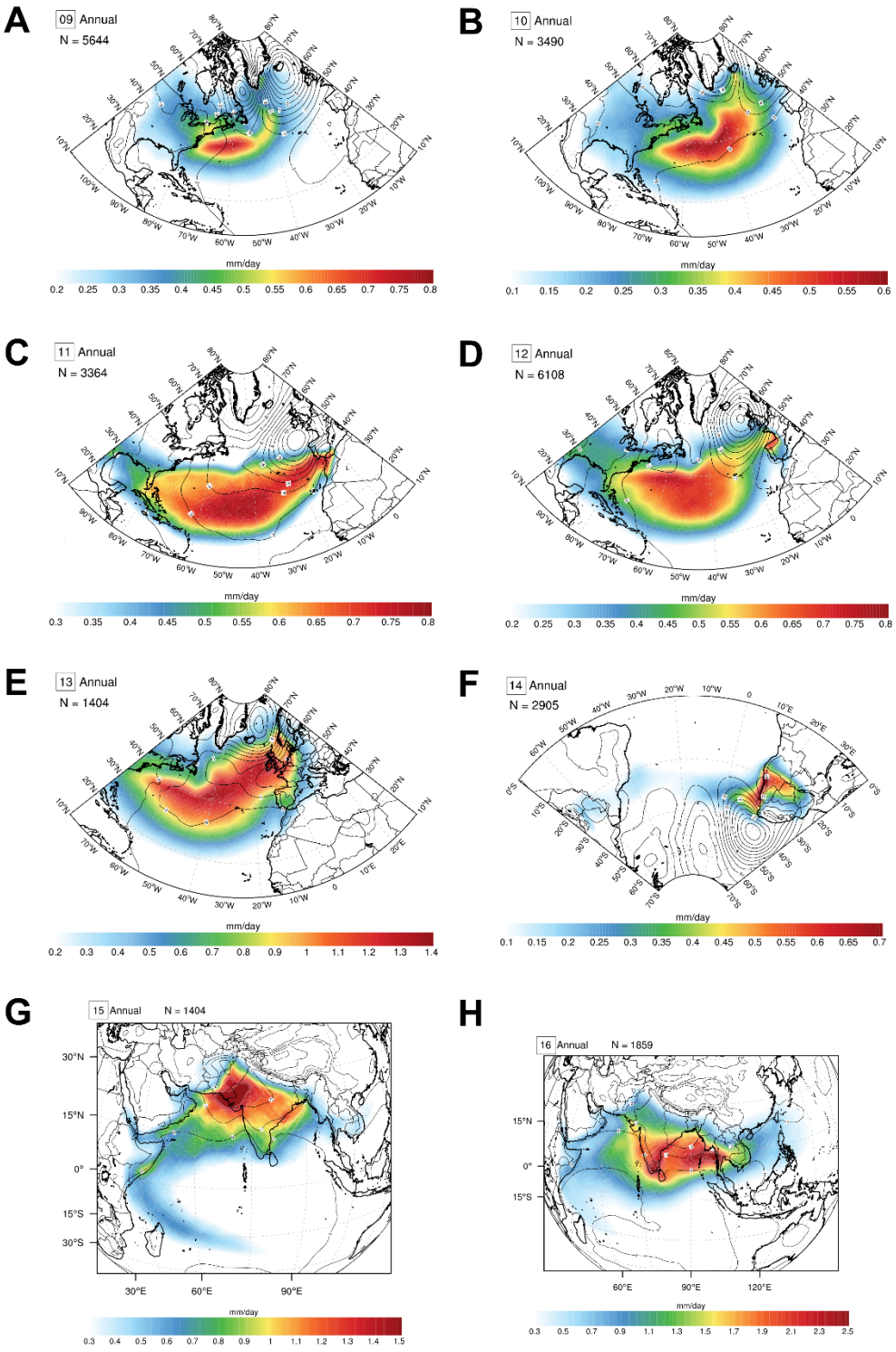

Fig S2. As Fig. S1. but for LAR regions from 9 to 16 identified in Fig.1

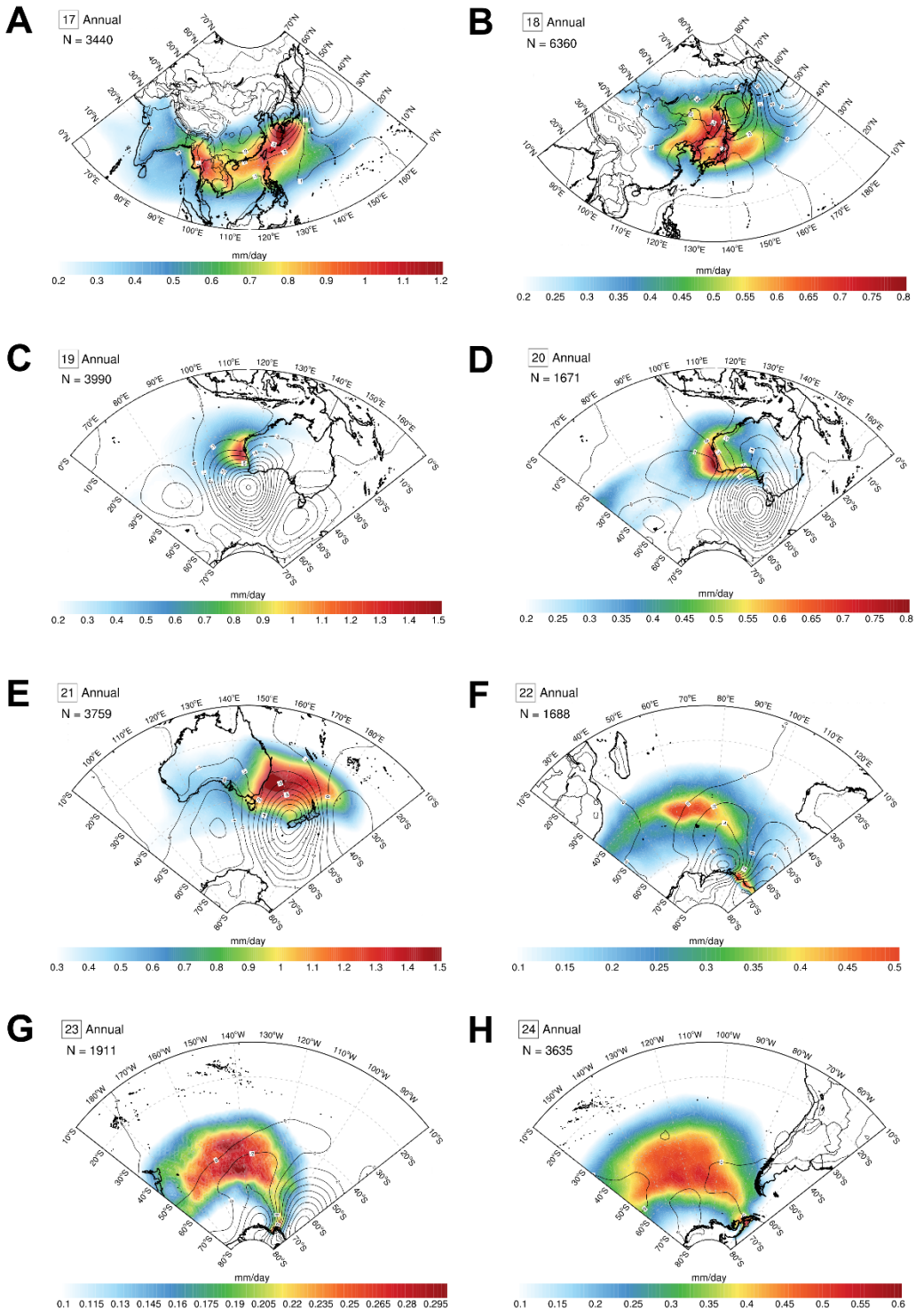

Fig S3. As Fig. S1. but for LAR regions from 17 to 24 identified in Fig.1

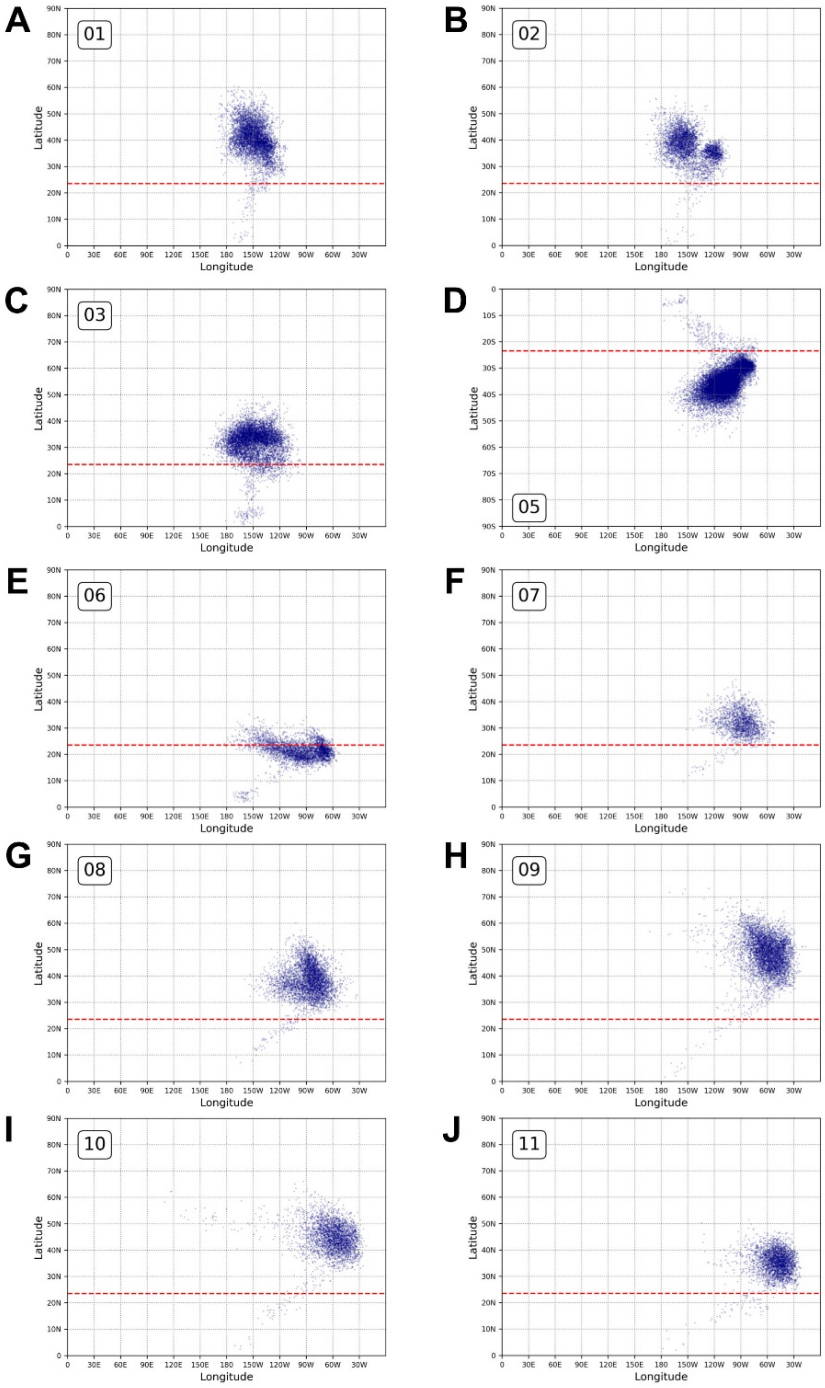

Fig S4. Weighted centroids of AMU for the LARs by region. Centroid position (blue points) of the area of AMU for each LAR (defined by the 90 percentile) weighted by each AMU value for region 1 to 11 identified in Fig.1. Red dashed line indicates the Tropic of Cancer (23.43ºN) or Capricorn (23.43ºS).

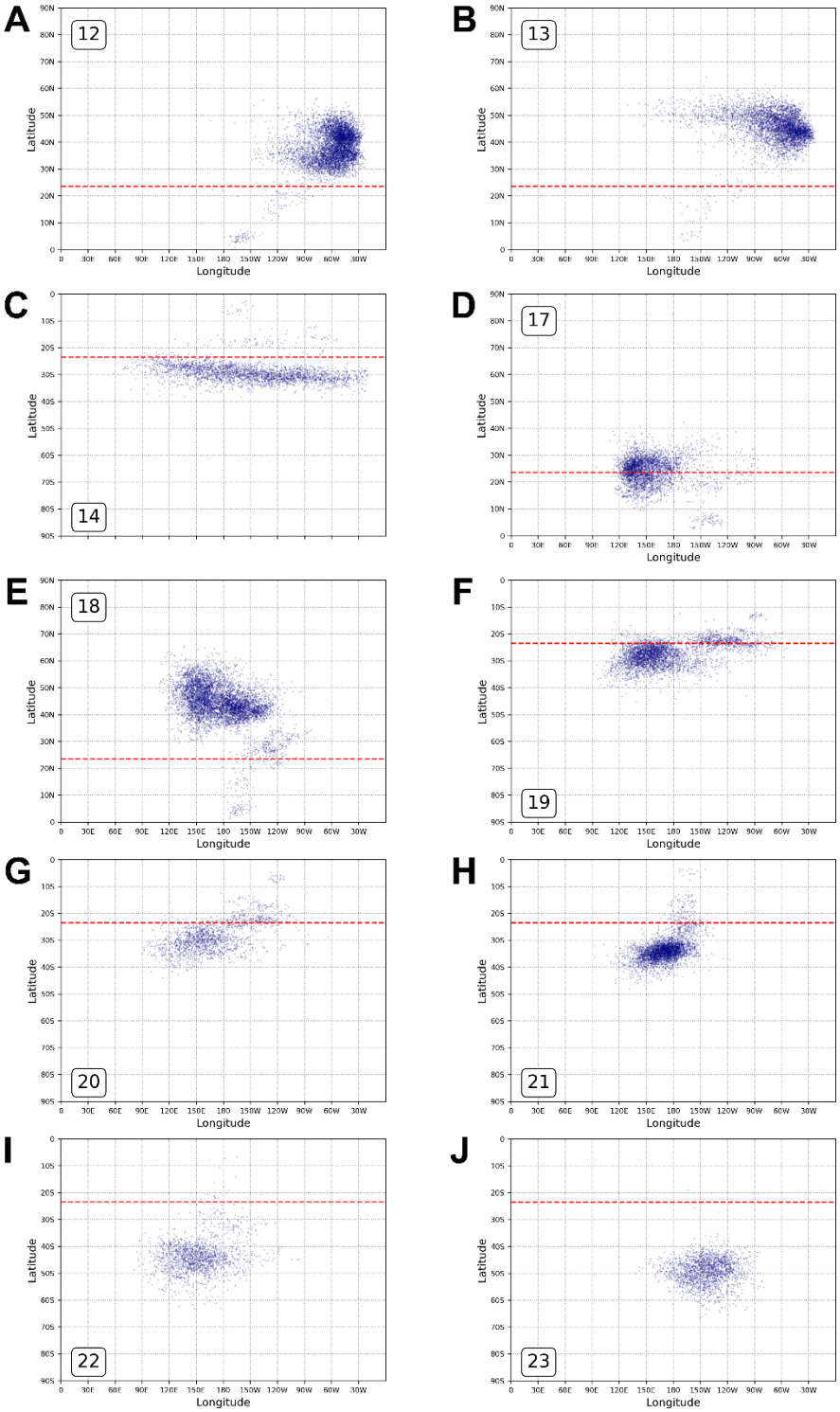

Fig S5. Weighted centroids of AMU for the LARs by region. As Fig. S4 but for LAR regions 12 to 23.

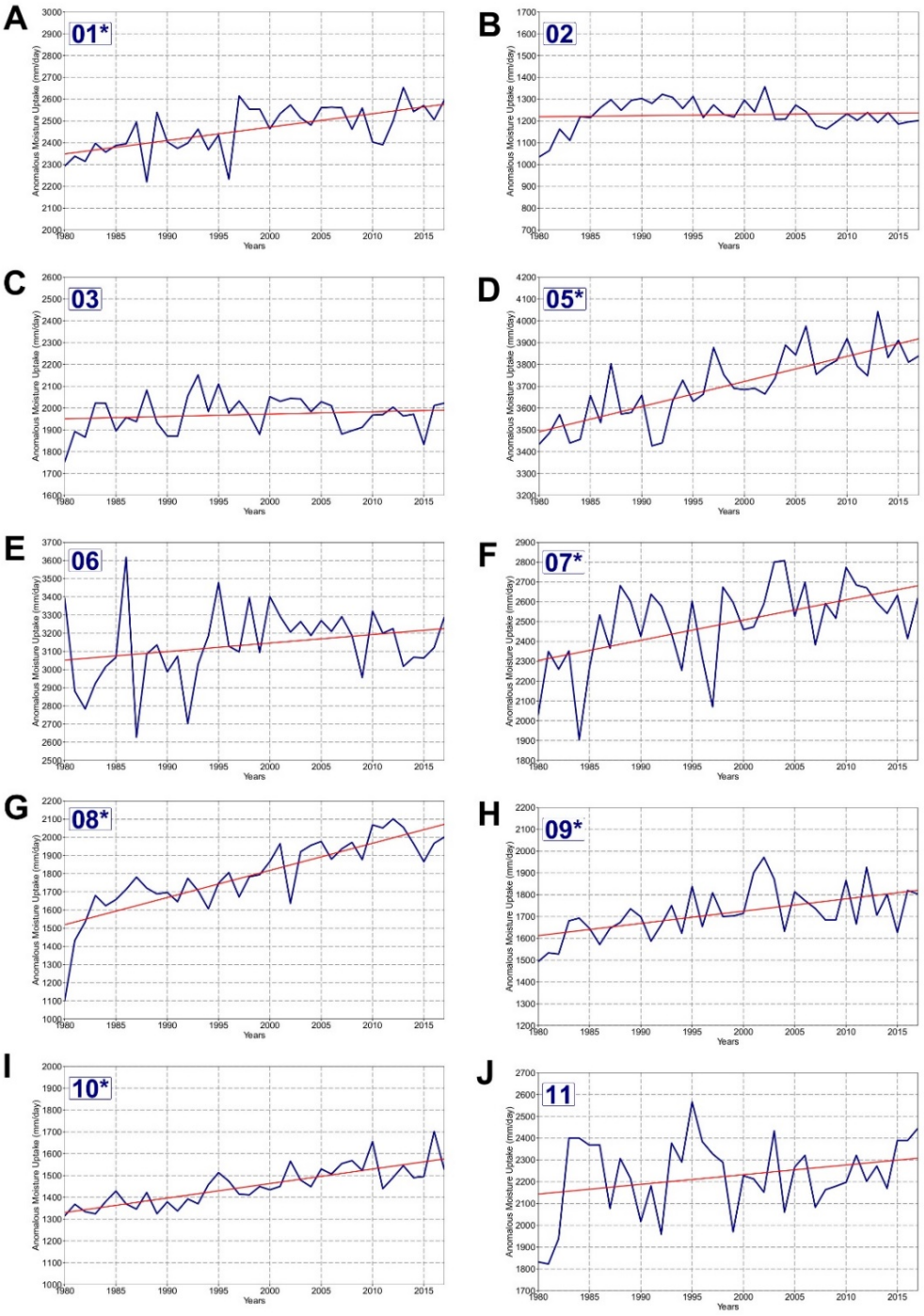

Fig S6. Interannual variability of AMU for each LAR region from 1980 to 2017. The red line shows the linear regression. Box (top left) shows the number of each LAR region in Fig. 1 (from 1 to 11). The asterisk indicates a significant trend (95%).

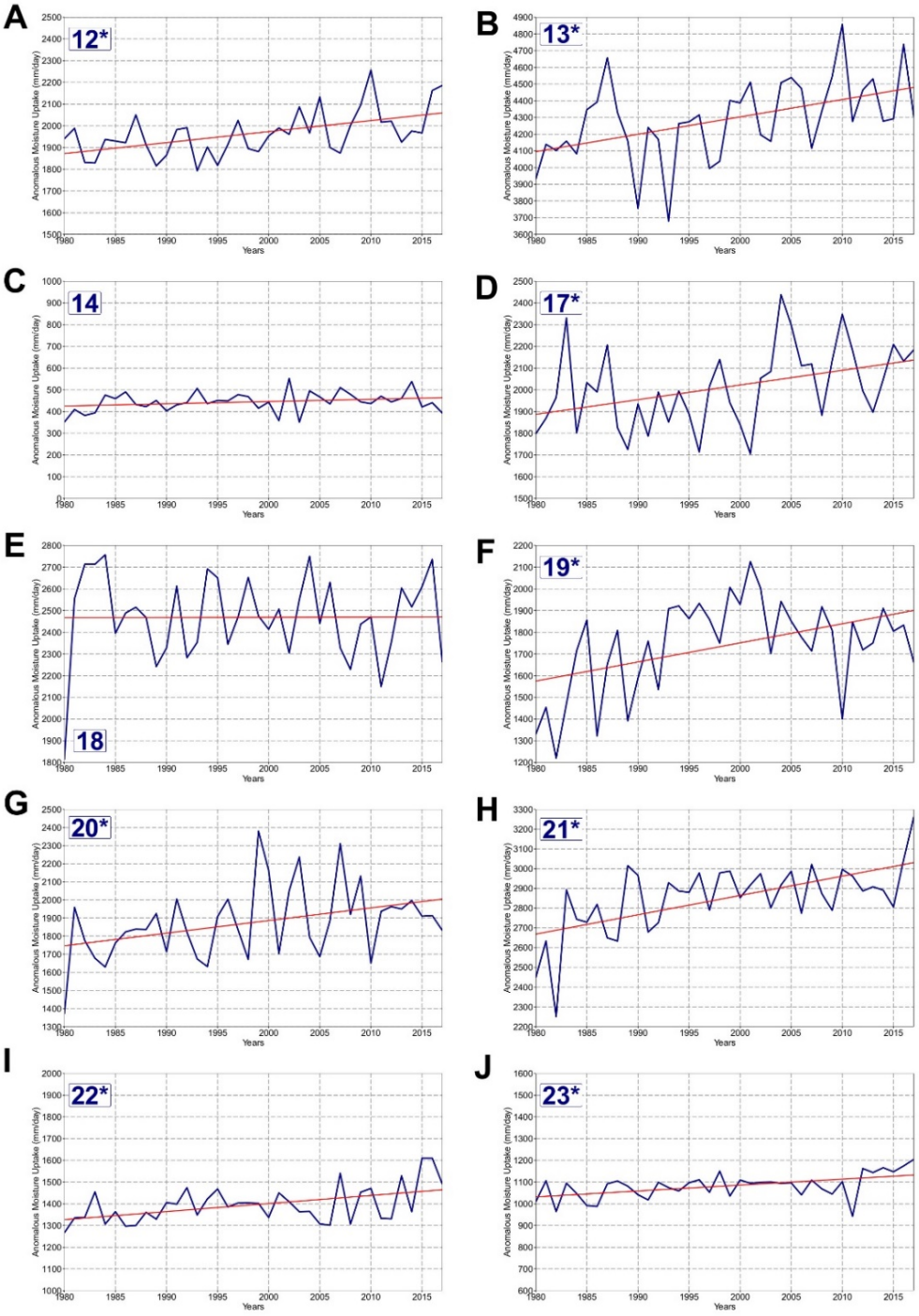

Fig S7. Interannual variability of AMU for each LAR region from 1980 to 2017. As Fig. S6 but for LAR regions 12 to 23.

REFERENCES AND NOTES

1. L. Gimeno, *et al.*, Major Mechanisms of Atmospheric Moisture Transport and Their Role in Extreme Precipitation Events. *Annu. Rev. Environ. Resour.* **41**, 117–141 (2016).
2. R. E. Newell, N. E. Newell, Y. Zhu, C. Scott, Tropospheric rivers? – A pilot study. *Geophys. Res. Lett.* **19**, 2401–2404 (1992).
3. Y. Zhu, R. E. Newell, A proposed algorithm for moisture fluxes from atmospheric rivers. *Mon. Weather Rev.* **126**, 725–735 (1998).
4. F. M. Ralph, M. C. L. D. Dettinger, M. M. Cairns, T. J. Galarneau, J. Eylander, Defining "Atmospheric river" : How the glossary of meteorology helped resolve a debate. *Bull. Am. Meteorol. Soc.* **99**, 837–839 (2018).
5. M. D. Dettinger, F. M. Ralph, T. Das, P. J. Neiman, D. R. Cayan, Atmospheric Rivers, Floods and the Water Resources of California. *Water* **3**, 445–478 (2011).
6. M. D. Dettinger, Atmospheric Rivers as Drought Busters on the U.S. West Coast. *J. Hydrometeorol.* **14**, 1721–1732 (2013).
7. T. W. Corringham, F. M. Ralph, A. Gershunov, D. R. Cayan, C. A. Talbot, Atmospheric rivers drive flood damages in the western United States. *Sci. Adv.* **5**, eaax4631 (2019).
8. D. A. Lavers, *et al.*, Winter floods in Britain are connected to atmospheric rivers. *Geophys. Res. Lett.* **38** (2011).
9. D. A. Lavers, G. Villarini, The nexus between atmospheric rivers and extreme precipitation across Europe. *Geophys. Res. Lett.* **40**, 3259–3264 (2013).
10. S. Pereira, A. M. Ramos, L. Rebelo, R. M. Trigo, J. L. Zêzere, A centennial catalogue of hydro-geomorphological events and their atmospheric forcing. *Adv. Water Resour.* **122**, 98–112 (2018).
11. L. Gimeno, *et al.*, Oceanic and terrestrial sources of continental precipitation. *Rev. Geophys.* **50** (2012).
12. L. Gimeno, *et al.*, Recent progress on the sources of continental precipitation as revealed by moisture transport analysis. *Earth-Science Rev.* **201** (2020).
13. I. M. Held, B. J. Soden, "Robust Responses of the Hydrological Cycle to Global Warming" (2006).
14. J. Bao, S. C. Sherwood, L. V. Alexander, J. P. Evans, Future increases in extreme precipitation exceed observed scaling rates. *Nat. Clim. Chang.* **7**, 128–132 (2017).
15. D. A. Lavers, G. Villarini, The contribution of atmospheric rivers to precipitation in Europe and the United States. *J. Hydrol.* **522**, 382–390 (2015).
16. V. Espinoza, D. E. Waliser, B. Guan, D. A. Lavers, F. M. Ralph, Global Analysis of Climate Change Projection Effects on Atmospheric Rivers. *Geophys. Res. Lett.* **45**, 4299–4308 (2018).
17. A. Gershunov, *et al.*, Precipitation regime change in Western North America: The role of Atmospheric Rivers. *Sci. Rep.* **9** (2019).
18. P. A. O'Gorman, C. J. Muller, How closely do changes in surface and column water vapor follow Clausius-Clapeyron scaling in climate change simulations? *Environ. Res. Lett.* **5** (2010).
19. A. M. Ramos, R. Tomé, R. M. Trigo, M. L. R. Liberato, J. G. Pinto, Projected changes in atmospheric rivers affecting Europe in CMIP5 models. *Geophys. Res. Lett.* **43**, 9315–9323 (2016).
20. E. C. Massoud, V. Espinoza, B. Guan, D. E. Waliser, Global Climate Model Ensemble Approaches for Future Projections of Atmospheric Rivers. *Earth's Futur.* **7**, 1136–1151 (2019).
21. Y. Tan, F. Zwiers, S. Yang, C. Li, K. Deng, The Role of Circulation and Its Changes in Present and Future Atmospheric Rivers over Western North America. *J. Clim.* **33**, 1261–1281 (2020).
22. A. Stohl, P. James, A Lagrangian analysis of

the atmospheric branch of the global water cycle: Part 1: Method description, validation, and demonstration for the August 2002 flooding in central Europe. *J. Hydrometeorol.* **5**, 656–678 (2004).

23. A. Stohl, C. Forster, A. Frank, P. Seibert, G. Wotawa, Technical note: The Lagrangian particle dispersion model FLEXPART version 6.2. *Atmos. Chem. Phys.* **5**, 2461–2474 (2005).

24. D. P. Dee, *et al.*, The ERA-Interim reanalysis: Configuration and performance of the data assimilation system. *Q. J. R. Meteorol. Soc.* **137**, 553–597 (2011).

25. A. Drumond, R. Nieto, L. Gimeno, On the contribution of the Tropical Western Hemisphere Warm Pool source of moisture to the Northern Hemisphere precipitation through a Lagrangian approach. *J. Geophys. Res. Atmos.* **116** (2011).

26. M. Dettinger, F. Ralph, D. Lavers, Setting the Stage for a Global Science of Atmospheric Rivers. *Eos (Washington. DC).* **96** (2015).

27. M. Dettinger, Climate change, atmospheric rivers, and floods in California - a multimodel analysis of storm frequency and magnitude changes. *J. Am. Water Resour. Assoc.* **47**, 514–523 (2011).

28. F. Dominguez, *et al.*, Tracking an atmospheric river in a warmer climate: From water vapor to economic impacts. *Earth Syst. Dyn.* **9**, 249–266 (2018).

29. P. M. Sousa, *et al.*, North Atlantic Integrated Water Vapor Transport – from 850-2100 CE: Impacts on Western European Rainfall. *J. Clim.* (2019) https:/doi.org/10.1175/jcli-d-19-0348.1.

30. A. F. Prein, *et al.*, Increased rainfall volume from future convective storms in the US. *Nat. Clim. Chang.* **7**, 880–884 (2017).

31. A. M. Ramos, R. M. Trigo, M. L. R. Liberato, R. Tomé, Daily precipitation extreme events in the Iberian Peninsula and its association with atmospheric rivers. *J. Hydrometeorol.* **16**, 579–597 (2015).

32. M. Viale, R. Valenzuela, R. D. Garreaud, F. M. Ralph, Impacts of atmospheric rivers on precipitation in Southern South America. *J. Hydrometeorol.* **19**, 1671–1687 (2018).

33. A. J. Simmons, *et al.*, A reassessment of temperature variations and trends from global reanalyses and monthly surface climatological datasets. *Q. J. R. Meteorol. Soc.* **143**, 101–119 (2017).

34. B. Guan, D. E. Waliser, Detection of atmospheric rivers: Evaluation and application of an algorithm for global studies. *J. Geophys. Res.* **120**, 12,514-12,535 (2015).

35. J. J. Rutz, W. James Steenburgh, F. Martin Ralph, Climatological characteristics of atmospheric rivers and their inland penetration over the western united states. *Mon. Weather Rev.* **142**, 905–921 (2014).

36. J. J. Rutz, W. James Steenburgh, F. Martin Ralph, The inland penetration of atmospheric rivers over western North America: A Lagrangian analysis. *Mon. Weather Rev.* **143**, 1924–1944 (2015).

37. A. E. Payne, G. Magnusdottir, An evaluation of atmospheric rivers over the North Pacific in CMIP5 and their response to warming under RCP 8.5. *J. Geophys. Res. Atmos.* **120**, 11,173-11,190 (2015).

38. H. M. Kim, Y. Zhou, M. A. Alexander, Changes in atmospheric rivers and moisture transport over the Northeast Pacific and western North America in response to ENSO diversity. *Clim. Dyn.* **52**, 7375–7388 (2019).

39. A. Stohl, P. James, A Lagrangian analysis of the atmospheric branch of the global water cycle. Part II: Moisture transports between earth's ocean basins and river catchments. *J. Hydrometeorol.* **6**, 961–984 (2005).

40. A. Numaguti, Origin and recycling processes of precipitating water over the Eurasian continent: Experiments using an atmospheric general circulation model. *J. Geophys. Res. Atmos.* **104**, 1957–1972 (1999).

41. R. J. Van Der Ent, O. A. Tuinenburg, The residence time of water in the atmosphere revisited. *Hydrol. Earth Syst. Sci.* **21**, 779–

790 (2017).

42. R. Nieto, L. Gimeno, A database of optimal integration times for Lagrangian studies of atmospheric moisture sources and sinks. *Sci. data* **6**, 59 (2019).

water

MDPI

Article

Atmospheric Rivers over the Arctic: Lagrangian Characterisation of Their Moisture Sources

Marta Vázquez [1,*], Iago Algarra [1], Jorge Eiras-Barca [1], Alexandre M. Ramos [2], Raquel Nieto [1] and Luis Gimeno [1]

[1] Environmental Physics Laboratory (EPhysLab), Facultade de Ciencias, Universidad de Vigo, Ourense 32004, Spain; ialgarra@uvigo.es (I.A.); jeiras@uvigo.es (J.E.-B.); rnieto@uvigo.es (R.N.); l.gimeno@uvigo.es (L.G.)

[2] Instituto Dom Luiz, Universidade de Lisboa, 1749-016 Lisboa, Portugal; amramos@fc.ul.pt

* Correspondence: martavazquez@uvigo.es

Received: 5 September 2018; Accepted: 19 December 2018; Published: 26 December 2018

Abstract: In recent years, the Arctic has become a subject of special interest due to the drastic effect of climate change over the region. Despite that there are several mechanisms that influence the Arctic region; some recent studies have suggested significant influences of moisture transport over the observed loss of sea ice. Moisture transport can affect the region in different ways: direct precipitation over the region, radiative effect from the cloud cover and through the release of latent heat. Atmospheric rivers (ARs) represent one of the main events involved in moisture transport from the tropics to the mid-latitudes and despite having been shown especially relevant on the northward advection, their effect over the Arctic has not been deeply investigated. The aim of this work was to establish the groundwork for future studies about the effect of ARs linked to moisture transport over the Arctic region. For this purpose, an automated algorithm was used to identify regions of maximum AR occurrence over the Arctic. This was done by analysing the number of AR detections every month over a band of 10° of latitude centred on 60° N. The Lagrangian model FLEXPART was used to find the areas where the ARs take their moisture to the Arctic. Using this model, the anomalous moisture contribution to these baroclinic structures was analysed taking into account only the dates of AR occurrence. From the results, it appears that the main moisture sources for AR events extend over the North Atlantic and North Pacific oceans; moreover, the local input of moisture over the region of maximum AR occurrence seems to be especially relevant. In general terms, moisture comes from major evaporative areas over the western part of the oceanic regions in the band between 30° and 40° N for most months in the year, showing a continental origin in the summer months. This behaviour agrees with the climatological moisture transport into the Arctic determined in previous studies. However, in special association with AR events, an intensification of local moisture uptake is observed over the area of maximum AR activity and nearby. The study of the origin of this moisture and associated anomalies for Arctic ARs is an important step in the analysis of the effect of these structures on the Arctic environment.

Keywords: atmospheric rivers; Arctic; moisture transport; FLEXPART

1. Introduction

Important changes have been observed in the Arctic region in recent decades, many of them being related to climate change in particular for example, [1,2]. On this topic, the change in sea ice extent that has occurred in recent years is especially relevant showing a downward trend in the last few decades. This decrease has occurred in all seasons [3–6] and has been more pronounced in late summer [7,8], when reaches its minimum annual value. The possible causes of the decrease in sea ice extent are

several and are triggered by feedback processes: increased temperatures, changing wind patterns and atmospheric moisture transport for example, [9–11]. Moreover, the changes in moisture transport from lower latitudes have been suggested to have an important influence over the Arctic region [12–14].

Multiple mechanisms are responsible for global moisture transport, Atmospheric Rivers (ARs) being one of the most important. ARs are usually associated with transient eddies and have been shown to dominate the transport of poleward moisture [15]. The transient moisture transport associated with the occurrence of extreme events has been estimated to contribute to the total poleward moisture transport across 60° N around 36–38% in winter and 32% in summer [16,17]. ARs are long and narrow corridors which transport water vapour along meridians from the tropics to the extra-tropics. Despite covering only about 10% of the Earth's circumference, these atmospheric structures account for over 80–90% of the total poleward water vapour transport at mid-latitudes [18,19] and are also associated with extreme precipitation events [20–23]. A mini review of the general characteristics of ARs was conducted by Gimeno et al. [24].

According to Sorterberg and Walsh [25], the interannual variability of moisture transport toward the Arctic is mainly triggered by the variability of cyclone activity over Greenland and the Eastern Siberia Sea. This cyclone activity also leads the AR activity in these latitudes. Despite that its formation may be independent of the genesis and development of cyclones, cyclone activity may still have an influence on ARs development [18,26]. Several studies have suggested the influence of cyclones and ARs on the extent of sea ice across the Arctic region. Hegyi and Taylor [27] have demonstrated that episodic Arctic ARs actively contribute to the evolution of Arctic sea ice during the ice growth season. Moreover, Komatsu et al. [28] investigated the influence of Siberian ARs entering the Arctic and noted an amplification of warming over the region in summer. The effects of enhanced moisture transport can be diverse. On the one hand, enhanced moisture transport may produce increased down-welling longwave fluxes, warming the Arctic and affecting the sea ice extent for example, [29]. On the other hand, precipitation can have different effects on the sea ice depending on the type of precipitation and its intensity [30].

Despite the importance of ARs in moisture transport and of their influence on Arctic warming for example, [31] and on the extent of sea ice [27,28], their influences on the region have not yet been deeply investigated in relation to the terms pointed out here. Some studies have investigated the moisture sources for ARs from a Eulerian [32] or a Lagrangian point of view for different regions in Europe for example, [33–35], North America [36–38] and South Africa [39]; however, as far as we know, no such studies have been performed for the Arctic region. The aim of this work was to take the first step in a more complete analysis of the evolution of ARs moving toward the Arctic and their influence over the region. To this end, the regions near the Arctic most affected by ARs were identified to determine the origins of the moisture associated with these ARs throughout the period 1997–2014.

2. Materials and Methods

2.1. Area of Maximum Occurrence of Atmospheric Rivers to the Arctic

In order to investigate the incidence of ARs over the Arctic region, the ARs database developed by Guan and Waliser [19] was used. This database provides the locations of the central axes of ARs on a global scale with horizontal resolution of 2.5° × 2.5° through the year with a time step of 6 h (00, 06, 12, 18 UTC). AR detection is based on computing of the vertically integrated horizontal water vapour transport (IVT) from 1000 to 300 hPa, taking into account the specific humidity and wind field retrieved from the ECMWF Interim reanalysis (ERA-Interim) [40]. In each grid cell, the 85th percentile was applied as a threshold with a fixed lower limit of 100 $kg{\cdot}m^{-1}s^{-1}$ (for polar regions). Once the threshold was applied, the coherence on the IVT direction was analysed by discarding those regions in which more than half of the grid cells showed deviations of more than 45° from the mean IVT and in those that did not have an appreciated poleward component. Further details can be found at Guan and Waliser [19]. From this procedure, a set of ARs was detected.

From the previous database, the regions of maximum occurrence of ARs were identified for every season of the year for the period 1997–2014. Only ARs reaching the Arctic region were taken into account. Thus, a 10° latitudinal band centred on 60° N all around the Arctic was selected to identify the areas of maximum occurrence. In order to define this area seasonally, the total number of AR events occurring between 55° and 65° N were calculated for every longitude. The 75th percentile was calculated for every longitudinal series to objectively define the maximum values of the field. So, the areas of maximum AR entrance into the Arctic was defined as those regions where the ARs frequency was greater than this value. The boxes defined for those longitudinal areas and between 55° and 65° N are hereinafter described as the 'ARs pathway boxes' to the Arctic.

2.2. Moisture Sources

In order to identify the source regions of moisture associated with the AR pathway boxes, the outputs of the FLEXPART v9.0 model [41] run in backward mode was used. ERA-Interim reanalysis data at 1° horizontal resolution was used to feed FLEXPART the initial and boundary conditions commonly used [41,42]. In our model configuration, the complete atmosphere is divided into the maximum number (about 2 million) of air parcels (or particles) which are dispersed following the 3-D wind field. For every air parcel, the specific humidity (q, measured in g/kg) and the position of the grid cell is stored every 6 h and moisture changes can be expressed as

$$\boldsymbol{e - p = m \ \ dq/dt} \tag{1}$$

in which $\boldsymbol{e}$ and p represent moisture increases and decreases, m is the mass of the particle expressed in kg and t is the time. If $(\boldsymbol{e - p})$ for all the particles at every grid position is considered, the total surface freshwater flux $(\boldsymbol{E - P})$ can be obtained as follows.

$$\boldsymbol{E - P} \ = \ \frac{\sum_{k=1}^{K} (\boldsymbol{e - p})}{\boldsymbol{A}} \tag{2}$$

where $(\boldsymbol{E})$ and $(\boldsymbol{P})$ are the rates of evaporation and precipitation per unit area, respectively; $\boldsymbol{A}$ is the area of the grid cell and $\boldsymbol{K}$ is the total number of particles in the atmospheric column. This methodology developed by Stohl and James [42,43] allows tracking of trajectories backward and forward in time. Forward tracking from source areas allows the study of moisture losses (regions where precipitation exceed evaporation) along the trajectories and then the identification of sinks of moisture $(E - P) < 0$). In addition, backward tracking from a specific area allows identification of those regions where particles gained moisture (evaporation exceed precipitation) before reaching the area of interest. In our case, in other words, moisture sources were indicated by $((E - P) > 0)$. This methodology has been widely used in moisture transport analysis over different areas and has been associated with different precipitation systems [33,44,45].

In this study, the backward methodology mentioned above was applied in order to find those regions where there is anomalous moisture available to be taken up by the ARs reaching the Arctic. The same procedure employed by Ramos et al. [33,39] was applied. Following this, backward trajectories were tracked for 10 days at 6 h intervals (40 time steps) for every AR event identified across the area of maximum AR occurrence every month. This period of 10 days is considered the average time of water vapour residence in the atmosphere [46] and for which Lagrangian trajectories can be considered relatively accurate [41].

With the purpose of computing the moisture uptake associated with ARs events, only positive values of $(E - P)$ were retained at each and every time step. The procedure used to obtain the area of anomalous moisture uptake is the following:

(a) Considering every case of AR occurrence at 6 h intervals (taking into account the 10 day backward trajectories), the moisture uptake $((\boldsymbol{E - P}) > \boldsymbol{0})$ is calculated individually for every case.

(b) The 'climatology' for the corresponding ARs cases is obtained, taking into account the moisture uptake for the corresponding time step over the entire period 1997–2014.

In this work, an AR case was defined as every one of the times at which an AR occurred within a 6 h interval. For example, if an AR took place from 00:00 UTC to 18:00 UTC on 15 September 1999, 4 AR cases would be considered (00, 06, 12 and 18 UTC). The climatology was calculated considering only the dates of ARs occurrence but included the entire 18-year period taken into account in this study (1997–2014). For instance, if an AR case was detected on 15 September 1999 at 12:00 UTC over the complete ARs pathway boxes previously defined, the climatology would consider the 15 September at 12:00 for every year within the period 1997–2014. This procedure was carried out for the sake of saving computing resources, by avoiding dates when AR activity was negligible.

The area of anomalous moisture uptake for every individual AR case was calculated by the difference between the (a) AR-case moisture uptake and (b) 'climatological' moisture uptake.

Once the anomalous moisture uptake was calculated for every case, the total amount associated with AR events was calculated by adding in the positive anomalies in moisture uptake for every individual case. Thus, we obtained those areas where the ARs gain more moisture along their trajectories. This result will be denoted hereinafter as $(E-P)ANOM > 0$. In the same way as for the moisture uptake anomalies, the total moisture uptake associated with ARs cases was obtained by adding the moisture sources ($(E-P) > 0$ values) for all the cases identified. These results are denoted as $(E-P)CLIM > 0$.

3. Results

3.1. Maximum Areas of AR Occurrence in the Arctic Region

In order to define the areas of maximum AR occurrence, Figure 1 shows the number of ARs for each longitude from 55° to 65° N (line plot) and their geographical distribution for every season (colour band map). On these figures, blue lines represent the longitudinal variability in the number of ARs and the horizontal red line represents the value of its 75th percentile. Embedded at the bottom for every month, the AR frequency that appears represents every grid point over the longitudinal band previously defined. On this plot, reddish colours represent higher occurrence and bluish colours represent lower AR frequency.

In general, the regions of major occurrence are located mainly over the Atlantic sector (from 80° W to 60° E) and the Pacific sector (from 120° to 240° E). The maximum AR activity on the edge of the Arctic occurs in autumn for the Atlantic sector and in summer for the Pacific sector (coloured map); however, minimal activity takes place in spring for both sectors.

For the Atlantic sector, most of the ARs that reach the Arctic region cross 60° N over the Norwegian Sea on a band between 50° W and 15° E for every season. Moreover, the Davis Strait is an important pathway for the ARs entering the Arctic. This region is the main entrance area in summer and shows high AR occurrence in spring and autumn too. Despite it was not defined as an ARs pathway region from the methodology applied, some entrance occurs over Europe in autumn, being especially relevant in October (see Supplementary Materials, Figure S1).

For the Pacific sector, three different regions of AR activity can be defined: the Gulf of Alaska, the Bering Sea and North Asia. In winter and autumn most of the ARs enter the Arctic across the Gulf of Alaska, between 190° and 240° E approximately. However, in the remaining seasons, AR pathway is displaced westward into the Bering Sea. This is especially relevant in summer when the ARs pathway box expands from 127° to 210° E including continental areas over Siberia, the complete Bering Sea and part of the Gulf of Alaska. In general terms the Pacific ARs pathway boxes show lower extension than Atlantic ones, being summer the only exception.

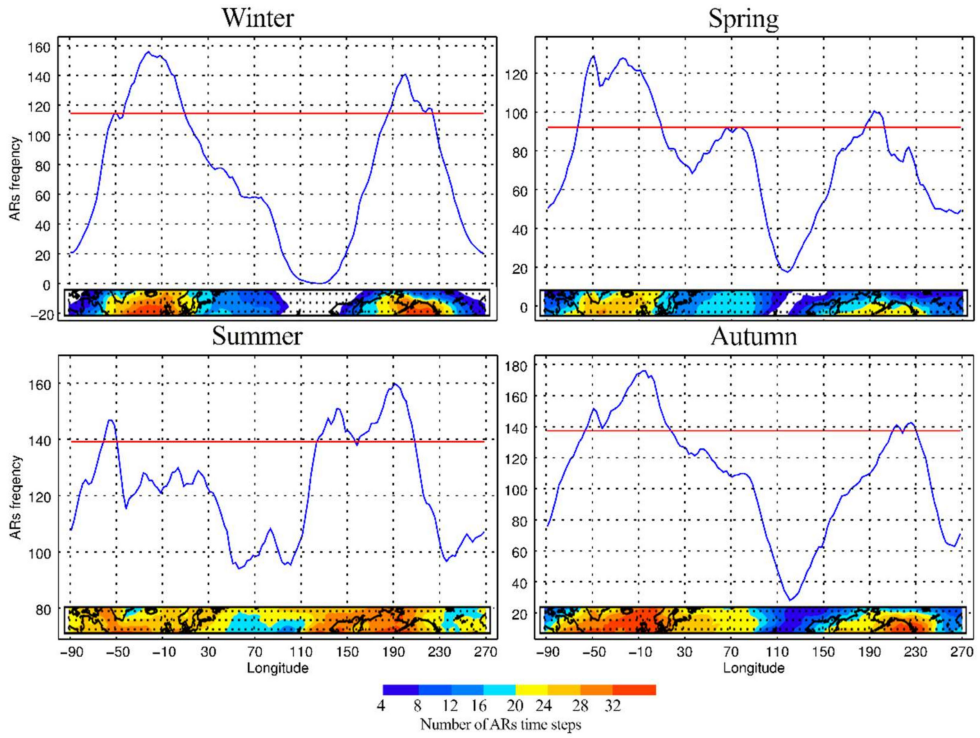

Figure 1. AR frequency over the area between 55° and 65° N over the period 1997–2014: The blue line represents the number of ARs for every longitude and the box embedded in the plot shows the spatial distribution of the ARs. Reddish colours represent areas with higher AR frequency and bluish colours those with lower. The red lines depict the 75th percentile of the distribution.

It is important to highlight the summer situation, not only for the higher Pacific box extension but also for the homogeneity on the AR occurrence. In this season more than 20 ARs time steps are identified at some grid point of the complete longitudinal band. Moreover, it shows high intraseasonal variability in this season (see Supplementary Materials, Figure S1). June show the lower AR occurrence, not only referred to summer but also to the whole year; however, in July and August, the occurrence highly increases especially over the Pacific sector in August. Important intraseasonal variability also occurs in autumn. The number of ARs time steps identified per longitude decreased from 20 to 73 in September to 2 to 56 in November. Moreover, the Atlantic pathway showed an important variability on its location.

3.2. Climatology for the Moisture Sources

Once the areas of the AR pathways into the Arctic were defined for every month, it was possible to analyse their sources of moisture. For this purpose, Figure 2 shows the climatological sources, those regions with $(E-P)CLIM > 0$ values, for every season for the entire period 1997–2014.

For the Atlantic sector, most of the moisture uptake occurs over the North Atlantic, the Labrador Sea and the Norwegian Sea. For all the season with the exception of summer, $(E-P)CLIM$ shows important moisture uptake over the western Atlantic Ocean between 30° and 40° N. These sources expand north-eastward toward the Arctic. The moisture uptake over this area is especially intense in autumn, being the main moisture source for the Atlantic pathway box. Intense moisture uptake also occurs over the northern part of the ocean, the Davis Strait and the Norwegian Sea with values higher than 2 mm/day over most of these areas. Finally, for this season, some continental moisture uptake occurs over the east coast of the United States, however this continental contribution has lower intensity than the oceanic contribution. A maximum of $(E-P)CLIM$ also occurs over the pathway area in winter and spring expanding toward the Norwegian Sea. In spring some $(E-P)CLIM$ values appear over continental areas in the eastern part of North America and over Europe, showing higher

values over the British Isles and northern Europe coast. In summer, continental moisture uptake highly increase referred to the previous season, especially over North America and the Scandinavian Peninsula. Concerning North America, the maximum $(E-P)CLIM$ occurs in areas over the Quebec Peninsula and the north-eastern part of the United States, however some moisture contribution appears from almost all of North America. Major moisture uptake in the oceanic areas is also found during this season, being located eastward of the ARs pathway box mainly to the east of Greenland and around 70°.

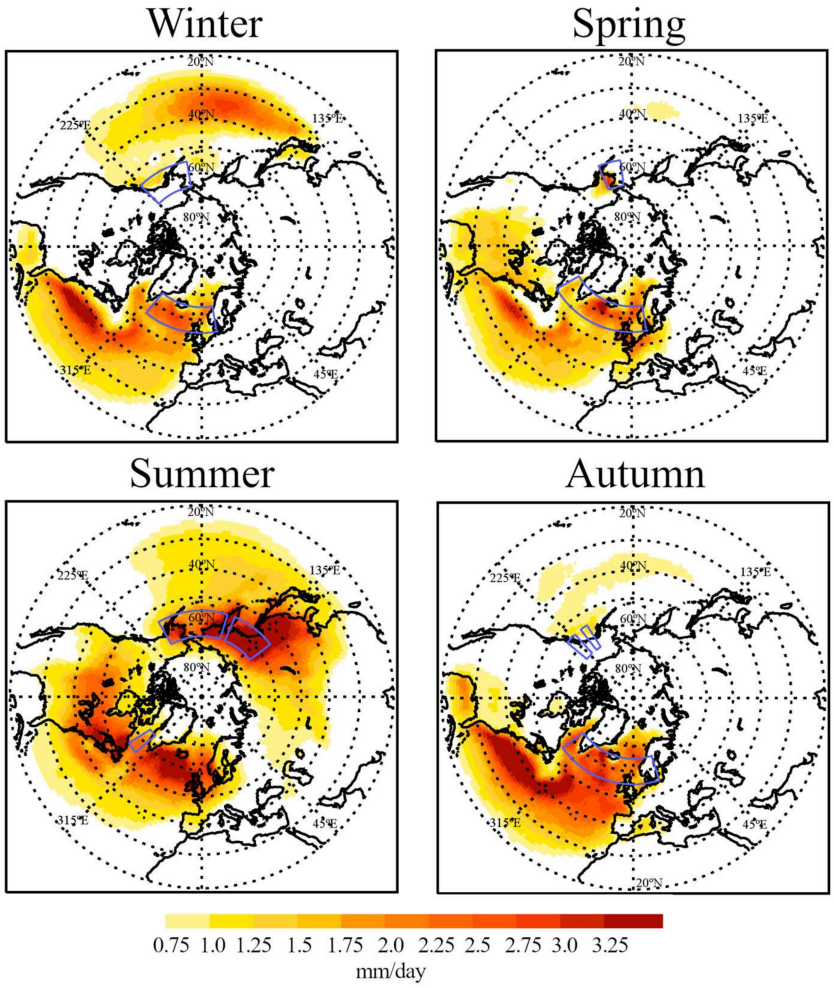

Figure 2. Climatological moisture sources ($(E-P)CLIM > 0$ regions) throughout the period 1997–2014 for the regions of maximum AR occurrence represented by blue boxes. Scale in mm/day.

For the Pacific sector, the moisture sources are located mainly over the Pacific Ocean and eastern Asia. In winter, moisture uptake regions expand along the ocean from the western North Pacific to the Gulf of Alaska, with maximum $(E-P)CLIM$ located westward on the band between 30° and 40° N. In summer, however, the highest values of $(E-P)CLIM$ are located over continental areas. These areas show a remarkably intense moisture uptake with values higher than 3 mm/day over western Alaska and eastern Eurasia. In general, some moisture contribution to the ARs pathway box is observed over most of northern Eurasia. Moisture uptake is also observed over oceanic areas south of 50° N in the western Pacific; however, it shows values lower than 1.5 mm/day for most of the area. Higher values appear on northern latitudes over the Bering Sea and the Sea of Okhotsk. In spring and autumn, $(E-P)CLIM$ shows low values and extension. In spring, a small area with values lower than 1 mm/day appears over western Pacific between 30° and 40° N. Higher moisture uptake occurs over continental areas in western Alaska, coinciding with the position of the ARs pathway box. Finally,

in autumn some moisture contribution to the box occurs over the Gulf of Alaska and a small area crossing the Pacific Ocean from west to east.

3.3. Anomalous Moisture Uptake

The climatological moisture sources for the AR pathway boxes (taking into count not only the ARs time steps) show where the moisture that feeds that region comes from, however the mechanism for the anomalous moisture uptake to the AR events can be different. In order to address which of those sources are specifically associated with AR events, Figure 3 shows anomalies in the moisture uptake for the AR events referring to the complete climatology for every season ($(E-P)ANOM$).

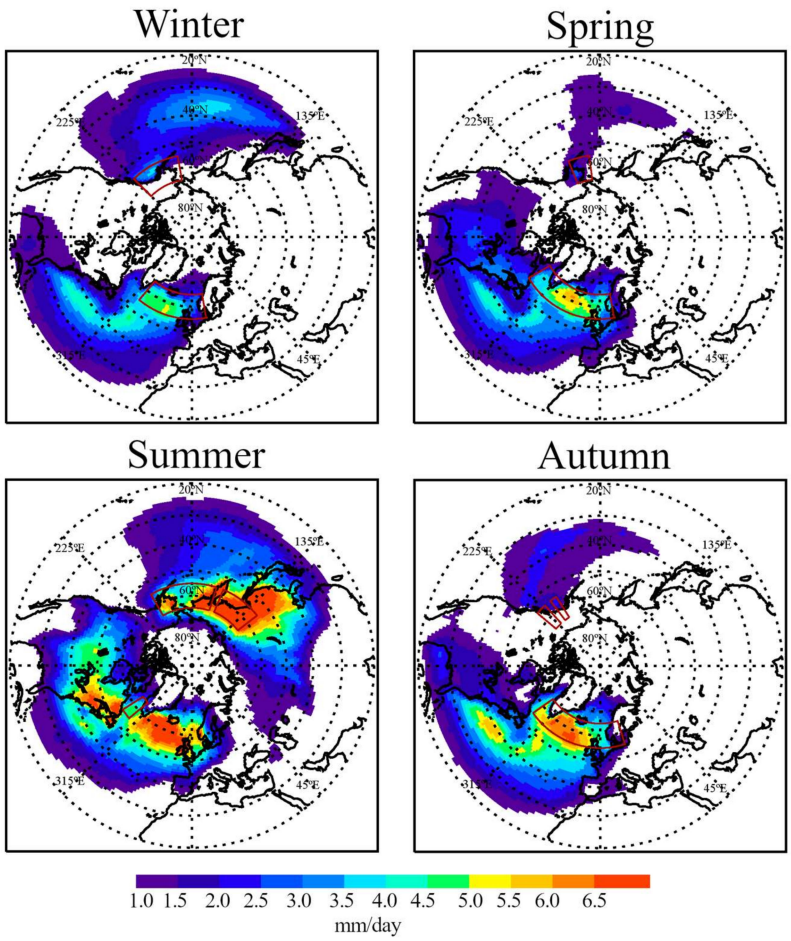

Figure 3. Anomalies for AR moisture uptake ($(E-P)ANOM > 0$) calculated for those days when an AR event was identified over the AR pathway regions (red boxes) and referring to the climatological value over the period 1997–2014. Scale in mm/day.

In general positive anomaly values are found over the main 'climatological' sources, reinforcing them, for Arctic AR events (Figure 2). However, some differences should be addressed.

Concerning the Atlantic sector in winter, positive anomalies of moisture uptake associated with AR events appear over most of the North Atlantic Ocean and the Gulf of Mexico, coinciding with the AR climatological sources (Figure 2). However, the maximum increase in moisture uptake occurs over the oceanic AR pathway box (from the area to the east of the southern coast of Greenland and the western British Isles coast). The anomaly is weaker over the southern part of the North Atlantic Ocean, where the maximum moisture uptake is observed for the AR events climatology. In spring the situation is quite similar, however, the intensification of the moisture uptake over the ARs pathway box is higher and it expands into the Norwegian Sea and the Davis Strait. In summer, anomalous and

climatological AR sources have a similar distribution. Higher values on $(E-P)ANOM$ for this season appear over the Quebec Peninsula and the northern Atlantic Ocean around 60° N. Finally, in autumn, the same pattern as for the winter and spring occurs. The highest increase of moisture uptake occurs over the pathway box. For these months some increase over continental areas of North America is also observed.

For the Pacific sector, in winter, despite that the main AR source is located over the North Pacific; this region shows similar increase in moisture uptake as that in the AR pathway box over the Gulf of Alaska. Moreover, positive anomalies occur over most of the ocean north of 30° N. In summer months, continental $(E-P)ANOM$ values show similar distribution as that of the climatological AR sources. Oceanic areas show lower anomalies than in the continental areas for these months. Finally, in spring and autumn, $(E-P)ANOM$ show the lower values. In spring, positive anomalies appear over the central part of the northern Pacific Ocean and expand westward between 30° and 40° N. In autumn the area showing the maximum positive anomaly expands south-westward from the Gulf of Alaska into the Pacific Ocean. In general, for spring and autumn, the $(E-P)ANOM$ shows a higher extension that the climatological ARs' source areas.

3.4. A Case of Study

To exemplify the described phenomena, we have analysed a case study of an AR reaching the Arctic during 6 September 1997 within the Atlantic AR pathway box. This AR shows the maximum spatially integrated vapour transport (IVT) activity in fall (when the ARs entrance is maxima over this area) during the completely studied period. Figure 4 shows the integrated column of water vapour (IWV) together with IVT for the case of study. Figure 4a–d show a well-defined AR and the four 6 h time steps highlight its evolution and illustrate the transient process which leads the advective transport from (sub)tropical latitudes to the Arctic. At 00 UTC, the AR reaches the southern coast of Greenland, displacing eastward in the following time steps and reaching the Iceland coast at 18 UTC.

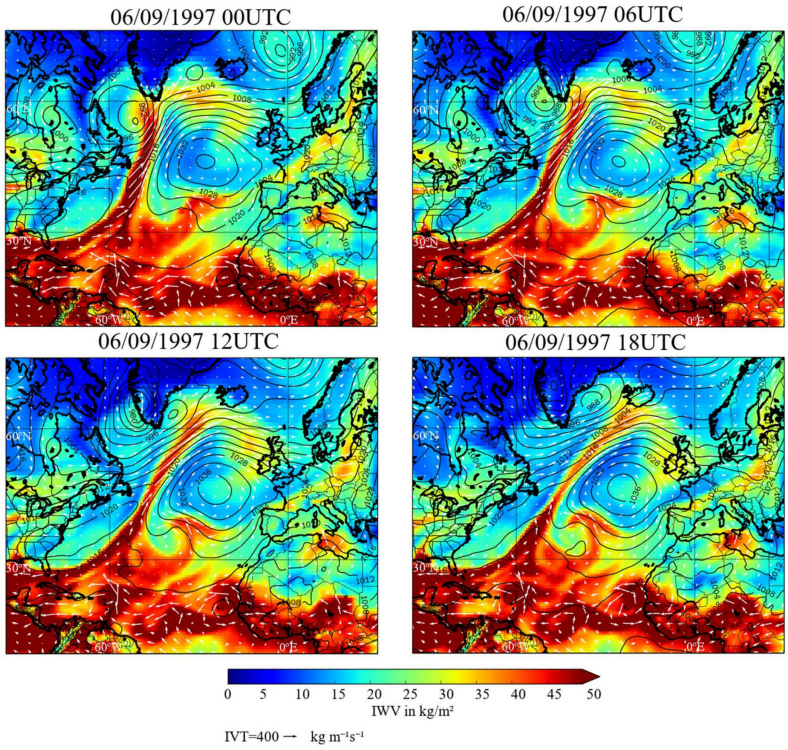

Figure 4. Integrated Water vapour column (IWV) and IVT for the AR event occurred on 6 September 1997. Black isolines represent the Mean Sea Level Pressure in hPa.

Figure 5 shows the budget E-P for every time-step stated in Figure 4. Negative values of E-P are located in regions of maximum IVT. Referred to moisture uptakes, they occur at both sides of the AR and mostly coincide with high-pressure centres (black isolines on Figure 4). On the right side, important moisture uptakes can be found over the North Atlantic in coincidence with a high-pressure area. The same occurs near to the US West Coast. Despite the maximum moisture uptake can be found at lower latitudes, the AR continues to gain moisture as it moves towards the Arctic, with moisture uptakes over the pathway box.

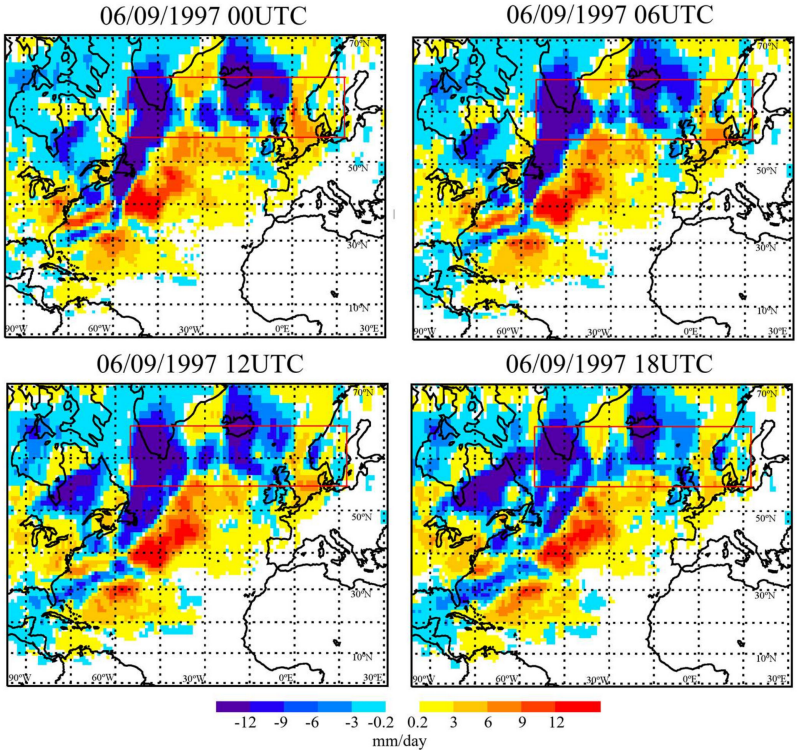

Figure 5. Total (E-P) values calculated for the 6 September 1997 (at every time step). The red box represents the ARs pathway box for the season. Scale in mm/day.

4. Discussion

In the present work, the area of maximum occurrence of the ARs reaching the Arctic (crossing the latitudinal band of 60° N) was located for every season. From the results, two different sectors of AR occurrence were defined: the Atlantic and the Pacific. In general terms, these areas are coincident with regions of extreme moisture intrusion over the Arctic found in previous studies [15,17]. Referring to the Atlantic sector, most of the ARs reach the Arctic region by crossing the Norwegian Sea. This is the most common way in the storm tracks into the Arctic [25] and their occurrence has been suggested to influence the Arctic Sea ice lost north of Eurasia [11,47,48]. Despite the general path followed by ARs, in late spring and summer (Figure 1 and Supplementary Materials, Figure S1), the AR activity moves westward occurring mainly over the Davis Strait. This seasonality in the AR pathway area is consistent with the previous study conducted by Liu and Barnes [16]. In the latter work, the relation between ARs and Rossby Wave Breaking (RWB) was analysed as they appeared in both the Davis Strait and the Norwegian Sea. In these areas, the maximum extreme moisture events were associated with cyclonic (C) and anticyclonic (A), RWB over the Davis Strait and the Norwegian Sea respectively. Despite from our results a relation between the ARs moisture uptake and RWB cannot be addressed, the seasonality of the CRWB and ARWB found previous work is consistent with the seasonality observed in the present work, occurring the highest moisture uptake over the Davis Strait in autumn coinciding with the strongest CRWB related transport. Referring to the Pacific sector, seasonal variability of the AR

pathway areas can also be addressed, they are located over the Gulf of Alaska in winter (Figure 1), late summer and early autumn (see Supplementary Materials, Figure S1); and over the Bering Sea in summer in August (see Supplementary Materials, Figure S1). These findings are also consistent with those described by Liu and Barnes [16]. In summer, an important AR entrance into the Arctic is observed to occur over continental areas in North Asia and Komatsu et al. [28] documented the existence of Siberian ARs reaching the Arctic in this season. The highest number of ARs entering the Arctic across the North Pacific region coincides with the previous results of Kamae et al. [49]. This work addressed the northward shift of the North Pacific AR peak occurrence area and found that in summer, ARs are most frequent over far eastern Eurasia.

Having analysed the moisture sources for the maximum AR areas of occurrence identified, it can be asserted that most of the moisture comes from the Pacific and the Atlantic Ocean for the respective sectors. Moreover, in general, important moisture support occurs over the AR pathway area itself, especially for the Atlantic sector. In summer the moisture taken up has mainly continental origins, being especially relevant over eastern Asia for the Pacific sector. This variability in the oceanic and continental origins seems to be related to the general moisture transport into the Arctic previously investigated by Vázquez et al. [50]. In summer, continental areas are more evaporative [51] and supply a greater amount of moisture to the Arctic region in general [50,52]. The main oceanic regions of moisture uptake are located along the paths of the global western boundary currents, where the strongest increase in evaporation was observed in the last decades [53]. These regions have been determined to be the main moisture sources for the Arctic system, especially in winter [50]. This suggests that these climatological moisture sources also have great influence on the transport of moisture by ARs and probably on their development. These oceanic areas were previously proposed as the path of winter ARs [15] and in general, were the most common path for Arctic cyclones [25]. Moreover, they are the most evaporative oceanic areas in the Northern Hemisphere [54] for this season.

Focusing attention on the anomalous moisture sources where the ARs take moisture up, it can be observed that the more important ones occur near the band of 60° N, northward to the climatological sources of moisture. This fact suggests that, despite climatological sources being crucial to the development of the ARs, enhanced continuous moisture uptake along the path of the ARs should exist along the northern transition of ARs into the Arctic. As suggested by previous studies, despite the tropical origin of ARs, most of them also incorporate mid-latitude sources and convergences of local vapour along their paths [55]. Over eastern Eurasia, where higher increases in moisture supply were found in summer, the precipitable water flux is much more intense in this season [52]. Sorteberg and Walsh [25] found a westward shift on the cyclone track that crosses the Bering Strait in this season, crossing the continental areas of far eastern Eurasia. This shift could affect not only the cyclone track but also the AR poleward path and increased moisture uptake over these continental areas. Moreover, Dufour et al. [56] associated most of the meridional moisture transport across 70° N to transient eddies, especially in winter. However, from the analysis of the case of study it can be addressed that the anomalous moisture uptake is not coincident with the maximum IVT value of the AR and it occurs on the edges of the AR pathway, being also important the increase of moisture uptake at the end of the path (over the AR pathway box). This result agreed with the finding of Ramos et al. [33].

5. Conclusions

To conclude, we investigated the main entrance paths for the ARs reaching the Arctic region using a systematic methodology. Moreover, the Lagrangian model FLEXPART was used to analyse the areas of maximum moisture uptake associated with the occurrence of Arctic ARs. From the results, two main sectors can be defined as AR entrance paths, the Atlantic sector and the Pacific sector. Most of the moisture taken up on the ARs trajectories comes from the Atlantic Ocean and the Pacific Ocean respectively; however, important continental moisture sources appear over North America and Eurasia, especially in the summer months. Southern moisture sources coincide in general terms with climatological evaporative areas proven to have an influence on poleward moisture transport

toward the Arctic. However, an increase on northern moisture uptake specifically associated with the occurrence of Arctic ARs was observed. This increase is especially relevant over the main pathway area along 60° N.

This work has taken the initial step toward analysis of the origin of moisture transported by Arctic ARs. Further analysis should be performed in order to characterise the influence of ARs on Arctic moisture transport and to understand the evolution of ARs toward the Arctic. The forward Lagrangian analysis from AR sources could be carried out to investigate the effectiveness of the poleward moisture transport from these meteorological structures. If positive trends are found in evaporation over the oceanic sources that influence major occurrences of ARs or in major transport of moisture that precipitates over the Arctic, these results could eventually lead to reasons for the further loss of sea ice extent during the last decades. These analyses would be the subject of future work.

Supplementary Materials: The following are available online at http://www.mdpi.com/2073-4441/11/1/41/s1, Figure S1. AR frequency over the area between 55° and 65° N over the period 1997–2014: The blue line represents the number of ARs for every longitude and the box embedded in the plot shows the spatial distribution of the ARs. Reddish colors represent areas with higher AR frequency and bluish colors those with lower. The red lines depict the 75th percentile of the distribution.

Author Contributions: Conceptualisation, R.N. and L.G.; Methodology, R.N. and A.M.R.; Software, M.V., I.A. and R.N.; Formal Analysis, M.V., I.A. and R.N.; Writing-Original Draft Preparation, M.V. and J.E.B.; Writing-Review & Editing, I.A., A.M.R., R.N and L.G.; Visualisation, M.V., I.A.; Supervision, R.N. and L.G.; Project Administration, L.G. and R.N.; Funding Acquisition, L.G. and R.N.

Funding: This research was funded by the Spanish Government within the EVOCAR (CGL2015-65141-R) project, which is also funded by FEDER. Alexandre M. Ramos was also supported by a FCT postdoctoral grant (FCT/DFRH/SFRH/BPD/84328/2012). This work was partially supported by Xunta de Galicia under Project ED431C 2017/64-GRC 'Programa de Consolidación e Estruturación de Unidades de Investigación Competitivas (Grupos de Referencia Competitiva).' Marta Vázquez and Jorge Eiras-Barca were also supported by Xunta de Galicia under grant ED481B 2018.

Acknowledgments: We acknowledge Bin Guan for providing the AR data.

Conflicts of Interest: The authors declare no conflict of interest. The funders had no role in the design of the study; in the collection, analyses or interpretation of data; in the writing of the manuscript or in the decision to publish the results.

References

1. Pithan, F.; Mauritsen, T. Arctic amplification dominated by temperature feedbacks in contemporary climate models. *Nat. Geosci.* **2014**, *7*, 181–184. [CrossRef]
2. Stroeve, J.; Holland, M.M.; Meier, W.; Scambos, T.; Serreze, M. Arctic sea ice decline: Faster than forecast. *Geophys. Res. Lett.* **2007**, *34*. [CrossRef]
3. Cavalieri, D.J.; Parkinson, C.L. Arctic sea ice variability and trends, 1979–2010. *Cryosphere* **2012**, *6*, 881–889. [CrossRef]
4. Comiso, J.C.; Hall, D.K. Climate trends in the Arctic as observed from space. *WIREs Clim. Chang.* **2014**, *5*, 389–409. [CrossRef] [PubMed]
5. Comiso, J.C.; Parkinson, C.L.; Gersten, R.; Stock, L. Accelerated decline in the Arctic sea ice cover. *Geophys. Res. Lett.* **2008**, *35*, L01703. [CrossRef]
6. Parkinson, C.L.; DiGirolamo, N.E. New visualizations highlight new information on the contrasting Arctic and Antarctic sea-ice trends since the late 1970s. *Remote Sens. Environ.* **2016**, *183*, 198–204. [CrossRef]
7. Stroeve, J.C.; Kattsov, V.; Barrett, A.; Serreze, M.; Pavlova, T.; Holland, M.; Meier, W.N. Trends in Arctic sea ice extent from CMIP5, CMIP3, and observations. *Geophys. Res. Lett.* **2012**, *39*, L16502. [CrossRef]
8. Serreze, M.C.; Holland, M.M.; Stroeve, J. Perspectives on the Arctic's Shrinking Sea-Ice Cover. *Science* **2007**, *315*, 1533–1536. [CrossRef]
9. Comiso, J.C. A rapidly declining perennial sea ice cover in the Arctic. *Geophys. Res. Lett.* **2002**, *29*, 17. [CrossRef]
10. Proshutinsky, A.Y.; Johnson, M.A. Two circulation regimes of the wind-driven Arctic Ocean. *J. Geophys. Res. Oceans* **1997**, *102*, 12493–12514. [CrossRef]

11. Parkinson, C.L.; Comiso, J.C. On the 2012 record low Arctic sea ice cover: Combined impact of preconditioning and an August storm. *Geophys. Res. Lett.* **2013**, *40*, 1356–1361. [CrossRef]
12. Mortin, J.; Svensson, G.; Graversen, R.G.; Kapsch, M.L.; Stroeve, J.C.; Boisvert, L.N. Melt onset over Arctic sea ice controlled by atmospheric moisture transport. *Geophys. Res. Lett.* **2016**, *43*, 6636–6642. [CrossRef]
13. Zhang, X.; He, J.; Zhang, J.; Polyakov, I.; Gerdes, R.; Inoue, J.; Wu, P. Enhanced poleward moisture transport and amplified northern high-latitude wetting trend. *Nat. Clim. Chang.* **2012**, *3*, 47–51. [CrossRef]
14. Simmond, I.; Keay, K. Extraordinay September Arctic sea ice reductions and their relationship with storm behavior over 1979–2008. *Geophys. Res. Lett.* **2009**, *36*, L19715. [CrossRef]
15. Newman, M.; Kiladis, G.N.; Weickmann, K.M.; Ralph, F.M.; Sardeshmukh, P.D. Relative Contributions of Synoptic and Low-Frequency Eddies to Time-Mean Atmospheric Moisture Transport, Including the Role of Atmospheric Rivers. *J. Clim.* **2012**, *25*, 7341–7361. [CrossRef]
16. Liu, C.; Barnes, E.A. Extreme moisture transport into the Arctic linked to Rossby wave breaking. *J. Geophys. Res. Atmos.* **2015**, *120*, 3774–3788. [CrossRef]
17. Woods, C.; Caballero, R.; Svensson, G. Large-scale circulation associated with moisture intrusions into the Arctic during winter. *Geophys. Res. Lett.* **2013**, *40*, 4717–4721. [CrossRef]
18. Zhu, Y.; Newell, R.E. A proposed algorithm for moisture fluxes from atmospheric rivers. *Mon. Weather Rev.* **1998**, *126*, 725–735. [CrossRef]
19. Guan, B.; Waliser, D.E. Detection of atmospheric rivers: Evaluation and application of an algorithm for global studies. *J. Geophys. Res. Atmos.* **2015**, *120*, 12514–12535. [CrossRef]
20. Gimeno, L.; Dominguez, F.; Nieto, R.; Trigo, R.; Drumond, A.; Reason, C.J.C.; Taschetto, A.S.; Ramos, A.M.; Kumar, R.; Marengo, J. Major mechanisms of atmospheric moisture transport and their role in extreme precipitation events. *Annu. Rev. Environ. Resour.* **2016**, *41*, 117–141. [CrossRef]
21. Ralph, F.M.; Neiman, P.J.; Wick, G.A.; Gutman, S.I.; Dettinger, M.D.; Cayan, D.R.; White, A.B. Flooding in California's Russian River: Role of atmospheric river. *Geophys. Res. Lett.* **2006**, *33*, L13801. [CrossRef]
22. Lavers, D.A.; Villarini, G. The nexus between atmospheric rivers and extreme precipitation across Europe. *Geophys. Res. Lett.* **2013**, *40*, 3259–3264. [CrossRef]
23. Leung, L.R.; Qian, Y. Atmospheric rivers induced heavy precipitation and flooding in the western U.S. simulated by the WRF regional climate model. *Geophys. Res. Lett.* **2009**, *36*, L03820. [CrossRef]
24. Gimeno, L.; Nieto, R.; Vázquez, M.; Laver, D.A. Atmospheir river: A mini-review. *Front. Earth Sci.* **2014**, *2*, 2.1–2.6. [CrossRef]
25. Sorteberg, A.; Walsh, J.E. Seasonal cyclone variability at 70°N and its impact on moisture transport into the Arctic. *Tellus A* **2008**, *60*, 570–586. [CrossRef]
26. Eiras-Barca, J.; Ramos, A.M.; Pinto, J.G.; Trigo, R.M.; Liberato, M.L.R.; Miguez-Macho, G. The concurrence of atmospheric rivers and explosive cyclogenesis in the North Atlantic and North Pacific basins. *Earth Syst. Dyn.* **2018**, *9*, 91–102. [CrossRef]
27. Hegyi, B.M.; Taylor, P.C. The Unprecedented 2016–2017 Arctic Sea Ice Growth Season: The Crucial Role of Atmospheric Rivers and Longwave Fluxes. *Geophys. Res. Lett.* **2018**, *45*, 5204–5212. [CrossRef]
28. Komatsu, K.K.; Alexeev, V.A.; Repina, I.A.; Tachibana, Y. Poleward upgliding Siberian atmospheric rivers over sea ice heat up Arctic upper air. *Sci. Rep.* **2018**, *8*, 2872. [CrossRef]
29. Woods, C.; Caballero, R. The role of moist intrusions in winter Arctic warming and sea ice decline. *J. Clim.* **2016**, *29*, 4473–4485. [CrossRef]
30. Vihma, T.; Screen, J.; Tjernström, M.; Newton, B.; Zhang, X.; Popova, V.; Deser, C.; Holland, M.; Prowse, T. The atmospheric role in the Arctic water cycle: A review on processes, past and future changes, and their impacts. *J. Geophys. Res. Biogeosci.* **2016**, *121*, 586–620. [CrossRef]
31. Baggett, C.; Lee, S.; Feldstein, S. An Investigation of the Presence of Atmospheric Rivers over the North Pacific during Planetary-Scale Wave Life Cycles and Their Role in Arctic Warming. *J. Atmos. Sci.* **2016**, *73*, 4329–4347. [CrossRef]
32. Eiras-Barca, J.; Dominguez, F.; Hu, H.; Garaboa-Paz, D.; Miguez-Macho, G. Evaluation of the moisture sources in two extreme landfalling atmospheric river events using an Eulerian WRF tracers tool. *Earth Syst. Dyn.* **2017**, *8*, 1247–1261. [CrossRef]
33. Ramos, A.M.; Nieto, R.; Tomé, R.; Gimeno, L.; Trigo, R.M.; Liberato, M.L.R.; Lavers, D.A. Atmospheric rivers moisture sources from a Lagrangian perspective. *Earth Syst. Dyn.* **2016**, *7*, 371–384. [CrossRef]

34. Liberato, M.L.R.; Ramos, A.M.; Trigo, R.M.; Trigo, I.F.; Durán-Quesada, A.M.; Nieto, R.; Gimeno, L. Moisture Sources and Large-Scale Dynamics Associated With a Flash Flood Event. In *Lagrangian Modeling of the Atmosphere*; Lin, J., Brunner, D., Gerbig, C., Stohl, A., Luhar, A., Webley, P., Eds.; American Geophysical Union: Washington, DC, USA, 2012.
35. Sodemann, H.; Stohl, A. Moisture Origin and Meridional Transport in Atmospheric Rivers and Their Association with Multiple Cyclones. *Mon. Weather Rev.* **2013**, *141*, 2850–2868. [CrossRef]
36. Moore, B.J.; Neiman, P.J.; Ralph, F.M.; Barthold, F.E. Physical processes associated with heavy flooding rainfall in Nashville, Tennessee, and vicinity during 1–2 May 2010: The role of an atmospheric river and mesoscale convective systems. *Mon. Weather Rev.* **2012**, *140*, 358–378. [CrossRef]
37. Rutz, J.J.; Steenburgh, W.J.; Ralph, F.M. The Inland Penetration of Atmospheric Rivers over Western North America: A Lagrangian Analysis. *Mon. Weather Rev.* **2015**, *143*, 1924–1944. [CrossRef]
38. Ryoo, J.-M.; Waliser, D.E.; Waugh, D.W.; Wong, S.; Fetzer, E.J.; Fung, I. Classification of atmospheric river events on the U. S. West Coast using a trajectory model. *J. Geophys. Res. Atmos.* **2015**, *120*, 3007–3028. [CrossRef]
39. Ramos, A.M.; Blamey, R.C.; Algarra, I.; Nieto, R.; Gimeno, L.; Tomé, R.; Reason, C.J.; Trigo, R.M. From Amazonia to southern Africa: Atmospheric moisture transport through Low Level Jets and Atmospheric Rivers. *Ann. N. Y. Acad. Sci.* **2018**. [CrossRef]
40. Dee, D.P.; Uppala, S.M.; Simmons, A.J.; Berrisford, P.; Poli, P.; Kobayashi, S.; Andrae, U.; Balmaseda, M.A.; Balsamo, G.; Bauer, P.; et al. The ERA-Interim reanalysis: Configuration and performance of the data assimilation system. *Q. J. R. Meteorol. Soc.* **2011**, *137*, 553–597. [CrossRef]
41. Stohl, A.; Forster, C.; Frank, A.; Seibert, P.; Wotawa, G. Technical note: The Lagrangian particle dispersion model FLEXPART version 6.2. *Atmos. Chem. Phys.* **2005**, *5*, 2461–2474. [CrossRef]
42. Stohl, A.; James, P.A. A Lagrangian Analysis of the Atmospheric Branch of the GlobalWater Cycle. Part I: Method Description, Validation, and Demonstration for the August 2002 Flooding in Central Europe. *J. Hydrometeorol.* **2004**, *5*, 656–678.
43. Stohl, A.; James, P.A. A Lagrangian Analysis of the Atmospheric Branch of the GlobalWater Cycle. Part II: Moisture Transports between Earth's Ocean Basins and River Catchments. *J. Hydrometeorol.* **2005**, *6*, 961–984.
44. Sorí, R.; Marengo, J.; Nieto, R.; Drumond, A.; Gimeno, L. The Atmospheric Branch of the Hydrological Cycle over the Negro and Madeira River Basins in the Amazon Region. *Water* **2018**, *10*, 738. [CrossRef]
45. Stojanovic, M.; Drumond, A.; Nieto, R.; Gimeno, L. Variations in Moisture Supply from the Mediterranean Sea during Meteorological Drought Episodes over Central Europe. *Atmosphere* **2018**, *9*, 278. [CrossRef]
46. Numagati, A. Origin and recycling processes of precipitation water over the Eurasian continent: Experiments using an atmospheric general circulation model. *J. Geophys. Res.* **1999**, *104*, 1957–1972. [CrossRef]
47. Zhang, J.; Lindsay, R.; Schweiger, A.; Steele, M. The impact of an intense summer cyclone on 2012 Arctic sea ice retreat. *Geophys. Res. Lett.* **2013**, *40*, 720–726. [CrossRef]
48. Simmonds, I.; Rudeva, I. The great Arctic cyclone of August 2012. *Geophys. Res. Lett.* **2012**, *39*. [CrossRef]
49. Kamae, Y.; Mei, W.; Xie, S.P.; Naoi, M.; Ueda, H. Atmospheric rivers over the Northwestern Pacific: Climatology and interannual variability. *J. Clim.* **2017**. [CrossRef]
50. Vázquez, M.; Nieto, R.; Drumond, A.; Gimeno, L. Moisture transport into the Arctic: Source-receptor relationships and the roles of atmospheric circulation and evaporation. *J. Geophys. Res. Atmos.* **2016**, 121. [CrossRef]
51. Jakobson, E.; Vihma, T. Atmospheric moisture budget in the Arctic based on the ERA-40 reanalysis. *Int. J. Climatol.* **2010**, *30*, 2175–2194. [CrossRef]
52. Groves, D.; Francis, J. Variability of the Arctic atmospheric moisture budget from TOVS satellite data. *J. Geophys. Res.* **2002**, *107*, 4785. [CrossRef]
53. Yu, L. Global variations in oceanic evaporation (1958–2005): The role of the changing wind speed. *J. Clim.* **2007**, *20*, 5376–5390. [CrossRef]
54. Gimeno, L.; Stohl, A.; Trigo, R.M.; Dominguez, F.; Yoshimura, K.; Yu, L.; Drumond, A.; Durán-Quesada, A.M.; Nieto, R. Oceanic and terrestrial sources of continental precipitation. *Rev. Geophys.* **2012**, *50*, RG4003. [CrossRef]

55. Dettinger, M.; Ralph, F.M.; Lavers, D. Setting the stage for a global science of atmospheric rivers. *Eos* **2015**, 96. [CrossRef]
56. Dufour, A.; Zolina, O.; Gulev, S.K. Atmospheric Moisture Transport to the Arctic: Assessment of Reanalyses and Analysis of Transport Components. *J. Clim.* **2016**, *29*, 5061–5081. [CrossRef]

ANNALS OF THE NEW YORK ACADEMY OF SCIENCES
Special Issue: *Climate Sciences*
ORIGINAL ARTICLE

From Amazonia to southern Africa: atmospheric moisture transport through low-level jets and atmospheric rivers

Alexandre M. Ramos,[1] Ross C. Blamey,[2] Iago Algarra,[3] Raquel Nieto,[3] Luis Gimeno,[3] Ricardo Tomé,[1] Chris J.C. Reason,[2] and Ricardo M. Trigo[1]

[1]Instituto Dom Luiz (IDL), Faculdade de Ciências, Universidade de Lisboa, 1749-016 Lisboa, Portugal. [2]Department of Oceanography, University of Cape Town, Rondebosch, South Africa. [3]EPhysLab (Environmental Physics Laboratory), Facultade de Ciencias, Universidade de Vigo, Ourense, Spain

Address for correspondence: Alexandre M. Ramos, Instituto Dom Luiz, Faculdade de Ciências, Universidade de Lisboa, Campo Grande, Edf. C8, Piso 3, Sala 8.3.1, 1749-016 Lisboa, Portugal. amramos@fc.ul.pt

A Lagrangian analysis is applied to identify the main moisture source areas associated with atmospheric rivers (ARs) making landfall along the west coast of South Africa during the extended austral winter months from 1980 to 2014. The results show that areas that provide the anomalous uptake of moisture can be categorized into four regions: (1) the South Atlantic Ocean between 10°S and 30°S, (2) a clear local maximum in the eastern South Atlantic, (3) a continental source of anomalous uptake to the north of the Western Cape, and (4) over South America at a distance of more than 7000 km from the target region. It emerges that the South American moisture source can be linked to a particular phase of the South American low-level jet, known as a no Chaco jet event (NCJE), which transports moisture to the western and central South Atlantic basin. Concisely, we provide strong evidence that the two margins of the South Atlantic Ocean appear connected by two meteorological structures, with the NCJE playing a key role of transporting moisture from South America to the western and central South Atlantic basin, feeding the AR that transports some of the moisture to the west coast of South Africa.

Keywords: South Africa; atmospheric rivers; South American low-level jet; South Atlantic Ocean; moisture sources

Introduction

Given the dependence of society on the availability of fresh water, the hydrological cycle is arguably the most important component of the Earth system. Globally, most of the moisture evaporated into the atmosphere is from the oceans, with the remainder coming from the continents.[1,2] On a regional scale, the hydrological cycle tends to be subtle with both local and remote sources having an impact, thereby introducing complexity. Understanding the location of moisture sources, the means of transport of this moisture, and the continental rainfall regime remains one of the important areas of climate research particularly so within the current climate change paradigm.

Over the South Atlantic Ocean and its continental margins, the two large-scale meteorological structures known to play an important role in moisture transport are atmospheric rivers (ARs) and low-level jet (LLJ) systems.[3] ARs are typically described as narrow filamentary bands of intense vertically integrated water vapor transport.[4,5] These features can be dynamically linked with the development and movement of extratropical cyclones and they are often associated with the large-scale dynamics, and thus, are generally more frequent during the winter months compared to the summer.[6] Considerable contributions from ARs to seasonal rainfall totals and also to extreme rainfall events have been identified for numerous locations, with most research to date focusing on the United States[7–10] and Western Europe.[11,12] Recent work by Blamey *et al.*[13] has highlighted the impact ARs can have on rainfall over western South Africa, bordering the South East Atlantic Ocean.

LLJs are narrow corridors of wind speed maximum within the lower atmosphere and are

doi: 10.1111/nyas.13960

typically associated with regional-scale features, including topography. These jets can carry much of the moisture transport from low to high latitudes or from warm oceans toward continental areas.[14,15] LLJs are primarily a warm season phenomenon, and the mechanisms that drive them are different from coastal or inland jets.[3] Coastal LLJs are generally associated with geostrophic balance and are associated with topography and daily cycles of land–sea temperature contrasts.[16] On the other hand, jets located inland are generally driven by topographic and/or inertial effects or may result from secondary circulations associated with upper level flows[17] where the topography can influence the behavior of an inland jet.

For South America, Refs. 3 and 18 explained the main mechanism that is involved in the moisture transport in the region as being related to the presence of the South American LLJ (SALLJ). The SALLJ is characterized as a narrow stream that channels the near-surface flow between the tropics and midlatitudes east of the Andes Mountain range. The SALLJ transports moisture from the Amazon region into the fertile lands of southern Brazil–Northern Argentina (as shown in the conceptual model in Ref. 18). It is important to note that throughout the year, the SALLJ is present in one of three possible configurations: the Chaco jet event (CJE), no CJE (NCJE), or the Argentinian low level jet (LLJA).[19] A key difference between the three is that during the austral winter, in which the NCJE is more frequent, the wind maxima do not cross 25°S and the flow turns more zonally to the east. Under this particular condition, it is possible that moisture coming from South America, in particular from the Amazonian region, will be available to be transported and have impact on South Africa as proposed by Ref. 20. These authors showed that strong teleconnections exist between South African daily rainfall and that over various areas of South America, with the latter leading by 4–5 days for winter.

Moisture that is required for South African rainfall is considered to be mainly transported from elsewhere. The Indian Ocean has often been portrayed as the major moisture source for the region, with wet and dry summers regularly linked to sea surface temperature (SST) anomalies in this oceanic domain.[21–25] Although the Indian Ocean is viewed as a dominant regional moisture source for summer rainfall (the most important rainy season), evidence also supports the South Atlantic Ocean as another important moisture source for both summer and winter (the rainy season in the southwest of the country).[26–30] Not all moisture is sourced from the neighboring oceans, with the tropical areas of continental Africa also considered a source region for rainfall over southern Africa.[31] However, a large amount of this understanding relates to the austral summer rainfall region, while the austral winter rainfall is poorly understood.

A global overview[32] and work that is more recent focusing on the west coast of South Africa[13] showed that ARs do make landfall in the region. Furthermore, they are responsible for extreme precipitation and contribute (in a high percentage) to the total precipitation there.[13] In addition, a study[33] analyzed the floods and water availability driven by ARs on a global scale and showed that for South Africa, the years with an absence/occurrence of ARs could lead to a hydrological drought/flood. Moreover, Ref. 34 studied the projected global-scale changes of ARs under a warming climate and found that for the South African domain a slight increase in the AR activity is projected for future climate scenarios. Despite the importance of winter rainfall to the local population and the economy (e.g., agriculture), relatively little is understood regarding the main drivers/processes behind the interannual variability or the key moisture sources. However, more important is that no previous work has put any attention on the link between both major mechanisms of moisture transport, the ARs and the LLJ (see Ref. 3), across the South Atlantic Ocean, linking South America to southern Africa. Therefore, the aim of our research is to provide a comprehensive linkage between both major mechanisms of moisture transport and to put them into a larger context of moisture availability and transport between the two continents.

Materials and methods

Atmospheric river database

The AR database used here is the one presented in Ref. 13, where the ARs are detected by means of an automated scheme based on the methodology as described in Refs. 11 and 12 for Western Europe. The method is based on vertically integrated horizontal water vapor transport (IVT) computed

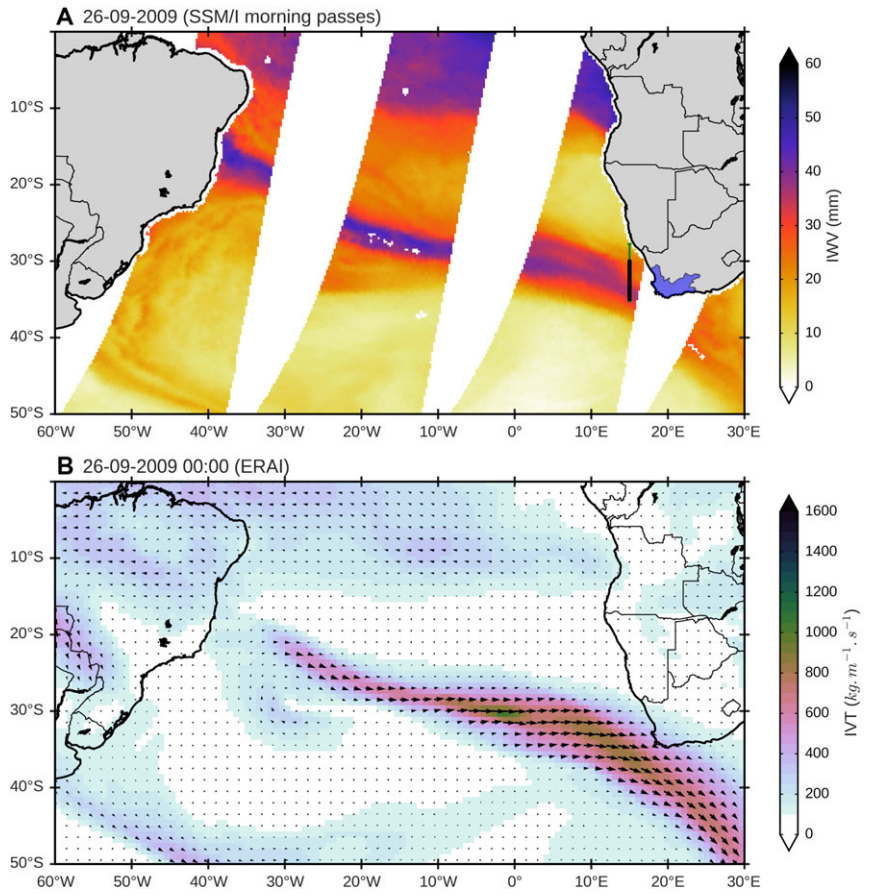

Figure 1. (A) An atmospheric river (AR) event is shown for September 26, 2009, using the integrated water vapor (IWV) retrieved from the SSM/I morning passes. Location of the reference meridian (15°E between 27.75° and 35.25°S, green line) is used for the computation of the atmospheric rivers (ARs) that reach the west coast of South Africa. The selected ARs correspond with the ones that during their lifetimes are located between 30° and 34.85°S at the 15°E reference meridian (black line). In addition, the Western Cape Province of South Africa is highlighted in blue and is the region where the particles were selected for the backward trajectory analyses. (B) The same AR event as in A is shown, but in this case using the IVT from ERA-Interim at 00UTC.

between 1000 and 300 hPa from reanalysis data. From the database, we have selected the ARs that were computed using the ERA-Interim reanalysis at a 0.75° resolution for the extended austral winter (AMJJAS).[35]

The AR database of Ref. 13 consists of the identification of the ARs that passes over the 15°E reference meridian and between 27.75° and 35.25°S that could eventually make landfall over the west coast of South Africa over the 1979–2014 period (see Fig. 1, green line). Over this 36-year period, 367 persistent ARs (at least three time steps in the reanalysis) were identified during the winter months. For additional information regarding the AR detection scheme, please see Ref. 13.

Since we are interested only in those ARs that have impacts over South Africa, we have filtered the ARs in order to ensure this. Therefore, we have selected only those ARs that during their lifetimes (by computing the mean position of the maximum IVT in each time step) are located somewhere between 30° and 34.85°S at the 15°E reference meridian (Fig. 1, black line). This new filtered AR database contained 193 persistent ARs in 1079 AR time steps for the 1980–2014 period.

The South American low-level jet

For the characterization of the SALLJ, we used an adaptation of the night LLJ (NLLJ) index grounded in the work of Ref. 14, which is based upon the

vertical structure of the wind's temporal variation, and the fact that these LLJs are more intense at local midnight. As the jet core is located in the first kilometer above the surface, sigma coordinates were used to take into account the elevation of the land. The wind variations are computed between 500 m (near the jet core) and 4000 m above ground level (AGL), which corresponds, approximately, with the sigma levels 53 and 42 at a resolution of 0.25° downloaded directly from the ERA-Interim reanalysis dataset at the ECMWF platform. The LLJ index was computed for the period between 1980 and 2014.

This LLJ index was calculated at each grid point over South America, and the two criteria must be satisfied simultaneously to have a jet day: (1) the winds at the jet core must be stronger at local midnight than at local noon and (2) the wind speed at the jet core must be stronger than that aloft (4 km AGL), similar to the criterion of Ref. 36. Therefore, the SALLJ index is a function between the difference of winds near the surface and at high levels, and the diurnal variation of the wind. According to this, the index is defined as follows:

$$\mathrm{NLLJ} = \lambda\varphi\sqrt{\left[\left(u_{00}^{L1} - u_{00}^{L2}\right) - \left(u_{12}^{L1} - u_{12}^{L2}\right)\right]^2 + \left[\left(v_{00}^{L1} - v_{00}^{L2}\right) - \left(v_{12}^{L1} - v_{12}^{L2}\right)\right]^2}, \quad (1)$$

where u and v are the zonal and meridional wind components, respectively. $L1$ represents the winds at sigma level 53 (500 m AGL, near the jet core) and $L2$ represents the wind at sigma level 40 (4000 m AGL, high level) above the jet core. To take into account the wind speed variation in the diurnal cycle, the subscripts 00 and 12 refer to local midnight and local moon, respectively. Two additional binary (0 or 1) terms are needed to take into account the temporal and vertical variation of the wind:

$$\lambda = \begin{cases} 0, & \mathrm{ws}_{00}^{l1} \le \mathrm{ws}_{12}^{l1} \\ 1, & \mathrm{ws}_{00}^{l1} > \mathrm{ws}_{12}^{l1} \end{cases} \text{ and } \varphi = \begin{cases} 0, & \mathrm{ws}_{00}^{l1} \le \mathrm{ws}_{00}^{l2} \\ 1, & \mathrm{ws}_{00}^{l1} > \mathrm{ws}_{00}^{l2} \end{cases} \quad (2)$$

The first, lambda (λ), refers to the temporal wind variation, so $\lambda = 1$ when the difference between the 500 m AGL wind speed (ws) at local midnight and local noon is positive. The second, phi (φ), refers to vertical variation and it requires to be $\varphi = 1$ that the 500 m AGL wind speed (ws) at local midnight to be greater than at 4000 m AGL at the same time.

Lagrangian moisture quantification

A method commonly applied to identify moisture sources is based on Lagrangian models. Essentially, the Lagrangian method is built around the changes in the water vapor content of air parcels (i.e., evaporation and precipitation) along their trajectories from the moisture sources to the region of interest. The method used in this work was developed by Ref. 37, which allows one to track the atmospheric moisture along Lagrangian trajectories of the air parcels in the atmosphere. The model used here is the version 9.0 of the FLEXPART Lagrangian model. For a comprehensive review, the reader is directed to Ref. 37, which provides further information on the FLEXPART model. In the model setup, it simulates the movement of approximately two million atmospheric parcels every 3 hours. Our global simulation was forced using the ERA-Interim reanalysis data from 1980 to 2014, which are accessible at approximately 80 km (T255 spectral) on 60 vertical levels from the surface up to 0.1 hPa. These particles are then advected using the reanalysis wind field, and in addition, Turbulence and convection parametrizations are taken in account, always maintaining the consistency of the atmospheric mass distribution.[38,39] The meteorological properties at each position (latitude, longitude, and elevation) of the air parcels, such as specific humidity or temperature among many others, are retained in the outputs of the FLEXPART model.

The transport time of the trajectories was limited in this work to 10 days, as this is the mean water vapor lifetime in the atmosphere.[40] Changes in specific humidity (q) and locations of air particles were recorded every 6 hours. The increases (e) and decreases (p) in moisture along each trajectory may be expressed by changes in specific humidity (q) by the following equation:

$$e - p = m\frac{\mathrm{d}q}{\mathrm{d}t}, \quad (3)$$

where m is the mass of the particle. By adding ($e - p$) values of all air particles residing at each time step over a specific area (in this case, over an area of 1.0° × 1.0° in latitude and longitude), it is possible to obtain the instantaneous values of $E - P$,

where E denotes evaporation and P the precipitation rate per unit area.

Following the trajectories in a backward mode, we are able to detect the sources of moisture for a selected region where $E-P$ is positive. This methodology for determining the sources of moisture has been extensively used over the past decade both for regional[41–44] and global studies.[45] The comprehensive review by Ref. 2 provides the details of the uncertainty and significance of this Lagrangian approach, as well as a comparison with other methods of estimating moisture sources.

We computed $E-P$ in a backward mode for the particles that are inside the Western Cape Province of South Africa (our sink region, blue area in Fig. 1), where the impacts of the ARs in extreme precipitation and precipitation regimes were already studied.[13] In addition, we computed the uptake of moisture for all the individual 193 persistent ARs for all time steps, retaining only positive values of $E-P$ every 6 h during the 10-day back trajectories (40 time steps). To check whether these areas (where the ARs take on moisture) differ from the climatology, we computed for each AR the anomaly between $(E-P) > 0$ of the ARs and the "climatology" for the corresponding AR dates. The climatology at this point corresponded with the same (Julian) time step but for all 36 years of the study (retaining again only the positive values of $(E-P)$ for each 6-h time step). This methodology is the same as the one applied in Ref. 46 that investigated the moisture source of the ARs that reached Western Europe.

The particles modeled by FLEXPART could be also followed in forward mode starting from a selected source of moisture. In this case, those areas in which $E-P$ is negative are considered as sinks of moisture. In addition, a forward analysis is also performed for some specific regions where the anomalous uptake of moisture is found during the back-trajectory analysis of the ARs that reach Western Cape Province of South Africa. This forward analysis will be explained in detail below.

Results

AR moisture sources

A brief analysis from an Eulerian approach will be made using the IVT and the sea-level pressure (SLP) before analyzing the moisture sources of the ARs reaching the Western Cape Province of South Africa. To do so, we have computed averages for IVT (intensity and components) and SLP using the 1079 AR time steps (from 193 persistent ARs) that affect the Western Cape and compare it with the extended austral winter long-term mean (Fig. 2). The austral winter climatological of the IVT mean values range between 200 and 300 kg m^{-1} s^{-1} for a large band of moisture crossing the entire South Atlantic Ocean basin in a westerly or west-northwesterly direction with the subtropical ridge being located between 30° and 40°S and extending its influence over the Western Cape, although the highest values are observed considerably to the south of South Africa (Fig. 2A). When analyzing the composite for the AR days that affect the Western Cape, an intensification of the advection of moisture clearly emerges (Fig. 2B), with values ranging from 240 kg m^{-1} s^{-1} to a maximum close to 420 kg m^{-1} s^{-1} (located immediately south of the Western Cape). In addition, there is a northward retreat of the subtropical ridge and clear trough is now visible to the southwest/west of South Africa.

The anomalies between the extended austral winter long-term mean and the composite for the AR days were also computed (Fig. 2C). Negative SLP anomalies are found south of the Western Cape ranging up to –12 hPa. In terms of the IVT anomalies, a dipole is found with positive anomalies occurring from the east coast of Brazil and over the South Atlantic Ocean toward the Western Cape (>30 kg m^{-1} s^{-1}). A maximum exists just off the Western Cape coast over the target domain (anomalies up to 270 kg m^{-1} s^{-1}). Negative IVT anomalies (up to –90 kg m^{-1} s^{-1}) are found south of 40°S to the southwest of South Africa. This increase in the IVT in the South Atlantic Ocean confirms the previous findings of Ref. 13, which suggest that ARs play a key role in transporting moisture into the Western Cape. Furthermore, the SLP anomaly pattern and the trough to the south of the Western Cape also indicate that cold fronts and associated extratropical cyclones are likely linked to ARs making landfall in South Africa.

Although the use of the IVT is an effective Eulerian approach for studying the temporal variability of moisture flows for specific locations around the globe (i.e., Fig. 2), it is not suitable for finding the main sources of moisture. For example, during an AR event, the Eulerian approach is not able to follow any specific *particle* transported by the AR. The use of Lagrangian models, such as FLEXPART,

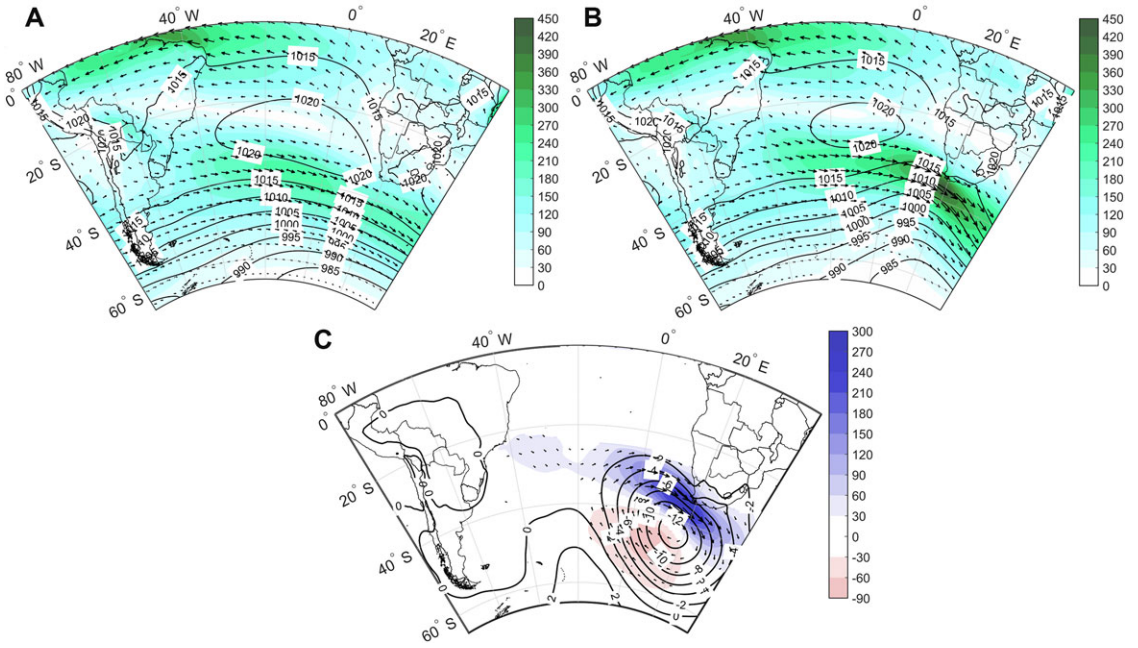

Figure 2. (A) Extended austral winter (AMJJAS) long-term mean (1979–2014) of the IVT direction (vectors) and intensity (kg m^{-1} s^{-1}; color shading) and SLP (hPa; contours) fields. (B) Mean composites of IVT direction (vectors) and intensity (kg m^{-1} s^{-1}; color shading) and SLP (hPa; contours) fields during the occurrence of the persistent ARs that affect the west coast of South Africa. (C) The anomalies between the long-term mean and the composites.

allows one to study air particle trajectories and thus characterize the history of the air parcels (e.g., their specific humidity) arriving at a specific location. As such, the use of Lagrangian models has previously been shown to be a worthwhile and important tool for analyzing the moisture sources in a case study of ARs in Western Europe,[46] Norway,[47] and the U.S. West Coast.[48]

It was shown in Figure 2 that there is typically an increase in the moisture transport over the South Atlantic Ocean in the presence of ARs, and, therefore, it is of paramount importance to understand where the anomalous moisture uptake occurs $(E-P) > 0$ (see above for the methodology). The backward trajectory analyses were performed for air particles residing over the area inside the Western Cape (blue area in Fig. 1) to the west of the AR detection for the climatological period and for days containing ARs.

The climatology of the moisture uptake for the austral winter, $(E-P)_{CLI} > 0$ for the non-AR days, is shown in Figure 3A, where one can see four major areas of uptake of moisture that arrive at the Western Cape: (1) over the western South Atlantic Ocean between 20°S and 30°S, (2) a maximum near the target region in the eastern South Atlantic and including the Agulhas Current retroflection south of South Africa, (3) the Agulhas Current, running along the east coast of South Africa, and (4) also some uptake of moisture from land areas to the north of the Western Cape, particularly northern and northwestern South Africa, Namibia, and Botswana. By comparison, when analyzing the moisture uptake for the austral winter for days where the ARs are present $(E-P)_{ARs} > 0$ over the Western Cape, a stronger signal emerges over the South Atlantic (Fig. 3B). An area extending from the central Brazilian coast across the South Atlantic toward western South Africa is evident. There is also a much stronger local moisture uptake immediately to the west and south of the Western Cape. In addition, there is also a strengthening of the moisture uptake over the land areas north of the domain (Namibia, Botswana), while less moisture uptake is observed in the Agulhas Current area. Thus, the analysis $(E-P)_{ARs} > 0$ for days in which AR events impact the Western Cape suggests that the South Atlantic Ocean, parts of South America, and to a lesser extent, countries

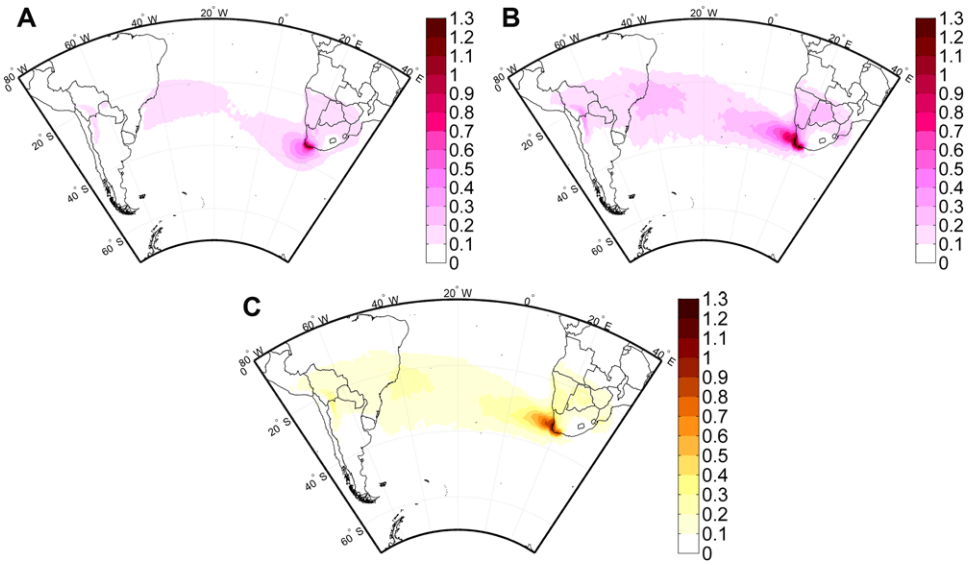

Figure 3. (A) Extended austral winter (AMJJAS) climatology for atmospheric river days (1979–2014) of the $(E-P) > 0$ $[(E-P)_{\mathrm{CLI}}]$, integrated backward for a 10-day period. (B) Mean composite considering only the atmospheric river days (1979–2014) of the $(E-P) > 0$ (mm) $[(E-P)_{\mathrm{ARs}}]$, integrated backward for a 10-day period. (C) Integrated backward for a 10-day period. $(E-P) > 0$ anomaly field for AR days $[(E-P)_{\mathrm{ANO}}]$. Units in mm day^{-1}.

north of South Africa, are the core areas of uptake of moisture. This moisture contributes to the enhancing of the ARs and favoring conditions for precipitation in the target region.

The role of specific regions acting as a moisture source is better visualized through the anomalous uptake of moisture $(E-P)_{\mathrm{ANO}} > 0$ which was simply obtained by subtracting the $[(E-P)_{\mathrm{ARs}} > 0 - (E-P)_{\mathrm{CLI}} > 0]$ (Fig. 3C; only the positive values are presented). The spatial $(E-P)_{\mathrm{ANO}} > 0$ field is very close to the one found for the $(E-P)_{\mathrm{ARs}} > 0$ (Fig. 3B). It shows anomalous uptake of moisture in four particular regions, which can be summarized as follows:

(1) A clear local maximum of anomalous uptake of moisture appears in the eastern South Atlantic, immediately to the west of the Western Cape.
(2) A continental source of anomalous uptake of moisture appears to the north of the Western Cape, in Namibia and Botswana.
(3) The South Atlantic Ocean between 10°S and 30°S (with a "hot spot" off the central coast of Brazil) associated with an increase of anomalous uptake of moisture from the tropical region during AR days, but also an intensification in the subtropical moisture uptake where there is convergence of moisture along cold fronts and associated extratropical cyclones that track eastward toward South Africa.
(4) Finally, it is also important to recognize and highlight the unusual anomalous uptake of moisture that occurred over some parts of the South American continent, which are located more than 7000 km from the target region. This last continental source of moisture over South America (that includes most of the large Paraná River Basin as well as the southern Amazon River Basin) is further analyzed below.

The South American connection

The last two anomalous regions indicating the uptake of moisture associated with the ARs listed above correspond with the parts of South America and the adjacent South Atlantic Ocean and are probably the most interesting in terms of dynamical analysis. To do this, we will analyze the mechanisms associated with this anomalous availability of moisture for uptake by the ARs that reach South Africa. Furthermore, we link two of the major structures for the moisture transport in the atmosphere:

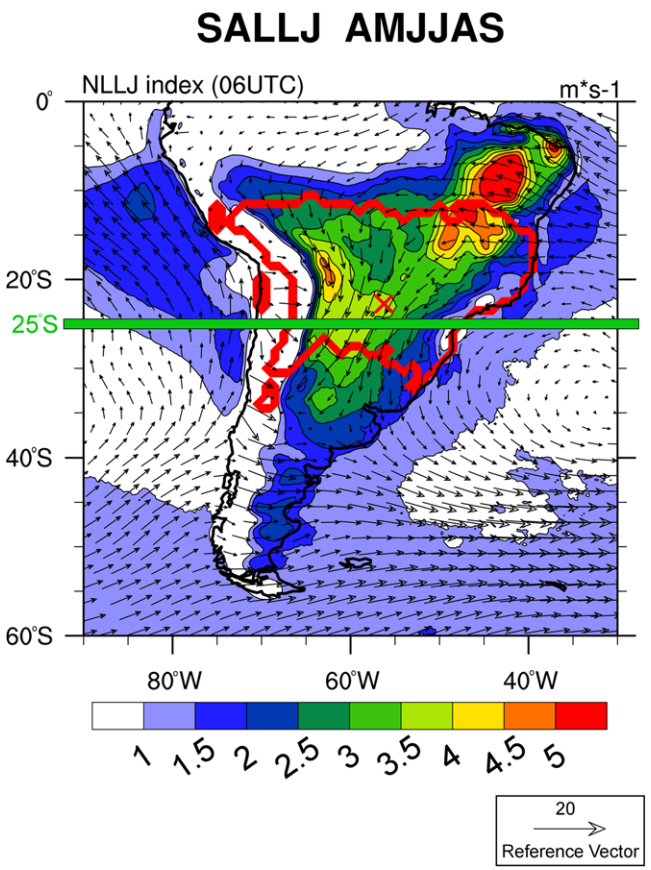

Figure 4. The climatological NLLJ index (colored contours), the wind field at 500 hPa (in m/s), and the continental source of moisture (red line) detected in Figure 3C, during austral winter. Red cross, at 22.75°S, 56.25°W, indicates the selected point to check changes in the behavior of the SALLJ. In addition, the 25°S parallel is also highlighted in green.

ARs (in this case landing in South Africa) and LLJs (the SALLJ in South America). As mentioned above, the NLLJ index was calculated at each grid point over South America region from April to September for the period 1980–2014. Figure 4 shows the climatological NLLJ index, the wind field at 500 hPa, and the boundaries of the continental source of moisture detected in Figure 3C. As commented on above, when the SALLJ is intense, the northerly wind dominates from 10° to 20°S and crosses southward past 25°S, and the LLJ is a CJE (Chaco jet event). However, when this wind pattern diminishes or is not present, a NCJE (no Chaco jet event) could occur, where the wind turns eastward before arriving at 25°S. The continental moisture source area, in southern Amazonia, extends just south of the 25°S latitude and is dominated by the SALLJ. The NLLJ index was used to perform a classification for the CJE and NCJE classes. Values greater than zero of the NLLJ index are associated with the CJE phase, while values equal to zero are associated with the NCJE phase of the SALLJ. The point selected to analyze changes in the behavior of the SALLJ is located at 22.75°S, 56.25°W (red cross, Fig. 4), which is north of 25°S and positioned in the middle of the South American source of moisture for the ARs (red contour) found in Figure 3C.

In order to evaluate the influence of a CJE and a NCJE in producing the moisture availability in the South Atlantic Ocean to feed the ARs in South Africa, we first computed the IVT composites for these two subgroups. As the South American source of moisture was detected using a 10-day backward analysis, a similar time-lag between the occurrence of the ARs in South Africa and the occurrence of the

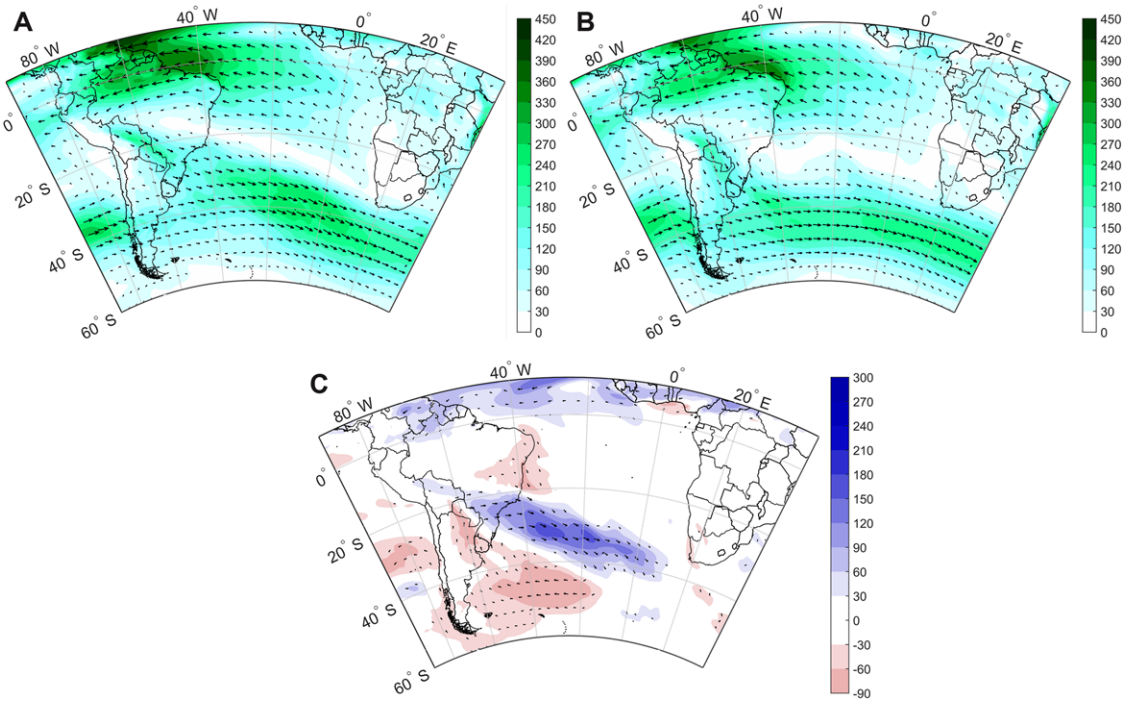

Figure 5. IVT composite (kg m^{-1} s^{-1}) for (A) days with NCJE and (B) days with a CJE for a 10-day lag period before the AR events that occurred in July. In addition, in C, the difference between NCJE IVT composite and CJE IVT composite is shown (kg m^{-1} s^{-1}).

SALLJ for the selected point at 22.75°S, 56.25°W was taken into account. More specifically, we generated lags from 1 to 10 days back in time and separated the events into days with a CJE or a NCJE. An example for which the IVT composite for these both subgroups is plotted is shown in Figure 5, for days with a NCJE shown in Figure 5A or days with a CJE in Figure 5B, both with a 10-day lag period before the AR events. For both cases, a maximum of IVT is detected in the easterlies near the equator and reaching the South American Atlantic coast. This zonal flow returns to the south, running parallel to the Andes mountain range, and then flows in a southeastward direction toward the southwest Atlantic. However, a clear difference occurs between CJEs and NCJEs regarding the intensity along the Andes, with CJEs being stronger, flowing further southward, while the westerly outflow also occurs at higher latitudes in CJEs. This last effect affects the IVT values over the South Atlantic Ocean, with a maximum of IVT found in a band centered around 35°S for a NCJE (Fig. 5A; between 240 and 270 kg m^{-1} s^{-1}) and with less intensity and occurring a little further south for a CJE (Fig. 5B; between 210 and 240 kg m^{-1} s^{-1}). To highlight this, the differences between both IVT composites ($IVT_{NCJE} - IVT_{CJE}$) are computed and shown in Figure 5C. The results show that, when the ARs strike the South Africa west coast, there is an important anomalous transport of moisture during the 10 days before along a southeastern shift band from 60°W to 10°E at the latitude around 25°S (up to 180 kg m^{-1} s^{-1}) during SALLJ events that are characteristic of its NCJE configuration. This confirms that the moisture available over this oceanic area for the South African ARs comes, largely, from the air masses transported by the SALLJ along the South America continental area.

The results of a similar analysis undertaken for the full winter climatology (Fig. 6) correspond reasonably well with that shown for the month of July (Fig. 5). The climatology illustrates the dipole configuration, with positive anomalies over continental South America and the South Atlantic Ocean (up to 180 kg m^{-1} s^{-1}) and negative values found further south with values reaching –90 kg m^{-1} s^{-1}. Therefore, the focus in the remaining analysis is on the mean April–September values. With the purpose

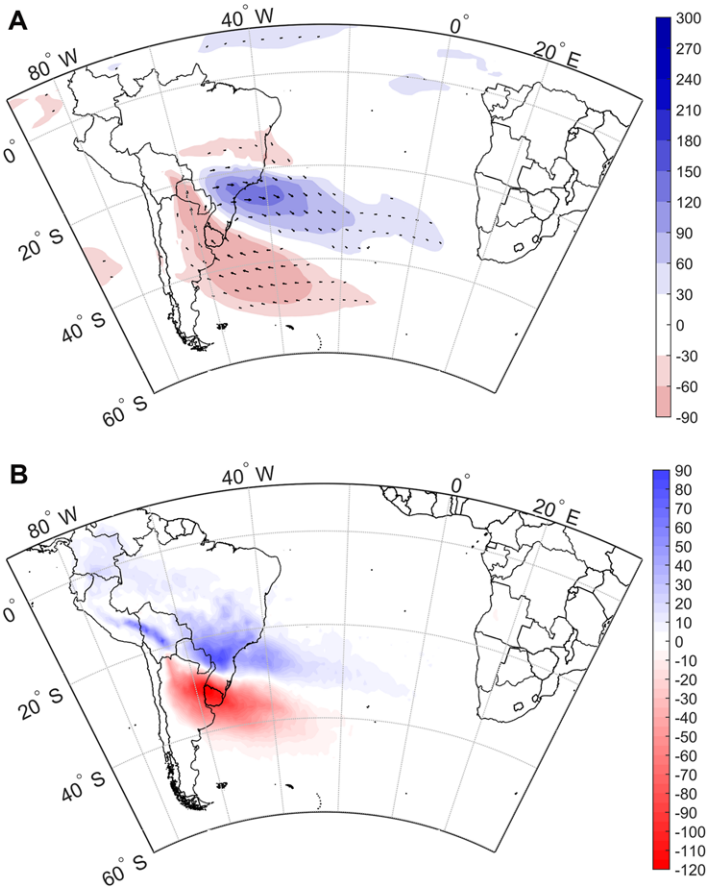

Figure 6. (A) The difference between NCJE IVT composite and CJE IVT composite is shown (kg m^{-1} s^{-1}) for a 10-day lag period before the AR events that occurred in the austral winter (AMJJAS). (B) Results for the difference between $(E - P < 0)_{NCJE}$ and $(E - P < 0)_{CJE}$ for each of the 10 days before the occurrence of ARs in South Africa; units in mm day^{-1}.

of corroborating the pattern of the IVT anomalies related with NCJEs (or not), we modeled the contribution of the South American moisture source detected in Figure 4 (red contour) by computing the FLEXPART outputs in its forward mode to detect the sink regions ($E - P < 0$) over the South Atlantic Ocean. As for the IVT analysis, the sinks for all 10-day lags are detected and separated between days of CJE and days with NCJE during the austral winter. Figure 6B shows the results for the difference between $(E - P < 0)_{NCJE}$ and $(E - P < 0)_{CJE}$ for each of 10 days before the occurrence of ARs in South Africa. The figure also reveals a dipole configuration with a clear anomalous transport of moisture over tropical–subtropical latitudes (in blue, with values up to 70 mm) during days with NCJEs, while a decreased moisture contribution occurs at higher latitudes (in red, with values reaching –110 mm). Compared to the climatological IVT composite ($IVT_{NCJE} - IVT_{CJE}$) in Figure 6A, the results show a similar pattern.

Discussion

Using a high-resolution FLEXPART simulation, our study here identifies the key regions where anomalous uptake of moisture associated with ARs making landfall over the southwestern part of South Africa occurs. ARs have previously been documented as important features for heavy rainfall events in southwestern South Africa.[13] Thus, the methods used here assist in locating important moisture source regions for South African winter rainfall. As alluded earlier, it has been well documented that the southwest and tropical Indian Ocean plays a key role in providing moisture for South Africa during the summer

months, with the tropical southeast Atlantic and central Africa being the other key source regions. In comparison, the understanding of moisture sources for the South African winter rainfall has remained relatively poor.

According to Ref. 39, the only air masses that cause net rainfall in South Africa are those that reach it from the Indian Ocean. However, when we look into the Western Cape region, some other studies have highlighted the contribution of the tropical southeast Atlantic to precipitation during summer and winter.[30,49,50] Additionally, in this study, we show that for southwestern South Africa, the South Atlantic is a key moisture source for ARs making landfall in South Africa during the winter months.

It was found that the maximum uptake in moisture for these ARs was located immediately off the coast of the Western Cape, extending westward. This region has previously been associated with winter rainfall variability over the Western Cape through changes in evaporation, air mass properties, and in the strength and position of cold fronts approaching the Western Cape.[27,51] Warm SST anomalies in this region may thus reinforce the ARs just upstream of the Western Cape. A similar pattern has been identified with ARs making landfall over the Iberian Peninsula, with a maximum in moisture uptake located over the waters located adjacent to the coastline.[46]

A continental moisture source was evident to the north of the Western Cape, in Namibia and Botswana. It has been shown that during the austral summer months, cloud bands, which develop through tropical–extratropical interactions, often extend diagonally NW–SE over southern Africa from the Angolan region out into the southwest Indian Ocean.[52–54] Thus, it is possible that the moisture sourced here during the extended winter is through similar mechanisms, but not as frequent as that during the summer months. Further analysis is required in order to establish whether this region acts as a moisture source throughout the entire winter period, or just the early or late winter months when cloud bands may still occur.

An interesting result of the AR moisture source analysis was the potential link between South American climate dynamics and winter rainfall in South Africa. A strong teleconnection exists between South African daily rainfall and that over various areas of South America.[20] The results here suggest that important anomalous uptake of moisture over South America was found for the ARs that strike South Africa. In order to understand the possible mechanism responsible for this uptake, we investigated the role of the SALLJ and its importance of moisture transport from the Amazon basin to the South Atlantic region. The key results linking the two continents are summarized in Figure 7, where we present a conceptual model of the combination of LLJs and ARs to transport moisture from Amazonia to southwestern South Africa.

From Figure 7, during the occurrence of ARs, negative SLP anomalies are found south of the Western Cape resulting from a trough configuration when the composite of the SLP during the AR event is analyzed. In terms of the IVT anomalies, a dipole is found with positive anomalies over the South Atlantic Ocean toward the Western Cape with a maximum occurring just off the coast over the target domain with an increase in the IVT in the South Atlantic Ocean (green area in Fig. 7). This result, therefore, confirms the previous findings by Ref. 13 that suggest ARs play a key role in transporting moisture into the Western Cape. Regarding the Lagrangian analysis, the main anomalous uptake moisture areas are delimited by the red curves in Figure 7 and encircle regions north of the Western Cape, in Namibia and Botswana where recycling of moisture occurs, the South Atlantic Ocean, and some parts of South America which are at the distance of more than 7000 km from South Africa. In addition, the configuration of the SALLJ in its NCJE phase explains the moisture availability coming from Amazon into the South Atlantic Ocean. This is also shown in Figure 7 as the South Atlantic appears as an anomalous sink of moisture (purple colored areas) from the South American source of moisture during days with NCJEs. This same area was revealed as an anomalous area of higher IVT during NCJEs. In Figure 7, both continental areas at the margins of the South Atlantic Ocean appear connected by two meteorological structures, the LLJ (under the NCJE configuration along South America) and the ARs. Thus, the SALLJ plays the key role of transporting moisture from South America to the western and central South Atlantic basin, while the ARs then transport some of the moisture to the west coast of South Africa.

To conclude, this study has provided the first compressive analysis of the moisture sources associated

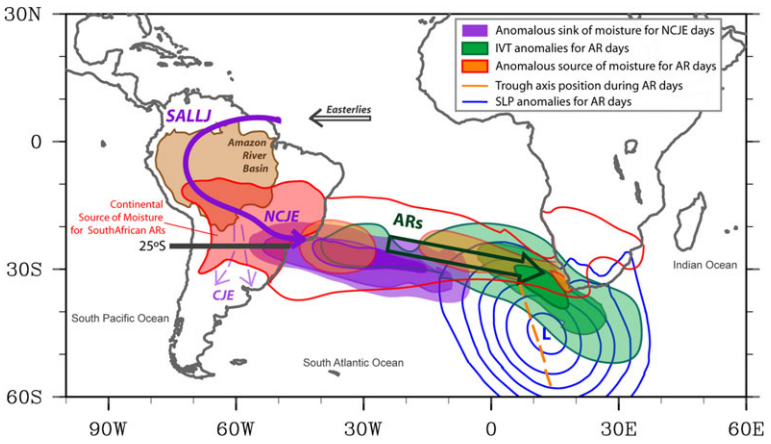

Figure 7. Conceptual model of the combination of the LLJ and ARs to transport moisture from Amazonia (brown area) to southwestern South Africa. Purple arrow indicates the South America low-level jet (SALLJ) in its both configurations; no Chaco jet events (NCJE) returning northern 25°S, and Chaco Jet Events (CJE, dashed lines) crossing southward 25°S. Purple contours are the sinks of moisture during NCJEs during the 10 days before the AR makes landfall in South Africa. Red contours are the sources of moisture during 10 days back for the AR days over South Africa; and the red-colored area over South America is the continental source of moisture. Greenish areas indicate the anomalies of IVT for AR days. Green big arrow indicates the common position of the AR track. Blue lines are the SLP anomalies and the orange dashed line is the trough axis position during AR days.

with the ARs that make landfall over southwestern South Africa. Results presented here indicate that areas of anomalous uptake for these South Atlantic ARs making landfall are mostly confined to the subtropics. The ARs in the North Atlantic, making landfall along Western Europe, have also been found to contain a strong uptake in moisture from the subtropics.[46]

Additionally, we show the combination of two of the most important structures for the moisture transport, the LLJ in South America and ARs over the South Atlantic Ocean, is responsible for the transport of moisture from Amazonia through to the southwestern tip of Africa. Thus, the results given here support the work of Ref. 20, suggesting a teleconnection between South American and South African rainfall.

Acknowledgments

A.M.R, R.M.T., C.R., L.G., and R.N. were supported by the project Improving Drought and Flood Early Warning, Forecasting and Mitigation using real-time hydroclimatic indicators (IMDROFLOOD) funded by Fundação para a Ciência e a Tecnologia, Portugal (FCT, Portugal) (WaterJPI/0004/2014), the Water Research Commission (K5-2618, South Africa), and the Ministerio de Economía y Competitividad, Spain (PCIN-2015-243 K639). A.M.R. was also supported by an FCT postdoctoral grant (FCT/DFRH/SFRH/BPD/84328/2012). R.B. and C.R. were also supported by the Natural Environment Research Council (NERC) Future Climate for Africa (FCFA) regional consortium project "UMFULA" (NE/M020223/1). R.N., L.G., and I.A. thank to the Programa de Consolidacion e Estructuracion de Unidades de Investigation Competitivas (ED431C 2017/64) by Xunta de Galicia. I.A. thanks the PhD grant received by the Ministerio de Economía y Competitividad, Spain (CGL2015-65141-R). Finally, we would like to thank the reviewers for their thoughtful comments and efforts toward improving the manuscript.

Author contributions

A.M.R., R.B., and R.N. conceived and designed the experiments; A.M.R., R.N., I.A., and R.T. performed the computations. A.M.R., R.B., I.A., R.N., L.G., C.R., and R.T. analyzed the data and wrote the paper.

Competing interests

The authors declare no competing interests.

References

1. Quante, M. & V. Matthias. 2006. Water in the Earth's atmosphere. *J. Phys. IV* **139:** 37–61.

2. Gimeno, L., A. Stohl, R.M. Trigo, *et al.* 2012. Oceanic and terrestrial sources of continental precipitation. *Rev. Geophys.* **50:** RG4003.
3. Gimeno, L., F. Dominghez, R. Nieto, *et al.* 2016. Major mechanisms of atmospheric moisture transport and their role in extreme precipitation events. *Annu. Rev. Environ. Resour.* **41:** 117–141.
4. Newell, R.E., N.E. Newell, Y. Zhu & C. Scott. 1992. Tropospheric rivers? A pilot study. *Geophys. Res. Lett.* **19:** 2401–2404.
5. Zhu, Y. & R.E. Newell. 1998. A proposed algorithm for moisture fluxes from atmospheric rivers. *Mon. Weather Rev.* **126:** 725–735.
6. Gimeno, L., R. Nieto, M. Vázquez & D.A. Lavers. 2014. Atmospheric rivers: a mini-review. *Front. Earth Sci.* **2:** 2.
7. Dettinger, M.D., F.M. Ralph, T. Das, *et al.* 2011. Atmospheric rivers, floods and the water resources of California. *Water* **3:** 445–478.
8. Rutz, J.J. & W.J. Steenburgh. 2012. Quantifying the role of atmospheric rivers in the interior western United States. *Atmos. Sci. Lett.* **13:** 257–261.
9. Ralph, F.M. & M.D. Dettinger. 2012. Historical and national perspectives on extreme west-coast precipitation associated with atmospheric rivers during December 2010. *Bull. Am. Meteorol. Soc.* **93:** 783–790.
10. Lavers, D.A. & G. Villarini. 2015. The contribution of atmospheric rivers to precipitation in Europe and the United States. *J. Hydrol.* **522:** 382–390.
11. Ramos, A.M., R.M. Trigo, M.L.R. Liberato & R. Tomé. 2015. Daily precipitation extreme events in the Iberian Peninsula and its association with atmospheric rivers. *J. Hydrometeorol.* **16:** 579–597.
12. Lavers, D.A., G. Villarini, R.P. Allan, *et al.* 2012. The detection of atmospheric rivers in atmospheric reanalyses and their links to British winter floods and the large-scale climatic circulation. *J. Geophys. Res.* **117:** D20106.
13. Blamey, R.C., A.M. Ramos, R.M. Trigo, *et al.* 2018. The influence of atmospheric rivers over the South Atlantic on winter rainfall in South Africa. *J. Hydrometeorol.* **19:** 127–142.
14. Rife, D.L., J.O. Pinto, A.J. Monaghan, *et al.* 2010. Global distribution and characteristics of diurnally varying low-level jets. *J. Clim.* **23:** 5041–5064.
15. Stensrud, D.J. 1996. Importance of low-level jets to climate: a review. *J. Clim.* **9:** 1698–1711.
16. Jiang, Q., S. Wang & L. O'Neil. 2010. Some insights into the characteristics and dynamics of the Chilean low-level coastal jet. *Mon. Weather Rev.* **138:** 3185–3206.
17. Parish T. 2000. Forcing of the summer low-level jet along the California coast. *J. Appl. Meteorol.* **39:** 2421–2433.
18. Marengo, J.A., W.R. Soares, C. Saulo & M. Nicolini. 2004. Climatology of the low-level jet east of the Andes as derived from the NCEP–NCAR reanalyses: characteristics and temporal variability. *J. Clim.* **17:** 2261–2280.
19. Salio, P. & M. Nicolini. 2006. Seasonal characterization of the diurnal cycle of convection frequency over southeastern South America under different low-level conditions. In *Proceedings of 8th ICSHMO*, Foz do Iguacu, Brazil.
20. Grimm, A.M. & C.J.C. Reason. 2015. Intraseasonal teleconnections between South America and South Africa. *J. Clim.* **28:** 9489–9497.
21. Mason, S. 1995. Sea-surface temperature—South African rainfall associations, 1910–1989. *Int. J. Climatol.* **15:** 119–135.
22. Reason, C.J.C. 1998. Warm and cold events in the southeast Atlantic/southwest Indian Ocean region and potential impacts on circulation and rainfall over southern Africa. *Meteorol. Atmos. Phys.* **69:** 49–65.
23. Landman, W. & S. Mason. 1999. Change in association between Indian Ocean sea-surface temperatures and summer rainfall over South Africa and Namibia. *Int. J. Climatol.* **19:** 1477–1492.
24. Reason, C.J.C & H.M. Mulenga. 1999. Relationship between South African rainfall and SST anomalies in the southwest Indian Ocean. *Int. J. Climatol.* **19:** 1652–1673.
25. Reason, C.J.C. 2001. Subtropical Indian Ocean SST dipole events and southern African rainfall. *Geophys. Res. Lett.* **28:** 2225–2227.
26. Rouault, M., P. Florenchie, N. Fauchereau & C.J.C. Reason. 2003. South east tropical Atlantic warm events and southern African rainfall. *Geophys. Res. Lett.* **30:** 8009–8013.
27. Reason, C.J.C. & D. Jagadheesha. 2005. Relationships between South Atlantic SST variability and atmospheric circulation over the South African region during austral winter. *J. Clim.* **18:** 3059–3075.
28. Reason, C.J.C., W. Landman & W. Tennant. 2006. Seasonal to decadal prediction of Southern African climate and its links with variability of the Atlantic Ocean. *Bull. Am. Meteorol. Soc.* **87:** 941–955.
29. Vigaud, N., Y. Richard, M. Rouault & N. Fauchereau. 2009. Moisture transport between the South Atlantic Ocean and southern Africa: relationships with summer rainfall and associated dynamics. *Clim. Dyn.* **32:** 113–123.
30. Nieto, R., R. Castillo, A. Drumond & L. Gimeno. 2014. A catalog of moisture sources for continental climatic regions. *Water Resour. Res.* **50:** 5322–5328.
31. D'Abreton, P.C. & J.A. Lindesay. 1993. Water vapour transport over southern Africa during wet and dry early and late summer months. *Int. J. Climatol.* **13:** 151–170.
32. Guan, B. & D.E. Waliser. 2015. Detection of atmospheric rivers: evaluation and application of an algorithm for global studies. *J. Geophys. Res. Atmos.* **120:** 12514–12535.
33. Paltan, H., D.E. Waliser, W.H. Lim, *et al.* 2017. Global floods and water availability driven by atmospheric rivers. *Geophys. Res. Lett.* **44:** 10387–10395.
34. Espinoza, V., D.E. Waliser, B. Guan, *et al.* 2018. Global analysis of climate change projection effects on atmospheric rivers. *Geophys. Res. Lett.* **45:** 4299–4308.
35. Dee, D.P., S.M. Uppala, A.J. Simmons, *et al.* 2011. The ERA-Interim reanalysis: configuration and performance of the data assimilation system. *Q. J. R. Meteorol. Soc.* **13:** 553–597.
36. Whiteman, C.D., X. Bian & S. Zhong. 1997. Low-level jet climatology from enhanced rawinsonde observations at a site in the southern Great Plains. *J. Appl. Meteorol. Climatol.* **36:** 1363–1376.
37. Stohl, A. & P. James. 2004. Lagrangian analysis of the atmospheric branch of the global water cycle. Part I: method

description, validation, and demonstration for the August 2002 flooding in Central Europe. *J. Hydrometeorol.* **5:** 656–678.
38. Stohl, A., M. Hittenberger & G. Wotawa. 1998. Validation of the Lagrangian particle dispersion model FLEXPART against largescale tracer experiment data. *Atmos. Environ.* **32:** 4245–4264.
39. Stohl, A. & P. James. 2005. A Lagrangian analysis of the atmospheric branch of the global water cycle. Part II: moisture transports between the Earth's ocean basins and river catchments. *J. Hydrometeorol.* **6:** 961–984.
40. Numaguti, A. 1999. Origin and recycling processes of precipitating water over the Eurasian continent: experiments using an atmospheric general circulation model. *J. Geophys. Res.* **104:** 1957–1972.
41. Nieto, R., L. Gimeno & R.M. Trigo. 2006. A Lagrangian identification of major sources of Sahel moisture. *Geophys. Res. Lett.* **33:** L18707.
42. Duran-Quesada, A.M., L. Gimeno, J.A. Amador & R. Nieto. 2010. Moisture sources for Central America: identification of moisture sources using a Lagrangian analysis technique. *J. Geophys. Res.* **115:** D05103.
43. Drumond, A., L. Gimeno & R. Nieto. 2011. On the contribution of the Tropical Western Hemisphere Warm Pool source of moisture to the Northern Hemisphere precipitation through a Lagrangian approach. *J. Geophys. Res.* **116:** D00Q04.
44. Sorí, R., R. Nieto, S.M. Vicente-Serrano, *et al.* 2017. A Lagrangian perspective of the hydrological cycle in the Congo River basin. *Earth Syst. Dynam.* **8:** 653–675.
45. Gimeno, L., A. Drumond, R. Nieto, *et al.* 2010. On the origin of continental precipitation. *Geophys. Res. Lett.* **37:** L13804.
46. Ramos, A.M., R. Nieto, R. Tomé, *et al.* 2016. Atmospheric rivers moisture sources from a Lagrangian perspective. *Earth Syst. Dynam.* **7:** 371–384.
47. Stohl, A., C. Forster & C. Sodemann. 2008. Remote sources of water vapor forming precipitation on the Norwegian west coast at 60°N: a tale of hurricanes and an atmospheric river. *J. Geophys. Res.* **113:** D05102.
48. Ryoo, J.-M., D.E. Waliser, D.W. Waugh, *et al.* 2015. Classification of atmospheric river events on the U.S. West Coast using a trajectory model. *J. Geophys. Res. Atmos.* **120:** 3007–3028.
49. Cook, C., C.J.C. Reason & B.C. Hewitson. 2004. Wet and dry spells within particular wet and dry summers in the South African summer rainfall region. *Clim. Res.* **26:** 17–31.
50. Hansingo, K. & C.J.C. Reason. 2009. Modelling the atmospheric response over southern Africa to SST forcing in the southeast tropical Atlantic and southwest subtropical Indian Oceans. *Int. J. Climatol.* **29:** 1001–1012.
51. Reason, C.J.C., M. Rouault, J.-L. Melice & D. Jagadeesha. 2002. Interannual winter rainfall variability in SW South Africa and large scale ocean–atmosphere interactions. *Meteorol. Atmos. Phys.* **80:** 19–29.
52. Harrison, M.S.J. 1984. A generalized classification of South African rain-bearing synoptic systems. *Int. J. Climatol.* **4:** 547–560.
53. Hart, N.C.G., C.J.C. Reason & N. Fauchereau. 2010. Tropical–extratropical interactions over Southern Africa: three cases of heavy summer season rainfall. *Mon. Weather Rev.* **138:** 2608–2623.
54. Hart, N.C.G., C.J.C. Reason & N. Fauchereau. 2013. Cloud bands over southern Africa: seasonality, contribution to rainfall variability and modulation by the MJO. *Clim. Dyn.* **41:** 1199–1212.

5

Summary and conclusions

Moisture transport is a fundamental component of the hydrological cycle, which constitutes a bridge between evaporation and precipitation. In this thesis, the main goal was to investigate the role of the two main mechanisms of transport of moisture, i.e., the Atmospheric rivers (ARs) and Low-Level Jets (LLJs) from a global approach. Both structures redistribute the available moisture in the atmosphere and play a fundamental role in the global and regional hydrological cycle. One particularly important in tropical and subtropical regions, i.e., the LLJs; whereas the other is especially relevant in the transport of moisture in extratropical regions, i.e., the ARs.

In the case of LLJ, the identification of LLJ events was performed using a night detection index based on the vertical variation of the temporal structure of the wind (using the methodology by Rife et al., 2010). For the detection of AR, the database developed by Guan and Waliser (2015) was used to define the significant coastal areas affected by these systems.

Both structures were subsequently investigated in terms of global and regional moisture transport. To address this goal, the Lagrangian model, i.e., FLEXPART, was applied. FLEXPART is a robust tool used to diagnose atmospheric motion and widely implemented in the investigation of moisture transport in the atmosphere.

The analysis period varied according to the availability of data, which were progressively updated at the start date of each analysis.

Each global study of both systems is accompanied by a regional study to focus on specific regions of occurrence or individual structures. Thus, for LLJs, the focus was on

the quantification of the moisture of the Great Plains LLJ (GPLLJ), in which an alternative approach for the study of moisture, i.e., WRF-TT (Insua-Costa and Miguez-Macho, 2018) was applied. On the other hand, for ARs, the focus was on those systems that reach the Arctic region. Finally, a relationship between both mechanisms of transport of moisture was found, linking the moisture transported by a particular phase of the South American LLJ over the South Atlantic Ocean and the ARs that make landfalling over the west coast of South Africa.

The main conclusive remarks derived from this thesis are presented below, following the same sequence of the articles presented in Chapter 4:

Low-level jets and associated moisture sources and sinks

Global distribution of nocturnal LLJs (NLLJ), during the warm season and over both hemispheres, was obtained using an objective index. The index is provided with the location of the main moisture sinks and sources associated with each LLJ. Moreover, changes between days of jet and no-jet are reported geographically in terms of evaporation and precipitation. Finally, a brief appointment is made in terms of water scarcity and the association with the LLJs occurrence.

- A total of 33 global regions of NLLJ occurrence were identified: 20 of which were identified during the boreal summer (over northern hemisphere) and the remaining 13 regions during the austral summer (over southern hemisphere). The NLLJ are mainly concentrated in tropical regions.
- The approach reported new regions of occurrence of NLLJ not analysed in previous studies, mainly in the eastern region of Brazil and western Asia.
- In the analysis of the moisture source-sink relationship, it was found that an essential modulation of the moisture transported by the NLLJs was highly asymmetric.
- In North America, where the GPLLJ dominates, the moisture transported is supported from the southern Gulf of Mexico and the Caribbean Sea.
- In South America, the primary source of moisture for the northern NLLJs is the tropical North Atlantic. Moreover, the transport of moisture is enhanced over the continent as it passes through the Amazon Basin, the primary source of moisture for the SALLJ.

- In Africa, NLLJs are not associated with a significant moisture advection. Nevertheless, the existing moisture mainly comes from the Mediterranean basin and continental recycling.
- In Asia, NLLJs are strongly linked to monsoon regimes, and the moisture comes mostly from the northern Indian Ocean, particularly from the oceanic regions of the Arabian Sea and the Gulf of Bengal.
- In Australia, moisture mainly comes from the Coral Sea due to the strong advection of the east winds, and there is a local source on the west coast that enhanced the transport of moisture by this LLJ.
- Moisture sink regions (i.e., where moisture contributes to precipitation) are those regions to which the NLLJ carries moisture, and these areas are especially vulnerable to changes in moisture transport through LLJs. Generally, days of LLJ are linked to a higher moisture advection, and the water vapour is transported towards more remote regions of maximum occurrence of LLJ, given the strong wind advection at low levels. In other words, in a day of LLJ, the sink of moisture is located farther away. However, during the days with no LLJ, moisture is concentrated in regions close to the area of maximum occurrence of NLLJ, and moisture transport is negligible.
- In North America, during the days of GPLLJ, the moisture is advected mainly towards the northeast of the United States, reaching the eastern and northern coast of the United States and Canada. Nevertheless, during the days of no GPLLJ, the moisture is confined in the central-western United States, close to the area of maximum occurrence of GPLLJ.
- In South America, the main pattern of moisture transport during days with LLJ occurs towards southern inland regions and to the southwest of South America, always in parallel to the Andes. The SALLJ sink region is located over the Rio de Plata basin and southeast of South America. During days with no LLJs, the pathway of moisture has a shorter route, and in some cases, it recurves eastward.
- In Asia, particularly China LLJ, the days of LLJ are linked to an intensification of the source of moisture, and the water vapour reaches the east of China. During a non-LLJ event, the moisture is mostly confined to central-south China.
- In the NLLJs that develop over Africa, moisture transport is lower compared to other regions identified above. One of the reasons is the fact that they are

developed over arid regions; therefore, these structures are more closely linked to the transport of dust.

- Some overpopulated regions are affected by the regimen of precipitation associated with the LLJs, and the amount of moisture transported compromises the availability of water resources as well as clearly the water scarcity, impacting in the socio-economic structures. North Africa and the Horn of Africa are particularly sensitive to changes in the behaviour to LLJs. Both regions are characterised by being arid and densely populated, which amplifies the hydraulic demand. Therefore, a minimal change in precipitation patterns linked to LLJ would have a knock-on effect on the already low availability of freshwater resources.

A case study: The Great Plains low-level jet (GPLLJ)

The Lagrangian and Eulerian techniques are used to examine moisture transport during the month of maximum activity of GPLLJ, which modulates the entry of moisture, and therefore the pattern of precipitation in the southeast of the United States. The primary source of moisture is identified, and then the moisture transported is quantified.

- The main source of moisture during July for the GPLLJ is detected over the oceanic region that extends from the Gulf of Mexico and part of the Caribbean Sea.
- The average wind advection of moisture by the GPLLJ can explain more than 80% of the precipitable water over the southern Great Plains region when a jet event occurs.
- The influence of orography curves the GPLLJ towards the east of the United States, which transports moisture to the east coast of the United States. The transported moisture ratio decreases as latitude increases. Nevertheless, the GPLLJ can explain almost half of the moisture than in the northeastern United States in the south of the Great Lakes.
- A major moisture advection is not necessarily linked to high NLLJ index values. In other words, a high NLLJ index value only shows a more significant wind shear.

Atmospheric Rivers and associated moisture sources

Anomalous moisture uptake (AMU) areas are reported for the primary regions of occurrence of ARs on a global scale. Then, an analysis of the interannual variability is performed to investigate trends in the regions that provide moisture to the ARs.

- A total of 20 regions of high-frequency AR were identified, which were mainly located on the western coastline of mid-latitudes.
- The results show a significant increase in the global AMU for landfalling AR events (LARs) in the current climate (0.9% per decade for 1980-2017). Extreme precipitation events will increase at the same rate as atmospheric moisture following the Clausius-Clapeyron (CC) ratio.
- The Western Hemisphere Warm Pool (WHWP) is identified as the main global contribution of anomalous moisture uptake.
- AMU highs values are found in areas near tropical latitudes, confirming the subtropical origin of transported moisture, and also in areas near where AR makes landfalling and along their paths, showing the importance of local convergence.

A case study: Atmospheric Rivers over the Arctic

The Arctic is one of the regions that are most sensitive to global warming. Atmospheric rivers represent one of the main events involved in moisture transport, hence, latent heat flow from the tropics to the height latitudes. Therefore, an increase in the moisture transport can be related to a decrease in the sea ice extent.

- The main entry gates for ARs that reach the Arctic are the North Atlantic Ocean, from 80° W to 60° E, and the North Pacific Ocean, from 120° to 240° E.
- The maximum AR activity occurs in autumn for the Atlantic sector and in summer for the Pacific one; the minimum activity occurs for both the Atlantic and Pacific during spring.
- The main sources of moisture for these systems are the basin of the northern oceans, in particular, the western part of the oceanic regions in the band between 30 °N and 40 °N. Nevertheless, essential sources of continental moisture appear in North America and Eurasia, especially during summer.

- In general terms, southern moisture sources coincide with climatological evaporative areas which influence poleward moisture transport toward the Arctic. In the Atlantic Ocean, an important moisture uptake is produced over the area of the AR pathway.
- During ARs events, anomalous moisture uptake occurs near 60 ºN, northward to the climatological sources of moisture. This fact suggests an enhanced continuous anomalous moisture uptake in the region of maximum AR activity and nearby along with the northern transition of ARs into the Arctic.

Linking moisture transport-associated to LLJs and ARs: a case study over the South Atlantic Ocean.

The primary anomalous moisture uptake areas linked to those ARs landfilling on the west coast of South Africa are investigated. The results focus on the role of the SALLJ and its importance in the transport of moisture from the Amazon Basin to the west coast of South Africa.

- For those ARs that reach west of South Africa, the anomalous moisture uptake occurs over confined subtropical areas. In total, four areas have been identified, i.e., (i) the South Atlantic Ocean between 10 °S and 30 °S, (ii) local maximum in the eastern South Atlantic, (iii) a continental source over the north of the Western Cape, and (iv) over South America, at a distance more than 7000 km.
- The mechanism responsible for this long-distance moisture uptake by ARs is based on a unique combination of meteorological events lagged in days:
    - First, a particular phase of the South American LLJ, known as No Chaco Jet event (NCJE), transport moisture from the northern South America Continent (that includes the Paraná River Basin and the southern Amazon River Basin) to the western and central South Atlantic Ocean basin, and eventually to the southern regions (which are the climatological sinks for the SALLJ).
    - This anomalous moisture over the western and central South Atlantic Ocean basin is captured by the ARs that reach the west coast of South Africa.

- Anomalous moisture sinks for the NCJE days and IVT anomalies for ARs days over central South Atlantic Ocean basin have been detected, thus confirming the existence of the link.

A

Supplementary Material

In this section is presented the supplementary material linked to each article that makes the main part of this thesis. All material related with published articles is available online by each journal.

Global climatology of nocturnal low-level jets and associated moisture sources and sinks

Iago Algarra[1], Jorge Eiras-Barca[1,2], Raquel Nieto[1], and Luis Gimeno[1]

[1]EPhysLab (Environmental Physics Laboratory), Facultade de Ciencias, Universidade de Vigo, Ourense, Galicia, Spain
[2]Department of Atmospheric Sciences, University of Illinois at Urbana-Champaign, Urbana, Illinois, United States

Correspondence to: Iago Algarra (ialgarra@uvigo.es)

Supplementary Material

Captions

Figure S1: Mean time height of wind speed within the jet core (in m/s), for each LLJ detected and during jets events. LST: Local Solar Time.

Figure S2: Wind vertical profile (in m/s) for each LLJ detected calculated at the point of maxima intensity (Black cross in fig. 1). Black line is the climatology for jet events at night hour. Dashed black line is the climatology for no-LLJ at night hour. Red line refers to climatology (LLJ and no LLJ) at midnight solar time and dashed red line refers to climatology (LLJ and no-LLJ) at noon solar time.

Figure S1

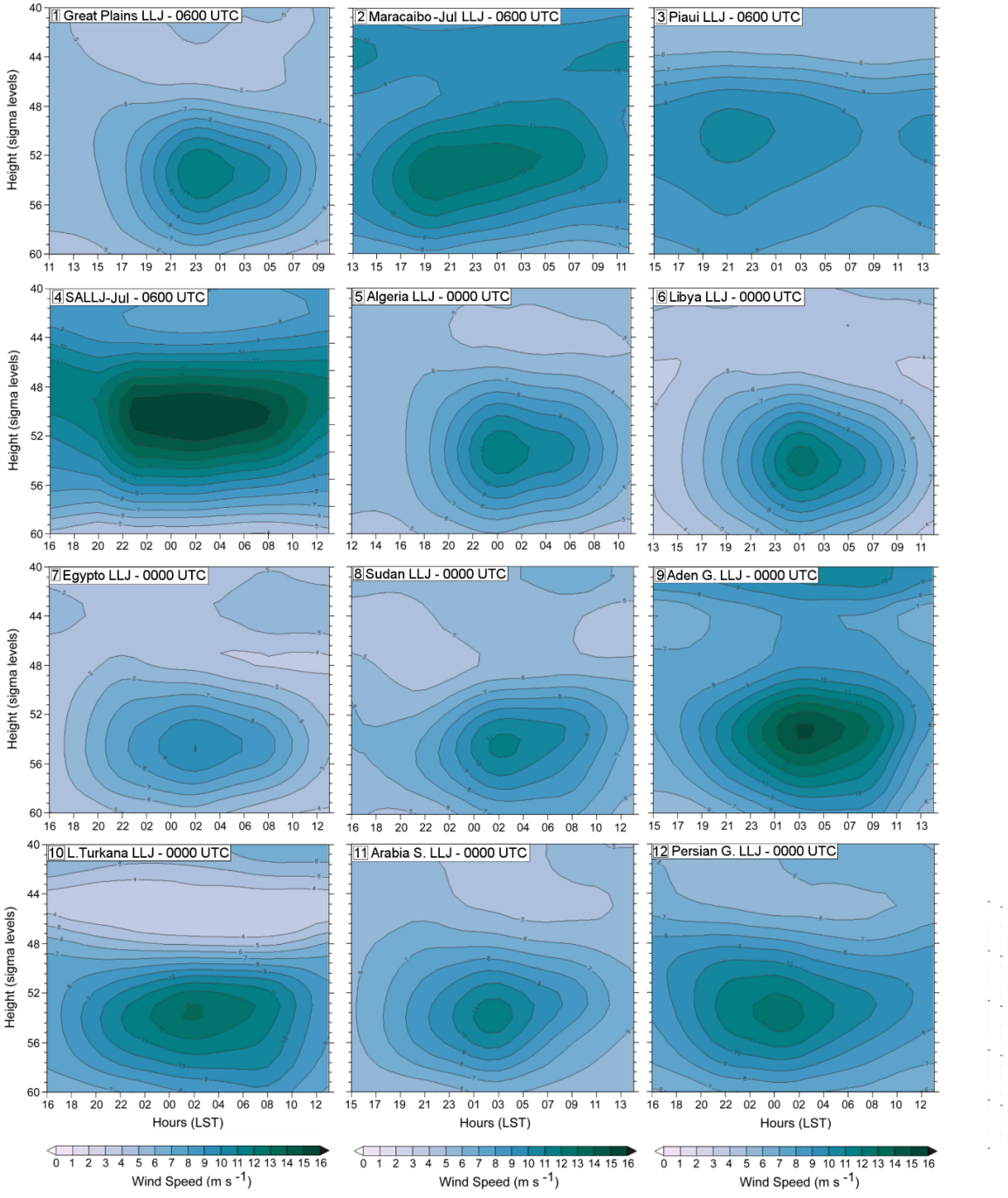
1 Great Plains LLJ - 0600 UTC
2 Maracaibo-Jul LLJ - 0600 UTC
3 Piaui LLJ - 0600 UTC
4 SALLJ-Jul - 0600 UTC
5 Algeria LLJ - 0000 UTC
6 Libya LLJ - 0000 UTC
7 Egypto LLJ - 0000 UTC
8 Sudan LLJ - 0000 UTC
9 Aden G. LLJ - 0000 UTC
10 L.Turkana LLJ - 0000 UTC
11 Arabia S. LLJ - 0000 UTC
12 Persian G. LLJ - 0000 UTC
Height (sigma levels)
Hours (LST)
Wind Speed (m s -1)

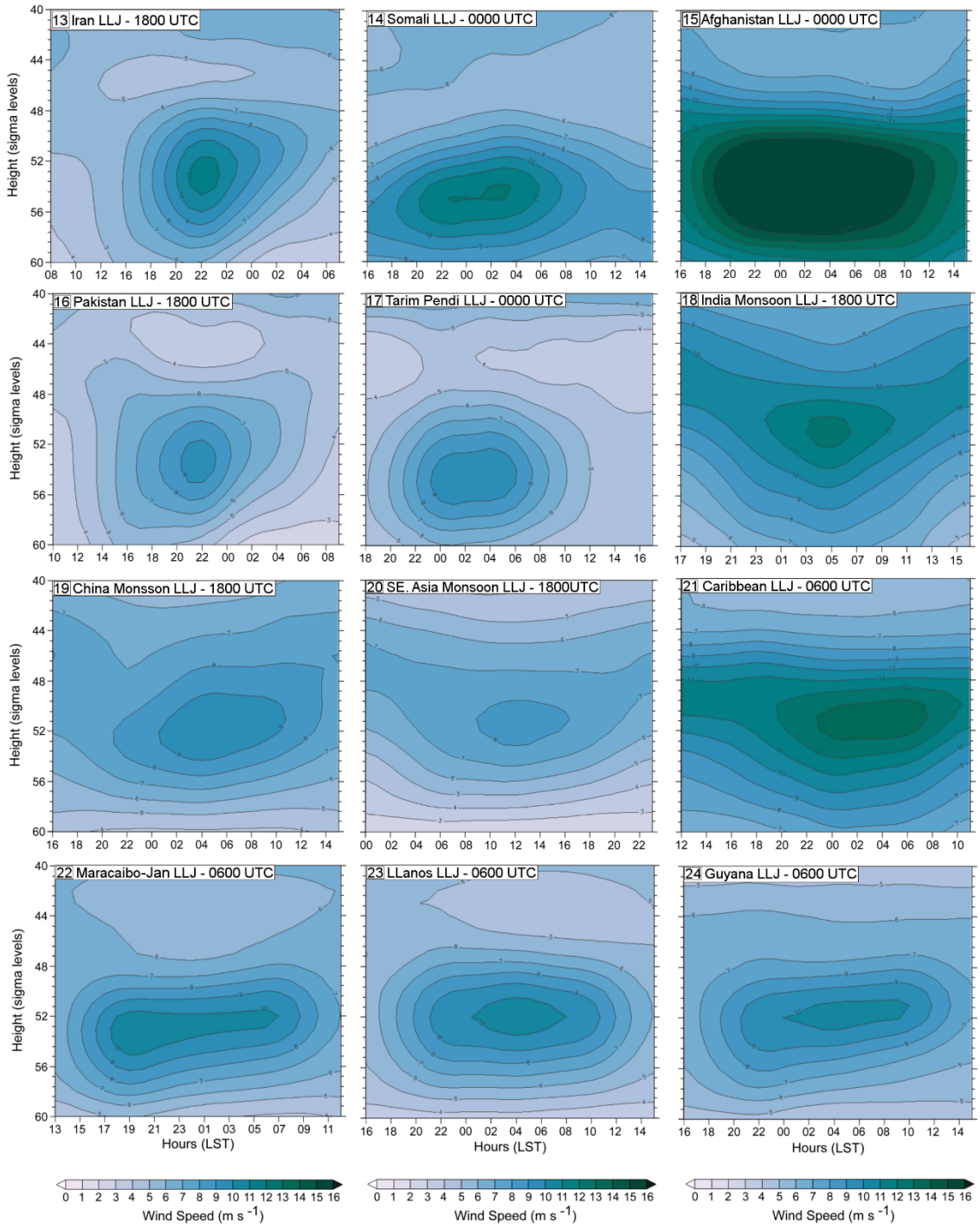
13 Iran LLJ - 1800 UTC
14 Somali LLJ - 0000 UTC
15 Afghanistan LLJ - 0000 UTC
16 Pakistan LLJ - 1800 UTC
17 Tarim Pendi LLJ - 0000 UTC
18 India Monsoon LLJ - 1800 UTC
19 China Monsson LLJ - 1800 UTC
20 SE. Asia Monsoon LLJ - 1800UTC
21 Caribbean LLJ - 0600 UTC
22 Maracaibo-Jan LLJ - 0600 UTC
23 LLanos LLJ - 0600 UTC
24 Guyana LLJ - 0600 UTC
Height (sigma levels)
Hours (LST)
Wind Speed (m s -1)

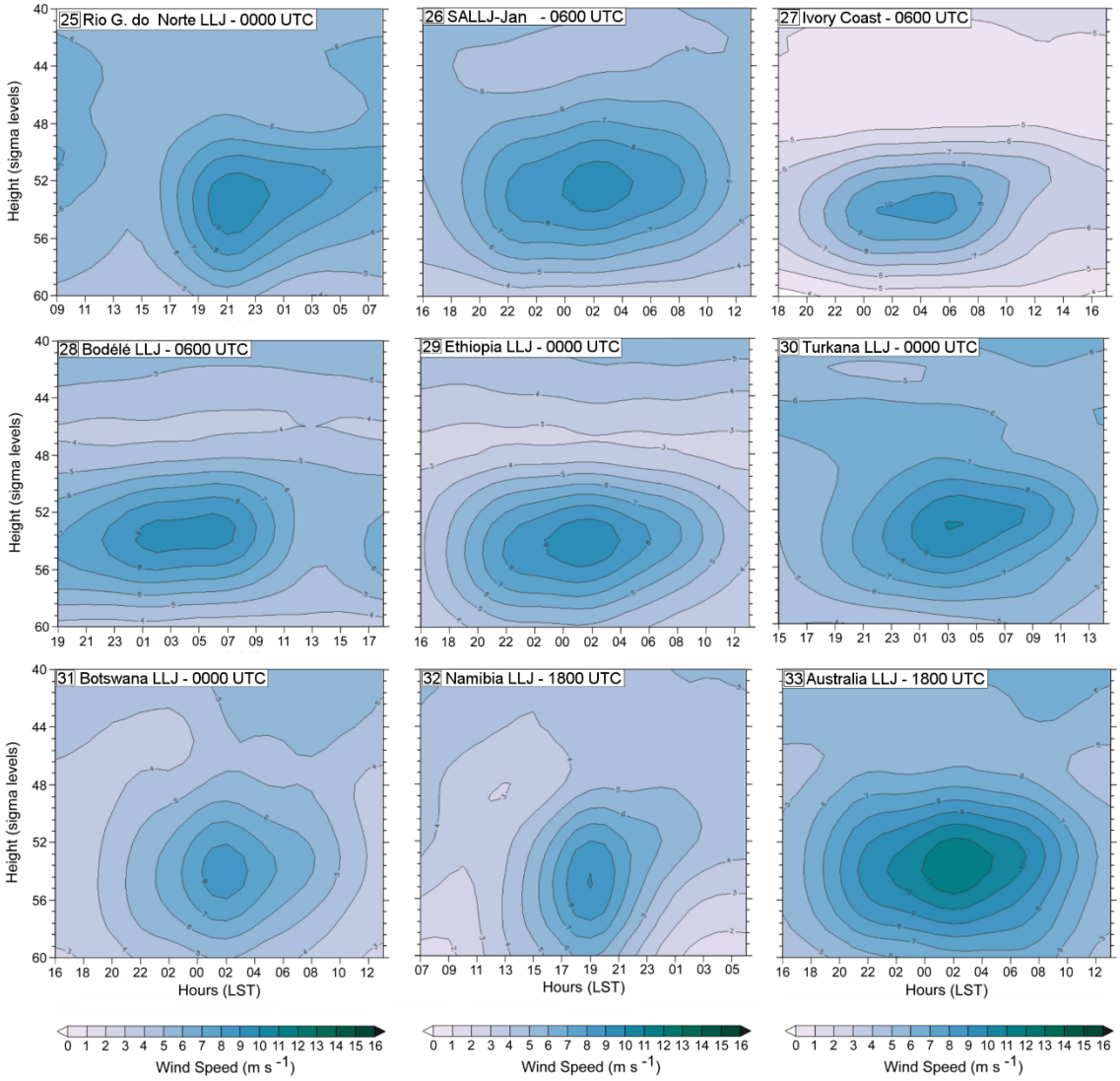
25 Rio G. do Norte LLJ - 0000 UTC
26 SALLJ-Jan - 0600 UTC
27 Ivory Coast - 0600 UTC
28 Bodélé LLJ - 0600 UTC
29 Ethiopia LLJ - 0000 UTC
30 Turkana LLJ - 0000 UTC
31 Botswana LLJ - 0000 UTC
32 Namibia LLJ - 1800 UTC
33 Australia LLJ - 1800 UTC
Height (sigma levels)
Hours (LST)
Wind Speed (m s -1)

Figures S2

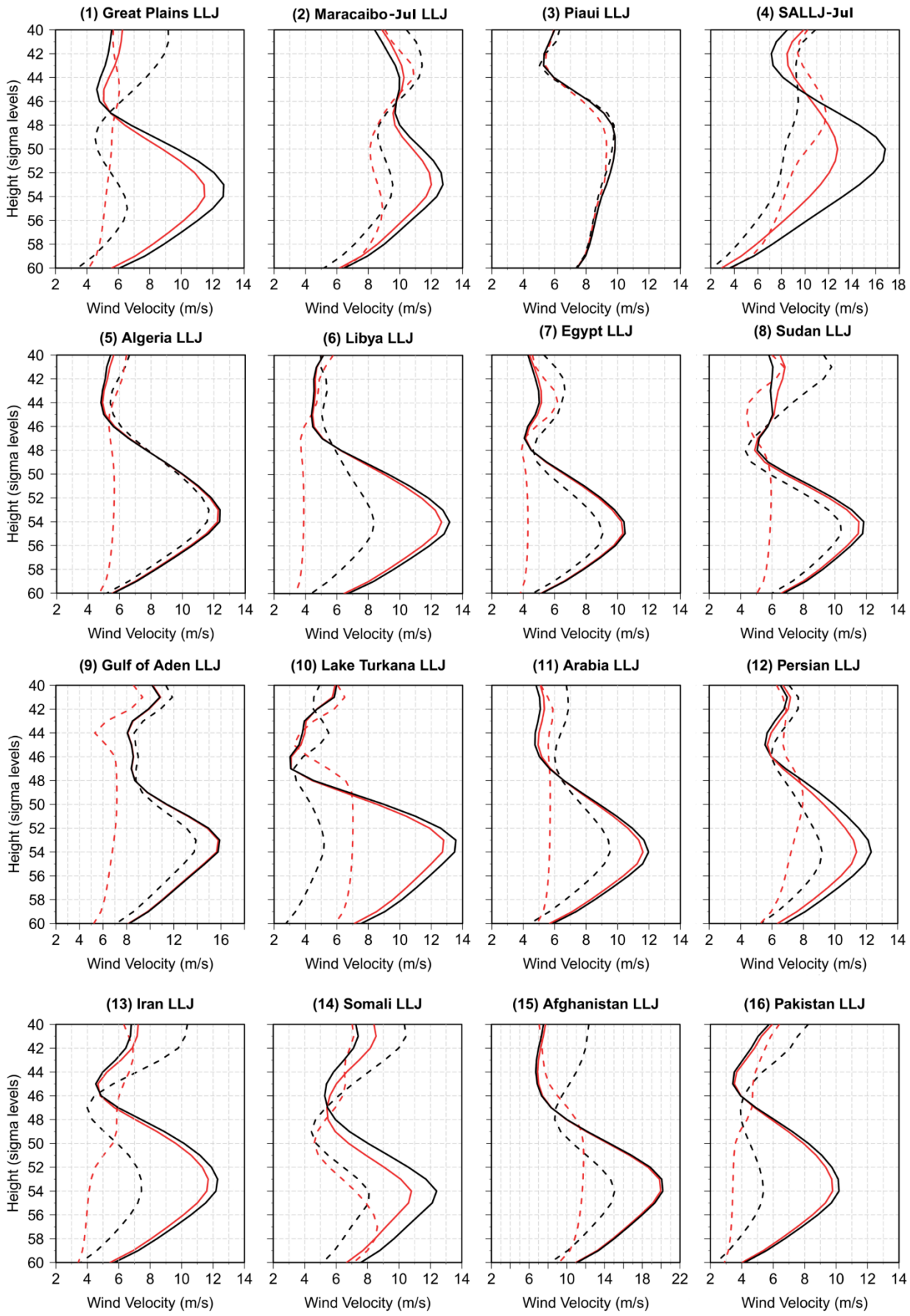
(1) Great Plains LLJ
(2) Maracaibo-Jul LLJ
(3) Piaui LLJ
(4) SALLJ-Jul
(5) Algeria LLJ
(6) Libya LLJ
(7) Egypt LLJ
(8) Sudan LLJ
(9) Gulf of Aden LLJ
(10) Lake Turkana LLJ
(11) Arabia LLJ
(12) Persian LLJ
(13) Iran LLJ
(14) Somali LLJ
(15) Afghanistan LLJ
(16) Pakistan LLJ
Height (sigma levels)
Wind Velocity (m/s)

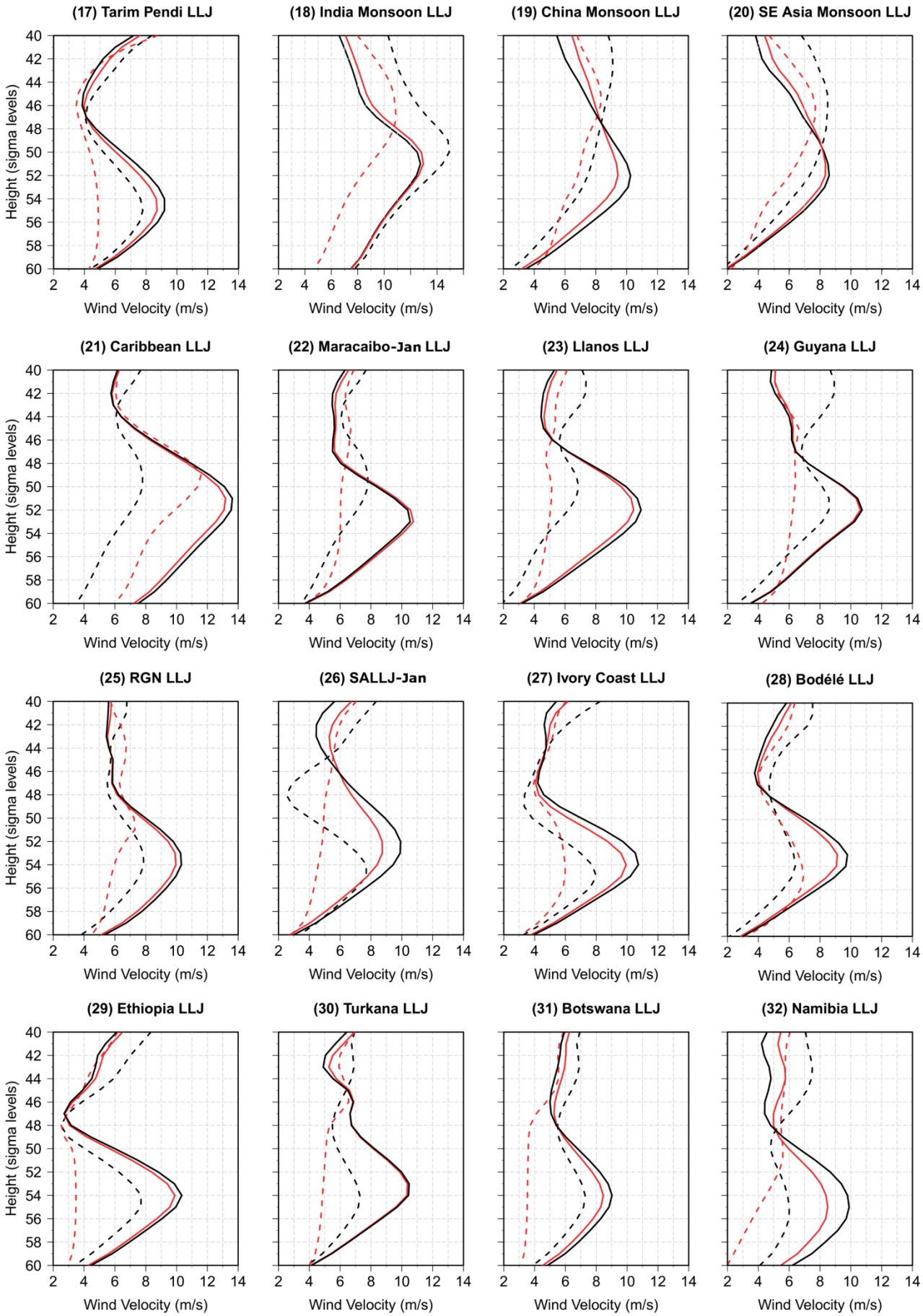
(17) Tarim Pendi LLJ
(18) India Monsoon LLJ
(19) China Monsoon LLJ
(20) SE Asia Monsoon LLJ
(21) Caribbean LLJ
(22) Maracaibo-Jan LLJ
(23) Llanos LLJ
(24) Guyana LLJ
(25) RGN LLJ
(26) SALLJ-Jan
(27) Ivory Coast LLJ
(28) Bodélé LLJ
(29) Ethiopia LLJ
(30) Turkana LLJ
(31) Botswana LLJ
(32) Namibia LLJ
Height (sigma levels)
Wind Velocity (m/s)

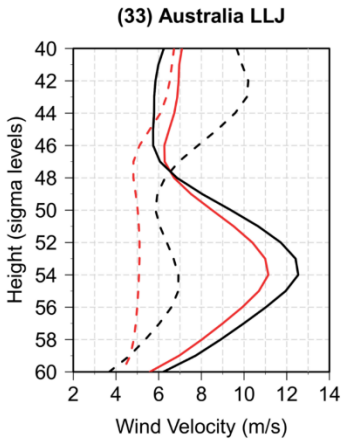
(33) Australia LLJ
Height (sigma levels)
40
42
44
46
48
50
52
54
56
58
60
2
4
6
8
10
12
14
Wind Velocity (m/s)

Supplement of Earth Syst. Dynam., 10, 107–119, 2019
https://doi.org/10.5194/esd-10-107-2019-supplement

Earth System Dynamics
Open Access
EGU

Supplement of

On the assessment of the moisture transport by the Great Plains low-level jet

Iago Algarra et al.

Correspondence to: Iago Algarra (ialgarra@uvigo.es)

Captions

Figure S1: Monthly variability of the percentage of GPLLJ days.

Figure S2: Moisture sources for the 6 case-studies analysed. Green line delimits the 75th percentile of (E - P) > 0 values. The vectors show the wind direction and intensity for each case study at surface level (~500m AGL). The purple line shows the position of the moisture-labelling wall used in the WRF simulation.

Figure S3: Comparison of 11-days accumulated precipitation for WRF simulations versus CPC gauge-analysis observations throughout the same periods.

Figure S4: (a-c) qTR in g kg^{-1} for the three vertical cross sections at the locations depicted with white lines in Fig. 5 for jet event of July 19, 1999 – Simulation 1. (d-f) same as (a-c) but for φTR in g m $(kg\ s)^{-1}$.

Figure S5: As Figure S4 but for jet event of July 23, 1983 – Simulation 2.

Figure S6: As Figure S4 but for jet event of July 28, 2002 – Simulation 4.

Figure S7: As Figure S4 but for jet event of July 14, 2016 – Simulation 5.

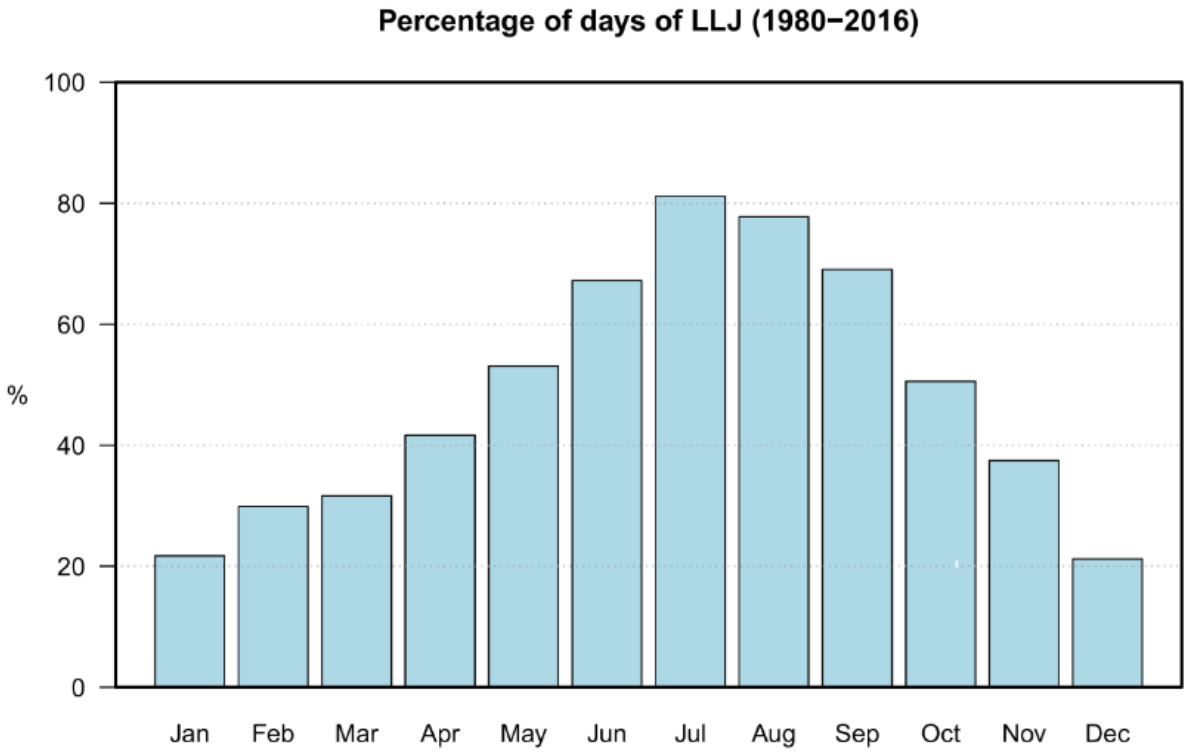
Percentage of days of LLJ (1980−2016)
100
80
60
40
20
0
%
Jan
Feb
Mar
Apr
May
Jun
Jul
Aug
Sep
Oct
Nov
Dec

Figure S1

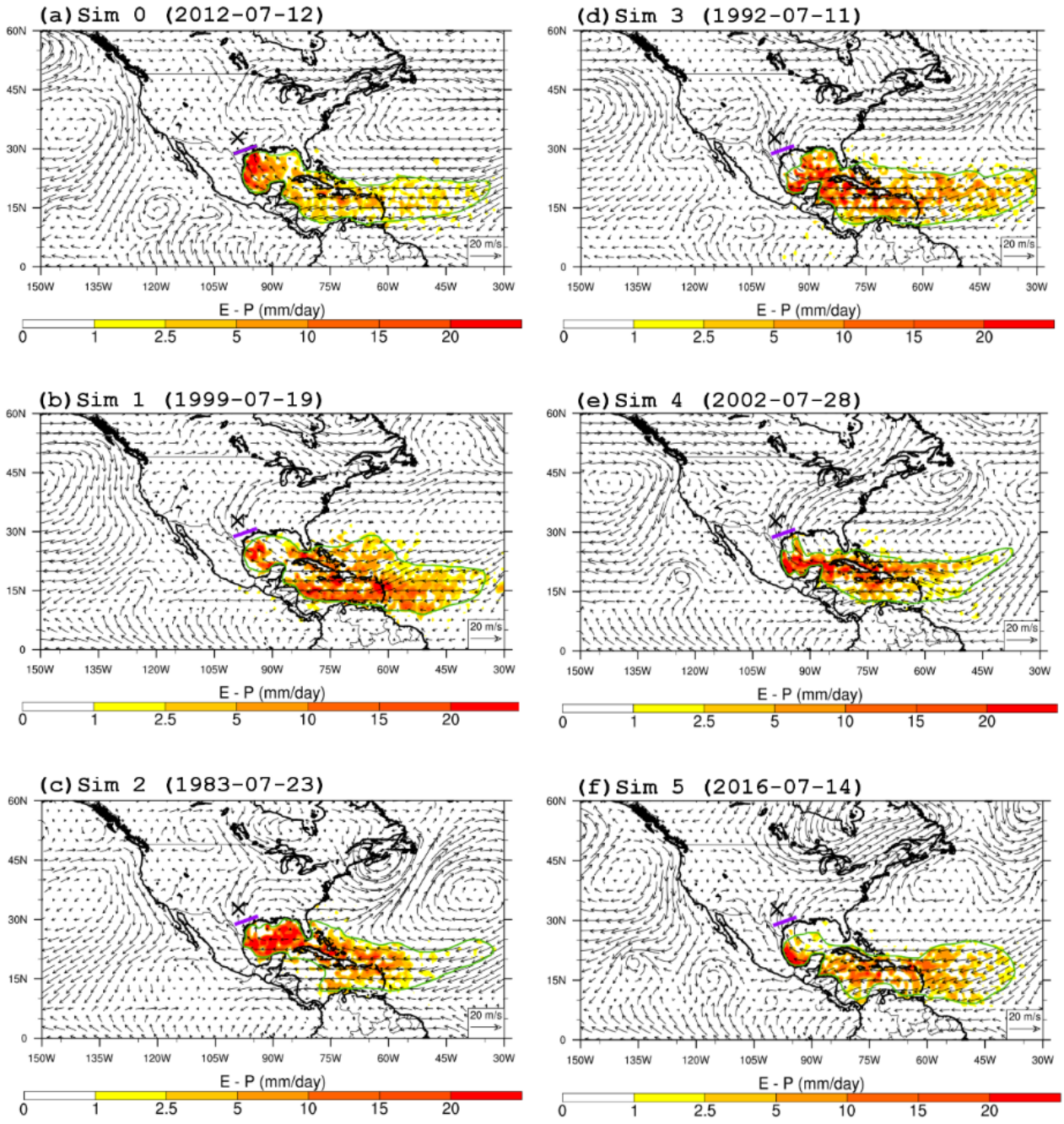
(a) Sim 0 (2012-07-12)
(d) Sim 3 (1992-07-11)
(b) Sim 1 (1999-07-19)
(e) Sim 4 (2002-07-28)
(c) Sim 2 (1983-07-23)
(f) Sim 5 (2016-07-14)
60N
45N
30N
15N
0
150W 135W 120W 105W 90W 75W 60W 45W 30W
20 m/s
E - P (mm/day)
0 1 2.5 5 10 15 20

Figure S2

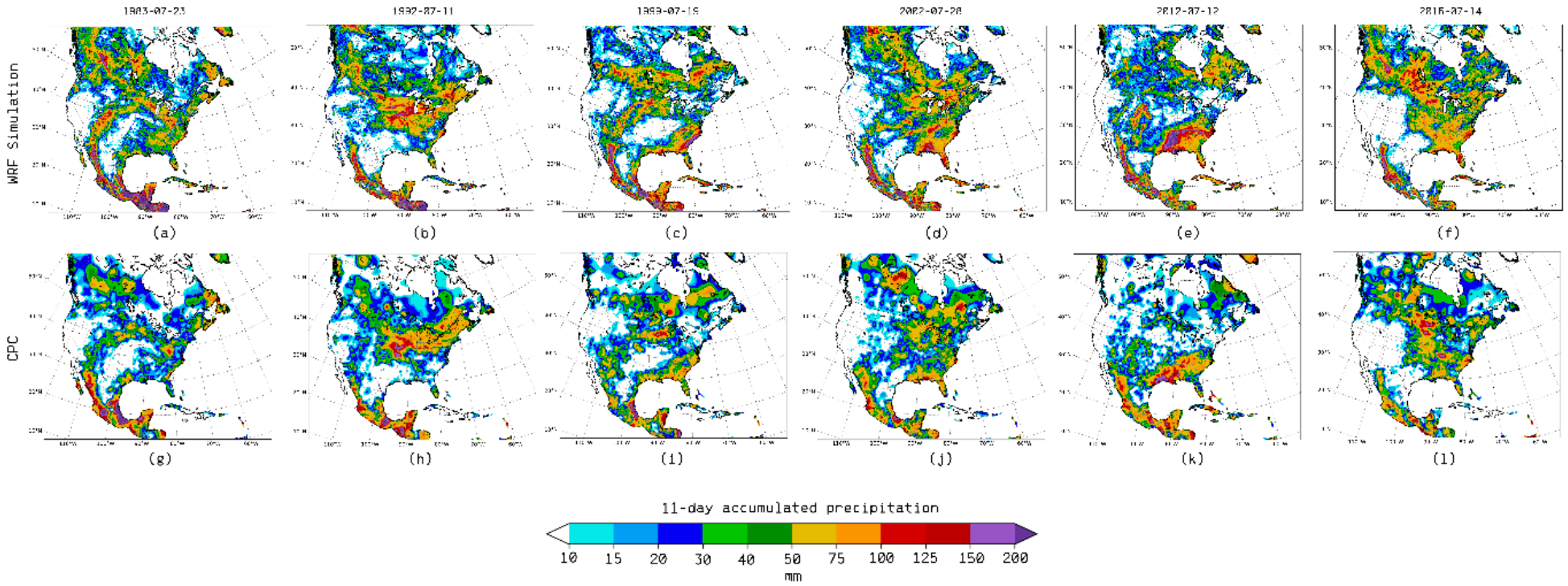
1983-07-23
1992-07-11
1999-07-15
2002-07-28
2012-07-12
2016-07-14
WRF Simulation
CPC
(a)
(b)
(c)
(d)
(e)
(f)
(g)
(h)
(i)
(j)
(k)
(l)
11-day accumulated precipitation
10
15
20
30
40
50
75
100
125
150
200
mm

Figure S3

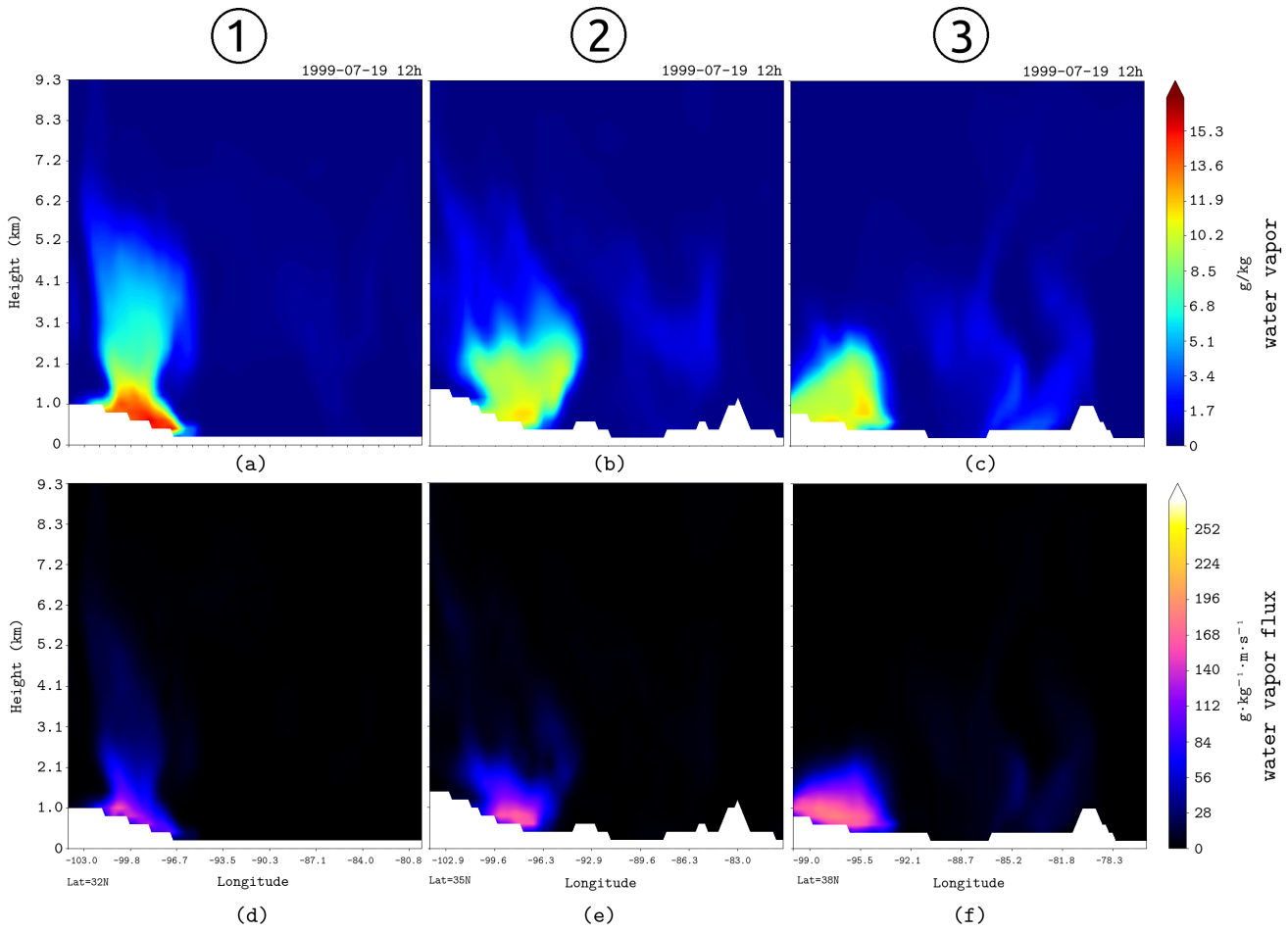
1
2
3
1999-07-19 12h
1999-07-19 12h
1999-07-19 12h
Height (km)
9.3
8.3
7.2
6.2
5.2
4.1
3.1
2.1
1.0
0
(a)
(b)
(c)
15.3
13.6
11.9
10.2
8.5
6.8
5.1
3.4
1.7
0
g/kg
water vapor
252
224
196
168
140
112
84
56
28
0
g·kg⁻¹·m·s⁻¹
water vapor flux
-103.0 -99.8 -96.7 -93.5 -90.3 -87.1 -84.0 -80.8
Lat=32N
Longitude
-102.9 -99.6 -96.3 -92.9 -89.6 -86.3 -83.0
Lat=35N
Longitude
-99.0 -95.5 -92.1 -88.7 -85.2 -81.8 -78.3
Lat=38N
Longitude
(d)
(e)
(f)

Figure S4

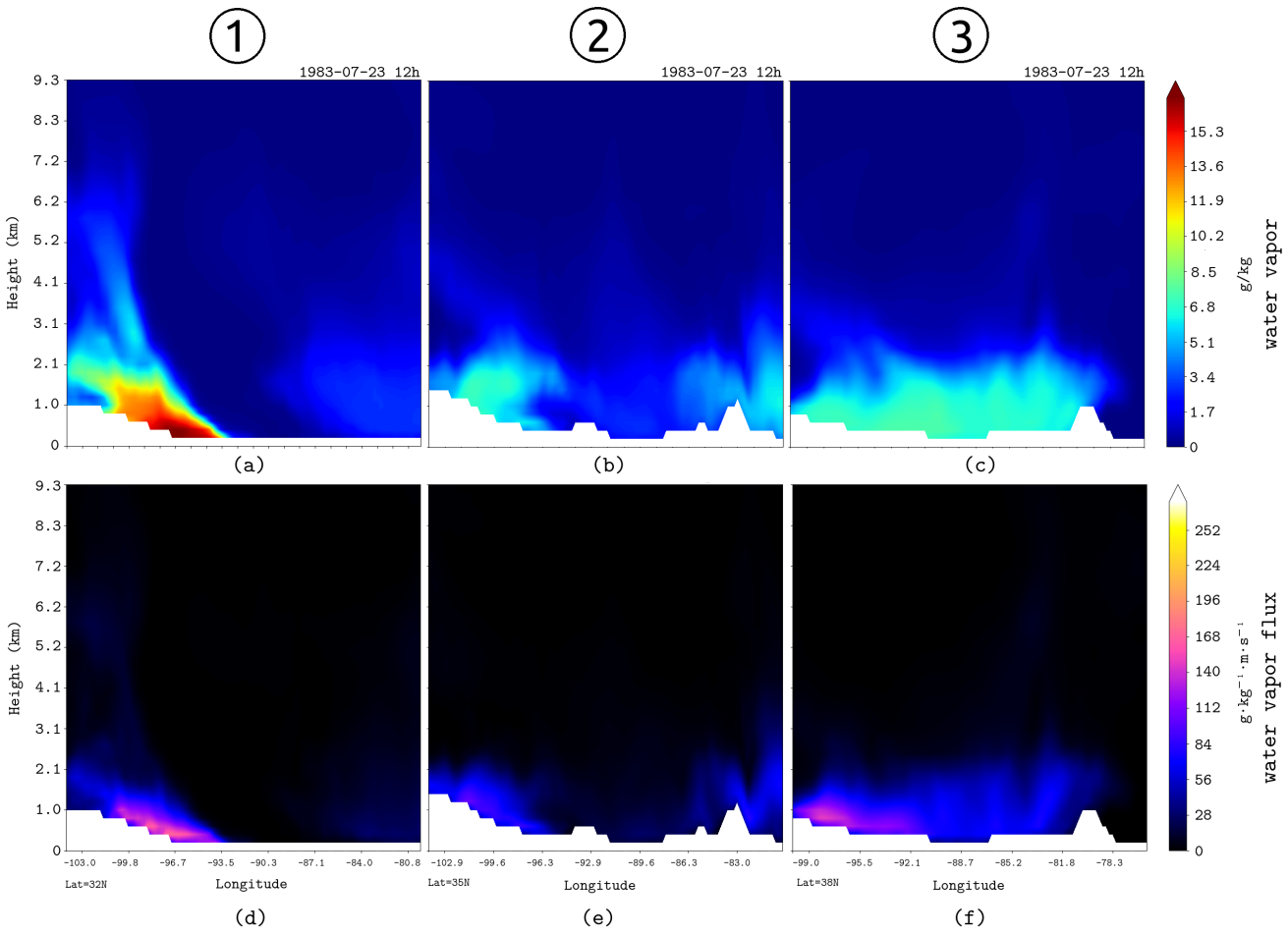
1
2
3
1983-07-23 12h
1983-07-23 12h
1983-07-23 12h
Height (km)
9.3
8.3
7.2
6.2
5.2
4.1
3.1
2.1
1.0
0
(a)
(b)
(c)
15.3
13.6
11.9
10.2
8.5
6.8
5.1
3.4
1.7
0
g/kg
water vapor
252
224
196
168
140
112
84
56
28
0
g·kg⁻¹·m·s⁻¹
water vapor flux
-103.0 -99.8 -96.7 -93.5 -90.3 -87.1 -84.0 -80.8
Lat=32N
Longitude
-102.9 -99.6 -96.3 -92.9 -89.6 -86.3 -83.0
Lat=35N
Longitude
-99.0 -95.5 -92.1 -88.7 -85.2 -81.8 -78.3
Lat=38N
Longitude
(d)
(e)
(f)

Figure S5

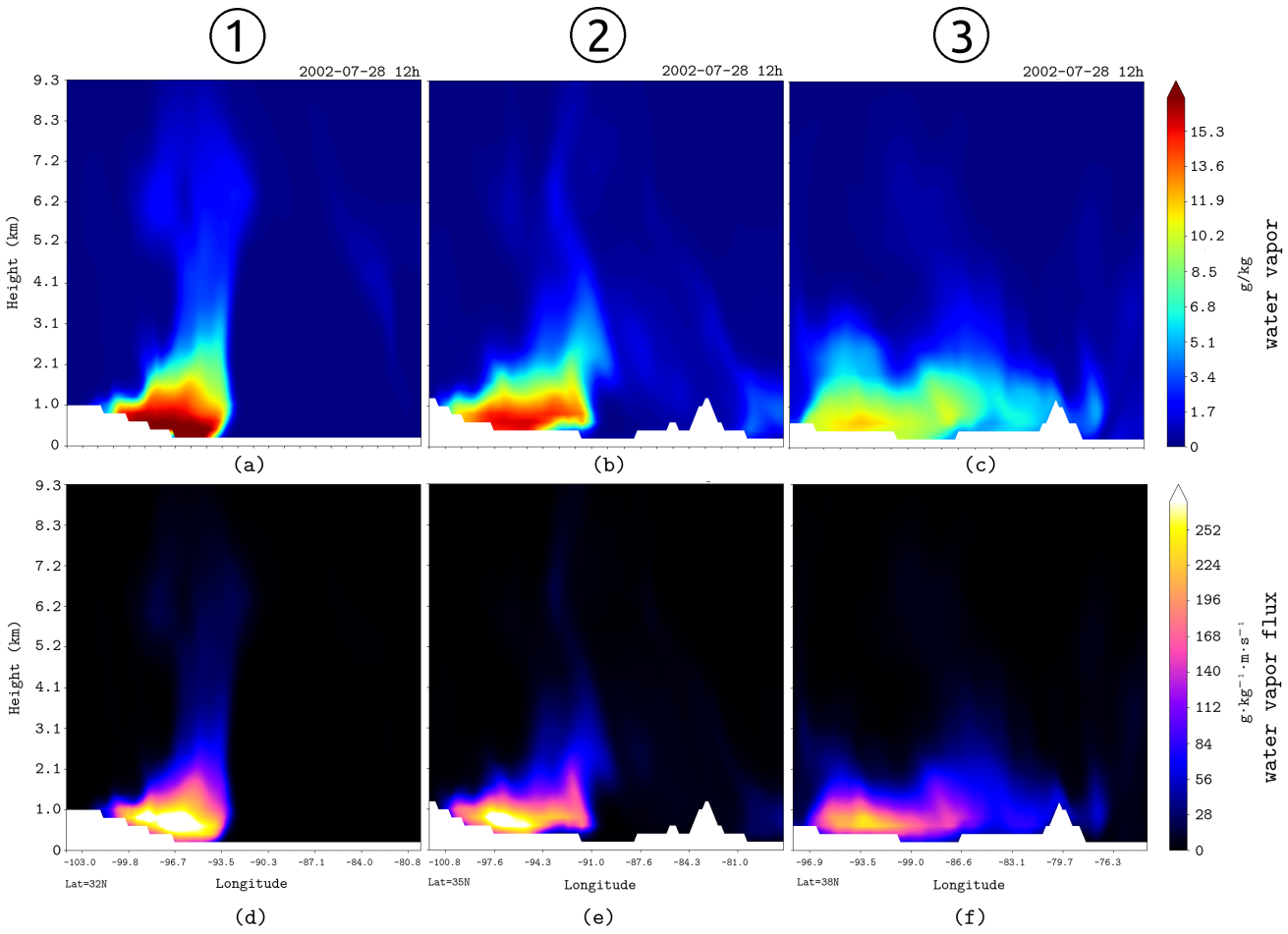
1
2
3
2002-07-28 12h
2002-07-28 12h
2002-07-28 12h
Height (km)
9.3
8.3
7.2
6.2
5.2
4.1
3.1
2.1
1.0
0
(a)
(b)
(c)
15.3
13.6
11.9
10.2
8.5
6.8
5.1
3.4
1.7
0
g/kg
water vapor
252
224
196
168
140
112
84
56
28
0
g·kg⁻¹·m·s⁻¹
water vapor flux
-103.0 -99.8 -96.7 -93.5 -90.3 -87.1 -84.0 -80.8
-100.8 -97.6 -94.3 -91.0 -87.6 -84.3 -81.0
-96.9 -93.5 -99.0 -86.6 -83.1 -79.7 -76.3
Lat=32N
Lat=35N
Lat=38N
Longitude
Longitude
Longitude
(d)
(e)
(f)

Figure S6

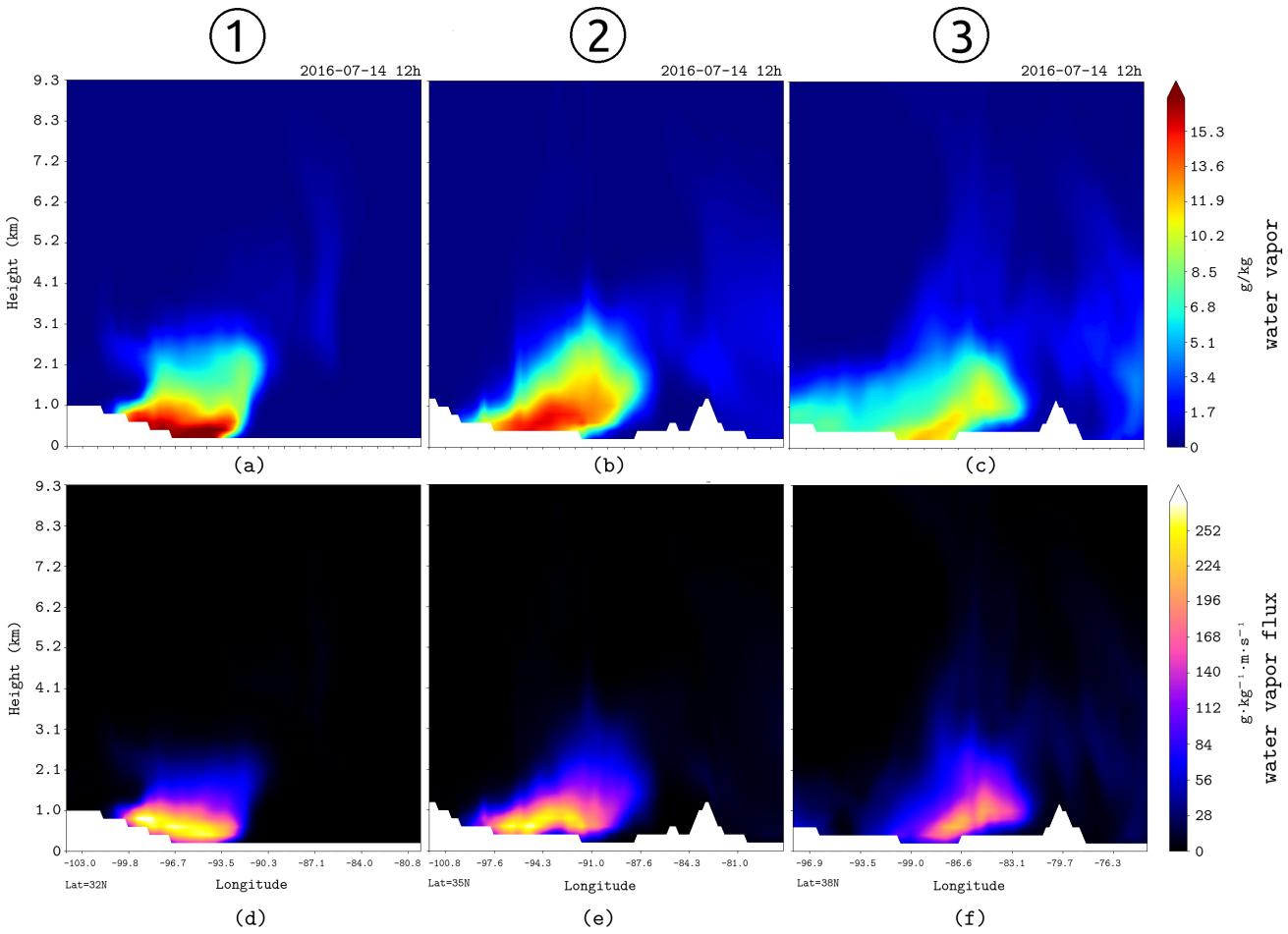
1
2
3
2016-07-14 12h
2016-07-14 12h
2016-07-14 12h
Height (km)
9.3
8.3
7.2
6.2
5.2
4.1
3.1
2.1
1.0
0
15.3
13.6
11.9
10.2
8.5
6.8
5.1
3.4
1.7
0
g/kg
water vapor
(a)
(b)
(c)
252
224
196
168
140
112
84
56
28
0
g·kg⁻¹·m·s⁻¹
water vapor flux
-103.0 -99.8 -96.7 -93.5 -90.3 -87.1 -84.0 -80.8
Lat=32N
Longitude
-100.8 -97.6 -94.3 -91.0 -87.6 -84.3 -81.0
Lat=35N
Longitude
-96.9 -93.5 -99.0 -86.6 -83.1 -79.7 -76.3
Lat=38N
Longitude
(d)
(e)
(f)

Figure S7

References

Adler, R. F., Huffman, G. J., Chang, A., Ferraro, R., Xie, P.-P., Janowiak, J., … Nelkin, E. (2003). The Version-2 Global Precipitation Climatology Project (GPCP) Monthly Precipitation Analysis (1979–Present). *Journal of Hydrometeorology*, *4*(6), 1147–1167. https://doi.org/10.1175/1525-7541(2003)004<1147:TVGPCP>2.0.CO;2

Baumgartner, A., & Reichel., E (1975). The World Water Balance. Elsevier., Amsterdam, 179 pp.

Beck, H. E., van Dijk, A. I. J. M., Levizzani, V., Schellekens, J., Miralles, D. G., Martens, B., & de Roo, A. (2017). MSWEP: 3-hourly 0.25° global gridded precipitation (1979–2015) by merging gauge, satellite, and reanalysis data. *Hydrology and Earth System Sciences*, *21*(1), 589–615. https://doi.org/10.5194/hess-21-589-2017

Beck, H. E., Wood, E. F., Pan, M., Fisher, C. K., Miralles, D. G., van Dijk, A. I. J. M., … Adler, R. F. (2019). MSWEP V2 Global 3-Hourly 0.1° Precipitation: Methodology and Quantitative Assessment. *Bulletin of the American Meteorological Society*, *100*(3), 473–500. https://doi.org/10.1175/BAMS-D-17-0138.1

Blackadar, A. K. (1957). Boundary Layer Wind Maxima and Their Significance for the Growth of Nocturnal Inversions. *Bulletin of the American Meteorological Society*, *38*(5), 283–290. https://doi.org/10.1175/1520-0477-38.5.283

Bonner, Wi. D. (1968). Climatology of the low-level jet. *Monthly Weather Review*, *96*(12), 833–850. https://doi.org/10.1175/1520-0493(1968)096<0833:cotllj>2.0.co;2

Castillo, R., Nieto, R., Drumond, A., & Gimeno, L. (2014). The role of the ENSO cycle in the modulation of moisture transport from major oceanic moisture sources. *Water Resources Research*, *50*(2), 1046–1058. https://doi.org/10.1002/2013WR013900

Chen, G., Norris, J., Neelin, J. D., Lu, J., Leung, L. R., & Sakaguchi, K. (2019). Thermodynamic and Dynamic Mechanisms for Hydrological Cycle Intensification over the Full Probability Distribution of Precipitation Events. *Journal of the Atmospheric Sciences*, *76*(2), 497–516. https://doi.org/10.1175/JAS-D-18-0067.1

Cordeira, J. M., Stock, J., Dettinger, M. D., Young, A. M., Kalansky, J. F., & Ralph, F. M. (2019). A 142-Year Climatology of Northern California Landslides and Atmospheric Rivers. *Bulletin of the American Meteorological Society*, *100*(8), 1499–1509. https://doi.org/10.1175/BAMS-D-18-0158.1

Corringham, T. W., Ralph, F. M., Gershunov, A., Cayan, D. R., & Talbot, C. A. (2019). Atmospheric rivers drive flood damages in the western United States. *Science Advances*, *5*(12), eaax4631. https://doi.org/10.1126/sciadv.aax4631

Dee, D. P., Uppala, S. M., Simmons, A. J., Berrisford, P., Poli, P., Kobayashi, S., … Vitart, F. (2011). The ERA-Interim reanalysis: Configuration and performance of the data assimilation system. *Quarterly Journal of the Royal Meteorological Society*, *137*(656), 553–597. https://doi.org/10.1002/qj.828

Dettinger, M. (2011). Climate Change, Atmospheric Rivers, and Floods in California - A Multimodel Analysis of Storm Frequency and Magnitude Changes1. *JAWRA Journal of the American Water Resources Association*, *47*(3), 514–523. https://doi.org/10.1111/j.1752-1688.2011.00546.x

Dettinger, M. D., Ralph, F. M., Das, T., Neiman, P. J., & Cayan, D. R. (2011). Atmospheric Rivers, Floods and the Water Resources of California. *Water*, *3*(2), 445–478. https://doi.org/10.3390/w3020445

Dominguez, F., Dall'erba, S., Huang, S., Avelino, A., Mehran, A., Hu, H., … Lettenmaier, D. (2018). Tracking an atmospheric river in a warmer climate: from water vapor to economic impacts. *Earth System Dynamics*, *9*(1), 249–266. https://doi.org/10.5194/esd-9-249-2018

Eiras-Barca, J., Dominguez, F., Hu, H., Garaboa-Paz, D., & Miguez-Macho, G. (2017). Evaluation of the moisture sources in two extreme landfalling atmospheric river events using an Eulerian WRF tracers tool. *Earth System Dynamics*, *8*(4), 1247–1261. https://doi.org/10.5194/esd-8-1247-2017

Espinoza, V., Waliser, D. E., Guan, B., Lavers, D. A., & Ralph, F. M. (2018). Global Analysis of Climate Change Projection Effects on Atmospheric Rivers. *Geophysical Research Letters*, *45*(9), 4299–4308. https://doi.org/10.1029/2017GL076968

Fairall, C. W., Bradley, E. F., Hare, J. E., Grachev, A. A., & Edson, J. B. (2003). Bulk Parameterization of Air–Sea Fluxes: Updates and Verification for the COARE

Algorithm. *Journal of Climate*, *16*(4), 571–591. https://doi.org/10.1175/1520-0442(2003)016<0571:BPOASF>2.0.CO;2

Gershunov, A., Shulgina, T., Clemesha, R. E. S., Guirguis, K., Pierce, D. W., Dettinger, M. D., … Ralph, F. M. (2019). Precipitation regime change in Western North America: The role of Atmospheric Rivers. *Scientific Reports*, *9*(1). https://doi.org/10.1038/s41598-019-46169-w

Gimeno-Sotelo, L., Nieto, R., Vázquez, M., & Gimeno, L. (2018). A new pattern of the moisture transport for precipitation related to the drastic decline in Arctic sea ice extent. *Earth System Dynamics*, *9*(2), 611–625. https://doi.org/10.5194/esd-9-611-2018

Gimeno, L. (2013). Grand challenges in atmospheric science. *Frontiers in Earth Science*, *1*. https://doi.org/10.3389/feart.2013.00001

Gimeno, L., Dominguez, F., Nieto, R., Trigo, R., Drumond, A., Reason, C. J. C., … Marengo, J. (2016). Major Mechanisms of Atmospheric Moisture Transport and Their Role in Extreme Precipitation Events. *Annual Review of Environment and Resources*, *41*(1), 117–141. https://doi.org/10.1146/annurev-environ-110615-085558

Gimeno, L., Drumond, A., Nieto, R., Trigo, R. M., & Stohl, A. (2010). On the origin of continental precipitation. *Geophysical Research Letters*, *37*(13), n/a-n/a. https://doi.org/10.1029/2010GL043712

Gimeno, L., Stohl, A., Trigo, R. M., Dominguez, F., Yoshimura, K., Yu, L., … Nieto, R. (2012). Oceanic and terrestrial sources of continental precipitation. *Reviews of Geophysics*, *50*(4). https://doi.org/10.1029/2012RG000389

Gimeno, L., Vázquez, M., Eiras-Barca, J., Sorí, R., Stojanovic, M., Algarra, I., … Dominguez, F. (2020, February 1). Recent progress on the sources of continental precipitation as revealed by moisture transport analysis. *Earth-Science Reviews*. Elsevier B.V. https://doi.org/10.1016/j.earscirev.2019.103070

Guan, B., & Waliser, D. E. (2015). Detection of atmospheric rivers: Evaluation and application of an algorithm for global studies. *Journal of Geophysical Research*, *120*(24), 12,514-12,535. https://doi.org/10.1002/2015JD024257

Harding, K. J., & Snyder, P. K. (2014). Examining future changes in the character of Central U.S. warm-season precipitation using dynamical downscaling. *Journal of Geophysical Research: Atmospheres*, *119*(23), 13,116-13,136. https://doi.org/10.1002/2014JD022575

He, J., Mao, H., Gong, S., Yu, Y., Wu, L., Liu, H., … Zou, C. (2017). Investigation of Particulate Matter Regional Transport in Beijing Based on Numerical Simulation. *Aerosol and Air Quality Research*, *17*(5), 1181–1189. https://doi.org/10.4209/aaqr.2016.03.0110

Held, I. M., & Soden, B. J. (2006). Robust Responses of the Hydrological Cycle to Global Warming. *Journal of Climate*, *19*(21), 5686–5699. https://doi.org/10.1175/JCLI3990.1

Insua-Costa, D., & Miguez-Macho, G. (2018). A new moisture tagging capability in the Weather Research and Forecasting model: formulation, validation and application to the 2014 Great Lake-effect snowstorm. *Earth System Dynamics*, *9*(1), 167–185. https://doi.org/10.5194/esd-9-167-2018

IPCC, 2014: Climate Change 2014: Synthesis Report. Contribution of Working Groups I, II and III to the Fifth Assessment Report of the Intergovernmental Panel on Climate Change [Core Writing Team, R.K. Pachauri and L.A Meyer (eds.)]. IPCC, Geneva, Switzerland, 151 pp.

Kim, H. M., Zhou, Y., & Alexander, M. A. (2019). Changes in atmospheric rivers and moisture transport over the Northeast Pacific and western North America in response to ENSO diversity. *Climate Dynamics*, *52*(12), 7375–7388. https://doi.org/10.1007/s00382-017-3598-9

Läderach, A., & Sodemann, H. (2016). A revised picture of the atmospheric moisture residence time. *Geophysical Research Letters*, *43*(2), 924–933. https://doi.org/10.1002/2015GL067449

Langford, A. O., Alvarez, R. J., Brioude, J., Evan, S., Iraci, L. T., Kirgis, G., … Yates, E. L. (2018). Coordinated profiling of stratospheric intrusions and transported pollution by the Tropospheric Ozone Lidar Network (TOLNet) and NASA Alpha Jet experiment (AJAX): Observations and comparison to HYSPLIT, RAQMS, and FLEXPART. *Atmospheric Environment*, *174*, 1–14.

https://doi.org/10.1016/j.atmosenv.2017.11.031

Langford, A. O., Senff, C. J., Alvarez, R. J., Brioude, J., Cooper, O. R., Holloway, J. S., … Williams, E. J. (2015). An overview of the 2013 Las Vegas Ozone Study (LVOS): Impact of stratospheric intrusions and long-range transport on surface air quality. *Atmospheric Environment*, *109*, 305–322. https://doi.org/10.1016/j.atmosenv.2014.08.040

Lavers, D. A., & Villarini, G. (2013). The nexus between atmospheric rivers and extreme precipitation across Europe. *Geophysical Research Letters*, *40*(12), 3259–3264. https://doi.org/10.1002/grl.50636

Marengo, J. A. (2005). Characteristics and spatio-temporal variability of the Amazon river basin water budget. *Climate Dynamics*, *24*(1), 11–22. https://doi.org/10.1007/s00382-004-0461-6

Massoud, E. C., Espinoza, V., Guan, B., & Waliser, D. E. (2019). Global Climate Model Ensemble Approaches for Future Projections of Atmospheric Rivers. *Earth's Future*, *7*(10), 1136–1151. https://doi.org/10.1029/2019EF001249

Martins, H., D. A. Sá, L., & L. L. Moraes, O. (2013). Low Level Jets in the Pantanal Wetland Nocturnal Boundary Layer – Case Studies. *American Journal of Environmental Engineering*, *3*(1), 32–47. https://doi.org/10.5923/j.ajee.20130301.06

Mekonnen, M. M., & Hoekstra, A. Y. (2016). Four billion people facing severe water scarcity. *Science Advances*, *2*(2), e1500323. https://doi.org/10.1126/sciadv.1500323

Monaghan, A. J., Rife, D. L., Pinto, J. O., Davis, C. A., & Hannan, J. R. (2010). Global Precipitation Extremes Associated with Diurnally Varying Low-Level Jets. *Journal of Climate*, *23*(19), 5065–5084. https://doi.org/10.1175/2010JCLI3515.1

Moore, B. J., Neiman, P. J., Ralph, F. M., & Barthold, F. E. (2012). Physical Processes Associated with Heavy Flooding Rainfall in Nashville, Tennessee, and Vicinity during 1–2 May 2010: The Role of an Atmospheric River and Mesoscale Convective Systems. *Monthly Weather Review*, *140*(2), 358–378. https://doi.org/10.1175/MWR-D-11-00126.1

Newell, R. E., Newell, N. E., Zhu, Y., & Scott, C. (1992). Tropospheric rivers? - A pilot

study. *Geophysical Research Letters*, *19*(24), 2401–2404. https://doi.org/10.1029/92GL02916

Nicholson, S. (2016). The Turkana low-level jet: mean climatology and association with regional aridity. *International Journal of Climatology*, *36*(6), 2598–2614. https://doi.org/10.1002/joc.4515

Nieto, R., Ciric, D., Vázquez, M., Liberato, M. L. R., & Gimeno, L. (2019). Contribution of the main moisture sources to precipitation during extreme peak precipitation months. *Advances in Water Resources*, *131*. https://doi.org/10.1016/j.advwatres.2019.103385

Nieto, R., & Gimeno, L. (2019). A database of optimal integration times for Lagrangian studies of atmospheric moisture sources and sinks. *Scientific Data*, *6*(1), 59. https://doi.org/10.1038/s41597-019-0068-8

Numaguti, A. (1999). Origin and recycling processes of precipitating water over the Eurasian continent: Experiments using an atmospheric general circulation model. *Journal of Geophysical Research Atmospheres*, *104*(D2), 1957–1972. https://doi.org/10.1029/1998JD200026

Nusbaumer, J., & Noone, D. (2018). Numerical Evaluation of the Modern and Future Origins of Atmospheric River Moisture Over the West Coast of the United States. *Journal of Geophysical Research: Atmospheres*, *123*(12), 6423–6442. https://doi.org/10.1029/2017JD028081

O'Gorman, P. A., & Muller, C. J. (2010). How closely do changes in surface and column water vapor follow Clausius-Clapeyron scaling in climate change simulations? *Environmental Research Letters*, *5*(2). https://doi.org/10.1088/1748-9326/5/2/025207

O'Gorman, P. A., & Schneider, T. (2009). The physical basis for increases in precipitation extremes in simulations of 21st-century climate change. *Proceedings of the National Academy of Sciences of the United States of America*, *106*(35), 14773–14777. https://doi.org/10.1073/pnas.0907610106

Oki, T. (2005). The hydrologic cycles and global circulation, Encyclopedia of Hydrological Sciences, edited by M. G. Anderson and J. McDonnell, pp. 13-22, John Wiley, New York

Peixoto, J. P., & Oort, A. H. (1992). Physics of Climate, AIP-Press, New York, NY Springer Verlag, New York Press

Pierrehumbert, R. T., Brogniez, H., Roca, R. (2008). On the relative humidity of the Atmosphere, Chapter 6

Pisso, I., Sollum, E., Grythe, H., Kristiansen, N., Cassiani, M., Eckhardt, S., … Stohl, A. (2019). The Lagrangian particle dispersion model FLEXPART version 10.3. *Geoscientific Model Development Discussions*, 1–67. https://doi.org/10.5194/gmd-2018-333

Ralph, F. M., Dettinger, M., Lavers, D., Gorodetskaya, I. V., Martin, A., Viale, M., … Cordeira, J. (2017). Atmospheric Rivers Emerge as a Global Science and Applications Focus. *Bulletin of the American Meteorological Society*, *98*(9), 1969–1973. https://doi.org/10.1175/BAMS-D-16-0262.1

Ralph, F. M., Neiman, P. J., Wick, G. A., Gutman, S. I., Dettinger, M. D., Cayan, D. R., & White, A. B. (2006). Flooding on California's Russian River: Role of atmospheric rivers. *Geophysical Research Letters*, *33*(13), L13801. https://doi.org/10.1029/2006GL026689

Ralph, F. M., Rutz, J. J., Cordeira, J. M., Dettinger, M., Anderson, M., Reynolds, D., … Smallcomb, C. (2019). A Scale to Characterize the Strength and Impacts of Atmospheric Rivers. *Bulletin of the American Meteorological Society*, *100*(2), 269–289. https://doi.org/10.1175/BAMS-D-18-0023.1

Ramos, A. M., Nieto, R., Tomé, R., Gimeno, L., Trigo, R. M., Liberato, M. L. R., & Lavers, D. A. (2016). Atmospheric rivers moisture sources from a Lagrangian perspective. *Earth System Dynamics*, *7*(2), 371–384. https://doi.org/10.5194/esd-7-371-2016

Ramos, A. M., Wilson, A. M., DeFlorio, M. J., Warner, M. D., Barnes, E., Garreaud, R., … Ralph, F. M. (2019). 2018 International Atmospheric Rivers Conference: Multi-disciplinary studies and high-impact applications of atmospheric rivers. *Atmospheric Science Letters*, *20*(9). https://doi.org/10.1002/asl.935

Rife, D. L., Pinto, J. O., Monaghan, A. J., Davis, C. A., & Hannan, J. R. (2010). Global Distribution and Characteristics of Diurnally Varying Low-Level Jets. *Journal of Climate*, *23*(19), 5041–5064. https://doi.org/10.1175/2010JCLI3514.1

Seidel, D. J. (2002). Water Vapor: Distribution and Trends. *Encyclopedia of Global Environmental Change, John Wiley and Sons, Ltd, Chichester*

Sousa, P. M., Ramos, A. M., Raible, C. C., Messmer, M., Tomé, R., Pinto, J. G., & Trigo, R. M. (2019). North Atlantic Integrated Water Vapor Transport – from 850-2100 CE: Impacts on Western European Rainfall. *Journal of Climate*. https://doi.org/10.1175/jcli-d-19-0348.1

Stensrud, D. J. (1996). Importance of low-level jets to climate: A review. *Journal of Climate*, *9*(8), 1698–1711. https://doi.org/10.1175/1520-0442(1996)009<1698:IOLLJT>2.0.CO;2

Stohl, A., Forster, C., Frank, A., Seibert, P., & Wotawa, G. (2005). Technical note: The Lagrangian particle dispersion model FLEXPART version 6.2. *Atmospheric Chemistry and Physics*, *5*(9), 2461–2474. https://doi.org/10.5194/acp-5-2461-2005

Stohl, A., Hittenberger, M., & Wotawa, G. (1998). Validation of the lagrangian particle dispersion model FLEXPART against large-scale tracer experiment data. *Atmospheric Environment*, *32*(24), 4245–4264. https://doi.org/10.1016/S1352-2310(98)00184-8

Stohl, A., & James, P. (2005). A Lagrangian Analysis of the Atmospheric Branch of the Global Water Cycle. Part II: Moisture Transports between Earth's Ocean Basins and River Catchments. *Journal of Hydrometeorology*, *6*(6), 961–984. https://doi.org/10.1175/JHM470.1

Trenberth, K. E. (1998). Atmospheric Moisture Residence Times and Cycling: Implications for Rainfall Rates and Climate Change. *Climatic Change*, *39*(4), 667–694. https://doi.org/10.1023/A:1005319109110

Trenberth, K. E., Fasullo, J. T., & Mackaro, J. (2011). Atmospheric Moisture Transports from Ocean to Land and Global Energy Flows in Reanalyses. *Journal of Climate*, *24*(18), 4907–4924. https://doi.org/10.1175/2011JCLI4171.1

Trenberth, K. E., Smith, L., Qian, T., Dai, A., & Fasullo, J. (2007). Estimates of the Global Water Budget and Its Annual Cycle Using Observational and Model Data. *Journal of Hydrometeorology*, *8*(4), 758–769. https://doi.org/10.1175/JHM600.1

van der Ent, R. J., & Savenije, H. H. G. (2011). Length and time scales of atmospheric

moisture recycling. *Atmospheric Chemistry and Physics*, *11*(5), 1853–1863. https://doi.org/10.5194/acp-11-1853-2011

van der Ent, R. J., Savenije, H. H. G., Schaefli, B., & Steele-Dunne, S. C. (2010). Origin and fate of atmospheric moisture over continents. *Water Resources Research*, *46*(9). https://doi.org/10.1029/2010WR009127

van der Ent, R. J., & Tuinenburg, O. A. (2017). The residence time of water in the atmosphere revisited. *Hydrology and Earth System Sciences*, *21*(2), 779–790. https://doi.org/10.5194/hess-21-779-2017

Vera, C., Higgins, W., Amador, J., Ambrizzi, T., Garreaud, R., Gochis, D., … Zhang, C. (2006, October 15). Toward a unified view of the American monsoon systems. *Journal of Climate*. https://doi.org/10.1175/JCLI3896.1

Wentz, F. J., Ricciardulli, L., Hilburn, K., & Mears, C. (2007). How much more rain will global warming bring? *Science*, *317*(5835), 233–235. https://doi.org/10.1126/science.1140746

Whiteman, C. D., Bian, X., & Zhong, S. (1997). Low-Level Jet Climatology from Enhanced Rawinsonde Observations at a Site in the Southern Great Plains. *Journal of Applied Meteorology*, *36*(10), 1363–1376. https://doi.org/10.1175/1520-0450(1997)036<1363:LLJCFE>2.0.CO;2

Zhang, Y., Sun, Y., Du, W., Wang, Q., Chen, C., Han, T., … Han, Y. (2016). Response of aerosol composition to different emission scenarios in Beijing, China. *Science of The Total Environment*, *571*, 902–908. https://doi.org/10.1016/j.scitotenv.2016.07.073

Zhu, Y., & Newell, R. E. (1998). A Proposed Algorithm for Moisture Fluxes from Atmospheric Rivers. *Monthly Weather Review*, *126*(3), 725–735. https://doi.org/10.1175/1520-0493(1998)126<0725:APAFMF>2.0.CO;2